Hydrodynamics of Jet Driven Gas-Liquid-Liquid Dispersion in Downflow Column and the Efficiency of Extraction

A Thesis
Submitted in Partial Fulfilment of the Requirement for the Degree of

Doctor of Philosophy

By

Goshika Bharath Kumar

Roll no. 136107021

Under the supervision of

Prof. Subrata Kumar Majumder

Department of Chemical Engineering

Indian Institute of Technology Guwahati

Guwahati, Assam – 781039

May, 2020

Dedicated to
My Supervisor and my family

INDIAN INSTITUTE OF TECHNOLOGY GUWAHATI
GUWAHATI - 781039, ASSAM, INDIA

DEPARTMENT OF CHEMICAL ENGINEERING

CERTIFICATE

This is to certify that the thesis entitled "***Hydrodynamics of Jet Driven Gas-Liquid-Liquid Dispersion in Downflow Column and The Efficiency of Extraction***" submitted by **Goshika Bharath Kumar** in fulfillment of the requirement of the *Degree of Doctor of Philosophy in Engineering*, is a record of bonafide research work carried out by him, in the Department of Chemical Engineering, Indian Institute of Technology, Guwahati, under my guidance and supervision. The work documented in this thesis has not been submitted to any other University or Institute for the award of any degree or diploma. In my opinion, the thesis has reached the standard fulfilling the requirements of the Ph. D. degree as prescribed in the regulations of this institute.

Dr. Subrata Kumar Majumder
Professor
Department of chemical Engineering
Indian institute of Technology Guwahati
Guwahati-781039, India.

ACKNOWLEDGEMENTS

I would like to express my gratitude to all those who helped me in different ways in completing this research work within the time span of four years, directly or indirectly. First and foremost, I would like to express my deep felt gratitude to my supervisor, **Prof. Subrata Kumar Majumder** for providing me continuous inspiration and guidance throughout the entire course of work. In addition, His philosophical guidance has built up a momentum inside me. His uncompromising approach to complete the experimental part, data analysis, writing manuscripts as well as thesis within the stipulated time period helped me a lot in completing my research work. The numerous brain storming sessions during the project meetings with him were very useful in enriching my analytical power. I also remain indebted for his understanding, support and caring during the times when I was really down and depressed due to personal problems. I also thank almighty for making me to feel fortunate to work under their great stewardship.

I wish to acknowledge my respectful thanks to **Prof. Bishnupada Mandal**, former HOD and **Prof. Anugrah Singh** present HOD, Department of Chemical Engineering, for extending all the necessary facilities for carrying out my research work. I am also grateful to all the professors in the department for their sincere cooperation.

I must also thank my doctoral committee members **Prof. Pallab Ghosh, Prof. Mihir K. Purkait,** of the Department of Chemical Engineering and **Prof. Ujjwal K. Saha** of the Department of Mechanical Engineering, for their valuable suggestions and contribution towards my research work.

I wish to thank all the non-teaching staff of our department for the help received from them.

I am grateful to my senior members from our group, *Dr. Anil K. Thandlam*, and *Dr. Rajeev Parmar*, for their co-operative assistance and suggestions in performing experiments. I also thank my present lab members *Mr. M. K. Fahad, Mr. Ritesh Prakash, Mr. Somen Mondal, Ms. Kumari Ruby, Ms. Surabhi Patel, Mr. Bongliba T Sangtam, Mr. Gaurav Singh, Mr Babban Mauriya* and *Ms. VVRS Bhavana*.

I cannot forget to thank my friends *Mr. M.M. Reddy, Mr. M. Venkatanarasimha Rao, Mr. T. Ramesh, Mr. Prudhviraj, Mr. Y. Santosh Kumar, Mr. Rambabu, Mr. Anudeep, Mr. E. Satyanarayan* and *Mr. Nagireedi Srinu*, for the lovely support in making my stay at IIT Guwahati memorable.

I would also like to thank my family who have not only supported me in the completion of my Ph.D. but also have stood by me throughout my life. They have patiently supported me at all instances in my research work. I feel proud and blessed to have such parents my mother, **Mrs. G. Shanti** Garu and my father **Mr. G. Pandu** Garu, and my sisters **Mrs. M. Nagaja** Garu, and **Ms. G. Sindhuja** Garu and my brother in law **Mr. M. Sandeep Kumar** Garu.

I am indebted to my wife **Chaitanya** whose constant encouragement, suggestion, patience and motivation, made me to achieve this endeavor in a peaceful and cheerful manner. She transformed all the odds into reality.

May, 2020

Place: IIT Guwahati

Goshika Bharath Kumar

CURRICULUM VITAE

Mr. GOSHIKA BHARATH KUMAR

Date of Birth: **20th August 1990**

Email: goshika@iitg.ac.in; gbk818@gmail.com

Educations:

Ph.D. pursuing

Department of Chemical Engineering
Indian Institute of Technology, Guwahati
Guwahati, Assam, India

M. Tech in Chemical Engineering

Department of Chemical Engineering
Indian Institute of Technology, Guwahati
Guwahati, Assam, India
2011- 2013

B. Tech in Chemical Engineering

Department of Chemical Engineering
Jawaharlal Nehru Technological University Anantapur
Anantapur, Andhra Pradesh, India
2007-2011

Higher Secondary in MPC

Sri Chaitanya Jr. College
Hydernagar, Hyderabad, Telangana, India
2005-2007

Secondary Education

Mallikarjuna High School, Choutuppal,
Yadadri Bhuvanagiri, Telangana, India
2005

AWARDS AND SCHOLARSHIPS

- MHRD Govt. of India scholarship for Ph.D. from July 2013 to July 2018
- MHRD Govt. of India scholarship for M.Tech. from July 2011 to June 2013
- Actively participated, in Environmental general quiz - 2010 organized by APPCB and department of chemical engineering JNTUCEA.

Journal Publications

- **Goshika, B. K.**; Majumder, S. K., 2019. Frictional pressure drop of gas-liquid-liquid dispersion in an ejector induced down flow column, Multiphase Science and Technology, 31, 151-174.
- **Goshika, B. K.**; Majumder, S. K., 2018. Dispersion of liquid-liquid phase by a jet-induced gas-liquid-liquid mixing column developed for separation of organic pollutant, Separation science and Technology, 54, 535-548.
- **Goshika, B. K**.; Majumder, S. K., 2018. Studies on gas entrainment and holdup in a new jet-driven gas-aided liquid-liquid solvent extraction column, Chemical Engineering Processing and Process Intensification, 125, 112-123.

Under preparation

- **Goshika, B. K.**; Majumder, S. K., 2019. Mixing Characteristics of gas-liquid-liquid dispersion in an ejector induced down flow column. (to be communicated)
- **Goshika, B. K.**; Majumder, S. K., 2019. Drop size Characteristics of gas-liquid-liquid dispersion in an ejector induced down flow column. (to be communicated)
- **Goshika, B. K**.; Majumder, S. K., 2019. Extraction efficiency of gas-liquid-liquid dispersion in an ejector induced down flow column. (to be communicated)

Conference Publications

- **Goshika, B. K.**; Majumder, S. K., Mixing characteristics of gas-liquid-liquid dispersion in a downflow column, RESEARCH CONCLAVE-2019, March 16-18, Indian Institute of Technology Guwahati, Guwahati, India.
- **Goshika, B. K.**; Majumder, S. K., Mixing characteristics of gas-liquid-liquid flow in an ejector induced down flow extraction column, REFLUX-2018, March 16-18, Indian Institute of Technology Guwahati, Guwahati, India.
- **Goshika, B. K.**; Majumder, S. K., drop size characteristics of gas-liquid-liquid flow in an ejector induced down flow extraction column , REFLUX-2017, March 24-26, Indian Institute of Technology Guwahati, Guwahati, India.
- **Goshika, B. K.**; Majumder, S. K., Pressure drop of gas-liquid-liquid flow in an ejector induced down flow extraction column , MPT-2017, Feb 01-03, Mahabalipuram, Chennai, India.
- **Goshika, B. K**.; Majumder, S. K., Studies on gas holdup in a modified gas-aided extraction column , *CHEMCON-2015*, December 27-30, Indian Institute of Technology Guwahati, Guwahati, India.
- **Goshika, B. K.**; Majumder, S. K., Gas-liquid-liquid flow holdup in an ejector induced down flow bubble column , *INCEE-2015*, March 20-21, NIT Warangal, Telangana state, India.

Other Journal Publications

- Dasari, A.; **Goshika, B.K**.; Majumder, S. K..; Mandal, T.K., 2015. Viscous oil-water flow through an inclined pipeline: Experimentation and prediction of Flow patterns, *Multiphase Science and Technology,* 27, 1-26
- Dasari, A.; **Goshika, B.K**.; Pilla, R. T..; Mandal, T.K., 2014. CFD simulation and validation of viscous oil-water flow through upward inclined pipe, *International Journal of Current Engineering and Technology*, 2, 453-460.
- Desamala, A.B.; Dasari, A.; Vijayan, V.; **Goshika, B.K**.; Dasmahapatra, A.K.; Mandal, T.K.; 2013. CFD simulation and validation of flow pattern transition boundaries during moderately viscous oil-water two-phase flow through horizontal pipeline, World Academy of Science, Engineering and Technology, *International Journal of Chemical, Materials Science and Engineering*, 7, 72-77.

Other Conference Publications

- **Goshika, B. K**.; Mandal, T. K., Experimental study of moderately viscous oil-water flow through inclined pipes, Cafe-2012, GLBITM, Greater Noida, India.
- **Goshika, B. K**.; Continuous extraction treatment process of ZINC from synthesis and industrial effluents using emulsion liquid membrane technique, Azoetrophy-2010**,** IIT Mumbai, India.

ABSTRACT

Gas-liquid-liquid dispersion is an important process for the mass transfer operation in chemical and biochemical industries. The presence of gas for the liquid-liquid dispersion increases the degree of mass transfer and reactions compared to other dispersion mechanisms. Some of the examples for gas-liquid-liquid operations are carbonylation, hydroformylation, and gas-aided mass transfer (e.g., extraction). The gas-aided mass transfer operation has now been extended to such various applications in the petrochemical industry, pharmaceuticals, hydrometallurgy, nuclear industry, and environmental protection. There are different types of commonly used extraction columns, pulsed sieve plate column, rotating disc contactor, Kuhni column, and spray column, Scheibel extractor, packed column, Oldshue-Rushton contactor, and reciprocating plate column. Various extraction model parameters, such as drop size, drop size distribution, slip velocity, mass transfer coefficient, and axial dispersion coefficient, play an important role in assessing the modeling of extraction columns. In order to increase the efficiency of columns, the contact time between the two liquid phases should be increased. The contact time is increased by the provisions of the sieve plates, disc, and doughnuts. Another way to increase the efficiency of an extraction column is the introduction of inert gas (air, nitrogen, oxygen) as a mixing agent in the two-phase liquid-liquid (L-L) system. This method of introduction of inert gas increases the turbulence within the three-phase gas-liquid-liquid (G-L-L) system, which causes an improved dispersion of droplets, and, consequently, a higher dispersed phase interfacial area and therefore a significant mass transfer efficiency. Sovilj and Kneževic (1994) reported that the extraction efficiency is nearly three times greater than that of conventional columns when the air is introduced into the extraction column, and claimed that the process is more efficient than by the use of stirring or pulsation of the column. The introduction of gas by liquid jet and its use for

liquid-liquid dispersion is gaining importance to the scientific, academic, and research and development organization for the development of liquid-liquid extraction device. The jet-driven downflow column has several advantages and applications described by (Majumder (2016)). Though several hydrodynamic studies such as gas-liquid and gas-solid-liquid like entrainment, holdup of phases, mixing characteristics has been reported, but for the direction of application in extraction in the jet-driven extraction column is missing. The present study focuses on some hydrodynamics and their effects on extraction in the jet-driven gas-aided liquid-liquid downflow extraction column.

The main objective of this study is to develop a jet-driven gas-aided liquid-liquid extraction system. Based on the literature survey and scope of the research, the following objectives of the work under this main objective are formulated as to study:

- Gas and dispersed liquid entrainment characteristics
- Gas holdup of the gas phase in the gas-liquid-liquid mixture.
- Frictional pressure drop and resistance of the flow
- Mixing characteristics of the phases in the proposed system
- Drop size and distribution and its analysis
- The efficiency of the gas-aided liquid-liquid extraction in the jet-driven extraction column

In chapter 3, the gas and liquid entrainment and its dispersion by liquid jet using paraffin liquid-water and kerosene-water is described. The gas entrainment increases with an increase in the gas and water jet velocities for paraffin liquid-water and kerosene-water. The decrease in gas entrainment is observed with an increase in the paraffin liquid and kerosene volume fraction from 5% to 35%, which is due to the increase in the flow resistance with an increase in the

effective viscosity of the liquid-liquid mixture. It can be concluded from the present study that the liquid entrainment can be extended based on the liquid jet kinetic energy. A generalized correlation is proposed for entrainment of gas and liquid as a function of various operating variables within the range of experimental conditions.

In chapter 4, a study focused on the gas holdup using paraffin liquid-water and kerosene-water, in the gas-liquid-liquid contactor is reported. The gas holdup characteristics are enunciated based on different operating conditions. The gas holdup varies with the gas and liquid flow rates and system properties. Gas holdup data were interpreted by Lockhart-Martinelli correlation and by, drift flux model.

In chapter 5, an extensive study for the frictional pressure drop of gas-liquid-liquid dispersion was reported based on the present study in a gas aided liquid-liquid column. Different models such as Lockhart-Martinelli, Kato, Wallis, and Gharat and Joshi models were considered to interpret the results based on the present operating conditions. A general correlation model was also developed based on the experimental results incorporating dynamic, geometric, and physical properties of the system.

In chapter 6, the mixing characteristics of a gas-liquid-liquid flow for the three-phase system are described. The residence time distribution method is enunciated for calculating the axial dispersion coefficient of liquid in the column. From the experimental result, it is observed that with increasing liquid and the gas velocities, the liquid axial dispersion coefficient of the three-phase system of air-water-paraffin liquid and the air-water-kerosene system increases. The liquid dispersion coefficient is analyzed by the velocity distribution model. The empirical models are developed for interstitial velocity and axial dispersion coefficient in terms of different dimensional groups consisting of dynamics, geometric, and the operating parameters of the

system.

In chapter 7, an extensive experimental study was conducted to enunciate the effect of superficial liquid and gas velocities and dispersed liquid volume concentration on drop size, drop size distribution, and the type of distribution function in a homogenous bubbly-drop flow regime. The drop size distribution observed to follow the log-logistic distribution. Correlations were developed for the prediction of each distribution parameters of the distribution functions. A generalized correlation model is also developed to predict the Sauter mean drop diameter and drop interfacial area in the three-phase.

Finally, In chapter 8, an attempt has been made to investigate the extraction and mass transfer efficiencies of the gas-liquid-liquid system in a jet-driven gas-aided downflow column using an air-water-paraffin liquid, and air-water-kerosene system are reported. The volume of the paraffin liquid is varied from 5 to 35% in the column. The extraction efficiency is found to be strongly affected by the superficial liquid velocity. It is observed that the extraction efficiency increased with an increase in superficial gas and liquid velocities. The effect of volume fraction of the paraffin liquid and kerosene on extraction efficiency is studied. The extraction efficiency is found to be higher with high solute concentration due to the lower surface tension of the water-propionic acid mixture. The mass transfer coefficient appeared to be a strong function of both the superficial liquid and gas velocities. The height of transfer unit (HTU_{cl}) and the mass transfer coefficient based on the continuous phase ($K_{cl}a$) are enunciated. The mass transfer coefficient of propionic acid as the solute in the kerosene phase is observed to be higher than that in the Paraffin liquid phase. The mass transfer coefficient is evaluated by dimensional analysis as a function of different operating system variables.

The present study may be useful for the understanding of process intensification in multiphase system for transport process.

Contents

LIST OF FIGURES

CHAPTER – 1

CHAPTER – 2

CHAPTER – 3

CHAPTER – 4

CHAPTER – 5

CHAPTER – 6

CHAPTER – 7

CHAPTER – 8

LIST OF TABLES

CHAPTER – 1

CHAPTER – 2

CHAPTER – 3

CHAPTER – 4

CHAPTER – 5

CHAPTER – 7

CHAPTER - 1

INTRODUCTION

1.1 Multiphase Flow

Multiphase flow means a mixture of two or more distinct phases flowing through a conduit. Generally, there are two categories of multiphase flow: disperse flows and separated flows. In disperse flow, drops or bubbles are dispersed in the continuous phase, whereas separated flows composed of multiple streams of unlike fluids divided by the interfaces. The multiphase flow reactors are widely used in the bulk chemical industries, pharmaceutical industry, fertilizer industry, petroleum industry, polymer industry, and petrochemical industry. Different types of multiphase reactors and their applications are given in Table 1.1. The simultaneous flow of three different phases is called three-phase flow. Three-phase gas-liquid-liquid flow can often be theoretically regarded as the two-phase flow that contains a mixture of two immiscible liquids along with gas. This mixture exhibits spatial and temporal variations in viscosity and density. This differs the three-phase flow significantly from a normal two-phase gas-liquid flow, and therefore it is needed to explore it separately as a different type of flow. The knowledge of the theories, methods, and correlations for the two-phase gas-liquid flow may be used as a preliminary step in the study of the three-phase flow because of its similarity with the two-phase gas-liquid flow. The nature of the interface between the two phases is of crucial importance in both gas-liquid and gas-liquid- liquid flows. However, in the latter flow, characteristics of the liquid-liquid interface can make the flow behavior very different from that of the gas-liquid flow case.

Table 1.1: Multiphase reactors and their applications

Reactor types	Phase	Applications
Gas-liquid	Two-phase	Absorption, olefin polymerization in the gas phase
Gas-solid	Two-phase	Coal gasification, catalytic cracking, reforming.
Liquid-liquid	Two-phase	Enzyme reactions, solution polymerization, bulk polymerization-casting.
Liquid-solid	Two-phase	Ion exchange, electrode reactions, liquid phase olefin polymerization, enzyme reactions, peptide synthesis.
Gas-liquid-solid	Three-phase	Hydrogenation, fermentation in airlift and stirred tank reactor, enzyme production, trickle bed filtration, coal liquefaction, wastewater treatment, electrolysis of water.
Gas-liquid-liquid	Three-phase	Carbonylation, hydroformylation in the petrochemical industry, solvent extraction

1.2 Multiphase Reactor

Multiphase reactors comprise three significant classes: fluidized bed reactor, a bubble column reactor, and a trickle bed reactor. A bubble column reactor is usually consisting of a cylindrical vessel where gas is injected from the bottom. These reactors are usually called slurry bubble column reactors when gas is dispersed as a dispersed phase of bubbles in a slurry. Figure 1.1 illustrates the various types of bubble column reactors. Over the years, the bubble column is extensively used in the study of liquid-phase catalytic oxidation processes (Deckwer and Field, 1992), metallurgical, chemical, petrochemical (Kantarci et al., 2005), biological wastewater treatment (Smith et al., 1996), fermentation processes (Kawase and Moo-Young, 1989), and

biochemical industries (Veera, 2001). Recent literature on bubble columns usually emphasizes on the studies of the gas holdup, flow regime transition, bubbles size and its distribution, local and average heat, and mass transfer characteristics. Also, a considerable study has been reported during the last two decades to overcome the drawbacks, and operational disadvantages of the bubble column, such as back mixing in both the phases (particularly in the continuous phase) and bubble coalescence phenomenon. This has given rise to several modified designs of the bubble column which have proved to be suitable for different industrial applications. Bubble column reactors have a wide range of applications in industrial scale due to the number of advantages compared to conventional both in terms of design and operations.

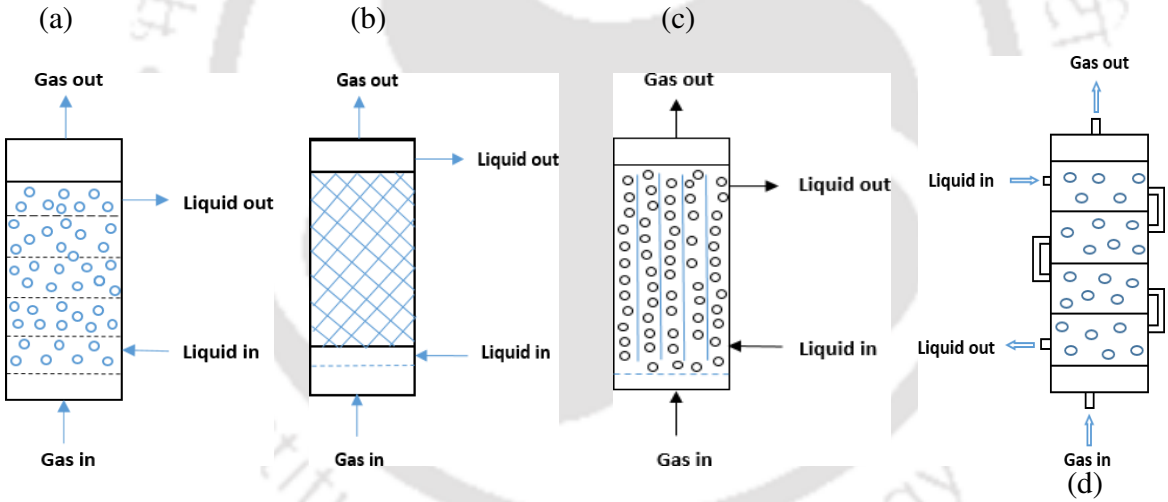

Figure 1.1: Types of reactors. (a) Cascade bubble column (b) Packed bubble column (c) Multi shaft bubble column (d) Multistage bubble column

1.3 Cocurrent Downflow Column

Recently cocurrent downflow columns have drawn interest for many chemical engineering

applications. The downflow column is suggested to use when the rate process is determined based on the interfacial area and contact time. A typical sketch of concurrent downflow column is shown in Figure 1.2. In recent literature, the downflow columns are categorized into two main types, sparger, and plunging jet system. In the plunging systems, ejectors are used where a liquid jet at higher velocity entrain the dispersed gas phase or liquid phase by its kinetic energy. The design of downflow columns is straightforward. It has the advantage to disperse the phase because of the entrainment of dispersed phase by high-velocity liquid jet. No extra energy is required for the dispersion (Majumder, 2016). In the downflow column, bubbles are enforced in the direction opposite to the buoyancy force, which increases the residence time of contact. Therefore, contact efficiency is higher than that of an up-flow column. The concurrent downflow column is also suitable when a small amount of dispersed phase is required to be contacted with a large amount of liquid. The dispersed phase entrainment by liquid jet in the downflow column can be used not only for the application of a highly volatile substance or gaseous reactants but also it can be used for the treatment of gases with an unpleasant odor (Yamagiwa et al., 1990). Some advantages of downflow column are given as follows:

- It is advantageous for slow reactions to be carried out by properly adjusting the liquid phase residence time (Mandal, 2010).
- A broad range of flowrates for liquid and gas can be controlled in the co-current downflow column compared to other conventional columns (Majumder, 2016).
- An ejector-induced downflow column can produce more uniform and finer bubbles or droplets that result in higher mass transfer rates, which helps in further improving the contact efficiency between phases (Cramers and Beenackers, 2001).
- It has a self-sucking capacity of dispersed phase due to jet kinetic energy and efficient

dispersion, which results in a significant volumetric mass transfer coefficient (Zahradnik et al., 1997).

- The other advantages of the co-current downflow column include; lower power consumption, no use of sparger, highly efficient gas utilization, applicable to both homogeneous and heterogeneous processes (Majumder, 2016).

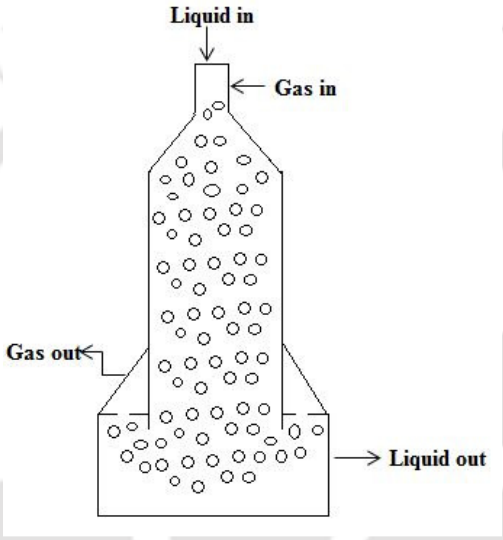

Figure 1.2: Typical sketch of Cocurrent downflow column

1.4 Applications of Downflow Column

Downflow bubble columns have wide applications in chemical industries, particularly in waste treatment and fermentation processes. Some of the practical examples in which the downflow column is used are given below.

- For the treatment of sewage wastewater, the plunging liquid jet aerators downflow bubble column was used by DSM Geleen in Netherland with a capacity of 220 m^3 (Majumder, 2016).
- Treatment of sludge in a downflow column using a plunging jet aerator (Ohkawa et al., 1986).

- In the steel industry, the transfer of liquid metal from one vessel to another is accomplished by the plunging of jet molten steel through the air (Kirchner, 1974).
- Evans (1990) has considered plunging liquid jet in the flotation industry. The system generated fine bubbles by shear force obtained by the plunging of a jet into the receiving pool of liquid. This type of system is useful to recover fine materials by floatation.

1.5 Origin of the proposed work

The liquid-liquid extraction process is used by the petroleum industries from the very beginning. Extraction is one of the essential processes which has been adopted in the nuclear industry, petrochemical industry, hydrometallurgy, and environmental protection (Law and Todd, 2008). Liquid-liquid extraction is one of the most important separation processes used by the chemical industries. Different types of extraction columns that are commonly used are packed column, rotating disc contactor, Kuhni column, Oldshue-Rushton contactor, Scheibel extractor, reciprocating plate column spray column, and pulsed sieve plate column. These are called the non-agitated extraction column. In order to increase the efficiency of non-agitated extraction columns, the contact time of the two liquid phases should be increased. The contact time is increased by the sieve plates, disc, and doughnuts in the extraction column. The introduction of inert gas (air, nitrogen) as a blending agent into the two-phase liquid-liquid (L-L) system can increase the efficiency of a non-agitated column. This gas introduction method increases turbulence in the three-phase gas-liquid-liquid (G-L-L) system, resulting in better dispersion of the immiscible liquids in the form of droplets. Therefore, a higher holdup of the dispersed phase provides a larger mass transfer area. Nowadays, various techniques are adopted for the process intensification of extraction based on the surface modification and the retention time of the phases. The term process intensification (PI) refers to technologies that replace bulky, costlier

and high-energy using equipment with smaller and cheaper equipment, based on the fluid-fluid interactions. Along with the miniaturization of the processes, it reduces investment costs, improved control, and energy efficiency as well as the quality of the products. It also includes the improvement in the process chemistry/steps, multifunctional reactors, the use of intensified processing methods such as the use of ultrasound and microwaves. Liquid-liquid extraction is generally a method of separating one component selectively from their mixture, where the solute transport from one phase to another depending on their relative solubilities. The aqueous phase contains the components to be separated, and the organic phase (used as the solvent) has a high affinity towards specific components present in the solution. The solute transfer from aqueous to solvent phase is called extraction and the solute transfer from organic to the aqueous phase is called stripping or back extraction. The immiscible liquids are then immediately separated after the mixing, based on the density difference of the two liquids. Modeling of the extraction columns is not as well known as that of the distillation column and still needs improvement. The design and control of the extraction column, however, is not yet complete and is still focused on laboratory test installations and relies on time-consuming and costly scaling methods (Drumm et al., 2010). The scale and design of an extraction column are mainly based on previous knowledge of hydrodynamics and flow models such as the dispersion or back-mixing model to describe the non-ideal flow, where a parameter explains all deviations from the ideal plug flow behavior (Thornton, 1992). These models are too simplified by assumptions that limit their application to minimal cases of the working range of the process and are unable to describe the actual hydrodynamic behavior, whereby one of the liquid phases is usually dispersed as droplets in the second continuous phase (Bart and Stevens, 2004). In principle, either of the phases can be dispersed into the other phases, if the volumetric flow rate of the two phases is relatively close to

each other. Very often, the dispersed phase is distributed at a higher volumetric flow rate because this results in a higher mass transfer area. An exception is spray and packed columns, where the smaller volumetric flow stream is dispersed in order to minimize axial dispersion. If the volumetric flow ratio is very high, it is difficult to disperse the higher flow rate phase. If the mass transfer resistance is significant on one side of the interface, it could be compensated by dispersing the phase with higher resistance. In columns with packing, if the dispersed phase of high viscosity would wet the packing, the droplets would coalesce, which reduces the mass transfer area. Generally, mass transfer from droplets to continuous phase enhances droplet coalescence, which reduces mass transfer area and reduces separation efficiency (Law and Todd, 2008)

1.6 Scope of the research work

Based on the literature, there is a scope of process intensification of extraction based on the enhancement of interfacial area and contact time of the phases. The jet-driven downflow gas-liquid-liquid extraction column can be used to enhance the interfacial area of the phases by producing fine droplets through which the mass transfer occurs (based on which extraction is done). Also, the downflow column can be used to increase the retention time of the phases by flowing it downward against its buoyancy. The details of the setup with its description are given in chapter 2.

1.7 Research Formulation

For the development of jet-driven downflow column for efficient gas-liquid-liquid dispersion and application for extraction, the present research has been undertaken for a systematic study based on the following objectives

1.7.1 Entrainment Characteristics

One of the important aspects of a jet-driven column is the gas entrainment by a plunging liquid jet. Liquid entrainment is the carryover of droplets of liquid by gas or bubbles. This phenomenon has been extensively observed in numbers of related process equipment where the phase separation takes place due to gravity such as industrial boiler, evaporators, and distillation columns and in a nuclear reactor (Bagul et al., 2013). It commonly occurs where liquid and gas are in contact. Liquid entrainment depends on various factors such as the size of the nozzle, velocity of liquid and droplets, nature of force on the drops, fluid properties viz., surface tension, viscosity, etc. The details of the study are described in chapter 3.

1.7.2 Gas Holdup Characteristics

Gas holdup (i.e., the volume fraction of gas in a dispersion volume of phases), is an essential hydrodynamic parameter for the design of phase contactors. It determines the mean residence time of the dispersed phase and influences the interfacial area per unit volume and, thereby, the mass transfer rate from one phase to another through interphase. The gas holdup depends on the bubble/droplet size distribution, mobility of bubble interface, physical properties of the liquid system, liquid, and gas velocities. Very few studies have so far been reported in the literature on hydrodynamics in gas-liquid-liquid systems. The details of the study on the gas holdup in the ejector-driven downflow column are described in Chapter 4.

1.7.3 Pressure Drop Characteristics

Pressure drop is one of the important parameters to assess the energy consumption in the multiphase unit. The pattern of energy dissipation required knowledge of pressure drop for the

modeling and the basic performance of the system (Majumder, 2016). The pressure drop is an important parameter, which not only affects the gas phase residence time but also related to the interfacial area (Jawad, 2009). One of the significant effects on pressure drop is because of the frictional force caused by the resistance of the fluid, change in elevation of the fluid, and friction within the pipe and fittings. The details of the study on pressure drop characteristics is given in chapter 5.

1.7.4 Mixing Characteristics

In most of the process industries, mixing is an essential and frequent operation where the multiphase system involved. A complete model of the reactor would require velocity vectors at each point of the system for both gas and liquid phases. This information is not always available because of the complicated nature of the fluid dynamics in multiphase flow, and the model needs computational efforts. The residence time distribution (RTD) of a reactor is a characteristic of the flow pattern that occurs in the chemical process unit, being one of the most informative characteristics of the unit. The RTD gives information on how long the various elements are in the process unit. As it provides a quantitative measure of the degree of mixing within a system, knowledge of the liquid RTD is essential, allowing for accurate kinetic modeling of the system and aid in design to achieve the desired flow pattern. Also, RTD allows for a more thorough comparison between systems with different configurations or different zones of the process unit and represents a tool in a successful process scale-up. In chapter 6, detailed studies on the mixing characteristics and how the degree of mixing is related to the flow resistance based on frictional pressure drop is described. A model has also been developed to interpret the mixing behavior, based on velocity distributional model.

1.7.5 Drop Size Distribution and Interfacial Area

Liquid-liquid mass transfer is a defining characteristic in the design and optimization of chemical and biological processes where the dispersed phase is a factor that limits mass transfer. The mass transfer rate is often determined empirically from the time profile of the concentration of the phase dispersed in the system. It is essential to know the size of the bubble or drop and its distribution, and the interface area in the specific system for different operating conditions to optimize processes based on mass transfer phenomena. This work is therefore intended to investigate the size of the drop and its size distribution in the down column. The details of drop size characteristics and interfacial area are described in chapter 7.

1.7.6 Extraction Efficiency

The final objective of the present work is to assess the extraction efficiency of the jet-driven downflow column based on the aforementioned studies of hydrodynamics. Two immiscible solvents were used to study the efficiency of the extraction of propionic acid in the jet-driven downflow column. The details of the study are described in chapter 8.

1.7 Outline of the thesis

This thesis is organized as the following chapters

Chapter 1: Introduction and objective of the research

Chapter 2: Experimental setup and techniques

Chapter 3: Entrainment characteristics of gas-liquid-liquid dispersion

Chapter 4: Gas holdup characteristics of gas-liquid-liquid dispersion

Chapter 5: Frictional pressure drop characteristics of gas-liquid-liquid dispersion

Chapter 6: Mixing characteristics of gas-liquid-liquid dispersion

Chapter 7: Drop size characteristics and its distribution of gas-liquid-liquid dispersion

Chapter 8: Extraction efficiency of gas-liquid-liquid dispersion

Chapter 9: Recommendations and scope of future work

CHAPTER - 2

EXPERIMENTAL SETUP, METHODOLOGY, AND MATERIALS

In the previous chapter, the growing importance of the three-phase gas-liquid-liquid downflow column has been mentioned. The objective of the study was also defined. Based on the objective, the studies of different hydrodynamics and mass transfer characteristics were carried out in a procured experimental setup. The details of the experimental setup and procedure are described in this chapter.

2.1 Experimental setup

A schematic diagram of jet-driven downflow gas-liquid-liquid contactor is shown in Fig. 2.1. It is procured with a gas-liquid-liquid separator SP, an ejector, a phase contactor, and the other accessories like rotameters, storage tanks, centrifugal pumps, manometer, control valves, solenoid valves, straight hole nozzle, etc. as per the concept of Majumder (2016). A column of transparent perspex pipe is used for visual observation of the flow. The inner diameter and the length of the column are 0.05 m and 1.60 m, respectively. The ejector assembly consists of a suction chamber, forcing nozzle, throat, and divergent diffuser and its dimensions are: The height and diameter of the suction chamber, as shown in Figure 2.1, are 0.05 m and 0.06 m, respectively. The size and the length of the throat are 0.019 and 0.183 m, respectively. The length of the diffuser is 0.25 m. The diameter of the nozzle is 0.005 m. The initial jet length from the nozzle to the surface of the liquid-liquid level in the column is 0.74 m. It is worth to mention that the jet length is changed with the change of height of fluid mixture in the column.

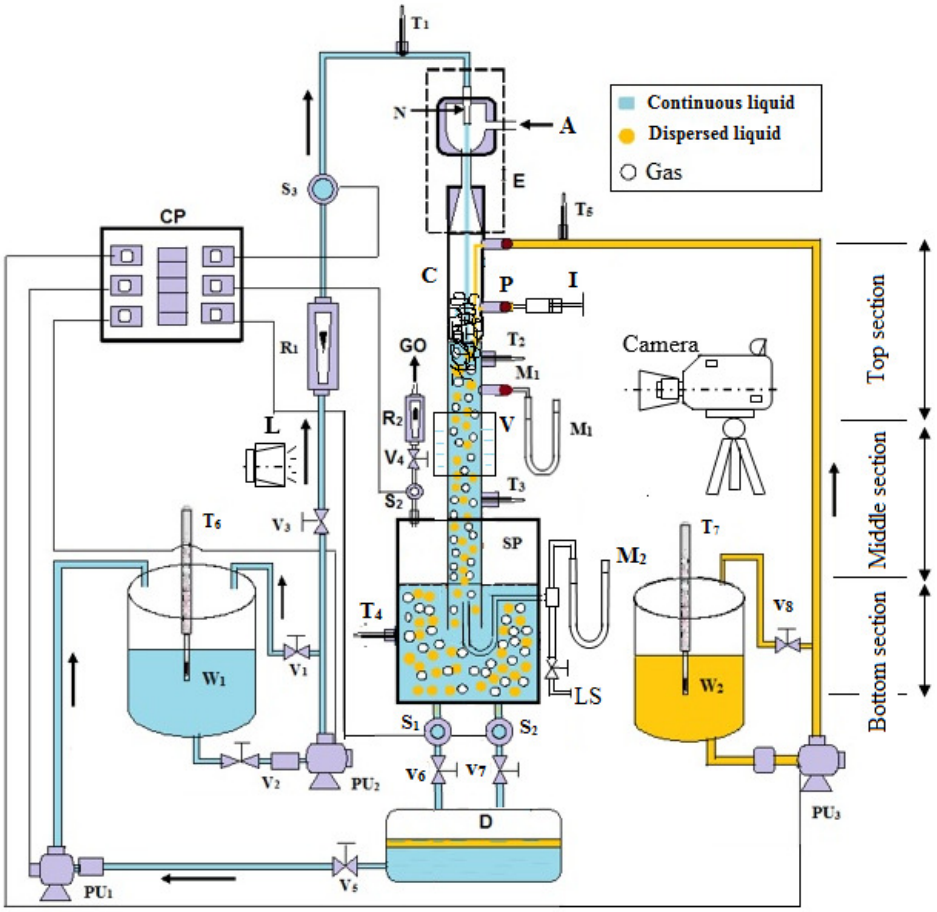

(a)

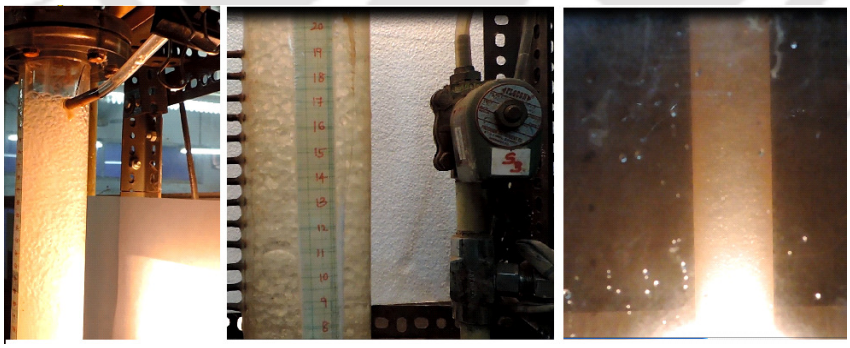

Top section Middle section Bottom section

(b)

Figure 2.1: Experimental setup: (a) schematic diagram, (b) typical snapshot of flow during experimental at high liquid jet (at u_j = 12.73 m/s and at 5% (v) paraffin liquid-water dispersion)

The different legends in Figure 2.1a are: E: Ejector assembly; N: Nozzle; M_1-M_2: Manometers; P: Port; C: Contactor; D: Decanter; PU_1- PU_3: Pumps; SP: Gas-liquid-liquid separator; S_1-S_3: Solenoid valves; V_1-V_8: Control valves; R_1-R_2: Rotameters; W_1: Primary tank; W_2: Secondary tank; A: Air inlet; GO: Gas outlet; T_1-T_7: Thermometer; CP: Control panel.

The column is extended to the separator for the uniform movement of the gas-liquid-liquid mixing and easy separation of the gas or dispersed liquid. The liquid-level inside the separator is maintained by operating the solenoid valves. The details of the sections are discussed as follows.

2.1.1 Ejector Assembly

The ejector assembly was designed based on the earlier investigations, as reported by Mukherjee et al. (1988). A sectional drawing of the ejector assembly is shown in Figure 2.2. It consists of a suction chamber, forcing nozzle, throat, and divergent diffuser.

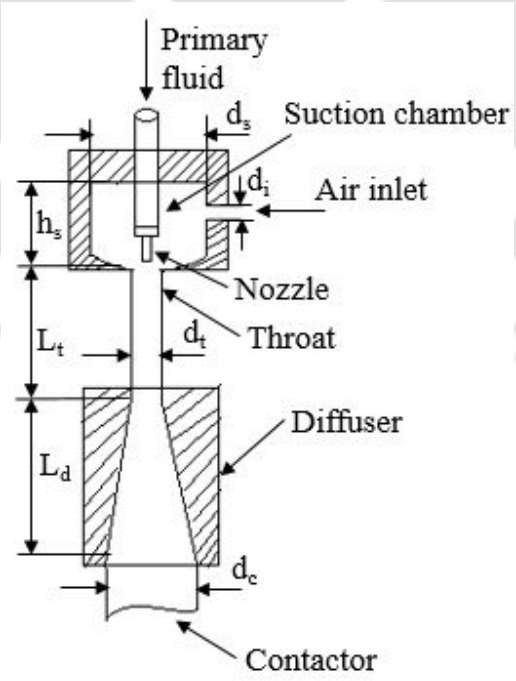

Figure 2.2: Schematic diagram of the ejector system

Earlier investigations carried out have shown that the suction chamber must be large enough to prevent shock and entry losses. It must not be too large for gas to circulate in the circulate in the chamber. So, to optimize these facts, the suction chamber selected was a cylindrical chamber of diameter 60 mm with a rounded bottom. This was provided with a secondary fluid inlet of 10.5 mm diameter, which was sufficiently significant to minimize entry losses at the inlet. The forcing nozzle was fixed in the suction chamber utilizing a spindle. A screw arrangement was provided to the spindle, which enabled the movement of the spindle axially to fix the nozzle at any position in the suction chamber.

The constant area and variable area throats are commonly used in the design of the ejectors. Previous authors (Lapple, 1951; Smith, 1951) have reported that the constant area throat produces a higher vacuum than that of the variable area throat. This is because the velocity distribution of gas (air) in a throat with a constant area is more uniform than that in the variable area throat. Hence, a constant area throat was selected in the present system. The length of the throat also plays an important role. Datta (1976) has shown that for the liquid gas discharge system, where the ejector was equipped with an extended parallel contactor, a groove length of 4 to 20 times the diameter gave essentially the same performance. In the present study, the length and diameter of the groove used were 184 mm and 19 mm, respectively. The throat inlet is well rounded to minimize the loss of secondary fluid (air) entering the throat.

A diverging diffuser was fitted after the groove to reduce the velocity of the liquid and to increase the static pressure. A sudden deviation causes unwanted effects. Previous authors (Kastner and Spooner, 1950; Smith, 1951) have reported that to optimize the performance, the divergent angle should be nearly 7° and the length of this section should be between 8 to 12 times the diameter of the throat (Davies et al., 1967a, b). In the present system, the diffuser angle

was chosen as 7.6° and length as 204 mm.

Two types of nozzles viz. convergent-divergent and straight hole nozzles are generally used in the ejector. Mitra and Roy (1963) studied that in the low-pressure range, there was an insignificant effect of the multi-hole nozzle on the performance of an ejector. In the present work, a single straight hole nozzle was used. The nozzle was accurately machined and properly shaped to avoid unnecessary shock and other losses.

2.1.2 Extended column as a contactor

One extended pipeline contactor, made of transparent perspex pipe was used in the experiments. The contactor had internal diameter 0.05 m, and length 1.45 m. The upper end of the contactor was connected to the end of the divergent diffuser by a flange, and the lower end projected 0.45 m inside the separator. This arrangement enables the uniform movement of the phases and also an easy separation of the gas from the mainstream (Majumder, 2016). Three manometer ports, M_1-M_3 were attached to the perspex column. The lower tapping was just at the bottom of the column to obtain the total pressure of the column. The other ports were attached at regular intervals to measure the pressures at different positions along with the height of the column.

2.1.3 Air-liquid-liquid Separator

It is an essential part of the apparatus, where down flowing gas-liquid-liquid mixture gets separated from each other. A rectangular mild steel vessel of 0.4 m × 0.4 m size and 0.87 m height were used as an air-liquid-liquid separator, which was sufficiently large to minimize the effects due to liquid leaving the system and air-liquid-liquid separation (Kundu et al., 1995). Three outlets, one at the top and two at the bottom, were provided for venting gas and draining liquid, respectively. The front and back of the separator were fitted with transparent Perspex

sheets to view the flow inside the separator.

2.1.4 Conductivity meter

For the study of mixing characteristics by the residence time distribution technique [Chapter 5], the variation of tracer concentration with time was measured by a digital electrical conductivity meter [Model: VSI-04 ATC Deluxe, VSI Electronics Pvt. Ltd., India].

2.1.5 Rotameter

Two rotameters were used for the flow rate measurement in the present experiment. In the present experiment rotameter, R_1 is used to maintain the volumetric flow rate of the water. The rotameter R_2 is used to measure the gas flow rate by varying the pressure in the gas-liquid-liquid separator SP. The range of rotameter R_1 (Make: Roth, India) is 100 – 1000 l/h and the range of rotameter R_2 (Make: Roth, India) is 0 – 5 l/min.

2.1.6 Pump

Three centrifugal pumps were used in the present experimental setup for fluid handling into the column. Pump (PU_1) was used for the circulation of water through the ejector into the column. The flow rate of water is adjusted with the help of bypass valve V_1 and by the control valves V_2 and V_3. The water collected into a decanter after the experimental run is recirculated into primary tank W_1 with a pump (PU_2). The dispersed liquid (Paraffin liquid or kerosene) from the secondary tank W_2 is circulated into the column with a pump (PU_3). The pumps PU_1 (370 W, 0.5 HP, 220/230 V, 1425 RPM), PU_2 and PU_3 (Mini Master II, 0.37 kW, 0.5 HP) were purchased from the Crompton Greaves, India.

2.1.7 Other accessories

A solenoid valve is an electrically operated valve, typically used for controlling the flow of liquid in the fluid flow system. Four solenoid valves ($S_1 - S_4$) were used in the present experimental setup for arresting the fluid in the column. A spring-loaded syringe (I) was used for the tracer injection into the column. Thermometers (T_1-T_7) were used for measuring the temperature of fluids in the column.

2.2 Fluid

In the present experimental study, tap water was used as the continuous fluid. Paraffin liquid and kerosene (supplied by Sigma-Aldrich, India) of different volume concentrations of range from 5 to 35% of the total volume of the column were used as the dispersed fluid. Atmospheric air was used as the gas phase. For the measurement of mixing characteristics, Sodium Chloride solution of concentration 40 kg/m^3 was used as a tracer. For the extraction characteristics, propionic acid of concentrations ranging from 0.01 to 0.05 M as a solute in the water was used.

2.3 Materials and their physical properties

In the present study, water is taken as a continuous phase. The dispersed liquids which were used for the present experiments are Paraffin liquid and Kerosene. The kerosene was dyed with blue anthraquinone of concentration (6 mg/l). The physical properties of the fluids are shown in Table 2.1. The density and viscosity of the liquid mixture were calculated by the equations given respectively by Stapelberg and Mewes (1994)

$$\rho_{dl-cl} = (1-\varepsilon_{dl})\rho_{cl} + \varepsilon_{dl}\rho_{dl} \tag{2.1}$$

$$\mu_{dl-cl} = (1-\varepsilon_{dl})\mu_{cl} + \varepsilon_{dl}\mu_{cl} \tag{2.2}$$

where the volumetric flow fraction (ε_{dl}) of the dispersed liquid is defined as

$$\varepsilon_{dl} = \frac{V_{dl}}{V_{cl} + V_{dl}} \tag{2.3}$$

where V_{dl}, V_{cl} are the volumes of dispersed liquid (*dl*) and continuous liquid (*cl*). The viscosity of liquid was measured using the Rheometer (Haake Rheostress 1, Thermo Electron Co., Germany). The surface tension of liquid was measured by Tensiometer (K9-Mk1, KRUSS GmbH Co., Germany).

To estimate the surface tension of the liquid-liquid mixture; it was assumed that the water and dispersed liquid (paraffin or kerosene), are to be in equilibrium with the immiscible phase. The liquid-bubble interface is considered as a thin phase by two dividing surfaces of different fluids (Eberhart, 1966). The bulk liquid phase is considered to have mole fractions x_w for water and x_d for dispersed liquid (paraffin or kerosene), while the bulk bubble phase has mole fractions z_w and z_d for water and dispersed liquid respectively. Overall mole fractions y_w and y_d assigning for water and dispersed liquid are obtained as per the material balance of the system. For water in the mixture, this condition is expressed as $n_w = n_L x_w + n_s y_w + n_b z_w$ where n_w is the total moles of water in the mixture and n_L, n_s, and n_b are the number of moles of water and dispersed liquid, surface, and bubble phases, respectively. The values of n_s and n_b are very smaller relative to n_L. Therefore x_w is equal to the overall mole fraction of water. The surface tension of liquid mixture $\sigma_{cl\text{-}dl}$, is then can be expressed as a linear function of moles in the surface layer (Eberhart, 1966).

$$\begin{aligned}\sigma_{cl-dl} &= y_{cl}\sigma_{cl} + y_{dl}\sigma_{dl} \\ &= \frac{(\alpha_{cl}V_{tot}\rho_{cl})/M_{cl}}{(\alpha_{cl}V_{tot}\rho_{cl})/M_{cl} + (\alpha_{dl}V_{tot}\rho_{dl})/M_{dl}}\sigma_{cl} + \frac{(\alpha_{dl}V_{tot}\rho_{dl})/M_{dl}}{(\alpha_{cl}V_{tot}\rho_{cl})/M_{cl} + (\alpha_{dl}V_{tot}\rho_{dl})/M_{dl}}\sigma_{dl}\end{aligned} \tag{2.4}$$

where σ_{cl-dl}, σ_{cl} and σ_{dl} are surface tensions of the mixture, aqueous phase, and dispersed

phase respectively. V_{tot} is the total volume of the liquid-liquid mixture, M is the molecular weight of the liquid.

Table 2.1: Physical properties of the system at 25 ± 1 ^{o}C

Liquid	**Density (kg/m^3)**	**Viscosity (kg/m.s)**	**Surface tension (N/m)**
Water	998.7	1×10^{-3}	0.071
Paraffin liquid (light)	840	5.61×10^{-3}	0.026
Water + P.A (0.01 M)	998.69	7.97×10^{-4}	0.069
Water + P.A (0.03 M)	998.67	7.98×10^{-4}	0.067
Water + P.A (0.05 M)	998.6	7.99×10^{-4}	0.065

2.4 Experimental procedure

The nozzle, the ejector assembly, and the extended pipeline column were perfectly aligned in a vertical position to attain an axially symmetric liquid jet. The nozzle was fixed at the optimum position at a distance of one throat diameter from the entry of the throat. This distance was decided from earlier investigations (Datta, 1976; Mukherjee et al., 1988) with a horizontal and vertical liquid-gas ejector system. Earlier investigators (Datta, 1976; Kundu et al., 1995; Mukherjee et al., 1988) reported that forcing air from the fluid inlet does not give any stable gas-liquid mixing system. Hence all the experiments have been carried out by entrainment of air. The experimental procedure can be explained on the basis of the sketches shown in Figures 2.3a to 2.3e.

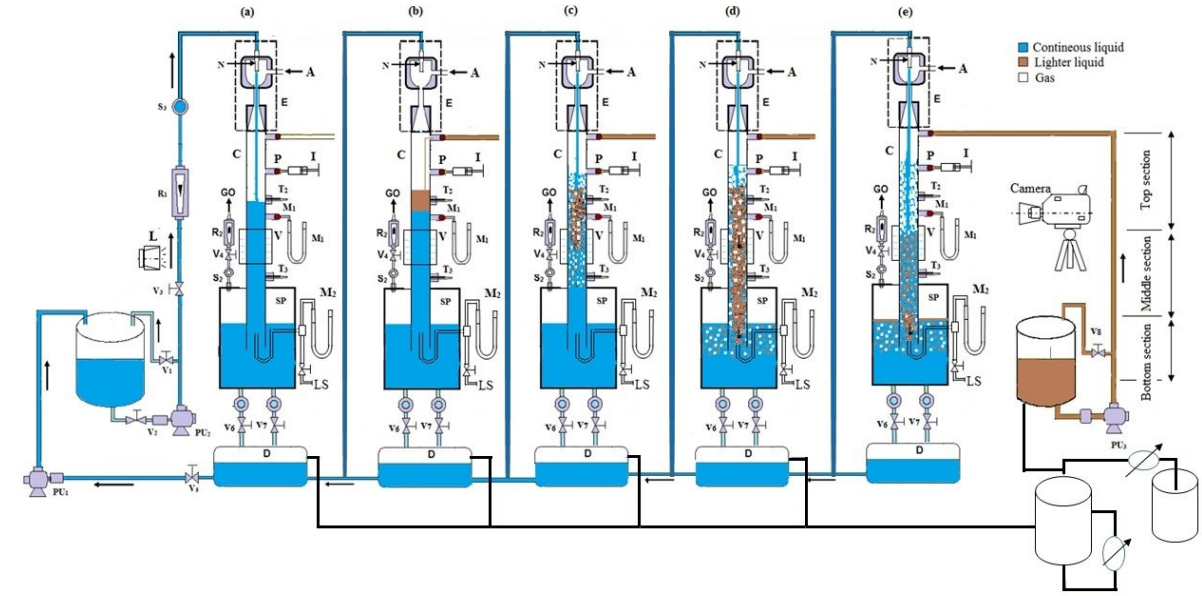

Figure 2.3: Schematic diagram of the experimental procedure

(a) To start the experiment, the liquid was pumped from the storage tank (ST) and allowed to emerge from the nozzle and flow through the center of the throat, divergent diffuser, and extended vertical column. Initially, the valves V_1, V_2, and V_3 were kept fully open, and liquid jet directly hit the bottom of the separator and went out through the valve V_6 and V_7. Then the valves V_6 and V_7 were closed, and the flowing of liquid was allowed to accumulate in the separator and column, as shown in Figure 2.3a. For each run, half of the downcomer column was filled with a continuous liquid phase, i.e., water at the beginning.

(b) The valve V_3 was then closed, and the liquid flowing in a liquid jet was allowed to accumulate in the column. The level of the continuous phase was noted as H_{cl}. Then, a certain volume % of dispersed liquid (Paraffin or Kerosene) was filled in the downcomer batch-wise, as shown in Figure 2.3b. The dispersed liquid volume was varied from 5 to 35 % in the column.

The height of the liquid-liquid mixture (H_{dl}) was noted for dispersed liquid and H_{cl} for continuous liquid.

(c) After saturation of the two liquids in the column, the valve V_3 was opened, and the liquid jet was allowed to flow into the column by adjusting the liquid flow rate to the desired value with the Rotameter R_1 as shown in Figure 2.3c. As soon as the liquid jet plunged into the accumulated liquid-liquid mixture, there was a sudden change in suction characteristics of the air due to the arresting of the liquid jet inside the column. At this liquid level, the suction of air was maximum. At this stage, an intense gas-liquid-liquid mixture is entrained throughout the column.

(d) The gas flow rate is then maintained with the Rotameter R_2 to a desired gas flow rate to allow the gas-liquid-liquid mixture to entrain into the separator, as shown in Figure 2.3d. At this stage, the intense mixing zone was completely spreaded in the extended column in the separator. The intense mixing zone is the zone where the jet penetrates the liquid, releases its energy, and disperses the gas and dispersed liquid. The gas-liquid-liquid mixture finally got separated in the separator. The liquid moved out through the valves, V_6 and V_7, while the air from the valve, V_4. The amount of air entrained is decreased by increasing the liquid height inside the separator. The extension of the column into the separator enabled smooth movement of the gas-liquid-liquid mixture and easy separation of the gas or dispersed liquid in the separator (Majumder, 2016). The liquid flowing from the separator through valves V_4 and V_5 are adjusted in order to maintain a constant liquid height in the column.

(e) The experimental data at a particular superficial gas and liquid velocity and dispersed liquid volume in the column were noted at a steady-state condition. While maintaining a constant liquid height in the column by adjusting the valves V_4 and V_5 after a certain time, the system attains a steady-state in the column, as shown in Figure 2.3e. At steady state condition, two distinct zones

were observed: at the top section of the column, an intense mixing zone of heterogeneous mixture of gas bubble, droplet and continuous liquid. The middle section and the bottom section of the column consisting of the uniform homogenous bubbly drop zone. When the liquid level entered the divergent diffuser, it was found that the ejector was suddenly filled up with the gas-liquid mixture, i.e., the ejector got flooded. As a result, the nozzle was submerged in the two-phase mixture, and its performance immediately dropped. Therefore, the plunging of the jet in the liquid was carefully operated so that the phase mixture height does not go up to the end of the divergent diffuser.

2.3.1 Measurement of gas and liquid entrainment

The jet coming from the nozzle sucks the gas and results in capturing the same by breaking the liquid surface at its plunging point (Majumder, 2016). The capturing amount of the gas depends on the energy transfer by the liquid jet. The capturing gas is then entrained by downward liquid momentum. The schematic representation of liquid jet plunging into the liquid surface is shown in Figure 2.4. The entrainment rate of a phase is defined as the rate of the volume of a dispersed phase captured in a continuous phase by the jet. For example: (i) the arresting of gas in a flowing liquid, as a dispersed phase of a bubble (ii) the holding of dispersed liquid as droplets into the other liquid which mutually immiscible. The entrained gas or liquid droplet disperses into the continuous liquid in the mixing zone (where liquid jet plunges to entrain the gas or dispersed liquid), are then carried downward by high momentum of the flow of fluid. A minimum jet velocity is required to move the bubbles/droplet downward by prevailing over their upward buoyant force.

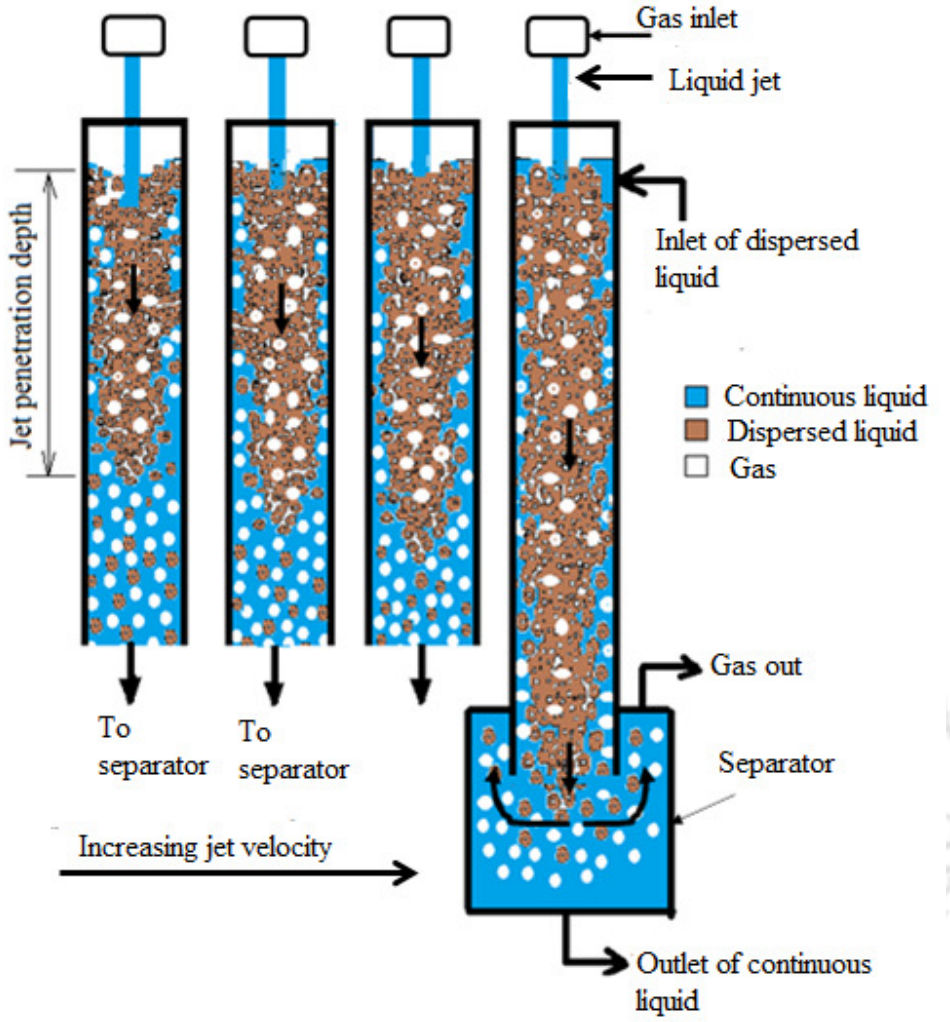

Figure 2.4: The schematic representation of liquid jet plunging into the liquid surface

The overall entrainment can be measured by measuring the amount of gas entrained (gas holdup) into the liquid in the column. The rate of gas entrainment was calculated by

$$Q_g = \frac{Q_{cl-dl}\varepsilon_g}{(1-\varepsilon_g)} \tag{2.5}$$

where Q_g is the gas entrainment, Q_{cl-dl} is the flow rate of the dispersed and continuous liquid-liquid mixture and ε_g is the overall holdup of gas in the column.

The entrainment of dispersed liquid is calculated as

$$Q_{dl} = \frac{Q_{cl-dl}\varepsilon_{dl}}{(1-\varepsilon_{dl})} \tag{2.6}$$

where ε_{dl} is the overall holdup of dispersed liquid in the column.

2.3.1 Measurement of gas holdup and dispersed liquid holdup

The overall gas holdup for the present system has been measured by the "phase isolation technique," as reported in the literature (Kundu et al., 1995). When a steady-state condition of the system was attained, the total height of the gas-liquid-liquid mixture in the column was noted. Then the four solenoid valves, SV_1, SV_2, SV_3, and SV_4 [Figure 2.1], were switched off simultaneously. This caused an immediate termination of the flow of fluids. The gas-liquid-liquid mixture arrested in the column was allowed to settle for some time till all gases are separated. The clear liquid height and the liquid-liquid mixture height inside the column were then noted. From the difference between the gas liquid-liquid mixing height and the corresponding clear liquid-liquid height the overall gas holdup was calculated by

$$\begin{aligned}\varepsilon_g &= \frac{\text{Volume of gas entrained}}{\text{Total volume of gas} - \text{liquid} - \text{liquid mixture}} \\ &= \frac{(\pi/4)d_c^2(H_{g-dl-cl} - H_{dl-cl})}{(\pi/4)d_c^2 H_{g-dl-cl}} = 1 - \frac{H_{dl-cl}}{H_{g-dl-cl}}\end{aligned} \tag{2.7}$$

The holdup of dispersed liquid was calculated by

$$\begin{aligned}\varepsilon_{dl} &= \frac{\text{Volume of dispersed liquid}}{\text{Total volume of dispersed liquid and continous liquid}} \\ &= \frac{(\pi/4)d_c^2(H_{dl-cl} - H_{cl})}{(\pi/4)d_c^2 H_{dll-cl}} = 1 - \frac{H_{dl}}{H_{dl-cl}}\end{aligned} \tag{2.8}$$

2.3.2 Measurement of pressure drop

Before starting the experiment, the column was filled with continuous liquid, and the manometer connection lines were flushed to remove all air bubbles present in the lines. The manometers were kept below the corresponding tapings so that the connecting lines between the tapping point and the manometric liquid were always filled with the working liquid. As explained in section 2.3, when the steady flow of liquid and gas was attained for a particular liquid level in the column, the manometer readings of the pressure drop were noted at different operating conditions. The pressure drops at different axial positions of the column have also been noted by changing the liquid flowrate, gas flowrate, and dispersed liquid concentration. The readings were repeated to ensure reproducibility. The total pressure drop (ΔP_{TP}) column is the sum of frictional pressure drop, hydrostatic pressure, and acceleration pressure drop, which can be written as

$$\Delta P_{TP} = \Delta P_{fTP} + \Delta P_h + \Delta P_a \tag{2.9}$$

From the total measured pressure drop, the frictional pressure drop was calculated based on the Equation (2.9) as

$$\Delta P_{ftp} = \left(\Delta P_{TP}\right)_{measured} - \Delta P_h - \Delta P_a \tag{2.10}$$

2.3.3 Residence time distribution (RTD) technique

The RTDs of the liquid phase were determined experimentally by using the classical tracer response technique. The tracer inputs were treated as a perfect impulse. When the steady-state condition was reached, the tracer, 20 ml of sodium chloride solution of concentration, 40.0 kg/m^3 in water was injected at a point 25 cm below the top of the column where the level of gas-liquid mixture crosses the level of injection. The volume of tracers used was kept small (1.0%) in relation to the total volume of the column according to (Levenspiel and Smith, 1957; Reith et al.,

1968). The injection was carried out as quickly (0.5 seconds) and smoothly as possible by a high-pressure spring-loaded syringe. The liquid phase sample collected was at every three-second interval at the column exit in the test tube. The small increment of time Δt was chosen so that the concentration of tracer (C), exiting between t and $t + \Delta t$ remained essentially constant. The concentration of the collected sample was then measured by digital electrical conductivity meter [Model 601E, M.S. Electronic India limited].

2.3.3.1 Calibration of conductivity meter

The range of this conductivity meter is about 0 - 999 micro Siemens per meter (μS/m). For the calibration of the conductivity meter, first of all, the conductivity probe was cleaned by using Millipore water, and then different samples of NaCl with tap water ranging from 5 moles/m^3 to 35 moles/m^3 were prepared. The samples were prepared in a beaker, and about 40 ml of each standard sample were prepared. After it, in each sample, the conductivity probe is inserted, and the reading of the conductivity meter is recorded. A graph of conductivity with concentration was plotted, which is shown in Figure 2.5. A correlation has been made with the data and can be represented as

$$C = 0.2379K - 0.0419,\ R^2 = 0.999 \tag{2.11}$$

2.3.4 Measurement of drop size

Drop size was measured by the photographic method. At steady-state conditions, the images were taken by illuminating the flow with uniform, diffused white light, and capturing the same with a digital Camera [Sony Cyber-shot, model: DSC-H300, 20.1 MP] placed in front of a light source. The camera was placed 200 mm away from the column with a field view of 200 mm × 200 mm. The combined high magnification and fast shutter speed used during the measurements

required high levels of lighting focused on a small area in order to obtain quality images [Hepworth et al. (2004)]. The digital photographs were processed and enhanced by using Image Processing Software [Digimizer, version: 4.2)]. The drop images were taken at the middle section of the column, where the homogenous bubbly drop zone is observed for different operating conditions. A scale was also photographed in order to calibrate the photographic measurements. Measured drop sizes may be susceptible to a distortion error due to the curvature of the column surface. In order to overcome the distortion issue, a rectangular box (20 cm × 20 cm × 20 cm) made of perspex pipe was filled with water and mounted on the perspex column surface like a window. Measurements were performed for the accuracy of the experiments by taking 4 to 7 images for each operating condition. The details have been discussed in Chapter 6.

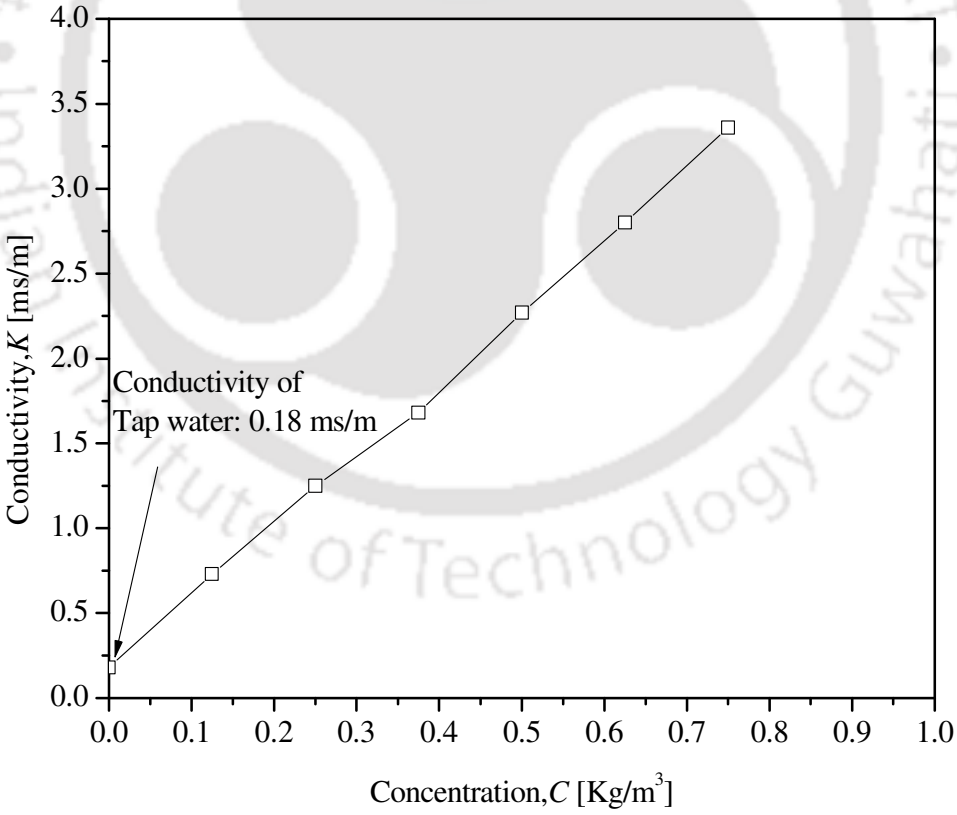

Figure 2.5: Calibration graph for conductivity meter

2.3.5 Extraction efficiency and mass transfer coefficient

For the extraction efficiency and mass transfer studies, the propionic acid is used as a solute in the water. The concentration of propionic acid in the water is varied from 0.01, 0.03, and 0.05 M according to the concentration of real effluent. Then the experimental procedure from 2.3a to 2.3e is followed. When the system attained steady-state condition, 20 ml of sample is collected from liquid sampler port and titrate with sodium hydroxide solution of concentration 0.05 N. The extent of extraction (E %) for continuous to dispersed phase was calculated by Mondal and Majumder (2018).

$$E(\%)=\frac{C_{cl,out}-C_{cl,in}}{C_{cl,in}}\times 100 \tag{2.12}$$

where $C_{cl,in,}$ and $C_{cl,out}$ are concentrations of solute in the inlet and outlet of aqueous solutions, respectively. The overall mass transfer coefficient based on the continuous phase is calculated using the following equation given by (Khawaja et al., 2017):

$$K_{cl}a=\frac{NTU_{cl}.u_{cl}}{H} \tag{2.13}$$

where $K_{cl}a$ is the mass transfer coefficient, NTU_{cl} is the number of transfer units, u_{cl} is the continuous phase velocity, H is the height of the column.

In the present study, the overall height of transfer unit and overall mass transfer coefficient are based on continuous phase and related to the number of transfer units and height of the column as (Khawaja et al., 2017):

$$HTU_{cl}=\frac{u_{cl}}{K_{cl}a}=\frac{H}{NTU_{cl}} \tag{2.14}$$

where NTU_{cl} is the overall number of transfer units based on the continuous phase, which is calculated using the experimental observations of inlet and exit molar concentrations of the

phases involved. The overall number of transfer units is defined by (Khawaja et al., 2017):

$$NTU_{cl} = \frac{1}{\left(\frac{\left(C_{cl,out} - C_{cl,in}\right)}{m.\left(C_{dl,out} - C_{dl,in}\right)}\right) - 1} \ln\left(\frac{C_{cl,in} - m \times C_{dl,out}}{C_{dl,out} - m \times C_{dl,in}}\right) \tag{2.15}$$

where, m is the equilibrium constant in the expression $y = mx$. The value of m was calculated experimentally by taking various concentrations of solute in virtually equal amounts of paraffin liquid/kerosene and water. y is the concentration of solute in the continuous phase, and x is the concentration of solute in the organic phase. The experimental value of m was obtained as 0.0605 for the propionic acid-water-paraffin liquid system and 0.2501 for the propionic acid-water-kerosene system.

CHAPTER - 3

ENTRAINMENT CHARACTERISTICS

In the previous chapter, the details of the experimental apparatus and the techniques of the experiments have been discussed. In this chapter, comprehensive studies on gas entrainment in the downflow column with an ejector system are reported. Models are developed for the gas entrainment in terms of different dimensionless groups consisting of operating variables, geometric variables, and system properties, which can be used to interpret the entrainment characteristics in gas-liquid-liquid downflow contactor.

3.1 Introduction

Multiphase flow (gas-liquid, Gas-liquid-liquid, Gas-liquid-solid) are essential in various chemical and biochemical processes. Many columns are being used for liquid-liquid operations in the presence of gas. The removal of an organic pollutant from wastewater by a liquid through the liquid-liquid interface is one of the important applications especially in the extraction process as shown in Table 3.1. In continuous large-scale operation, some of the examples for gas-liquid-liquid are carbonylation, hydroformylation in the petrochemical industry, and gas-aided extraction process. The performance of gas-aided mass transfer, especially extraction, is approximately three times higher than liquid-liquid mass transfer without gas (Assmann and von Rohr, 2011). The addition of inert gas is more economical and efficient compared to other removal methods. The efficiency of mass transfer can be increased by intense mixing among the phases by proper designing the column. The mixing can be increased by plunging one phase into another phase. In this case, movement of the dispersed phase against its buoyancy and formation of internal phase circulation vertically in the plunging zone is enhanced.

Table 3.1: Examples of gas-liquid-liquid operations for contaminant removal

Reference	Mixing device	System
Vermijs and Kramers (1954)	Rotating disc liquid-liquid column	water-acetic acid-methyl isobutyl ketone
Sohn and Doungdeethaveeratana (1998)	A liquid-liquid column with gas injection	$Cuso_4$- H_2SO_4-H_2O-LIX 860-Kerosene
Venkatanarasaiah and Varma (1998)	Pulsed liquid-liquid column	Kerosene –water
Wang et al. (2002)	Modified rotating liquid-liquid column	1-butanol-succinic acid-water
Din et al. (2009)	Pulsed liquid-liquid column	Water-Kerosene
Napeida et al. (2010)	Hanson mixer–settler	toluene–water, n-butyl acetate–water, butanol–water
Sa et al. (2010)	Liquid-liquid column	n-butyl alcohol – water
Samdavid et al. (2016)	Perforated liquid-liquid column	Kerosene - water
Present study	Jet driven gas-liquid-liquid downflow column	Paraffin-water; Kerosene-water

The introduction of inert gas (air, nitrogen, oxygen) in the column may increase the further

efficiency of the mass transfer. The inert gas acts as a mixing agent to increase the energy in the liquid-liquid (L-L) system. This increased energy causes an increase in dispersion of phases, and hence, more efficiency of the liquid-liquid mass transfer can be achieved (Dehkordi, 2002; Lü et al., 2005; Saien et al., 2006; Sohn and Doungdeethaveeratana, 1998; Tan et al., 2011).

The jet induced downflow mixing column (as shown in Figure 2.1) has many advantages over other conventional columns since it has the capability of phase dispersing into the column with a continuous phase without any external power requirement. It made attention to the scientific community for process intensification for achieving higher mass transfer and multiphase reaction. With the increasing energy costs and emission of harmful gases, the conventional extraction columns are under a challenge for the new technologies in order to reduce energy consumption and to meet requirements for emissions and safety. These shortcomings have led to the consideration in our research to look for a system of downflow gas-liquid-liquid ejector induced mixing column, in which the back-mixing is reduced for continuous phase, and there is no need for external energy requirement for the gas introduction (Babu et al., 1999; Majumder, 2008; Sivaiah and Majumder, 2013b). Since the efficiency of gas-liquid-liquid mass transfer is higher compared to liquid-liquid mass transfer without gas, in the present work, the gas-liquid-liquid ejector-induced downflow mixing column is designed. The phase entrainment and its dispersion is one of the critical design parameters to characterize the hydrodynamics of gas-liquid-liquid flow in the column. The entrainment rate influences the mass transfer between phases as it determines the interfacial area for their transport and mixing of the fluid in the column. Gas entrainment is a very complicated process and controlled mainly by the jet velocity. Lin and Donnelly (1966) studied the mechanism of air entrainment by the vertical plunging liquid jet. They reported that entrainment for turbulent jets result from free surface disturbances

caused by jet instability, while entrainment by laminar jets results from the formation of a thin shell of gas at the point of entry. Kumagai and Endoh (1982) studied that the rate of entrainment was independent of the surface tension that contrasted with all previous observations. Ohkawa et al. (1985) discussed the entrainment characteristics of the gas between two vertical liquid jet systems with and without a downcomer. They observed that with increasing the nozzle diameter, the gas entrainment increases, and with the increasing height of the downcomer, gas entrainment decreases. Evans et al. (1996) developed a gas entrainment model for a confined plunging liquid jet, taking into account the re-entrainment of the recirculated gas. Their model was based on the effective jet diameter as a function of free jet length. Miwa et al. (2018) studied experimental investigation of the air entrainment by the vertical plunging liquid jet. It was found that the gas entrainment rate depends on the product of Weber number and Laplace length scale, and entrainment ratio, defined as the entrained air flow rate divided by impinging jet flow rate. In this chapter, the liquid entrainment characteristics and its dispersion phenomena in the gas-liquid-liquid jet-driven downflow mixing column are explained based on the experiment study.

3.2 Experimental setup and procedure

The representative diagram of the jet-driven downflow gas-liquid-liquid mixing column is shown in Figure 2.1 in chapter 2. It is procured with a gas-liquid-liquid separator SE, an ejector, a phase downcomer, and the other accessories like rotameters, storage tanks, centrifugal pumps, manometer, control valves, solenoid valves, straight hole nozzle, etc. The details of the experimental setup and techniques are discussed in chapter 2. The ejector, as shown in Figure 2.1, consists of a suction chamber, a throat, a divergent diffuser, and forcing nozzle. Through the suction chamber, the jet coming from the nozzle, which sucks the gas and results in capturing the

same by breaking the liquid surface at its plunging point. The capturing amount of the gas depends on the energy transfer by the liquid jet. The capturing gas is then entrained by downward liquid momentum.

The entrainment rate of a phase is defined as the rate of the volume of a dispersed phase captured in a continuous phase by the jet. During the entrainment, the following characteristics are observed: (i) the arresting of gas in a flowing liquid, as a dispersed phase of bubbles (ii) the dispersion of dispersed liquid as droplets into the gas-liquid-liquid which are immiscible to each other. The entrainment of phase and their flows downward in a vertical downcomer is happened against the buoyancy force that developed based on the particular size of bubble or droplet of dispersed phases. This is because of the gas bubbles or liquid droplets in the continuous phase (other than dispersed liquid) have a natural tendency to rise due to its buoyancy force. Therefore, to get the downward flow of gas bubbles or liquid droplets, the carrier liquid (continuous phase) velocity must be higher than the bubble rise or droplet rise velocity.

The overall entrainment can be measured by measuring the amount of gas entrained (gas holdup) into the liquid in the column. The rate of gas entrainment was calculated from the material balance in the mixing column as

Gas entrainment rate = Gas holding rate in the mixing column, which implies

$$Q_g = \left(Q_{cl-dl} + Q_g\right)\varepsilon_g \tag{3.1}$$

or,

$$Q_g = \frac{Q_{cl-dl}\varepsilon_g}{1-\varepsilon_g} \tag{3.2}$$

where Q_g is the gas entrainment rate, Q_{cl-dl} is the flow rate of the dispersed and continuous liquid-liquid mixture and, ε_g is the overall holdup of gas in the column. The subscripts *g*, *cl*, *dl*

refer the gas, continuous liquid, and dispersed liquid, respectively.

The entrainment of dispersed liquid is calculated as

$$Q_{ll} = \frac{Q_{cl-dl}\varepsilon_{dl}}{(1-\varepsilon_g)} \tag{3.3}$$

where ε_{dl} is the overall holdup of dispersed liquid in the column. The phase isolation method is followed to estimate the overall gas holdup. At the beginning of each run, the downcomer was filled with continuous phase (dispersed liquid - water) up to half of the downcomer. After filling, the level of the continuous phase (H_{cl}) was recorded. Then, the dispersed liquid (liquid paraffin, kerosene) was introduced to the downcomer in a batch-wise with a certain volume %. At this moment, the height of the liquid-liquid mixture was noted as H_{dl} for dispersed liquid and H_{cl} for continuous liquid, which was introduced as a liquid jet through the nozzle in the column. The liquid jet induced the gas, which is entrained through the liquid surface in the downcomer at a certain minimum liquid jet velocity.

During the operation, the height of the interface ($H_{g\text{-}dl\text{-}cl}$) of the gas-liquid-liquid mixture was noted at a certain operating condition. After reaching the steady-state condition, the flow of liquids was suddenly stopped by a solenoid valve and allowed to settle down. During the settlement of liquid, the gas is disengaged or isolated from the mixture. After a certain time, when the gas was isolated or disengaged completely from the gas-liquid-liquid mixture, the final height of the liquid-liquid mixture is noted, which is denoted by $H_{cl\text{-}dl}$. The overall gas holdup is then estimated by

$$\varepsilon_g = \frac{\text{Volume of gas entrained}}{\text{Total volume of gas - liquid - liquid mixture}} = \frac{(\pi/4)d_c^2(H_{g-\text{cl-dl}} - H_{\text{cl-dl}})}{(\pi/4)d_c^2 H_{g-\text{cl-dl}}} = 1 - \frac{H_{\text{cl-dl}}}{H_{g-\text{cl-dl}}} \tag{3.4}$$

The holdup of dispersed liquid based on the total volume of the gas-liquid-liquid mixture was calculated by

$$\varepsilon_{dl} = \frac{\text{Volume of dispersed liquid}}{\text{Total volume of gas - liquid - liquid mixture}} = \frac{(\pi/4)d_c^2 H_{\text{dl}}}{(\pi/4)d_c^2 H_{\text{g-cl-dl}}} = \frac{H_{dl}}{H_{\text{g-cl-dl}}} = \frac{Q_{dl}}{Q_{\text{g-cl-dl}}} = \frac{Q_{cl-dl}\alpha_{dl}}{Q_{\text{g-cl-dl}}} = (1-\varepsilon_g)\alpha_{dl} \quad (3.5)$$

where,

$$\alpha_{dl} = \frac{Q_{dl}}{Q_{cl-dl}} \quad (3.6)$$

3.3 Results and discussion

3.3.1 Entrainment mechanism

The entrainment of gas and dispersed liquid occurs by plunging the liquid jet into the mixing column. The liquid jet plunges vertically in a pool, which entrains gas by sucking it from the source (here air from the atmosphere) at a certain minimum value of liquid jet velocity. A typical photographic representation of gas entrainment by liquid jet is shown in Figure 3.1. When the liquid (here water) jet impinges the surface of the liquid level in the downcomer as shown in Figure 3.1 (a) at a velocity of u_j = 1.41 m/s, the entrainment of gas into the liquid phase in the downcomer was not observed. At this velocity, there was not sufficient energy transfer by the liquid jet to break the surface of the liquid. A slight increase in liquid jet velocity of u_j = 2.12 m/s causes a little entrainment of gas in the liquid pool by breaking the surface of the liquid, as shown in Figure 3.1.(b), which may be represented as minimum liquid jet velocity for entrainment. With further increasing jet velocity of u_j = 2.83 m/s, the jet penetration depth increases (Figure 3.1 (c)). When the liquid jet velocity in the mixing column was fixed at 3.18

m/s, it was seen that a uniform dispersion of gas and liquid was observed with more depth of jet penetration, which is shown in Figure 3.1 (d). The high liquid jet velocity results in the bubble and droplet dispersion through the whole mixing column and bubble and droplets of less buoyancy flow downward by the downward high liquid momentum.

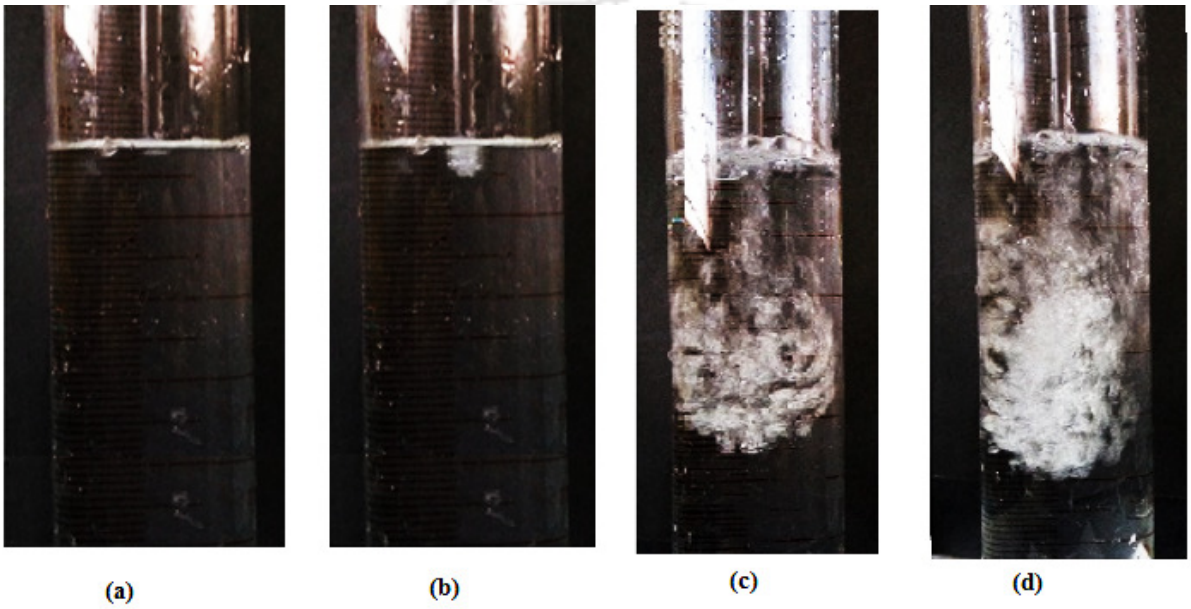

Figure 3.1: Gas and dispersed liquid entrainment in water at low liquid jet velocity (a) u_j = 1.41 m/s, (b) u_j = 2.12 m/s, (c) u_j = 2.83 m/s, (d) u_j = 3.18 m/s

The gas entrainment by liquid jet in Paraffin liquid-water and Kerosene-water systems are shown in Figure 3.2 and Figure 3.3, respectively. The different subsequent phases of the entrainment by the liquid jet, as shown in Figure 3.2 and Figure 3.3 (a) to (e) are shown at the low velocity of liquid jet above relative to the minimum jet velocity for entrainment.

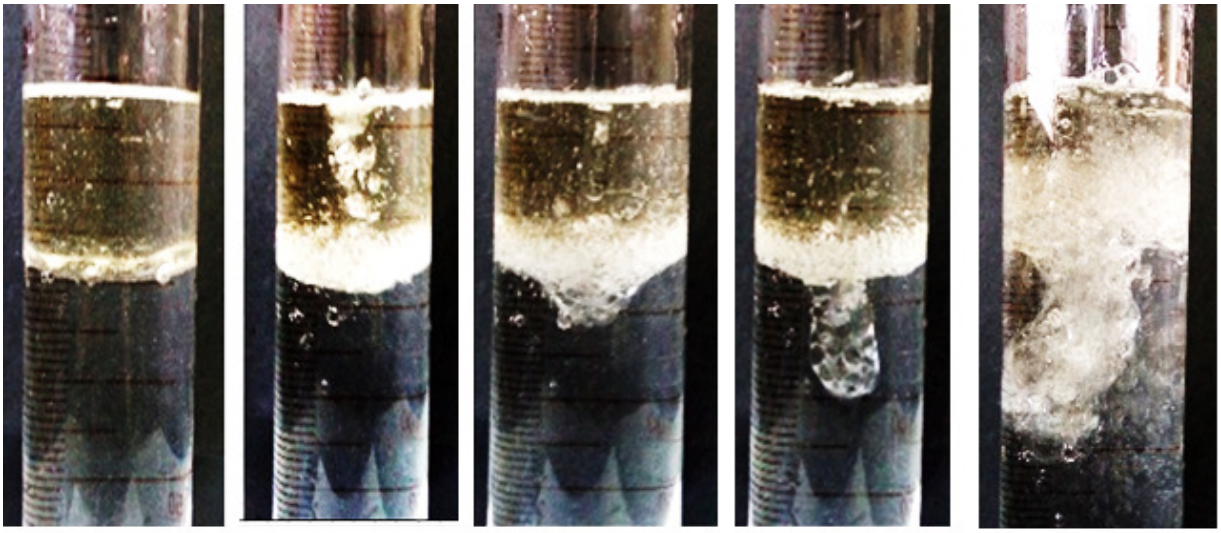

Figure 3.2: Mechanism of gas entrainment in paraffin liquid – water at low liquid jet velocities (a) $u_j = 0$, (b) $u_j = 1.41$ m/s, (c) $u_j = 2.12$ m/s, (d) $u_j = 2.83$ m/s, (e) $u_j = 3.18$ m/s

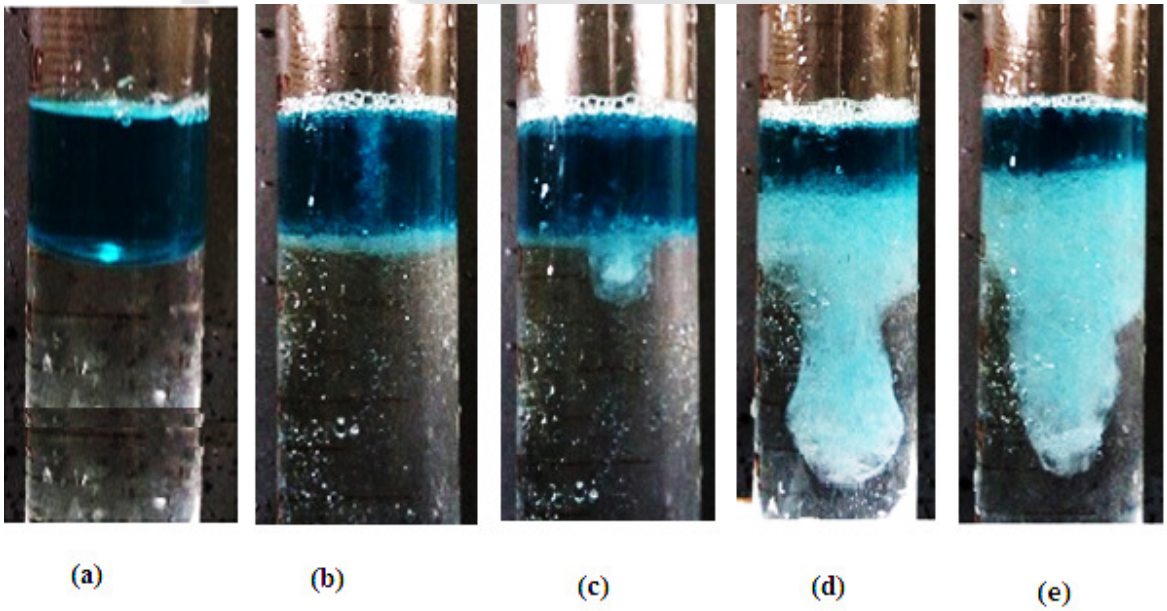

Figure 3.3: Mechanism of gas entrainment in kerosene-water at low liquid jet velocities (a) $u_j = 0$, (b) $u_j = 1.41$ m/s (c) $u_j = 2.12$ m/s, (d) $u_j = 3.18$ m/s, (e) $u_j = 3.53$ m/s

At higher jet velocity, the jet penetrates the liquid, and the lower part of the liquid oscillates,

which consequently breaks up into bubbles and droplets. Since the kerosene is less viscous than the paraffin liquid, the gas entrainment is higher in the kerosene-water system, as shown in Figure 3.2 (c) and Figure 3.3 (c).

It is to be noted that the dye concentration, which is mixed with kerosene, does not affect the gas dispersion as a bubble. At very high water jet velocity, it was seen that entrainment and dispersion of both gas and dispersed liquids in the water were increased. Even after high liquid jet velocity beyond 3.53 m/s, it was seen the significant dispersion of both the gas and dispersed liquid in the whole downcomer and separated in the phase separator, as shown in Figure 2.1(b) typically for the air-paraffin-water system.

3.3.2 Effect of gas and water jet velocities on gas entrainment

The effects of the gas and water jet velocities on gas entrainment for paraffin and kerosene at a volume fraction of 5% are shown in Figure 3.4 (a) and Figure 3.4 (b). It was observed that with increasing the water jet velocity and gas velocity, the gas entrainment increases. The momentum of the jet increases with increasing liquid flow rate, which results in higher gas entrainment into the liquid. It was observed that an increase in the gas or liquid velocity leads to increase in the mixing of phases due to an increase in the intensity of the momentum transfer. Enhancement in the momentum transfer results in increase of bubble formation which improves the gas entrainment. u_{sg} is the superficial gas velocity, which is defined as the volumetric gas flow rate divided by the cross sectional area. The gas entrainment was seen higher for paraffin liquid-water (Figure 3.4 (a)) than that for kerosene-water (Figure 3.4 (b)).

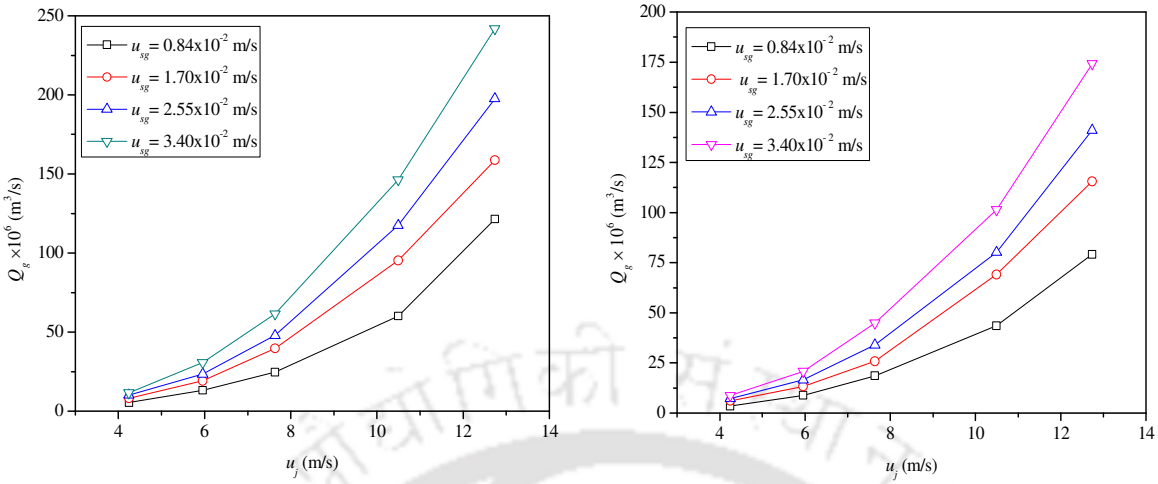

Figure 3.4: Effects of gas and higher liquid jet velocity on gas entrainment (a) for 5% (v) paraffin liquid, (b) for 5% (v) kerosene

The viscosity of kerosene is less than the paraffin liquid. The kerosene disperses quickly into the continuous liquid, which makes the gas entrainment less in kerosene than the paraffin liquid. Figure 3.5 (a) and Figure 3.5 (b) represent the effect of gas and liquid jet velocities on gas entrainment for 25% volume fraction of paraffin liquid-water and kerosene-water.

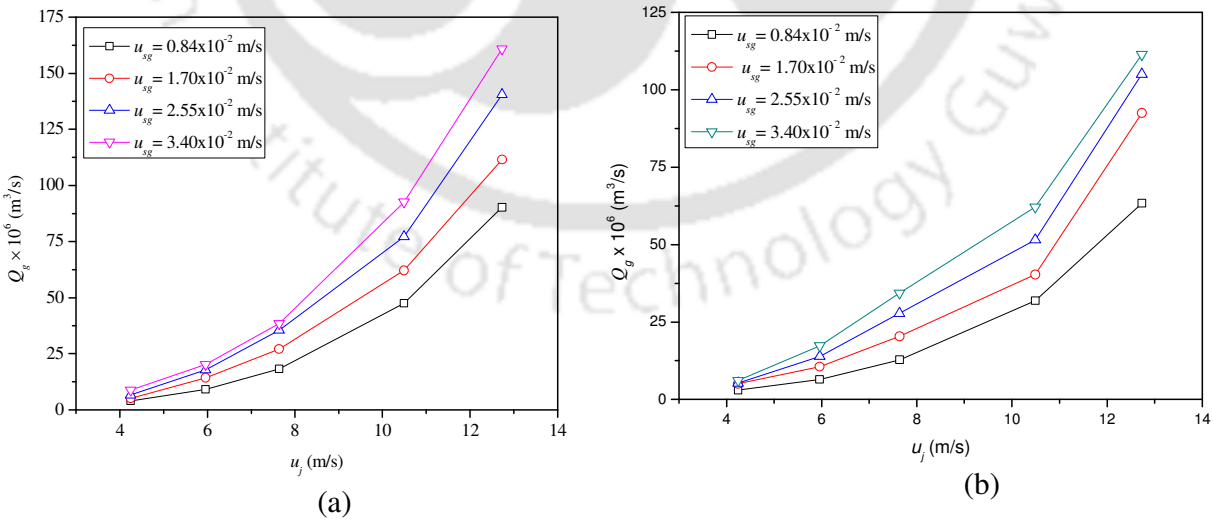

Figure 3.5: Effects of gas and higher liquid jet velocity on gas entrainment (a) for 25% (v) paraffin liquid, (b) for 25% (v) kerosene

3.3.3 Effect of volume fractions of dispersed liquid on gas entrainment

The effect of gas entrainment with different dispersed liquid volume concentrations at a constant gas flow rate is shown in Figure 3.6. It is observed that the entrainment of the gas is lesser at the higher volume of paraffin liquid (35%) compared to that at the lower volume fraction of paraffin liquid (5%), as shown in Figure 3.6 (a). With an increase in the volume of dispersed liquid, the effective viscosity of dispersed liquid and continuous liquid mixture increases, which increases the resistance of the liquid jet flow into the liquid-liquid mixture, thus the gas entrainment decreases with increasing dispersed liquid volume. A similar trend is observed for kerosene-water, as shown in Figure 3.6 (b).

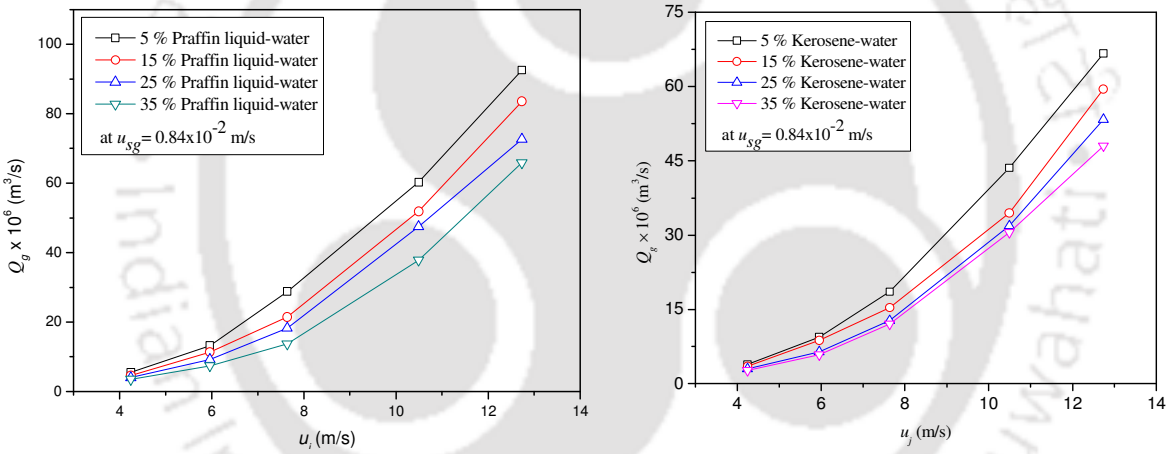

Figure 3.6: Variation of gas entrainment with a liquid jet velocity at different volume concentrations of (a) paraffin liquid, (b) kerosene

3.3.4 Depth of penetration of plunging liquid jets

Liquid or gas entrained by a vertical plunging jet penetrates to some maximum depth in the liquid pool in the column. The maximum depth cannot be identified properly due to the continuous fluctuation of the lower limit of the bubble-droplet swarm. In this regard, a time average of the same can be taken. Several authors measured the maximum depth of jet

penetration in the plunging jet system (Bonsignore et al., 1985; Kusabiraki et al., 1990; Ohkawa, 1986; Ohkawa et al., 1987). The penetration depths of the plunging liquid jet at different jet velocities are shown typically in Figure 3.7.

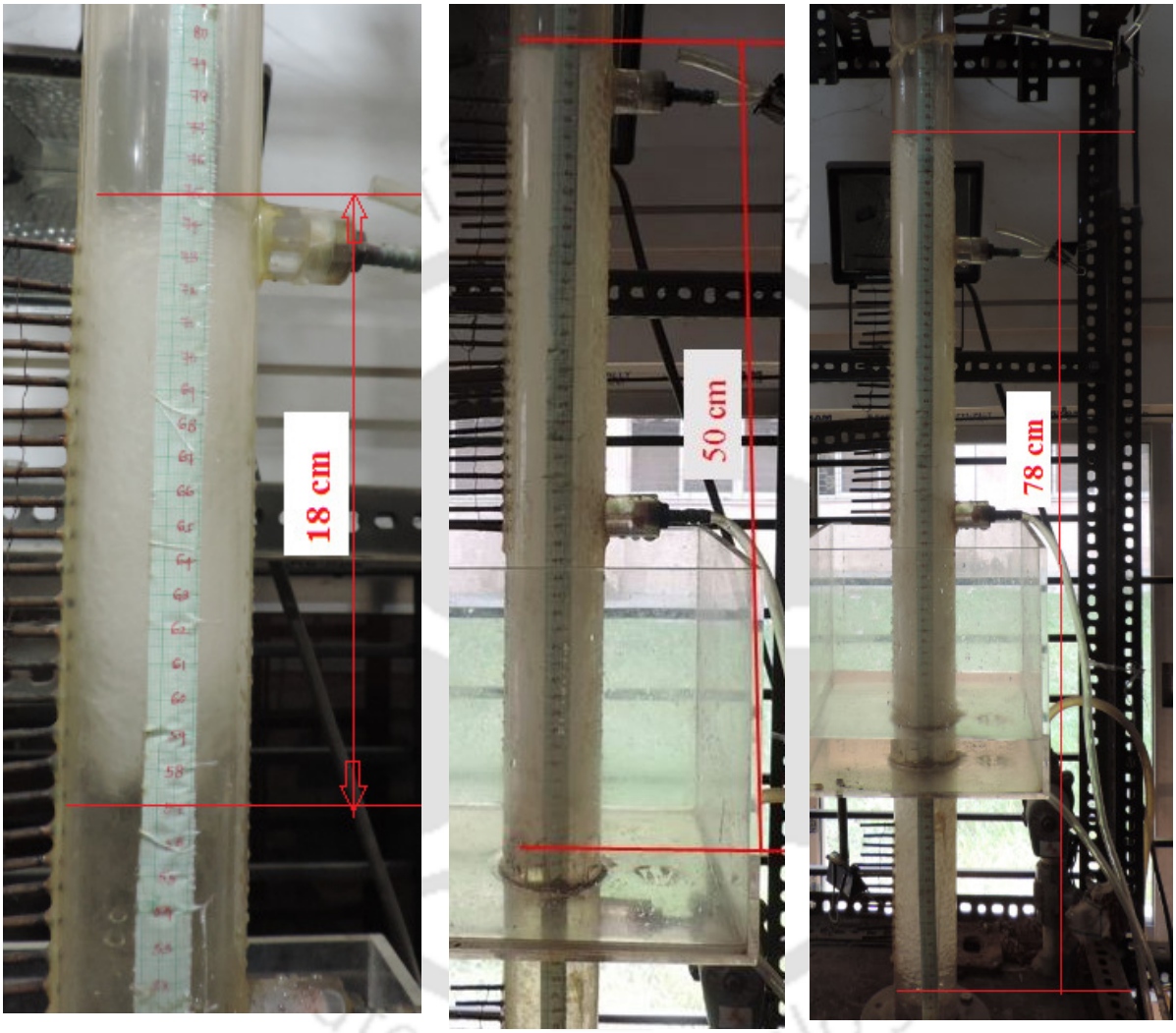

(a) at u_j = 4.24 m/s; u_{sg} = 0.0084 m/s; H_p = 0.18 m

(b) at u_j = 7.63 m/s; u_{sg} = 0.0084 m/s; H_p = 0.50 m

(c) at u_j = 10.49 m/s; u_{sg} = 0.008 m/s; H_p = 0.78 m

Figure 3.7: The penetration depth at different jet velocities at 5% (v) paraffin liquid

According to the Suciu and Smigelschi (1976) theory, based on the assumption that, at the maximum depth of penetration, the local liquid velocity in the submerged jet at that point should

be equal to the bubble/droplet rise velocity. That resulted in a direct linear relationship between the maximum bubble penetration depth and the jet diameter and jet velocity product. However, the analysis is convoluted by the buoyancy force resulting from the entrained phase. Cumming (1975) predicted theoretically that the maximum penetration depth should be related to the square of the jet velocity and the entrainment ratio, whereas many investigators (Bonsignore et al., 1985; McKeogh and Ervine, 1981; Van de Donk, 1981; Van de Sande and Smith, 1975) suggested purely empirical correlations for such complicated system. Those correlations are applicable for both small and large diameter jets. Ohkawa et al. (1987) stated that the depth of penetration is dependent on the nozzle geometry and the ratio of jet length to nozzle diameter. Both these effects are insignificant if the ratio of jet length to nozzle diameter is higher than 20. The effect of the jet length on penetration depth is significant only for short jet lengths. Ohkawa et al. (1986) and Ohkawa et al. (1987) correlated their data on penetration depth, with a rather complicated relationship that involves the jet Froude number and the jet length to nozzle diameter ratio. Based on the analysis of present experimental data, the penetration depth is correlated with the operating variables in terms of jet length to nozzle diameter ratio and the jet Froude number, etc. as follows:

$$H_{pR} = 2.13\times10^{-4}\,\mathrm{Re}_j^{\,0.336} Fr_j^{\,0.643} L_{jR}^{\,0.993} \tag{3.7}$$

where

$$H_{pR} = \frac{H_p}{d_n};\ \mathrm{Re}_j = \frac{d_n u_j \rho_{cl-dl}}{\mu_m};\ Fr_j = \frac{u_j}{\sqrt{g d_n}};\ L_{jR} = \frac{L_j}{d_n}$$

The correlation was developed by multiple linear regression analysis based on experimental data. The correlation coefficient and the standard error for the above correlation (Equation 3.7) are found to be 0.998 and 0.025, respectively.

3.3.5 Minimum entrainment velocity

The minimum entrainment velocity depends on the turbulent intensity of the jet (McKeogh and Ervine, 1981). The gas or liquid entrainment occurs beyond a critical value of liquid jet velocity. In the present experimental system, there is almost complete recirculation of the entrained phase at a higher jet velocity (Majumder, 2016). Thus, a minimum liquid jet velocity is required to move the phase downward. As per the present experimental data, a correlation is developed to predict the minimum entrainment velocity of phase which can be expressed as

$$\frac{u_{e,\min}}{\Gamma^{2/3}} = p + q\sqrt{M} \tag{3.8}$$

where

$$\Gamma = \frac{\sigma_{cl-dl}}{\left(\rho_{cl-dl}\mu_{cl-dl}d_n\right)^{0.5}} \tag{3.9}$$

$$M = \frac{\rho_g \mu_g L_j}{\rho_{cl-dl}\mu_{cl-dl}d_n} \tag{3.10}$$

The density and viscosity of liquid-liquid used in the present system were calculated by the equations given by Hermstapelberg and Mewes (Stapelberg and Mewes, 1994) respectively as follows:

$$\rho_{cl\text{–}ll} = (1-\varepsilon_{dl})\rho_{cl} + \varepsilon_{dl}\rho_{dl} \tag{3.11}$$

$$\mu_{cl\text{–}ll} = (1-\varepsilon_{dl})\mu_{cl} + \varepsilon_{dl}\mu_{dl} \tag{3.12}$$

where the volumetric flow fraction (ε_{dl}) of dispersed liquid is defined as

$$\varepsilon_{dl} = \frac{V_{dl}}{V_{cl} + V_{ll}} \tag{3.13}$$

The surface tension of liquid-liquid mixture $\sigma_{cl\text{-}dl}$, is then assumed to be a linear function of the

surface layer mole fraction, which is expressed as (Eberhart, 1966).

$$\sigma_{cl-dl} = y_{cl}\sigma_{cl} + y_{dl}\sigma_{dl}$$
$$= \frac{(\alpha_{cl}V_{tot}\rho_{cl})/M_{cl}}{(\varepsilon_{cl}V_{tot}\rho_{cl})/M_{cl} + (\varepsilon_{dl}V_{tot}\rho_{dl})/M_{dl}}\sigma_{cl} + \frac{(\alpha_{dl}V_{tot}\rho_{dl})/M_{dl}}{(\varepsilon_{cl}V_{tot}\rho_{cl})/M_{cl} + (\alpha_{dl}V_{tot}\rho_{dl})/M_{dl}}\sigma_{dl} \quad (3.14)$$

where σ_{cl-dl} , σ_{cl} and σ_{dl} are surface tensions of the mixture, aqueous phase, and organic phase respectively. V_{tot} is the total volume of the liquid-liquid mixture, M is the molecular weight of the liquid.

The unknown parameters p and q as defined in equation (3.8) can be obtained from the experiment. In the present experimental system for the whole experimental set of data the parameters p and q are found to be 4.85 and 1.48 respectively.

3.3.6 Minimum energy required for phase entrainment

Bińk (1988) reported that minimum kinetic energy is required to move the gas bubbles downward. Based on fluid properties and the diameter of the nozzle, a correlation is proposed for the minimum energy required for gas entrainment in the mixing column which can be expressed as

$$\frac{\dot{E}_{\min}\rho_{cl-dl}}{\mu_{cl-dl}^2 d_n} = 3.05\times10^2\left(\frac{d_n\sigma_{cl-dl}\rho_{cl-dl}}{\mu_{dl}\mu_{cl-dl}}\right)^{2.19} \quad (3.15)$$

The correlation coefficient and the overall standard error of the Equation (3.15) are found to be 0.981 and 0.041, respectively. In the present experimental study the range of E_{min} for the paraffin liquid-water is 11.15-10.66 W, and for the kerosene-water system is 6.62-6.27 W.

3.3.7 Efficiency of gas-liquid-liquid dispersion column

The entrainment efficiency of the gas-liquid-liquid dispersion in the column is evaluated by the equation given by Bin and Smith (Bin and Smith, 1982) as

$$\dot{E}_s = \frac{\pi \rho_{dl} d_n^2 u_j^3}{8} \tag{3.16}$$

The energy used for the mixing of three-phase gas-liquid-liquid system is then expressed by

$$\dot{E}_{um} = \eta_m \dot{E}_s \tag{3.17}$$

For the present experimental system, the energy efficiency for the dispersion of the three phases is 44-361 KW s/m^3 within the range of present operating conditions. The efficiency of the present system for gas entrainment is compared with other systems as given in Table 3.2.

Table 3.2: Efficiency of the present system for gas entrainment compared with other systems

Authors	Type of contactor	E_s/Q_g (kWs/m^3)
Fukuda et al. (1968)	Aerated-stirred fermenter	80 – 140
Topiwala and Hamer (1974)	Hollow impeller	300 – 700
Zundelevich (1979)	Turbo aerator	60 – 800
Matsumura et al. (1982)	Tank-type gas entrainer	100 – 1000
Ohkawa et al. (1986)	Water jet aeration in pool system	15 – 300
Sivaiah et al. (2012)	Ejector induced downflow (gas-slurry system)	101 – 210
Present work	Ejector induced downflow (gas-liquid-liquid)	41 – 246

3.3.8 Prediction of dispersed liquid entrainment rate by developing a general correlation

The cumulative entrainment rate of the dispersed liquid (here paraffin) at the end of the downer

can be predicted by the following model

$$f_{v,cum} = \alpha \exp[-\exp(-\beta(t-\gamma))] \tag{3.18}$$

where α, β and γ are parameters which can be obtained by fitting this model with the experimental value. As per the present experimental data, the parameters can be expressed as

$$\alpha = 0.1362\exp(2.211\varepsilon_{dl}) \tag{3.19}$$

$$\beta = 0.045\exp(1.918\varepsilon_{dl}) \tag{3.20}$$

$$\gamma = 61.835 - 39.71\varepsilon_{dl} \tag{3.21}$$

The cumulative entrainment of the dispersed liquid with time at a particular location (1.26 m from the insertion point of dispersed liquid) of the downer is shown in Figure 3.8.

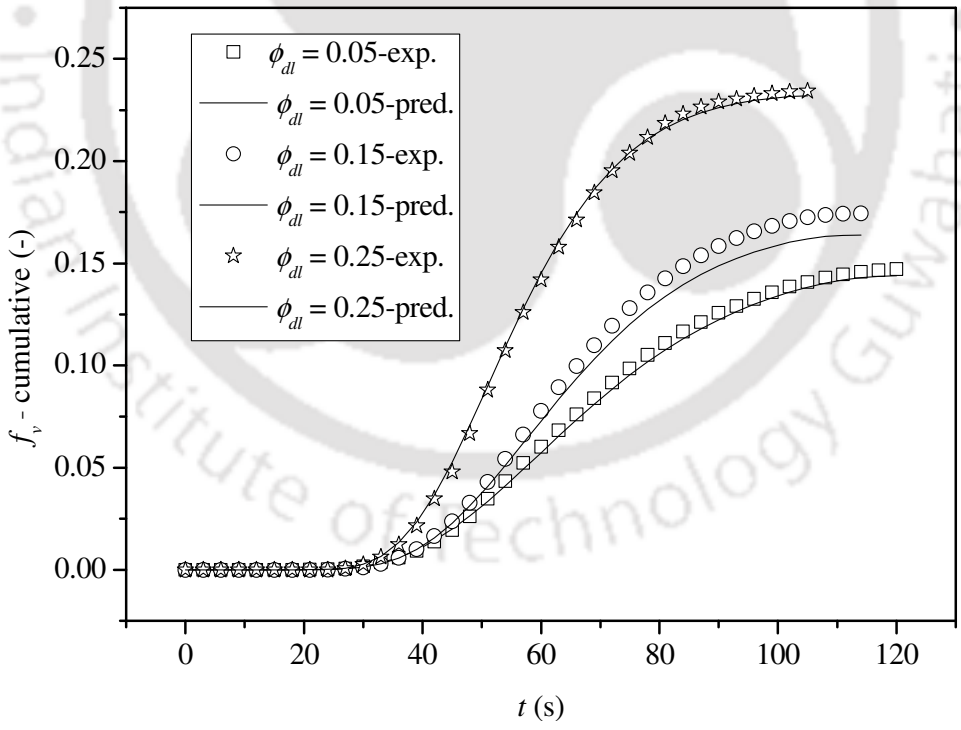

Figure 3.8: Cumulative profile of the fraction of the dispersed liquid with time

The initial volume fraction of the entrained dispersed liquid (paraffin here) depends on the liquid

jet velocity, which is shown in Table 3.3.

Table 3.3: The paraffin fraction entrained out of the total volume of a downer at its respective minimum time at a location z = 1.26 m from the inlet of the liquid jet velocity 4.24 m/s

Min. time (s) of entrainment	Volume fraction of paraffin entrained [f_v (-)]		
	5% Praffin	15% paraffin	25% paraffin
18	8.60×10^{-6}	–	–
24	–	9.80×10^{-5}	–

3.3.9 Prediction of gas entrainment rate by developing a general correlation

The gas entrainment is depending on the different operating variables. The functionality of gas entrainment rate based on the present experimental system can be expressed as

$$\frac{Q_g}{Q_{cl}} = f\left(u_j, \rho_{cl-ll}, \mu_{cl-ll}, \sigma_{cl-ll}, g, d_c, h_m\right) \tag{3.22}$$

The correlation for gas entrainment in terms of various operating variables is developed by dimensional analysis. Based on the dimensional analysis, the following function can be developed in terms of the different dimensionless groups. The generalized correlation for the whole range of experimental condition by multiple regression analysis can be expressed as

$$\frac{Q_g H_r^{0.88} We^{1.95}}{Q_{cl} Fr^{2.70}} = 2.56 \mathrm{Re}_j^{0.46} \mathrm{Re}_g^{0.67} \tag{3.23}$$

The calculated values by Equation (3.23) against the experimental values are shown in Figure 3.9.

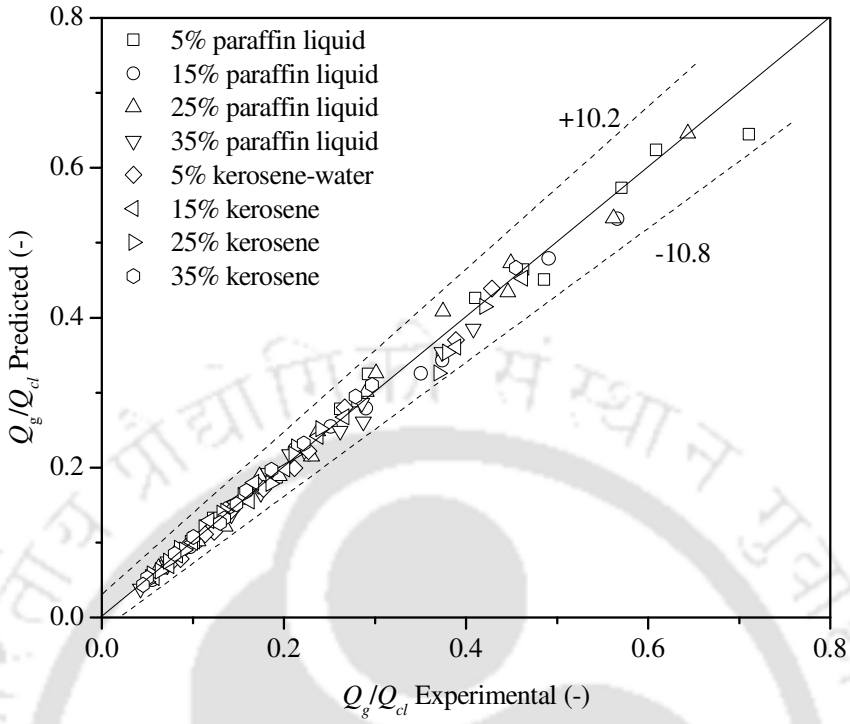

Figure 3.9: Parity plot of calculated values and experimental values of gas entrainment rate

The correlation coefficient and the overall standard error of the Equation (3.23) are 0.972 and 0.054, respectively. The overall percentage error between experimental and predicted values is found to be +10.2% and -10.8%. The ranges of the variables at which the correlation is valid: $27.82 < Re_g < 111.28$, $81514.4 < Re_j < 731406.7$, $1.30 < We < 17.36$, $0.06 < Fr < 0.18$, $19 < H_r < 41$. The basic theory which was followed for the analysis of variance is given in appendix-1.

3.4 Conclusions

In the present work, a gas-liquid-liquid mixing column is developed to study the liquid-liquid dispersion. In the present chapter, the gas, and liquid entrainment and its dispersion by liquid jet is enunciated. It can be concluded from the present study that the liquid entrainment can be extended based on the liquid jet kinetic energy. The penetration depth is correlated with the

operating variables in terms of jet length to nozzle diameter ratio, Reynolds number, and the jet Froude number. It is observed that the degree of dispersion is related to the penetration depth. If the penetration depth of the jet is increased the degree of entrainment and the phase dispersion is increased. The penetration depth of the liquid jet also depends on the system properties. A generalized correlation is proposed for entrainment of gas and liquid as a function of various operating variables within the range of experimental conditions.

CHAPTER - 4

GAS HOLDUP CHARACTERISTICS

In the preceding chapter, details of the gas entrainment by liquid jet and subsequent dispersion into the liquid phase in the column have been discussed. In this chapter, comprehensive studies on gas holdup is reported. Models are developed for the gas holdup in terms of different dimensionless groups consisting of operating variables, which can be used to interpret the holdup characteristics of the phases in the gas-liquid-liquid downflow contactor.

4.1 Introduction

The gas holdup is one of the important design parameters to characterize the hydrodynamics of gas-liquid-liquid flow in the contactor. The gas holdup influences the mass transfer between phases as it determines the interfacial area for their transport and mixing of the fluid in the column. Some studies on the phase holdup in the conventional liquid-liquid contactor reported by different investigators are shown in Table 4.1.The gas-liquid-liquid pseudo-three phase system, e.g., gas emulsion, was studied by Botton et al. (1978) for estimating the effect of high gas throughput on holdup values for several bubble columns including the draft tube. Kato et al. (1984) studied gas holdup in two multistage gas-liquid-liquid bubble columns of 0.066 m and 0.122 m diameter. The gas holdup in the column was determined and was correlated to superficial gas velocity only, but the effect of liquid composition was not considered. Bandyopadhyay et al. (1988) measured the average gas holdup of air in a bubble column with a multiple nozzle sparger plate, operated batch-wise. They found that the fractional holdup depends on the gas velocity, liquid properties, phase inversion in the liquid mixture, as well as on the spreading coefficient of the organic liquid. The holdup is minimum at the phase inversion point of the liquid with a negative spreading coefficient. However, the reverse is valid for a

liquid with a positive coefficient of spreading.

Table 4.1: Summary of the studies executed by various investigators

Author	Extraction device	System	Device geometry	Range of phase flow rate	Range of liquid holdup
Vermijs and Kramers (1954)	Rotating disc liquid-liquid contactor	water-acetic acid-methyl isobutyl ketone	i.d: 0.041 m	Q_{dl} : 1.94 $\times10^{-6}$-4.166 $\times10^{-6}$ m^3/s	ε_{dl} = 3.1 $\times10^{-2}$ - 19.2 $\times10^{-2}$
Sohn and Doungdeethaveeratana (1998)	Liquid-liquid contactor with gas injection	$Cuso_4$- H_2SO_4-H_2O-LIX 860-kerosene	i.d: 0.1425 m	Q_{cl} : 4.1$\times10^{-6}$ m^3/s	ε_{dl} = 0.03 - 0.4
Venkatanarasaiah and Varma (1998)	Pulsed liquid-liquid column	kerosene – water	i.d: 0.043 m	Q_{cl} : 4.57 $\times10^{-6}$ — 1.04$\times10^{-5}$ m^3/s	ε_{dl} =0.182 - 0.189
Wang et al. (2002)	Modified rotating liquid-liquid contactor	1-butanol-succinic acid-water	i.d: 0.10 m	Q_{cl} : 0 - 4.44 $\times10^{-4}$ m^3/s	ε_{dl} =0.05 - 0.45
Din et al. (2009)	Pulsed liquid-liquid contactor	water-kerosene	i.d: 0.05 m	Q_{cl} : 7.26 $\times10^{-6}$ - 9.26$\times10^{-6}$ m^3/s	ε_{dl} = 0.25 - 0.45
Napeida et al. (2010)	Hanson mixer–settler	toluene–water, n-butyl acetate–water, butanol–water	h_c: 1.72 m	Q_{cl} : 8.33 $\times10^{-6}$ -3.33 $\times10^{-5}$ m^3/s	ε_{dl} =0.083 - 0.073; 0.108 - 0.048; 0.112-0.053
Sa et al. (2010)	Liquid-liquid contactor	n-butyl alcohol – water	i.d: 0.092 m	Q_{cl} : 5.84 $\times10^{-5}$- 2.72 $\times10^{-5}$ m^3/s	ε_{dl} =0 - 0.2
Samdavid et al. (2016)	Perforated liquid-liquid column	kerosene - water	i.d: 0.06 m	Q_{cl} : 0 - 5.55 $\times10^{-5}$ m^3/s	ε_{dl} =0.05 - 0.6
Present study	Jet driven gas-liquid-liquid contactor	paraffin-water; kerosene-water	i.d: 0.05 m	Q_{cl} : 0.83 – 2.50 $\times10^{-4}$ m^3/s	ε_{dl} =0.04-0.46; 0.03-0.41

Asai and Yoshizawa (1991) presented the gas holdup experimental results, in an air-water two-phase and air-water-kerosene three-phase system. The average gas holdup calculation in the three-phase air-water-kerosene system is based on the G-L system relationship. Wang Li et al. (2007) presented an empirical expression for the prediction of the gas phase holdup in a gas-agitated sieve plate extraction column. The effects of superficial gas velocity on the gas holdup were widely investigated in various liquid-liquid and gas-liquid-liquid systems.

In the present work, the gas holdup characteristics in the gas-liquid-liquid jet-driven downflow column are studied experimentally, which has not been reported yet in the literature with the gas-liquid-liquid three-phase system.

4.2 Theories to analyze the gas holdup by various models

4.2.1 Lockhart-Martinelli correlation model

Gas holdup data has been analyzed by Lockhart – Martinelli (Lockhart and Martinelli, 1949) model. Butterworth (Butterworth, 1975) presented the Lockhart–Martinelli relation for gas holdup based on quality (x), and fluid properties such as density (ρ), viscosity (μ) as

$$\frac{1-\varepsilon_g}{\varepsilon_g} = a_1\left(\frac{1-x}{x}\right)^{a_2}\left(\frac{\rho_g}{\rho_{cl-dl}}\right)^{a_3}\left(\frac{\mu_{dl}}{\mu_g}\right)^{a_4} \tag{4.1}$$

The parameters a_1, a_2, a_3, a_4 are coefficients depends on experimental conditions.

4.2.2 Drift-flux model

Zuber and Findlay (1965) developed their drift flux model based on the existence of local slip. The drift flux model is generally applied to analyze the overall holdup of the gas in a vertical column. This model considers the effect of non-uniform flow and concentration distribution

across the duct as well as the effect of local relative velocity between the phases. To analyze the gas holdup data by drift flux model the average gas velocity is plotted against the gas-liquid mixture velocity, which is given by the following equation as,

$$\frac{u_{sg}}{\varepsilon_g} = C_o\left(u_{sg} + u_{sl}\right) + u_d \tag{4.2}$$

where C_o is the velocity distribution coefficient, and u_d is the gas phase drift velocity, which are obtained by experiment. The distribution coefficient accounts for the interaction of the velocity and gas holdup distributions. u_d accounts for the effect of local relative velocity between bubbles and liquid.

4.2.3 Slip velocity model

The slip velocity model is also a suitable tool to analyze the holdup in multiphase flow in a vertical column (Behringer, 1952). In the present work, this model is also used for the present gas-liquid-liquid co-current downward flow in the vertical column. The slip velocity is defined by the velocity of bubbles relative to the downward flow of gas-liquid-liquid mixture as:

$$u_s = \pm\{u_b - u_{sl}\} = \pm\left\{u_b - \frac{u_{sl}}{1-\varepsilon_g}\right\} \tag{4.3}$$

The bubble rise velocity is calculated by (Stokes, 1880)

$$u_b = \frac{g d_b\left(\rho_{cl-dl} - \rho_g\right)}{18\mu_{cl-dl}} \tag{4.4}$$

where the stable average bubble diameter can be estimated by (Evans et al., 1992)

$$d_b = \left(We_{cl-dl}\sigma_{cl-dl}/2\right)^{3/5}\rho_{cl-dl}^{-1/5}\bar{\in}^{-2/5} \tag{4.5}$$

The parameter $\bar{\in}$ is the average energy dissipation rate per unit volume. According to the work

of (Evans et al., 1992), the critical Weber number for downward flow is 1.2 since the break-up of the bubble is related to the energy dissipation rate. The energy dissipation rate is calculated by,

$$\overline{\epsilon} = \frac{1}{2}\frac{K_m \rho_{cl-dl} u_j^3 d_n^2}{d_c^2 \Delta z} \tag{4.6}$$

where K_m is the mixing loss coefficient. A correlation for K_m in terms of physical properties of liquid and gas and geometric variables is given by (Mandal et al., 2004)

$$K_m = 1.426\times10^{-2}\,\mathrm{Re}_j^{0.604} A_r^{0.590} H_r^{-0.072} Mo^{0.144} \tag{4.7}$$

Various authors used the slip velocity to interpret the flow behavior in churn turbulent flow condition as (Lapidus and Elgin, 1957; Majumder, 2008)

$$u_s = u_b f(\varepsilon_g) \tag{4.8}$$

where u_b is the bubble terminal rise velocity, and its functionality corresponds to the interaction of surrounding bubbles in the column.

4.3 Experimental setup and methodology

The details of the experimental setup and techniques have been discussed in chapter 2. The gas holdup was measured by the "phase isolation technique" in which operating (aerated) and liquid levels are measured after stopping both gas and liquid flow, as discussed in section 2.1. The studies of gas holdup were performed at different dispersed liquid concentrations at and different liquid and gas flowrates. The readings were repeated several times (at least four times) to check reproducibility.

4.3.1 Uncertainty analysis

The mean and standard deviation of data obtained the repeated experiment were calculated

respectively as

$$\bar{x} = \frac{1}{N}\sum_{i=1}^{N} x_i \tag{4.9}$$

$$\text{STDEV} = \sqrt{\frac{\sum_{1}^{N}(x_i - \bar{x})^2}{N-1}} \tag{4.10}$$

The standard uncertainty of the mean value is calculated by the Equation (4.13) as

$$U = \frac{\text{STDEV}}{\sqrt{N}} \tag{4.11}$$

The ranges of uncertainties of different parameters are given in Table 4.2.

Table 4.2: Typical uncertainties of the gas holdup

u_{sl} (m/s)	Volume fraction of dispersed liquid in the column (%)	Range of mean	Range of STDEV	Range of uncertainty ($\times 10^{-3}$)	Range of relative uncertainty (%)
0.045-0.236	0.069	0.044-0.234	0.0028-0.0029	1.17-1.20	2.64-0.51
0.044-0.217	0.183	0.044-0.215	0.0028-0.0022	1.17-0.91	2.64-0.42
0.044-0.199	0.273	0.044-0.196	0.0028-0.0029	1.17-1.17	2.64-0.59
0.044-0.205	0.344	0.044-0.204	0.0028-0.0029	1.17-1.17	2.64-0.57

4.4 Results and discussion

4.4.1 Effect of gas and liquid jet velocity on gas holdup

The effect of liquid jet velocity on the gas holdup is shown in Figure 4.1. It is observed that with increasing the jet velocity and gas velocity, the gas holdup increased at a constant dispersed liquid volume fraction (Paraffin liquid). The momentum of the jet increases with increasing liquid flow rate, which results in higher gas entrainment into the liquid. From Figure 4.1 (a), it is seen that increase in the gas or liquid velocity leads to increase the mixing of phases due to increase in the intensity of the momentum transfer, thereby increase in the bubble formation, which enhances the gas holdup. When the dispersed liquid (Paraffin liquid) volume fraction is increased by 25% of the total volume of the column, it follows the same trend as discussed above which is shown in Figure 4.2 (a).

The effect of liquid jet velocity on gas holdup at a constant kerosene volume fraction is shown in Figure 4.1 (b). It is observed that with increasing the water and gas velocities, the overall holdup of gas increases at a constant kerosene volume fraction. In this case, the liquid jet entrains gas with increasing water flow rate. As the viscosity of kerosene is less, the entrainment of gas is easier than that with paraffin liquid, which results in more gas holdup. As the dispersed liquid volume fraction (kerosene) in the column increases, the viscosity increases, which results in less gas entrainment with the same trend of decreasing gas holdup with liquid flow rate as shown in Figure 4.2 (b).

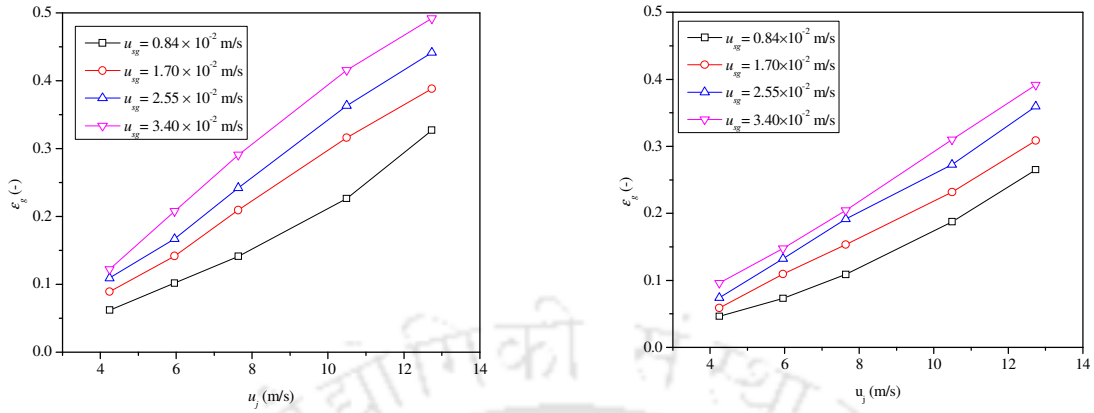

(a) (b)

Figure 4.1: Variations of gas holdup with liquid jet velocity at different gas velocity (a) for 5% (v) of paraffin liquid, (b) for 5% (v) of kerosene

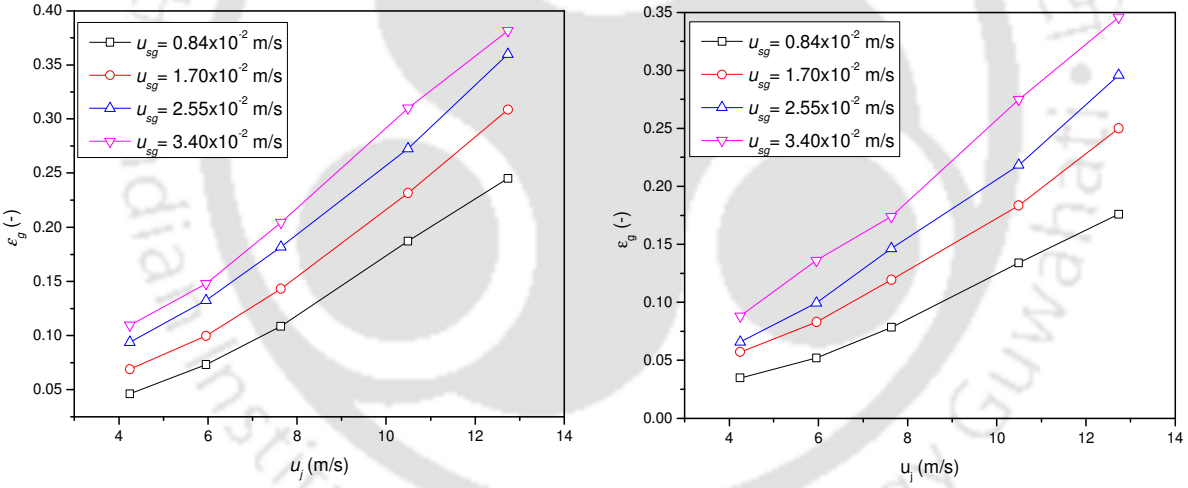

(a) (b)

Figure 4.2: Variations of gas holdup with liquid jet velocity at different gas velocity (a) for 25% (v) of paraffin liquid, (b) for 25% (v) of kerosene

4.4.2 Effect of dispersed liquid volume fractions on overall gas holdup

The changes in the overall holdup of the gas with different dispersed liquid volume fraction at a constant gas flow rate is shown in Figure 4.3 (a). It is observed from the experimental result that

the overall holdup of the gas is lesser at the lower volume of paraffin liquid than that at a higher volume in the column. This is occurred due to the higher viscosity of the fluid at a higher concentration of paraffin liquid. The deviation in overall holdup of the gas with different concentrations of kerosene at a constant gas flow rate is shown in Figure 4.3 (b). It is observed that the overall holdup of the gas is gradually increasing with respect to the water flow rate. This is due to the lower viscosity of the fluid. The deviation in overall holdup of gas at different volume fractions of the paraffin liquid and kerosene at a higher flow rate of gas is shown in Fig.4.4. It is seen that the overall holdup of gas increases with increasing flow rate of gas. Also it can be seen from the figures that the range of holdup is higher at higher gas flowrate.

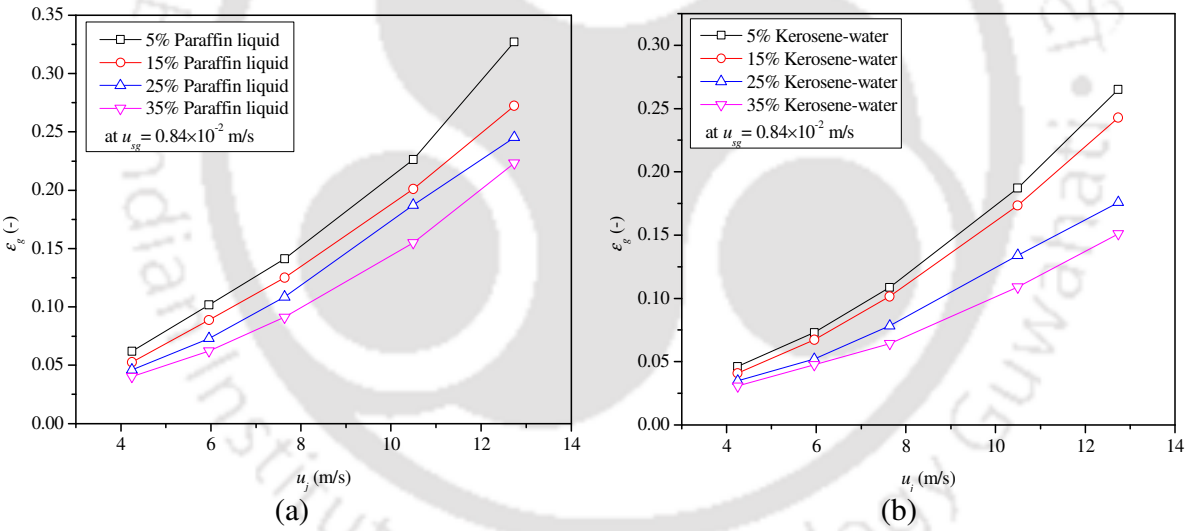

Figure 4.3: Variations of gas holdup with liquid jet velocity at different (a) paraffin liquid (b) kerosene volume concentrations

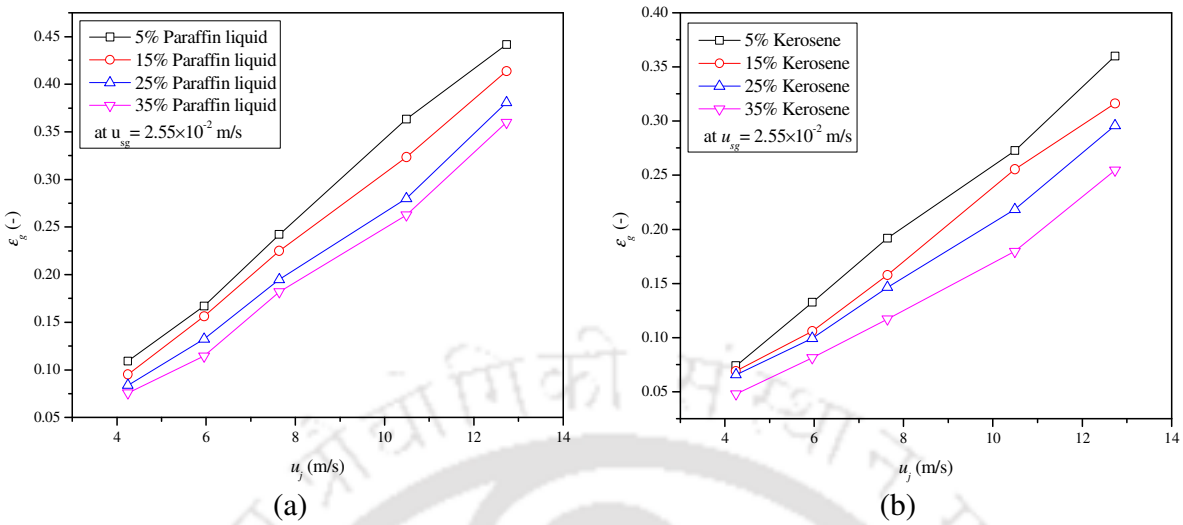

Figure 4.4: Variations of gas holdup with liquid jet velocity at different (a) paraffin liquid (b) kerosene volume concentrations

4.5 Gas holdup analysis by different correlations and models

The overall holdup of the gas data of the present system was analyzed with different models, which are described in the following sections.

4.5.1 Correlation model

A general correlation has been made by dimensional analysis to predict the overall holdup of the gas. The overall holdup of the gas as a function of different variables can be expressed as

$$\varepsilon_g = f\left(u_j, u_g, \rho_{cl-dl}, \rho_g, \mu_{cl-dl}, \mu_g, \sigma_{cl-dl}, g, d_c, h_m\right) \tag{4.12}$$

Combining the dimensional groups as per the dimensional analysis, the resulting functional form was formed as,

$$\varepsilon_g = f\left(\mathrm{Re}_j, \mathrm{Re}_g, We, Fr, H_r\right) \tag{4.13}$$

The regression analysis of experimental data yields,

$$\varepsilon_g = 3.48 \times \mathrm{Re}_j^{0.238}\, \mathrm{Re}_g^{0.586}\, We^{-1.42}\, Fr^{2.162}\, H_r^{-1.081} \quad (4.14)$$

The correlation was developed based on 160 experimental data at different operating conditions. The predicted values ε_g from the correlation were compared with the experimental values, which are shown in Figure 4.5. The overall percentage error between experimental and predicted values was found to be +12% and -12%. The ranges of the variables of groups for which the correlation is valid are: $27.82 < Re_g < 111.28$, $81514.4 < Re_j < 731406.7$, $1.30 < We < 17.36$, $0.06 < Fr < 0.18$, $19 < H_r < 41$. The theory based on which it was followed for the analysis of variance is given in Appendix I.

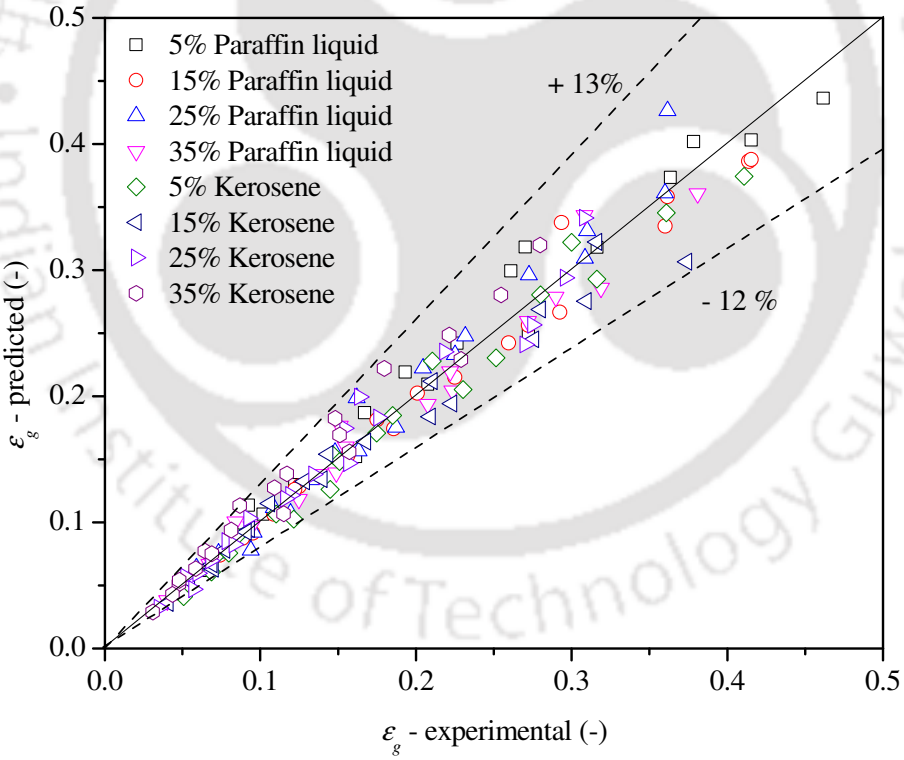

Figure 4.5: Parity plot of calculated values and experimental values of gas holdup for different concentrations of paraffin liquid and kerosene

4.5.2 Analysis by Lockhart-Martinelli correlation

In the present analysis, it is found that the model Equation (4.1), which is developed for horizontal flow, does not fit well with the experimental values of vertical downflow, so an attempt has been made to modify the correlation in terms of quality (x). The quality is given by the ratio of the mass flow rate of gas and the mass flow rate of a gas-liquid-liquid mixture, which is expressed as

$$x = \frac{\dot{m}_g}{\dot{m}_m} = \frac{\rho_g Q_g}{\rho_g Q_g + \rho_{cl-dl} Q_{cl-dl}} \tag{4.15}$$

The volumetric flow rate of gas Q_g is calculated from the volumetric flow rate of liquid $Q_{cl\text{-}dl}$ and the gas holdup as

$$Q_g = \frac{\varepsilon_g Q_{cl-dl}}{(1-\varepsilon_g)} \tag{4.16}$$

By substituting Equation (4.16) in the Equation (4.15) the gas holdup can be expressed as,

$$\varepsilon_g = \frac{1}{\left(1 + \frac{\rho_g}{\rho_{cl-dl}} \frac{(1-x)}{x}\right)} \tag{4.17}$$

Based on the present study, the quality (x) is correlated with the physical and operating conditions of the present experiment. The correlation can be expressed by different significant dimensionless groups based on the dimensional analysis. The functionality of the correlation can be obtained by the multiple regression analysis (by Microsoft Excel data analysis tool) which is expressed as

$$\frac{1-x}{x} = 1.15 \times 10^{10}\ \mathrm{Re}_j^{-0.65}\ \mathrm{Re}_g^{-0.66}\ H_r^{-1.90}\ X^{-0.53} \tag{4.18}$$

By substituting Equation (4.18) in the Equation (4.17) the gas holdup can be expressed as,

$$\varepsilon_g = \frac{1}{\left(1+\left(\frac{\rho_g}{\rho_{cl-dl}}\right)\left(1.15\times10^{10}\,\mathrm{Re}_j^{-0.65}\,\mathrm{Re}_g^{-0.66}\,H_r^{-1.90}\,X^{-0.53}\right)\right)} \tag{4.19}$$

Comparisons between the predicted values of gas holdup (ε_g) by modified Lockhart– Martinelli correlation and the experimental data are shown in Figure 4.6. It is seen that the correlation Equation (4.19) fits well within the range of experimental conditions. The correlation coefficient (R^2) and the standard error (SE) are 0.96 and 0.21, respectively. The overall percentage error between experimental and predicted values is found to be +16% and -18%. The correlation valid within the ranges: $27.82 < Re_g < 111.28$, $81514.4 < Re_j < 731406.7$, $5.81 < X' < 60.71$.

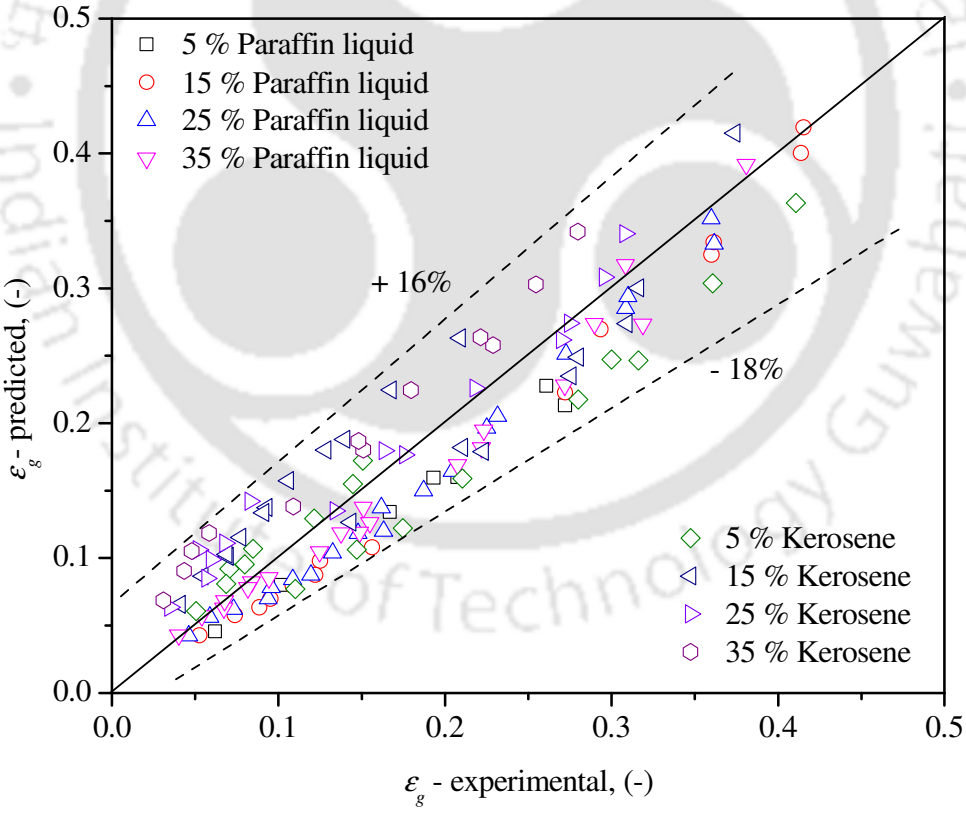

Figure 4.6: Parity plot of calculated values and experimental values of gas holdup (ε_g) by modified Lockhart- Martinelli correlation (Equation (4.19))

4.5.3 Analysis by drift-flux model

The drift flux model is applied in this study for gas-liquid-liquid flow in the downflow column. For a homogeneous flow, the values of C_o and u_d correspond to one and zero, respectively. The drift velocity for upward gas-liquid two-phase flow is given by

$$u_d = \sqrt{2}\left(\frac{g\sigma_{cl-dl}\left(\rho_{cl-dl} - \rho_g\right)}{\rho_{cl-dl}^2} \right)^{1/4} \tag{4.20}$$

By using Equation (4.20) and Equation (4.2), the distribution coefficient (C_o) can be expressed for downflow gas-liquid-liquid system as follows:

$$C_o = \frac{\left(\frac{u_{sg}}{\varepsilon_g}\right) - \left(-\sqrt{2}\left(\frac{g\sigma_{cl-dll}\left(\rho_{cl-dl} - \rho_g\right)}{\rho_{cl-dl}^2} \right)^{1/4} \right)}{u_{sg} + u_{sl}} \tag{4.21}$$

The entrainment occurs beyond a minimum entrainment velocity for which the dispersion of gas occurs and results in the fluid circulation inside the column. The circulation of fluid may occur by counteracting the buoyancy effect of gas bubbles and insoluble liquid in the column. At the center of the column the jet kinetic energy is higher than the radial positions. Due to this energy distribution, along the column wall, the gas bubble and the other insoluble liquid move upward and get circulated in the column.

Based on present experimental data, a correlation has been made by dimensional analysis of Buckingham Pi theorem to obtain the values of C_o within the range of liquid velocity of 0.04 to 0.14 m/s and the gas velocity of 0.85×10^{-2} to 2.55×10^{-2} m/s. The range of drift flux velocity for paraffin-water system is -6.57 to -5.71 and for kerosene-water system is -6.60 to -5.84 as per present experimental conditions. The correlation can be expressed as

$$C_o = 24.5 \mathrm{Re}_j^{-0.08}\, \mathrm{Re}_g^{0.23}\, Mo^{-0.029} Fr^{-0.42} \tag{4.22}$$

By regression analysis of Equation (4.22), the correlation coefficient and standard error are found to be 0.977 and 0.050, respectively. The parity plot of experimental versus calculated values of C_o by Equation (4.22) is shown in Figure 4.7. The correlation shows good prediction of the experimental values. The overall percentage error between experimental and predicted values is found to be +10% and -7%. The correlation is valid within the range of $27.82 < Re_g < 111.28$, $81514.4 < Re_j < 731406.7$, $1.44 \times 10^{-11} < M_o < 1.01 \times 10^{-9}$, $0.06 < Fr < 0.18$.

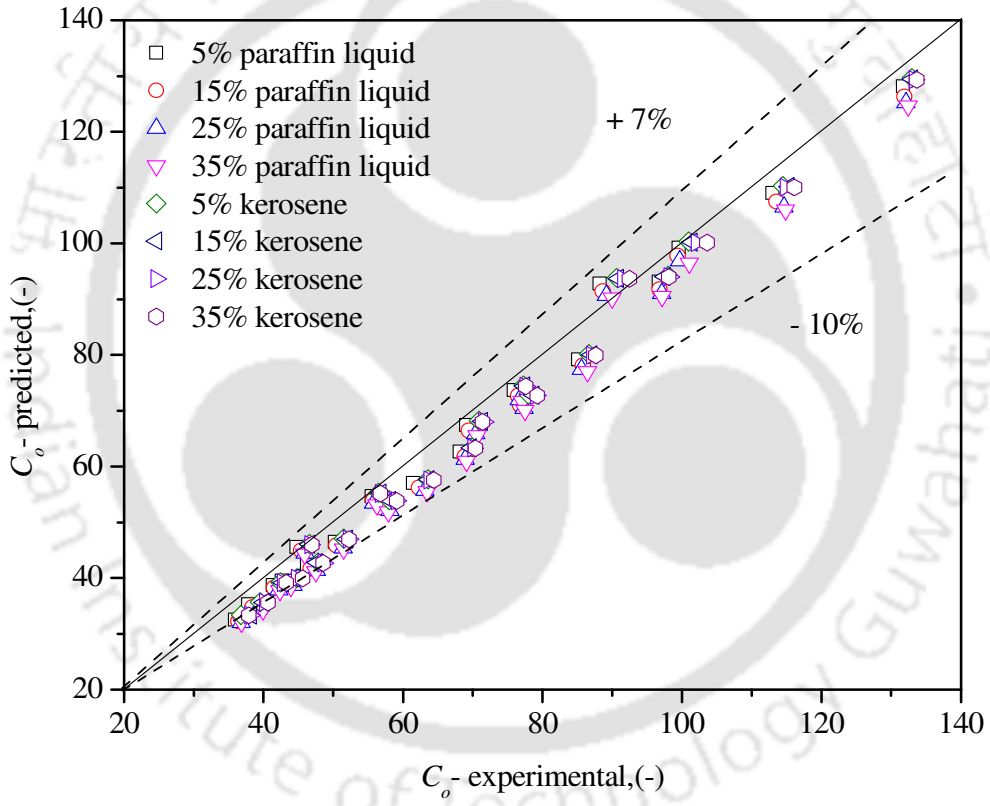

Figure 4.7: Parity plot of calculated values and experimental values of distribution parameter (C_o)

4.5.4 Interpretation of gas holdup by slip velocity model

In the present downflow column, the slip velocity is found to be positive or negative. The

positive values of slip velocity specify the higher rise velocity of bubbles relative to downward velocity of liquid. The negative value indicates the downward movement of bubbles with the liquid. Based on the present experimental study, the following relation is developed,

$$\frac{u_s}{u_b} = \alpha\varepsilon_g + \beta \tag{4.23}$$

where

$$\alpha = -4.64\times10^{-5}\,\mathrm{Re}_j^{0.78}\,We^{-2.91}\,Fr^{2.74} \tag{4.24}$$

and β = 1.245. The slip velocity is positive for u_{sl} < 0.10 m/s and d_b < 0.66 mm. From the Fig.4.8, it is seen that the slip velocity is a function of concentrations of dispersed liquid. Typical profiles of slip velocity as a function of bubble size for paraffin liquid-water and kerosene-water are shown in Figure 4.9a and Figure 4.9 b, respectively. The slip velocity increases with the bubble size for the respective dispersed liquids. The average bubble size for paraffin liquid-water and kerosene-water system are 1.21 and 0.76 mm, respectively, within the range of present experimental conditions.

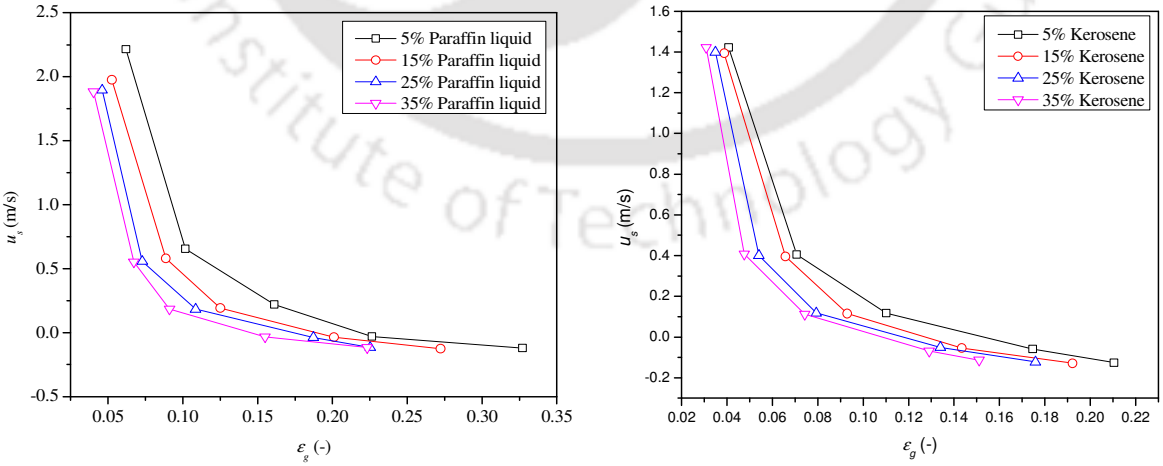

(a) (b)

Figure 4.8: Variations of slip velocity with gas holdup at u_{sg} = 0.84×10^{-2} m/s, for different concentrations of (a) paraffin liquid (b) kerosene

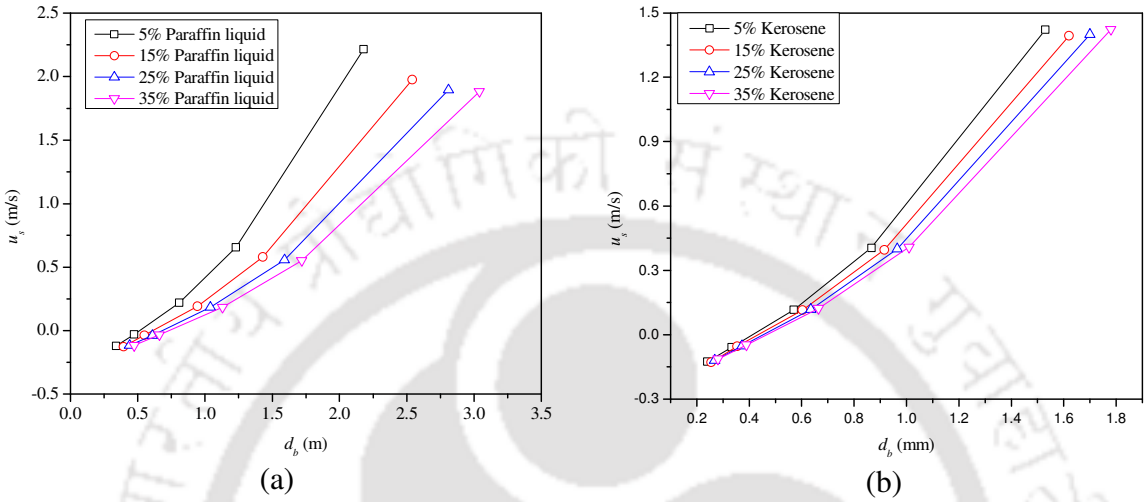

Figure 4.9: Variations of slip velocity with bubble size at u_{sg} = 0.84×10^{-2} m/s, for 5% of dispersed liquid (a) paraffin liquid (b) kerosene

4.6 Conclusions

From the present work, it can be concluded that the holdup of gas is strongly dependent on the liquid jet velocity. The gas holdup varies also with system properties. Gas holdup data were analyzed by Lockhart-Martinelli correlation with its modifications and drift flux model. The slip velocity is also used to interpret the bubble relative velocity, which indicates the interaction of the bubbles along with the liquid movement. This enables to bubble and droplet breakup to enhance the turbulence in the column which may be useful for intensification of the mass transfer process. A generalized correlation was proposed for gas holdup as a function of various operating variables. The correlations developed are within the range of the experiments for the gas holdup.

CHAPTER - 5

FRICTIONAL PRESSURE DROP CHARACTERISTICS

In the preceding chapters, characteristics of gas entrainment and gas holdup in the ejector induced downflow column have been reported. This chapter presents a systematic study on the frictional and total pressure drop of gas liquid-liquid flow. An empirical correlation is developed for frictional pressure drop and friction factor as a function of various operating variables and the system properties.

5.1 Introduction

For scale-up and the proper design of the downflow column with the liquid-liquid system, several hydrodynamic characteristics and the transport processes are essential to study and its interpretation for the suitability of industrial-scale operation. Recently the chemical operations in the downflow column and its feasibility aspects are gaining interest in the scientific community for its several advantages such as a finer droplet generation, higher degree of mixing and mass transfer, the high residence time of the droplet. The previous chapters regarding entrainment and holdup characteristics (Goshika and Majumder, 2018, 2019a) reveals the proof of concept of the feasibility of liquid-liquid operation in the downflow column. Pressure drop affects the gas phase residence time and also relates indirectly to the interfacial area. The understanding of pressure drop gives the energy dissipation and the assessment of the performance of the reactor (Poettman and Carpenter, 1952).

Spedding et al. (2000) studied in detail the existence of flow patterns and how they affect the pressure drop of gas-liquid-liquid flow in the vertical pipe. Descamps et al. (2006) reported the effect of gas injectors and the influence of different injectors on the phase inversion in a vertical

pipe. It was reported that the pressure drop rises during the phase inversion from oil to water. The gas injection did not affect the concentration of oil in liquid. However, the effect on the pressure drop was significant. Xu et al. (2012) investigated the effect of gas injection in oil-water two-phase flow and observed that the total pressure gradient of gas-liquid-liquid flow is higher than that in oil-water flow at the phase inversion region. Pietrzak et al. (2017) studied the influence of gas injection on two immiscible liquid mixtures in a vertical pipe. They observed that variation of the continuous liquid phase in three-phase flow has a considerable effect on the variation of frictional pressure drop. The changes in pressure drop depend on the water and gas flow rates. Khooshechin et al. (2013) studied the pressure drop in the absence of mass transfer in the pulsed packed extraction column. They observed that the pressure drop is affected by the continuous and dispersed phase flow rate and pulsation intensity. The ejector induced downflow column has the advantage of dispersing the gas without external power requirement, as reported by Majumder (2016). In the ejector induced downflow column, the continuous liquid jet sucks the gas from the atmosphere into the column through the ejector assembly mounted on the top of the column contactor. The downflow column has the advantage of forming uniform oil drops and gas bubbles, a negligible coalescence of drops, and reduction of back-mixing in the column (Goshika and Majumder, 2018, 2019a). Most of the past literature for the study of pressure drop in downflow column fitted with ejector induced are shown for gas-liquid (Babu et al., 1999; Kundu et al., 1995) liquid-liquid (Ghosh et al., 2011; Hu and Angeli, 2006) and gas-liquid-solid (Sivaiah et al., 2012) systems. The present work aims to study the pressure drop of paraffin liquid-water and kerosene-water flow in the ejector induced gas-liquid-liquid downflow column which is not yet reported in the literature. The study on the pressure drop is used to enunciate the dispersion of phases in the column.

5.2 Theoretical background

5.2.1 Frictional pressure drop and friction factor

The total pressure drop of gas-aided liquid-liquid flow (ΔP_{TP}) in the present jet-driven downflow column is a sum of frictional pressure drop, hydrostatic pressure, and pressure drop due to acceleration, which can be expressed as

$$\Delta P_{TP} = \Delta P_{fT} + \Delta P_h + \Delta P_a \tag{5.1}$$

The hydrostatic pressure drop of the gas-liquid-liquid flow in the column is expressed as,

$$\Delta P_h = h_m \rho_{dl-cl} \left(1 - \varepsilon_g\right) g \tag{5.2}$$

In the present system, when the continuous liquid plunges the surface of the liquid in the column, the gas-liquid-liquid mixture bears a sudden impact which changes the pressure inside the column. This pressure (ΔP_a) is defined by the ratio of force applied by the liquid jet and the column cross- sectional area which can be expressed as

$$\Delta P_a = \frac{F_j}{A_c} = \frac{ma_j}{A_c} = \frac{Q_{dl-cl} \rho_{dl-cl} \left(u_j - v_{dl-cl}\right)}{A_c} \tag{5.3}$$

As per continuity equation, one can write

$$u_j A_j = v_{dl-cl} A_c (1 - \varepsilon_g) = u_{dl-cl} A_c = Q_{dl-cl} \tag{5.4}$$

or

$$u_j = u_{dl-cl} \frac{A_c}{A_j} \tag{5.5}$$

and

$$v_{dl-cl} = \frac{u_{dl-cl}}{(1 - \varepsilon_g)} \tag{5.6}$$

Substituting Equations (5.5) and (5.6) in Equation (5.3), it can be written as

$$\Delta P_a = u_{dl-cl}^2 \rho_{dl-cl} \left[\frac{d_c^2}{d_j^2} - \frac{1}{(1-\varepsilon_g)} \right] \tag{5.7}$$

By substituting Equations (5.2) and (5.7) into the Equation (5.1) the three-phase frictional pressure drop can be expressed as,

$$\Delta P_{fT} = \Delta P_{TP} - \left(h_m \rho_{dl-cl} (1-\varepsilon_g) g\right) - \left(u_{dl-cl}^2 \rho_{dl-cl} \left[\frac{d_c^2}{d_j^2} - \frac{1}{(1-\varepsilon_g)} \right] \right) \tag{5.8}$$

The single phase frictional pressure drop ΔP_{fO} over a dispersion height of h_m is given by,

$$\Delta P_{fO} = \frac{2\rho_O f_O u_O^2 h_m}{d_c} \tag{5.9}$$

Similarly, the gas-liquid-liquid frictional pressure drop based on liquid superficial velocity may be defined as

$$\frac{\Delta P_{fT}}{g\rho_{dl-cl} h_m} = \frac{2 f_{TPL} u_{dl-cl}^2}{g d_c} \tag{5.10}$$

By substituting Equation (5.10) in Equation (5.8) friction factor (f_{TPL}) for gas-liquid-liquid system can be expressed as

$$f_{TPL} = \left(\frac{g d_c}{2 u_{dl-cl}^2} \right) \left(\frac{\Delta P_f}{g \rho_{dl-cl} h_m} - (1-\varepsilon_g) - \left(\frac{u_{dl-cl}^2}{g h_m} \left[\frac{d_c^2}{d_j^2} - \frac{1}{(1-\varepsilon_g)} \right] \right) \right) \tag{5.11}$$

5.2.2 Different models to analyze the frictional pressure drop

5.2.2.1 Lockhart–Martinelli model

Lockhart and Martinelli (1949) suggested a correlation for the analysis of frictional pressure drop in the horizontal pipe for different gas and liquid flow mixtures. According to the model the parameters $\phi_{dl\text{-}cl}$, ϕ_g and X as follows

$$\Delta P_{fT} = \phi_{dl-cl}^2 \Delta P_{fodl-cl} \tag{5.12}$$

$$\Delta P_{fT} = \phi_g^2 \Delta P_{fog} \tag{5.13}$$

$$X = \frac{\phi_g}{\phi_{dl-cl}} = \sqrt{\left(\frac{\Delta P_{fodl-cl}}{\Delta P_{fog}}\right)} \tag{5.14}$$

The frictional pressure drop of single phase ΔP_{fO} for height of h_m of the column is

$$\Delta P_{f0} = \frac{2\rho_0 f_0 V_0^2 h_m}{d_c} \tag{5.15}$$

The single phase friction factor (f_0) for laminar and turbulent flow respectively are given by (McCabe and Smith, 1976; Chhabra and Richardson, 1999)

$$f_0 = 16/\mathrm{Re}_0 \qquad \text{for Re} < 2100 \tag{5.16}$$

and

$$f_0 = 0.079/\mathrm{Re}_0^{0.25} \qquad \text{for Re} > 4000 \tag{5.17}$$

The single phase friction factor (f_0) for transition flow (2100 < Re < 4000) is given by (Desouky, 1991),

$$f_0 = 0.125\left(0.0112 + \mathrm{Re}_0^{-0.3185}\right) \tag{5.18}$$

Davis (1963) recommended Lockhart-Martinelli's correlation for a vertical column by modifying the term X by introducing Froude number (Fr) to add velocity and gravity effect as

$$X_{\mathrm{mod}} = 0.19 Fr^{0.185} X \tag{5.19}$$

Chisholm (1967) suggested a model in terms of the Lockhart-Martinelli parameter for

$$\phi_{dl-cl}^2 = f(X) = \left(1 + \frac{C}{X} + \frac{1}{X^2}\right) \tag{5.20}$$

$$\phi_g^2 = f(X) = \left(1 + CX + X^2\right) \tag{5.21}$$

The parameter C depends on the laminar or turbulent flow of the gas and liquid phase. The different values of C are given in Table 5.1. For the present experimental data the value of C is 10 as the gas phase is laminar flow and liquid phase is turbulent flow.

Table 5.1: Values of the constant C in Chisholm (1967) correlation for different flow mechanisms

Flow Mechanism (Liquid-Gas)	Value of C
Laminar-laminar	5
Turbulent-laminar	10
Laminar-turbulent	12
Turbulent-turbulent	20

5.2.3.2 Kato (1958) model

Kato (1958) suggested a modified Lockhart-Martinelli parameter, ϕ_l in the vertical column with the air-water flow which is expressed as,

$$\phi_k^2 = K\left(\frac{\dot{m}_{dl-cl}}{\dot{m}_G}\right)^{k_1} \frac{\mathrm{Re}_g^{k_2}}{X^2} \tag{5.22}$$

For the gas-liquid system, Kato (1958) found the values of K, k_1, and k_2 respectively as 36.8×10^{-3}, 1.27 and 0.25.

5.2.3.3 Wallis (1969) model

Wallis (1969) proposed the correlation of the phase multiplier, which is dependent on the flow quality (x) of the system. The proposed correlation is,

$$\phi_w^2 = \lambda_w \left(1 + x\frac{\rho_{cl-dl} - \rho_g}{\rho_g}\right)\left(1 + x\frac{\mu_{cl-dl} - \mu_g}{\mu_g}\right)^{w_1} \tag{5.23}$$

For the gas-liquid system, Wallis (1969) found the values of λ_w and w_1, respectively, as 1 and -0.25.

5.2.3.4 Gharat and Joshi (1992) model

Gharat and Joshi (1992) suggested a model to predict pressure drop based on the combined effect of the friction and the velocity which is given by

$$\Delta P_{fT} = \Delta P_{f0} + \Delta P_{fAT} \tag{5.24}$$

$$\Delta P_{f0} = \frac{2 f_{f0} u_0^2 \rho_0 \Delta z}{d_c} \tag{5.25}$$

$$\Delta P_{fAT} = \frac{2 f_{fAT} u_{dl-cl}^2 \rho_{dl-cl} \Delta z}{d_c}$$

(5.26)

$$f_{Tp} = \frac{f_0}{\varepsilon_l^2} + f_{AT} \tag{5.27}$$

The overall friction factor depends on turbulence intensity ($u_y^{'}$) of the flow and slip velocity (u_s), which can be expressed as

$$f_{AT} = 2\left(\frac{u_y^{'}}{u_s}\right)^2 \tag{5.28}$$

For homogeneous flow,

$$u_y^{'} = 1.5\varepsilon_g u_s \tag{5.29}$$

$$u_s = -\frac{u_{sg}}{\varepsilon_g} + \frac{u_{dl-cl}}{1-\varepsilon_g} \tag{5.30}$$

The two-phase multiplier can then be expressed as

$$\phi_l^2 = \frac{\Delta P_{ft}}{\Delta P_{f0}} = \frac{\Delta P_{f0} + \Delta P_{fAT}}{\Delta P_{f0}} \tag{5.31}$$

or

$$\phi_l^2 = \frac{1}{\varepsilon_l^2} + \frac{f_{AT}}{f_0}\left(\frac{u_s}{u_{dl-cl}}\right)^2 \tag{5.32}$$

or

$$\phi_l^2 = \frac{1}{\varepsilon_l^2} + \frac{2}{f_0}\left(\frac{u_y'}{u_{dl-cl}}\right)^2 \tag{5.33}$$

The model equations shown in Equations (5.22), (5.23) and (5.33) were adapted to the present gas-liquid-liquid dispersion in downflow column.

5.3 Experimental setup and procedure

5.3.1 Experimental setup

The details of the experimental setup and procedure are discussed in Chapter 2. A schematic diagram of the jet-driven downflow gas-liquid-liquid dispersion column is shown in Figure 2.1. When the steady-state was attained for a particular gas-liquid-liquid mixing height in the column, the pressure readings of all the manometers connected at different levels of the column were noted. Experiments have been carried out with paraffin liquid-water and kerosene-water system. At the start of a run, the column was filled with water up to 2/3rd of the column. The dispersed liquid (paraffin liquid or kerosene) was introduced into the column batch-wise within a range of 5 to 35 % by volume.

5.3.2 Procedure

For each run, half of the downcomer was filled with a continuous liquid phase, i.e. water at the beginning. The level of the continuous phase was noted as H_{cl}. Then, a certain volume % of dispersed liquid was filled in the downcomer batch-wise. Immediately, the height of the liquid-liquid mixture (H_{ll}) was noted for dispersed liquid and H_{cl} for continuous liquid. At a fixed water flow rate, when the liquid from the nozzle plunges the liquid-liquid mixture in the column, a sudden increase in pressure occurs through the column, which enables the water to suck the gas from the atmosphere in the ejector assembly. The gas flow rate is then controlled in the column with the valve V_4. During the operation, the height of the gas-liquid-liquid interface was recorded as $H_{g\text{-}ll\text{-}cl}$. Once the steady-state is achieved, the flow of liquids was suddenly stopped by closing the solenoid valves and allow it to settle down. After a certain time, the final height of the liquid-liquid mixture ($H_{ll\text{-}cl}$) was noted when the gas is completely isolated from the liquid-liquid mixture. The gas-liquid-liquid mixture height in the column is maintained by controlling the valve V_6. A level of liquid is maintained in the column by adjusting the pressure in the separator. When the system reached the steady-state at particular gas and liquid flows, readings for the pressure were noted from the manometer connected to the column.

5.4 Results and discussion

5.4.1 Variations of frictional pressure drop with different variables

5.4.1.1 Effect of the gas holdup on the three-phase frictional pressure drop

In the previous chapter, the effect of superficial gas velocity on the gas holdup in the presence of water-paraffin liquid and water-kerosene in the gas-liquid-liquid downflow contactor was reported (Goshika and Majumder, 2018). It was observed that the gas holdup of the downflow contactor increases with an increase in the concentration of water-paraffin liquid and water-

kerosene systems with varying gas superficial velocity. In this chapter, the effect of the gas holdup on a three-phase frictional pressure drop in the presence of water-paraffin liquid and the water-kerosene is analyzed. The impact of the gas holdup on a three-phase frictional pressure drop with varying superficial gas velocity for 15% (v) paraffin liquid is shown in Figure 5.1a. It is observed that frictional pressured drop increases with an increase in the gas holdup and superficial gas velocity. As the gas holdup of the system increases, the contact among the paraffin droplets generates more friction and turbulence with an increase in the gas-liquid-liquid mixture velocity. The frictional pressure drop variation with the gas holdup with kerosene of 15% (v) at a different gas flow rates is shown in Figure 5.1b. The frictional pressure drop increases with an increase in overall gas holdup (ε_g). But the frictional pressure drop in case of kerosene is less than that of the paraffin liquid. This is due to the lower viscosity of the kerosene than that of the paraffin liquid.

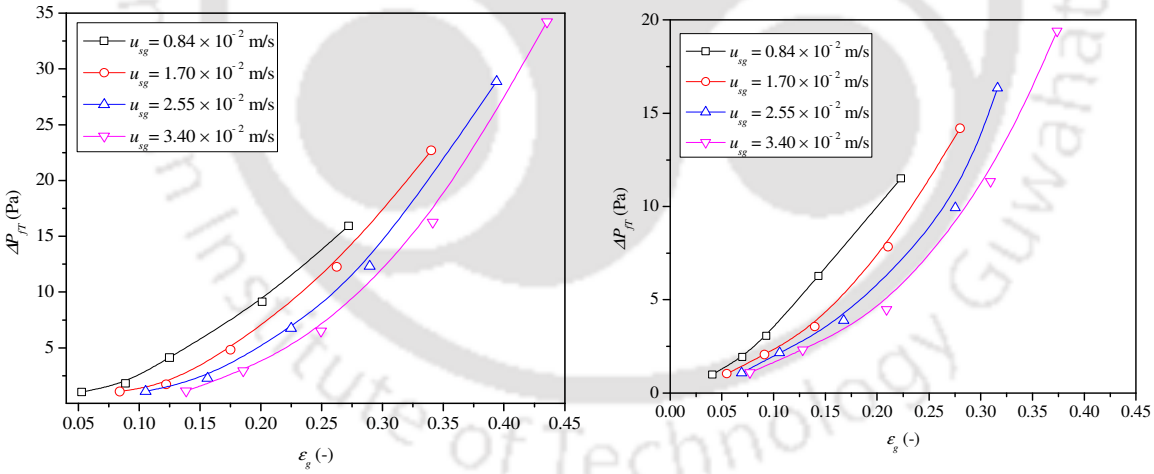

(a) (b)

Figure 5.1: Variations of frictional pressure drop with gas holdup at different gas velocity (a) for 15% (v) of paraffin liquid, (b) for 15% (v) of kerosene

Figure 5.2a and Figure 5.2b represent the deviation of a frictional pressure drop along with the

corresponding gas holdup of dispersed liquid, paraffin liquid, and kerosene of 35% volume. The frictional pressure drop rises with a rise in overall gas holdup (ε_g), but the frictional pressure drop in case of dispersed liquids of higher volume (35%) is more than that at the lower volume (15%) due to the higher resistance of the fluids as the liquid-liquid mixture viscosity increases with the volume of dispersed liquid.

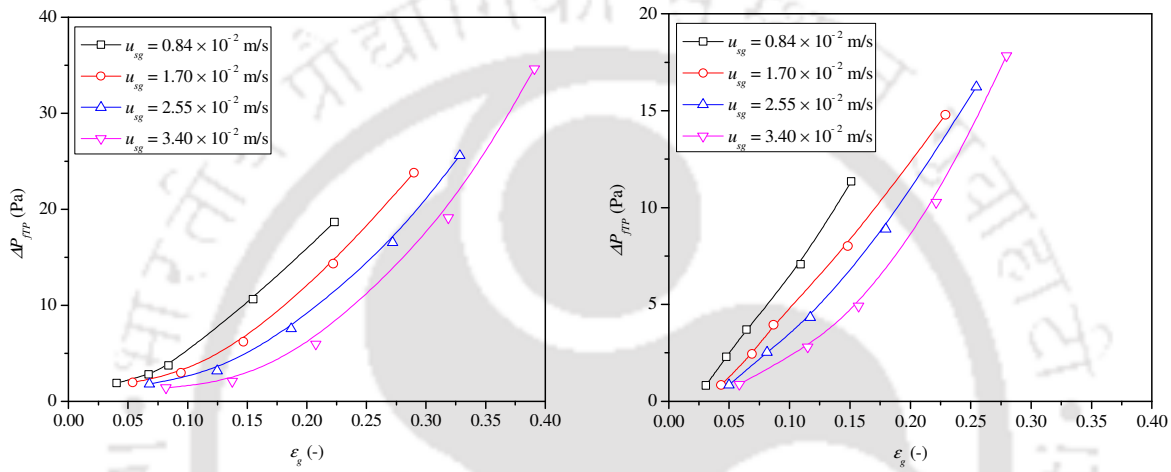

Figure 5.2: Variations of frictional pressure drop with gas holdup at different gas velocity (a) for 35% (v) of paraffin liquid-water, (b) for 35% (v) of kerosene-water

5.4.1.2 Effect of gas and liquid-liquid mixture Reynolds number on frictional pressure drop

The frictional pressure drop variation with gas and liquid-liquid mixture Reynolds number is shown in Figure 5.3a. The frictional pressure drop rises with a rise in liquid-liquid mixture and gas Reynolds number. By increasing the superficial gas velocity, the flow area of the liquid-liquid mixture inside the column decreases due to higher gas holdup, which led to a rise in the frictional pressure drop. A similar trend is also reported by many researchers (Kundu et al., 1995; Babu et al., 1999; Sivaiah and Majumder, 2012; Majumder, 2016). At a fixed superficial gas velocity, with the increase in liquid velocity, the intensity of liquid-liquid mixture inside the

column leads to the coalescence of drops to generate bigger size drops which cause a rise of friction in the column. The frictional pressure drop variation with liquid-liquid mixture and gas Reynolds number at 15% (v) kerosene is shown in Figure 5.3b. It is seen that the frictional pressure drop rises with a rise in liquid-liquid mixture Reynolds number. The frictional pressure drop of kerosene is less than that for the paraffin liquid.

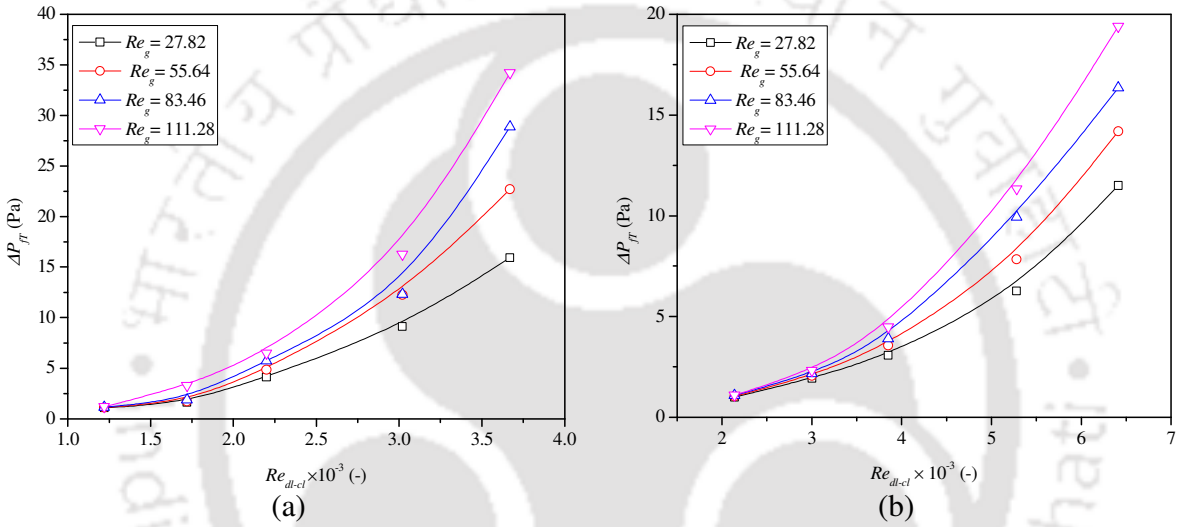

Figure 5.3: Variations of frictional pressure drop with liquid-liquid mixture Reynolds number (a) for 15% (v) of paraffin liquid, (b) for 15% (v) of kerosene

The variations of frictional pressure drop with mixture (liquid-liquid) Reynolds number for a certain holdup of paraffin and kerosene are shown in Figures 5.4a and 5.4b, respectively. It is observed that the frictional pressure drop rises with an increase in the volume of liquid-liquid mixture Reynolds number. However, the frictional pressure drop of dispersed liquids of higher volume (35%) is more than that for the lower volume (15%). This is owed to the higher resistance of the fluid as the liquid-liquid mixture viscosity increases with the amount of dispersed liquid.

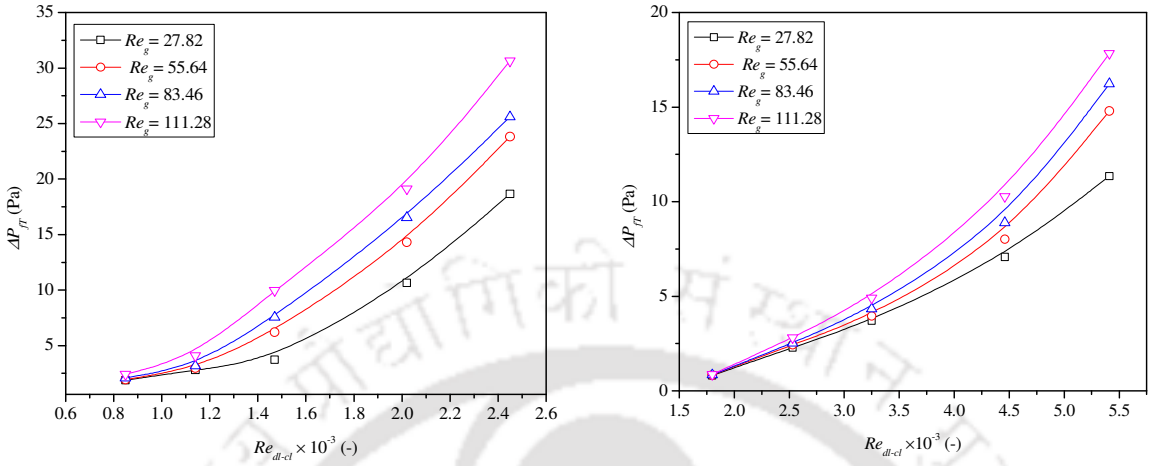

(a) (b)

Figure 5.4: Variations of frictional pressure drop with liquid-liquid mixture Reynolds number (a) for 35% (v) of paraffin liquid, (b) for 35% (v) of kerosene

5.4.1.3 Effect of different dispersed liquid volume on frictional pressure drop

The variation of frictional pressure drop with dispersed liquid volume (for paraffin liquid) is shown in Figure 5.5a. It is found that the increase in dispersed liquid volume increases the frictional pressure drop and the viscosity of the gas-liquid-liquid mixture. Those mentioned above hindered the movement of drops which leads to a decrease in column friction. As increasing the dispersed liquid concentration, the interstitial liquid velocity decreased by the higher friction losses between drops and the viscous liquid medium. The variation of frictional pressure drop with dispersed liquid volume for kerosene is shown in Figure 5.5b. The frictional pressure drop rises with a rise in dispersed liquid volume. The frictional pressure drop is higher for kerosene than that for the paraffin liquid due to the lower viscosity of kerosene.

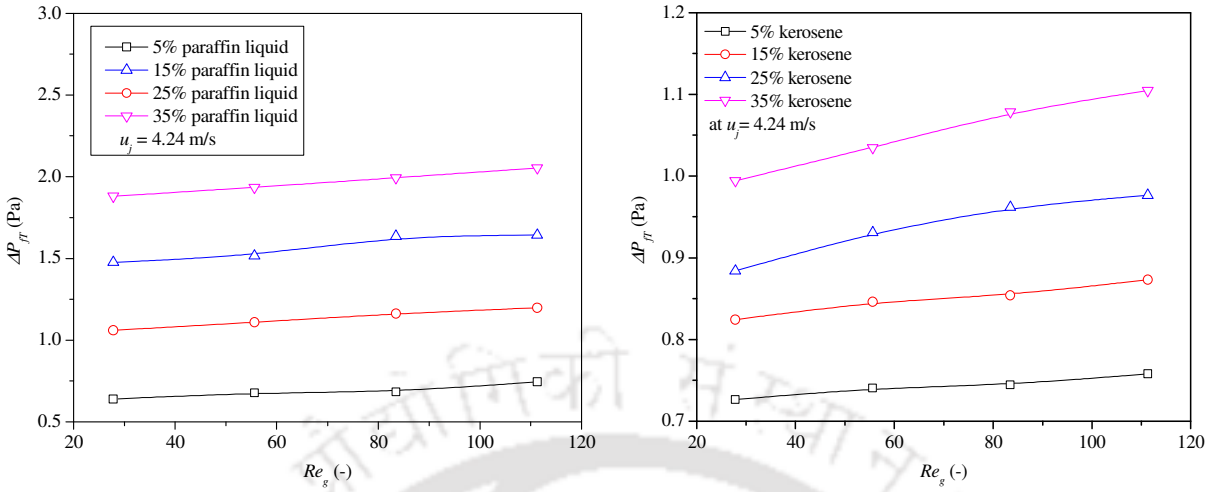

Figure 5.5: Variations of frictional pressure drop with gas Reynolds number at different dispersed concentrations of (a) paraffin liquid, (b) kerosene

5.4.2 Analysis of frictional pressure drop by different models

5.4.2.1 Analysis by Lockhart Martinelli's Model

From the present experimental system, the parameter $\phi_{dl\text{-}cl}$ is correlated as a function of various non-dimensional parameters as:

$$\phi_{dl-cl}^2 = 4.49\times10^{-4}\,\mathrm{Re}_{dl-cl}^{0.25}\,\mathrm{Re}_g^{1.05}\,H_r^{1.66}\,X_{\mathrm{mod}}^{1.87} \tag{5.34}$$

The correlation coefficient (R^2) and the standard deviation (SD) of Equation (5.34) are found to be 0.961 and 0.225, respectively. The frictional pressure drop of the gas-liquid-liquid system is then calculated by the Equation (5.35) as:

$$\Delta P_{fT} = \phi_{dl-cl}^2 \Delta P_{fodl-cl} \tag{5.35}$$

The predicted values of the Lockhart-Martinelli parameter calculated from the Equation (5.34) are plotted against the experimental data are presented in Figure 5.6. From the Figure 5.6, the parity plot between the predicted and experimental values of the Lockhart– Martinelli multiplier

gives the satisfactory results within the range of the system variables of 27.82 < Re_g < 111.28, $8.15\times10^4 < Re_{ll\text{-}cl} < 7.31\times10^4$, 5.81 < X< 60.71 and 19 < H_r < 41.

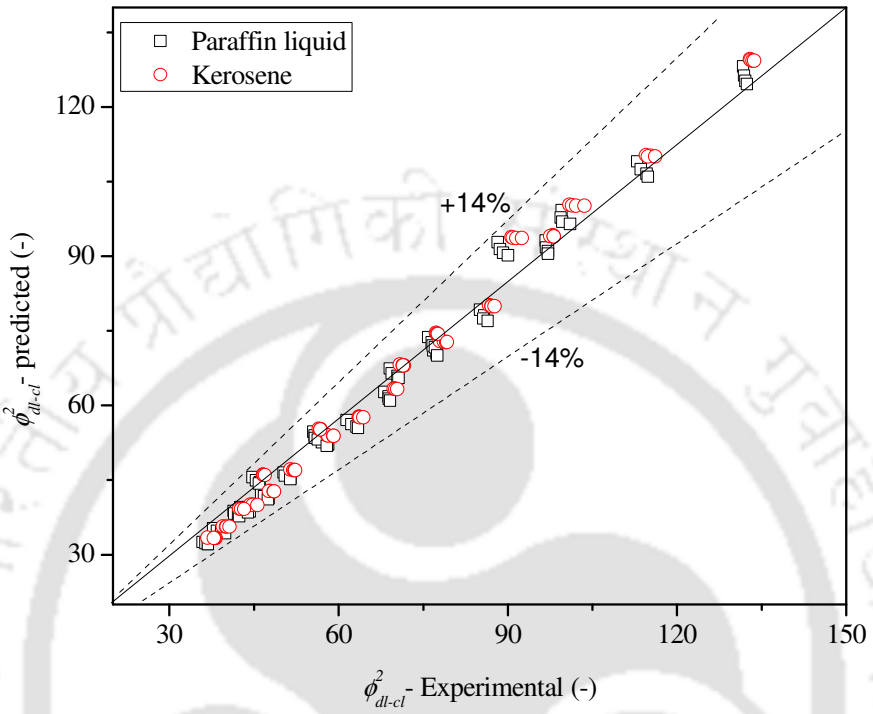

Figure 5.6: Parity plot of calculated values and experimental values of the Lockhart-Martinelli parameter

5.4.2.2 Analysis by Kato (1958) model

The coefficients of the equation (5.22) are obtained by fitting with the present experimental data of the downflow gas-liquid-liquid system. After substituting the coefficient, the Equation (5.22) can be expressed as

$$\phi_{lk}^2 = 4.07\times10^{17}\left(\frac{\dot{m}_{ll-cl}}{\dot{m}_g}\right)^{-3.52}\frac{\mathrm{Re}_g^{-2.46}}{X^2} \tag{5.36}$$

The correlation coefficient and the standard error for the fitted experimental data are 0.712 and 1.094, respectively. The values of the friction multiplier, ϕ_{lk} from Equation (5.36) are used to

calculate the frictional pressure drop as per the Equation (5.35) as follows:

$$\Delta P_{fTP} = \phi_{lk}^2 \Delta P_{f0ll-cl} \tag{5.37}$$

The predicted frictional pressure drop values from Equation (5.37) are compared with the present experimental results for water-paraffin liquid and water-kerosene system of 15% volume of dispersed liquid, as shown in Figure 5.7.

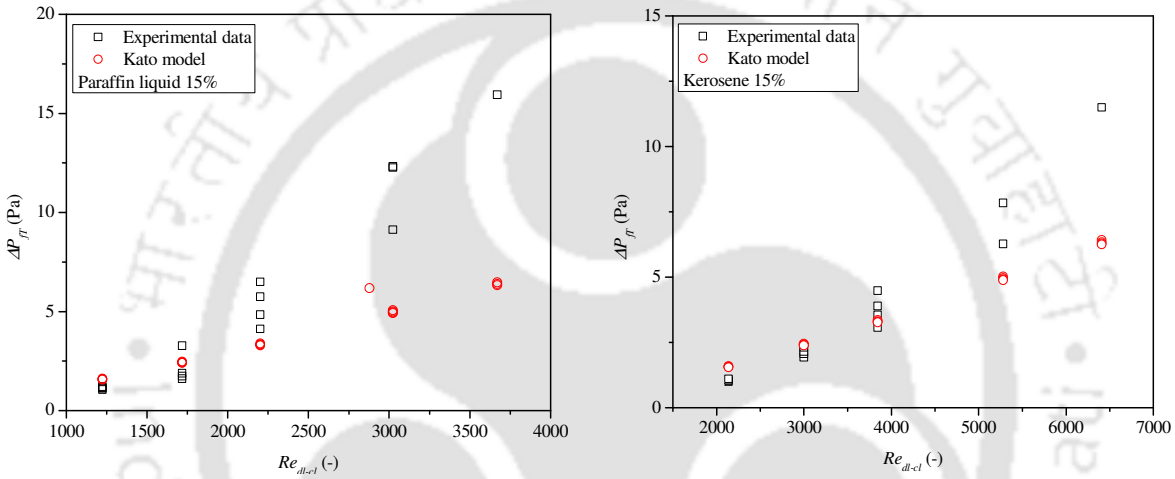

(a) (b)

Figure 5.7: Comparison of experimental data with Kato model (a) for 15% (v) of paraffin liquid (a) for 15% (v) of kerosene

The accuracy of the predicted values to the experimental values is calculated by average absolute percentage error. The average absolute relative percentage error (*AAPE*) is calculated by

$$AAPE = \left[\frac{1}{n} \sum_{i=1}^{n} \left[\left(\frac{\text{predicted} - \text{experimental}}{\text{experimental}} \right)^2 \right]^{1/2} \right] \times 100 \tag{5.38}$$

The average absolute percentage error values of frictional pressure drop for the present experimental data with the values of Kato model is shown in Table 5.2. The frictional pressure drop by the Kato model shows an error of 7.54% with experimental values for water-paraffin

liquid and 5.04% for the water-kerosene system within the range of superficial liquid velocity 0 < u_{sl} ≤ 0.076 m/s.

Table 5.2: Error analysis of different models for 15% of dispersed liquid volume

Model	AAPE (%) of water-paraffin liquid	AAPE (%) of water-kerosene
Lockhart-Martinelli (1949)	1.34	0.96
Kato (1958)	7.54	5.04
Wallis (1969)	27.54	24.10
Gharat and Joshi (1992)	20.82	18.91

5.4.2.3 Analysis by Wallis (1969) model

By fitting the Wallis model with our present experimental data, the model for the downflow gas-liquid-liquid system can be expressed as,

$$\phi_w^2 = 96.63\left(1 + x\frac{\rho_{dl-cl} - \rho_g}{\rho_g}\right)\left(1 + x\frac{\mu_{dl-cl} - \mu_g}{\mu_g}\right)^{6.51} \tag{5.39}$$

The values of the friction multiplier, ϕ_w from Equation (5.39) are used to estimate the frictional pressure drop as per the Equation (5.35) as follows:

$$\Delta P_{fTP} = \phi_w^2 \Delta P_{fodl-cl} \tag{5.40}$$

The predicted frictional pressure drop values from Equation (5.40) are compared with the present experimental results for water-paraffin liquid and the water-kerosene system, as shown in Figure 5.8.

The average absolute percentage error values of frictional pressure drop for the present

experimental data with the values of Wallis model is shown in Table 5.2. The frictional pressure drop values of the Wallis model shows an error of 27.54% with experimental values for water-paraffin liquid and 24.10% for the water-kerosene system within the superficial liquid velocity range of $0 < u_{sl} \leq 0.076$ m/s.

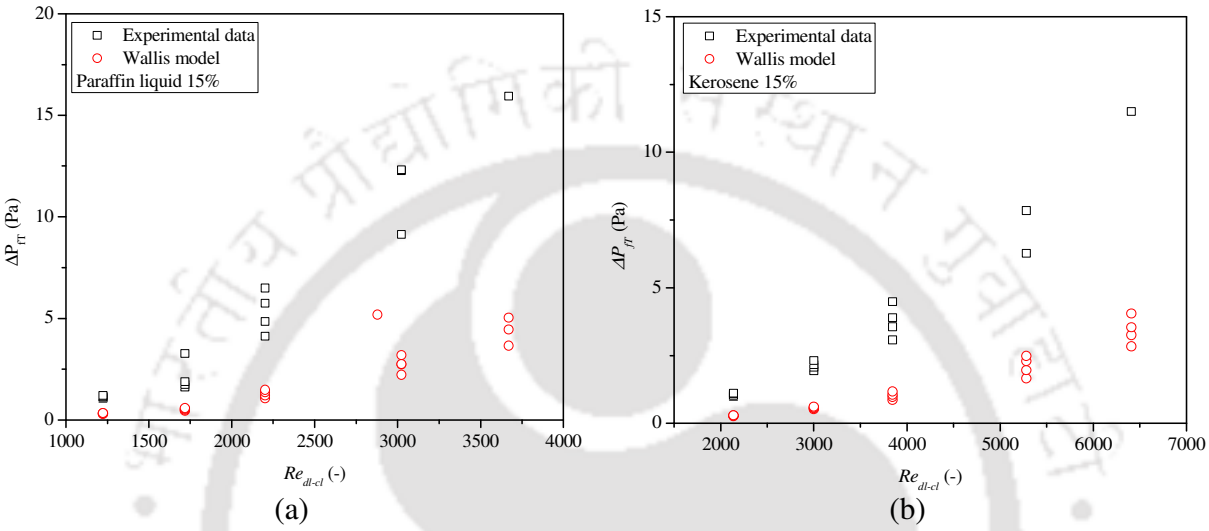

Figure 5.8: Comparison of experimental data with Wallis model (a) for 15% (v) of paraffin liquid (a) for 15% (v) of kerosene

5.4.2.4 Analysis by Gharat and Joshi (1992) model

The two-phase multiplier given by Gharat and Joshi model is modified based on the concept of Clark and Flemmer (1985a,b) within a liquid velocity of 0 to 0.8 m/s, for the downflow column which can be expressed as,

$$\phi_l^2 = \frac{1}{\varepsilon_l^2} + \frac{5.45\varepsilon_g u_s}{\varepsilon_l u_{dl-cl}} \tag{5.41}$$

The Equation (5.41) is used to calculate the frictional pressure drop values as,

$$\Delta P_{fT} = \phi_l^2 \Delta P_{foll-cl} \tag{5.42}$$

The calculated frictional pressure drop values by Equation (5.42) are compared with the present

experimental results, it is found to be satisfactory. The parity plot is shown in Figure 5.9. In Table 5.2, the average absolute percentage error values of frictional pressure drop for the present experimental data with the values of Gharat and Joshi model is shown. The frictional pressure drop values of the Gharat and Joshi model shows an error of 20.82% with the experimental values for water-paraffin liquid and 18.91% for the water-kerosene system within the superficial liquid velocity range of $0 < u_{sl} \leq 0.076$ m/s.

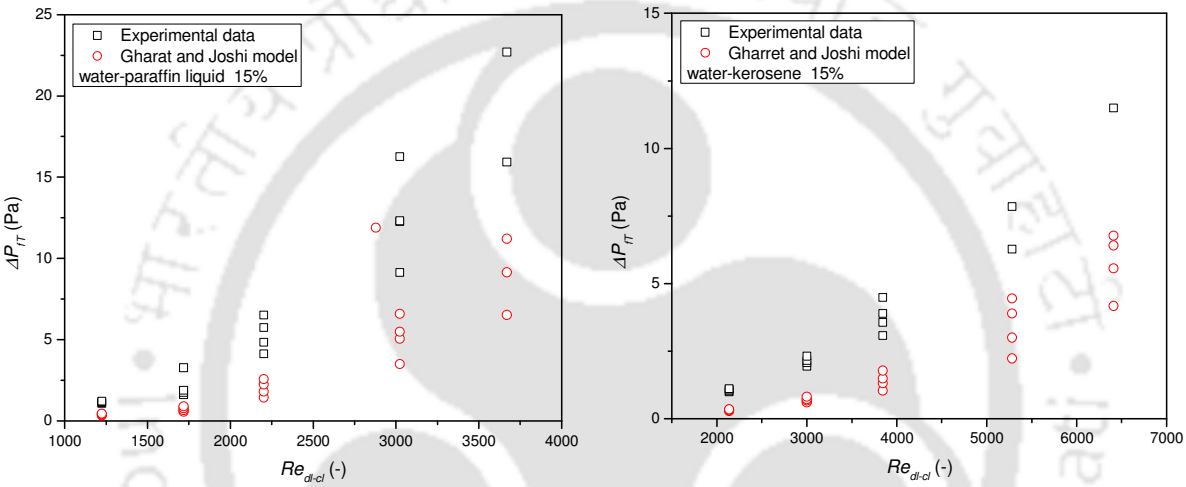

Figure 5.9: Comparison of experimental data with Garret and Joshi model. (a) for 15% (v) of paraffin liquid (a) for 15% (v) of kerosene

The error values shown in Table 5.2 confirm that the modified Lockhart-Martinelli correlation for the present experimental values shows good prediction compared to the Kato (1958), Wallis (1969) models, and Gharat and Joshi (1992) model. The Wallis model shows the highest percentage error and not recommended for the prediction of frictional pressure drop in the downflow column. The Lockhart-Martinelli model can predict the experimental values within an acceptable range for both low and high mixture Reynolds number and can be recommended for the calculation of frictional pressure drop in the ejector induced downflow column.

5.4.3 Prediction of frictional pressure drop by developing a correlation

The three-phase frictional pressure drop correlation is analyzed by dimensional analysis as a function of different operating, geometric variables, and the physical properties of the system. The frictional pressure drop ΔP_{ftp} is expressed as a function of all these different variables of the system as:

$$\Delta P_{ft} = f(u_{cl-dl}, u_G, \rho_G, \rho_{cl-dl}, \mu_G, \mu_{cl-dl}, d_c, g) \tag{5.43}$$

By the dimensional analysis of Equation (5.43) and rearranging dimensional groups, the following functional relation can be written

$$Eu = \lambda \mathrm{Re}_G^{a_1} \mathrm{Re}_{cl-dl}^{a_2} Mo^{a_3} \tag{5.44}$$

From the multiple regression analysis of Equation (5.44) with the present experimental data, the functional form can be represented as

$$Eu = 2.04\times10^{5} \mathrm{Re}_G^{-2.04} \mathrm{Re}_{cl-dl}^{-0.009} Mo^{-0.506} \tag{5.45}$$

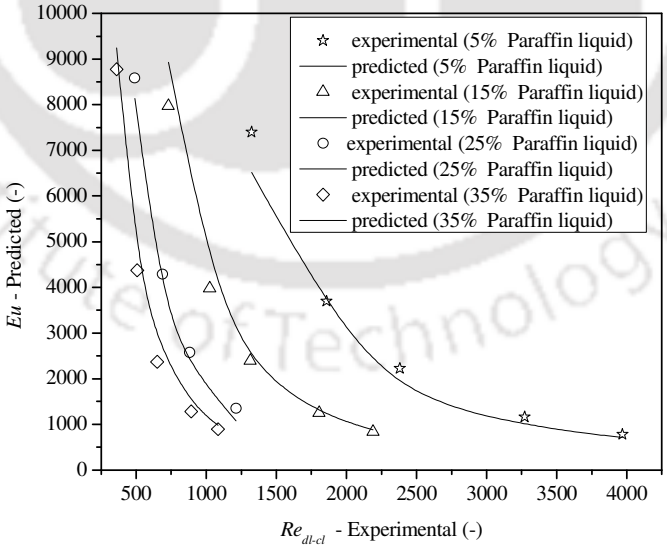

Figure 5.10: Comparison of predicted Euler number with experimental values

The predicted values of the Equation (5.45) is plotted against the experimental data. The predicted values are in excellent agreement with the experimental values, as shown in Figure 5.10 within the overall error of -19 % and +17%.

5.4.4 Prediction of friction factor with dimensional analysis

A correlation for friction factor (as defined in Equation (5.11)) has also been developed by dimensional analysis with different operating variables, geometric variables, and physical properties of the system. The functionality can be expressed as

$$f_{TPL} = f(u_{dl-cl}, u_g, \rho_g, \rho_{dl-cl}, \mu_g, \mu_{dl-cl}, d_c, g) \tag{5.46}$$

By dimensional analysis and regression with the experimental data, the following correlations are resulted

For $\mathrm{Re}_{dl-cl} < 2100$ (Laminar Flow)

$$f_{TPL} = 8.47\times10^{-2}\,\mathrm{Re}_{dl-cl}^{-0.188}\,\mathrm{Re}_g^{0.014}\,Mo^{0.004}\,H_r^{-0.215} \tag{5.47}$$

For $2100 < \mathrm{Re}_{dl-cl} < 4000$ (Transition Flow)

$$f_{TPL} = 4.57\times10^{-2}\,\mathrm{Re}_{dl-cl}^{-0.403}\,\mathrm{Re}_g^{-0.049}\,Mo^{-0.070}\,H_r^{0.065} \tag{5.48}$$

For $\mathrm{Re}_{dl-cl} > 4000$ (Turbulent Flow)

$$f_{TPL} = 1.50\times10^{-1}\,\mathrm{Re}_{dl-cl}^{-0.32}\,\mathrm{Re}_g^{-0.02}\,Mo^{-0.013}\,H_r^{-0.107} \tag{5.49}$$

The predicted values of the friction factor by the above equations are plotted against the experimental data. The predicted values are in good agreement with the experimental values, as shown in Figure 5.11.

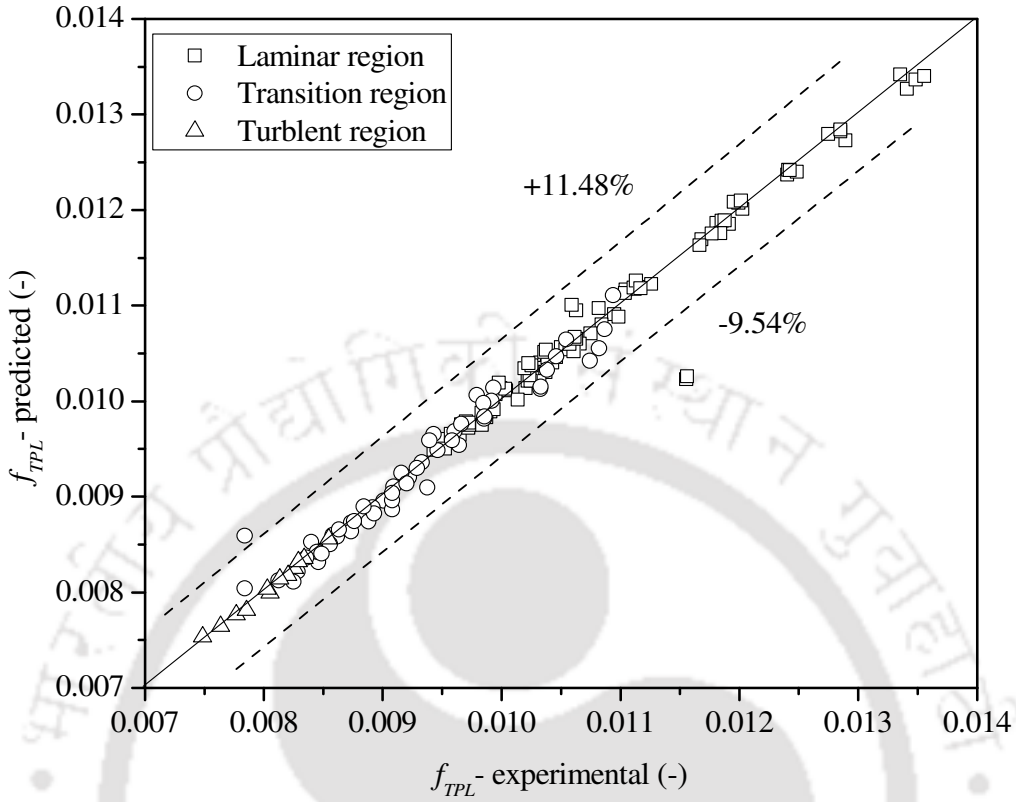

Figure 5.11: Comparison of predicted friction factor with experimental values

5.5 Conclusion

The frictional pressure drop of the gas-liquid-liquid system was experimentally investigated in a jet-driven gas-aided downflow column using two different systems of air-water-paraffin liquid and air-water-kerosene system. The volume fractions of the dispersed liquid is varied from 5 to 35% in the column. The frictional pressure drop rises with a rise in water and gas velocities. The variation of frictional pressure drop is more significant at higher gas velocity as compared to the lower gas velocity. With the rise in the gas holdup of the system, the contact among the droplets and the liquid interface rises, and dispersed liquid droplets generate more friction and turbulence with the gas-liquid-liquid mixture. At a fixed superficial gas velocity, with a rise in liquid jet velocity, the intense mixing by higher momentum exchange inside the column leads to an

increase the friction in the column. With the rise in dispersed liquid concentration, the velocity in the column is decreased due to the higher friction among drops and the viscous liquid mixture. The modified Lockhart-Martinelli model gives good results compared to the Kato, Wallis, and Gharat and Joshi models for both low and high mixture Reynolds number and is recommended for the prediction of frictional pressure drop in the jet-driven downflow column. An empirical correlation is developed for frictional pressure drop and friction factor as a function of various operating variables and the system properties. The correlation has been found to be satisfactory within the range of the experimental data.

CHAPTER - 6

MIXING CHARACTERISTICS

In the previous chapters, characteristics of a gas holdup, entrainment, and pressure drop in the jet-driven downflow column have been reported. This chapter is about the investigations on mixing characteristics as well as the development of a model to analyze the intensity of mixing in the jet-driven downflow column.

6.1 Introduction

Gas-liquid-liquid mixing is an important process for mass transfer in the chemical and biochemical processes. The presence of inert gas in liquid-liquid operation increases the degree of mass transfer and reactions compared to other mixing mechanisms. Some examples of industrial applications of the gas-liquid-liquid system are hydroformylation, carbonylation, and gas-aided physical operations like extraction. The three-phase catalytic reactions are also one of the significant applications of gas-liquid-liquid systems commonly accounted in chemicals and pharmaceutical industries. The catalytic reactions of gas-liquid-liquid three-phase were studied in the conventional unit by several authors (Baidossi et al., 1993; Chaudhari et al., 1995). However, there is a lack of study in the downflow column with the gas-liquid-liquid system though it has a potential advantage for the same on a pilot scale. For scale-up and the proper design of the downflow column with the gas-liquid-liquid system, several hydrodynamic characteristics and the transport processes are essential to study and its interpretation for the suitability of the industrial-scale operation. Recently the chemical operations in the downflow column for various applications are gaining interest in the scientific community for its several advantages such as a finer droplet generation, higher degree of mixing and mass transfer, the

high residence time of the droplet. The previous chapters regarding entrainment and holdup characteristics (Goshika and Majumder, 2018), frictional pressure drop studies (Goshika and Majumder, 2019b) described the proof of concept of the feasibility of gas-liquid-liquid operation in the downflow column.

The residence time distribution of the reactor (RTD) is one of the most informative characteristics of the processing unit, which provides information on the degree of mixing in the unit. Din et al. (2009) studied the residence time (RTD) distribution for a frequency range and amplitude of pulsation on the liquid-liquid extraction in a column of pulsed sieve plates with dispersed water and continuous-phase kerosene. It was reported that the axial mixing and holdup of dispersed phase increases with increasing frequency and amplitude of the pulses until a maximum value is reached. Cheng et al. (2012) studied the mixing time of the continuous phase of gas-liquid-liquid dispersions in a mechanically agitated stirred tank. They reported that the gas-liquid-liquid mixing in the stirred tank was almost similar to that in liquid-liquid, and gas-liquid stirred tanks. The results showed that the mixing is increased at higher gas holdup while it is decreased at lower gas holdup. Velmurgan et al. (2015) studied the residence time distribution of various solvents at a different superficial gas velocity in an external-loop airlift reactor. RTD studies were carried out using a stimulus-response tracer technique. They reported that a reduction in the residence time with increasing gas velocity was due to the intense mixing that lead to the early outcome of the fluid. Most of the past literature for the study of mixing characteristics in the jet-driven downflow column is shown for a two-phase and three-phase flow system. The jet-driven downflow column has the advantage of dispersing the gas without external power requirement, as reported by Majumder (2016). In the jet-driven downflow column, the continuous liquid jet sucks the gas from the atmosphere into the column through the

ejector assembly mounted on the top of the column contactor. The downflow column has the advantage of uniform oil drops and gas bubbles, negligible coalescence of drops, and reduction of back-mixing in the column (Goshika and Majumder, 2018, 2019b). Upadhyay et al. (2009) studied the mixing characteristics in a gas-liquid jet-driven downflow column. The effect of liquid and gas velocity on dispersion number was reported. The dispersion number was found to increase with liquid and gas velocities. Majumder (2008) and Sivaiah and Majumder (2013a) have studied the mixing characteristics in a downflow bubble column. They reported that the longitudinal dispersion coefficient of liquid is significantly influenced by interstitial liquid velocity, gas velocity, and the nozzle and column diameter of the column. At low superficial gas velocity, the dispersion coefficient is to be constant, as reported by Majumder (2008). The mean residence time was found to be higher at lower gas velocity. Also, at higher gas and slurry velocity, the kinetic energy between gas-liquid-solid increased, which enhanced a more mixing in the column and thus increased the dispersion and reduced the residence time of the tracer particle as reported by Sivaiah and Majumder (2013a). When the gas velocity increased, the gas tends to accelerate the liquid in the downward direction and hence the residence time of the fluid decreased in the column. They also observed that with an increase in the superficial gas velocity and slurry velocity, the dispersion coefficient increased. With an increase in the gas or slurry velocity create intense turbulence inside the column, which enhances the mixing of phases and increases the dispersion coefficient. The present work aims to study the mixing characteristics of paraffin liquid-water and kerosene-water flow in the jet-driven gas-liquid-liquid downflow column, which may be useful for the application of gas-aided liquid-liquid extraction in such column for process intensification of extraction.

6.2 Experimental setup and procedure

The details of the experimental setup are described in Chapter 2. At the initial stage, the system was allowed to attend steady-state, from the port P_2, 10 ml tracer of 0.1 N NaCl solution was quickly injected inside the column, and for every 3 seconds, time interval the liquid mixture samples were collected in the tubes at the column outlet. The collected samples were measured using the electrical conductivity meter (Model: VSI-04 ATC Deluxe, VSI Electronics Pvt. Ltd., India). This RTD study was conducted at different liquid and gas flow rates within the ranges: 11×10^{-5} – 2.06×10^{-5} m^3/s and, 1.67×10^{-5} – 5.0×10^{-5} m^3/s respectively and at three different concentrations by volume of dispersed liquid (paraffin liquid and kerosene) at ambient condition.

6.3 Theory of estimation of the intensity of mixing

Due to the penetration of the liquid jet, the dispersed liquid is dispersed in the downer. At low liquid jet velocity, the dispersion is limited to the mixing zone of the plunging jet. However, at the high liquid jet velocity, the dispersed liquid is dispersed through the whole column. The degree of dispersion (defined by dispersion number, N_d) depends on the kinetic energy of the liquid jet. It is seen that for a higher liquid jet, due to higher kinetic energy, to disperse the dispersed liquid and to reach it to an endpoint of a downer, it takes some minimum time due to balance of the downward flow of dispersed liquid against its buoyancy. After the minimum time, the liquid is dispersed and reside in the downer. The residence time is estimated by collecting the sample from the end of the downer with respect to time and measuring the concentration of the collected sample. The results of changing the concentration with time are analyzed by the axial dispersion model (Rathilal et al., 2013) as follows

$$\frac{\partial c}{\partial t} = D_{ax}\frac{\partial^2 c_v}{\partial x^2} \tag{6.1}$$

where the parameter D_{ax}, is called longitudinal or axial dispersion coefficient, uniquely characterizes the degree of axial dispersion flow. Generally, for column diameter, smaller than 5 cm is considered a negligible effect of radial distribution compared to axial or longitudinal dispersion. The axial mixing is mainly due to fluid velocity gradients. In a dimensionless form where z = (ut + x)/L and $\theta = t/\bar{t} = tu/L$, the primary differential equation representing the dispersion model becomes

$$\frac{\partial c}{\partial \theta} = N_d \frac{\partial^2 c}{\partial z^2} - \frac{\partial c}{\partial z} \tag{6.2}$$

where the dimensionless group (N_d), called the vessel dispersion number (D_{ax}/uL), is the parameter that measures the degree of axial dispersion. Thus $N_d \rightarrow 0$ indicates negligible dispersion, hence plug flow whereas $N_d \rightarrow \infty$ indicates large dispersion and hence mixed flow. The solution for the model based on open-open boundary condition can be expressed which is expressed as (Levenspiel, 1972)

$$c(t) = \frac{\int_0^t c(t)dt}{2t_m\sqrt{\pi\theta N_d}} \exp\left[-\frac{(1-\theta)^2}{4\theta N_d}\right] \tag{6.3}$$

where c is the concentration of tracer in the gas-liquid-liquid mixture in the column. As per moment method, the parameters of the model can be estimated by

$$t_m = \frac{\sum(t_i c_i)}{\sum c_i} \tag{6.4}$$

$$N_d = \frac{1}{8}\left[\sqrt{1+8\sigma_\theta^2} - 1\right] \tag{6.5}$$

where

$$\sigma_\theta^2 = \frac{1}{t_m^2}\frac{\sum(t^2 c_i)}{\sum c_i} - 1 \tag{6.6}$$

6.4 Results and discussion

The degree of mixing in the downflow column is influenced by superficial liquid velocity, gas velocity, and dispersed liquid concentration. The effects of the different operating variables on the mixing intensity are discussed in the subsequent section.

6.4.1 Effect of different variables on residence time distribution (RTD)

6.4.1.1 Effect of gas and liquid flow rate

The effects of superficial gas velocity for paraffin liquid-water and kerosene-water on the residence time of the tracer is shown in Figure 6.1. It is observed that just after the tracer injection, the tracer concentration is zero initially up to a certain time. When the tracer is injected into the column, the particles of the tracer begin to mix into the column, and mixing of the tracer occurs after a certain time. When the tracer moves downwards, a more intense mixing is observed. Figure 6.1 shows the variation of tracer concentration collected with the time at the lower gas velocity. The tracer concentration is found to be higher compared to that at the higher gas velocity. It is because, at the lower gas velocity, there is a uniform mixing of the liquid-liquid mixture, which enhanced the rate of liquid dispersion and the more residence time for tracer particles inside the column. The effect of the velocity of the liquid on the residence time of the tracer particle is shown in Figure 6.2. It is observed that the residence time of the tracer particle decreases with the increase in the superficial liquid velocity. At a higher liquid velocity (u_{sl} = 0.104 m/s), more energy is dissipated for the gas-liquid-liquid mixture, which improves the dispersion of the liquid in the column. This allows the residence time distribution (RTD) of the tracer particle to vary with the superficial liquid velocity. At a lower liquid velocity (u_{sl} = 0.042 m/s), the entrainment of the gas is relatively low and causes no internal circulation in the gas-liquid-liquid mixture. At a higher liquid velocity (u_{sl} = 0.104 m/s), the flow fluctuations and the

internal circulation of the gas-liquid-liquid mixture in the column will be higher. This can vary the area under the curves, as shown in Figure 6.2.

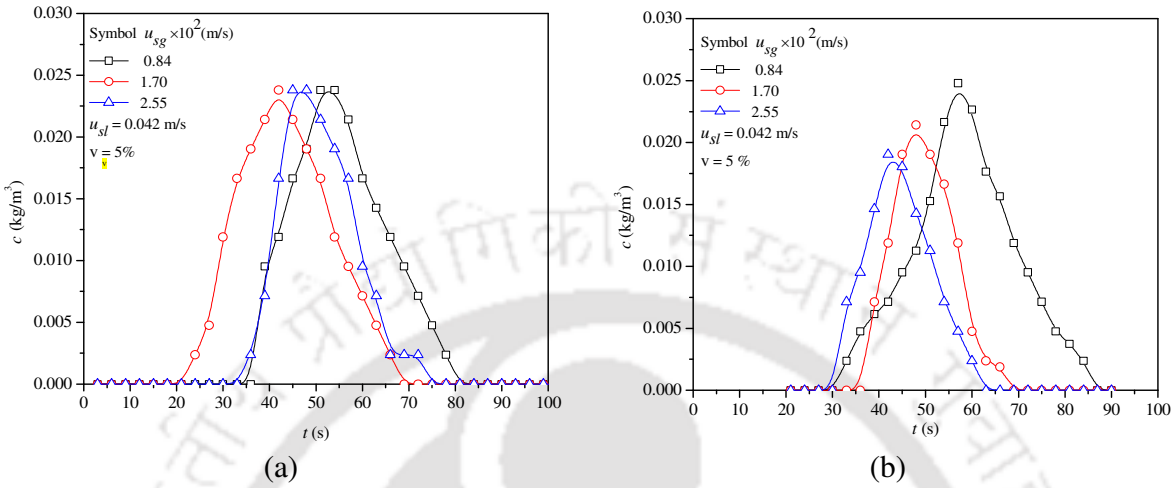

Figure 6. 1: Variations of residence time distribution of tracer with gas velocity for (a) paraffin liquid and, (b) kerosene

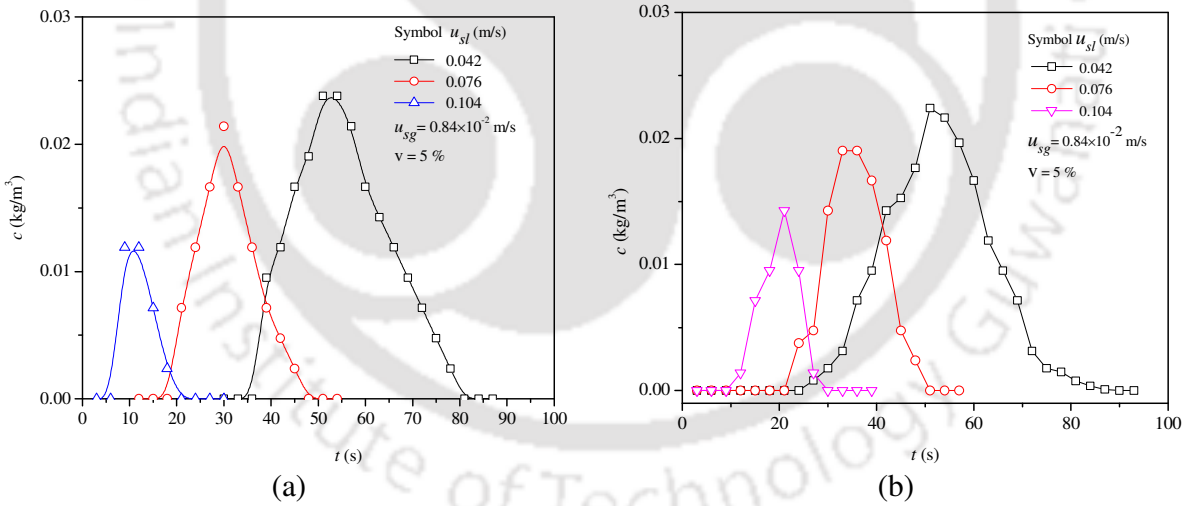

Figure 6. 2: Variations of residence time distribution with liquid velocity for (a) paraffin liquid and, (b) kerosene

6.4.1.2 Effect of dispersed liquid volume on RTD

The variation in the residence time of the tracer particle with the dispersed liquid volume

concentration is shown in Figure 6.3. At constant liquid and gas velocities, it is observed that the residence time of the tracer particles increases with an increase in the dispersed liquid volume concentration. As the concentration of dispersed liquid increases, the viscosity of the liquid-liquid mixture increases, which resists the downward movement of the tracer particles in the column. From Figures 6.3a and 6.3b, it is observed that the residence time of the tracer particle of the paraffin liquid is higher than that of the kerosene. The flow resistance of the tracer particle is higher in the paraffin liquid because the viscosity of the paraffin liquid is higher than that of kerosene.

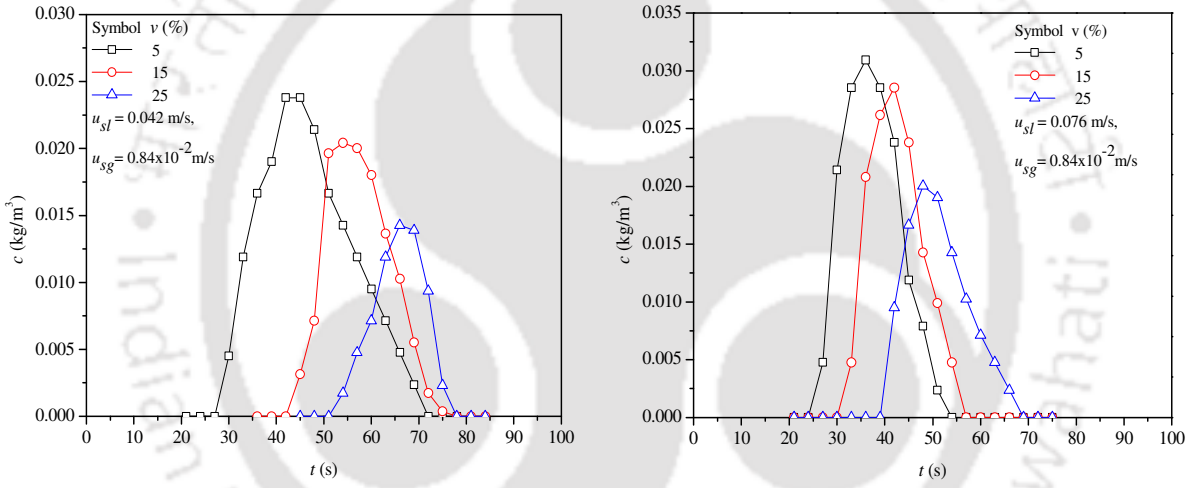

Figure 6.3: Variations of residence time distribution of tracer with dispersed liquid volume concentration (a) paraffin liquid and, (b) kerosene

6.4.2 Effect of gas and liquid flow rate on mean residence time

The effect of the gas and liquid superficial velocity on the mean residence time with a volume of dispersed liquid of 5% is shown in Figure 6.4. From Figure 6.4, it is observed that with an increase in the superficial velocity of the gas and liquid, the mean residence time of the trace

particles in the column decreases. With an increase in the superficial velocity of the gas, the volume of liquid-liquid mixture in the column decreases due to the increase in gas holdup, which decreases the mean residence time. As the superficial gas velocity increases, the axial dispersion in the column increases (Majumder, 2008). The mean residence time decreases with an increase in the superficial liquid velocity from Figure 6.4. As the velocity of the superficial liquid increases, the momentum of the jet increases the gas-liquid-liquid mixture down, which decreases the mean residence time.

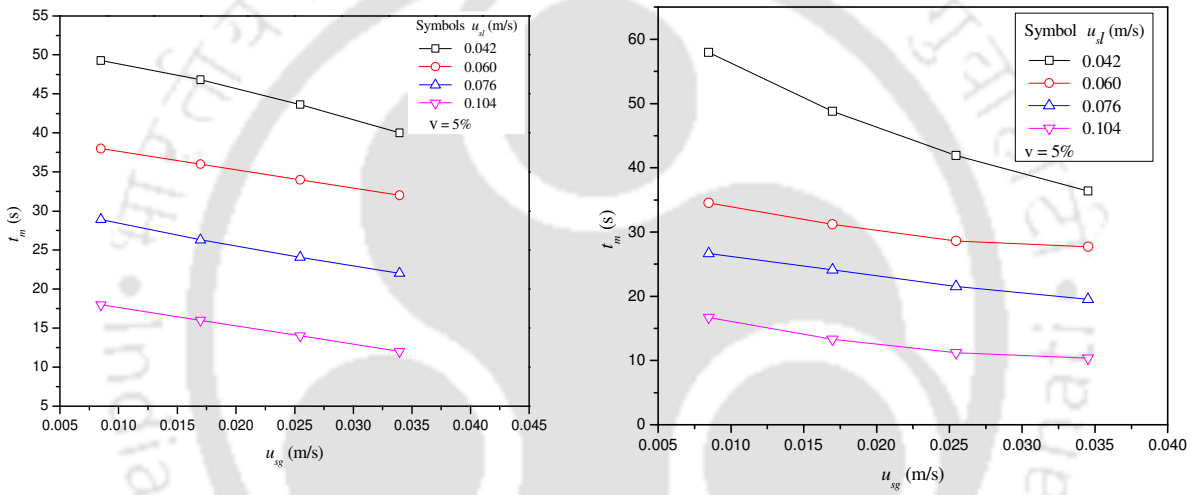

Figure 6.4: Variations of mean residence time with gas and liquid velocities for (a) paraffin liquid and, (b) kerosene

6.4.3. Effect of different variables on dispersion number

6.4.3.1. Effect of gas and water flow rate on the dispersion number

The variation in dispersion number as a function of superficial gas and liquid velocity for 5% v of dispersed liquid is shown in Figure 6.5. It is noticed that the dispersion number increases with an increase in both gas and liquid velocity. The increase in the dispersion number is attributed to the intense mixing of the fluids because of the increase in gas and liquid velocity. From Figure

6.5, at the higher superficial liquid velocity, the dispersion number is high because of the more intense mixing due to the high liquid momentum transfer. The high momentum transfer creates more intense mixing of the gas-liquid-liquid mixture, which increases the turbulence in the column. This can lead to an increase in the dispersion number with the increase in superficial liquid velocity.

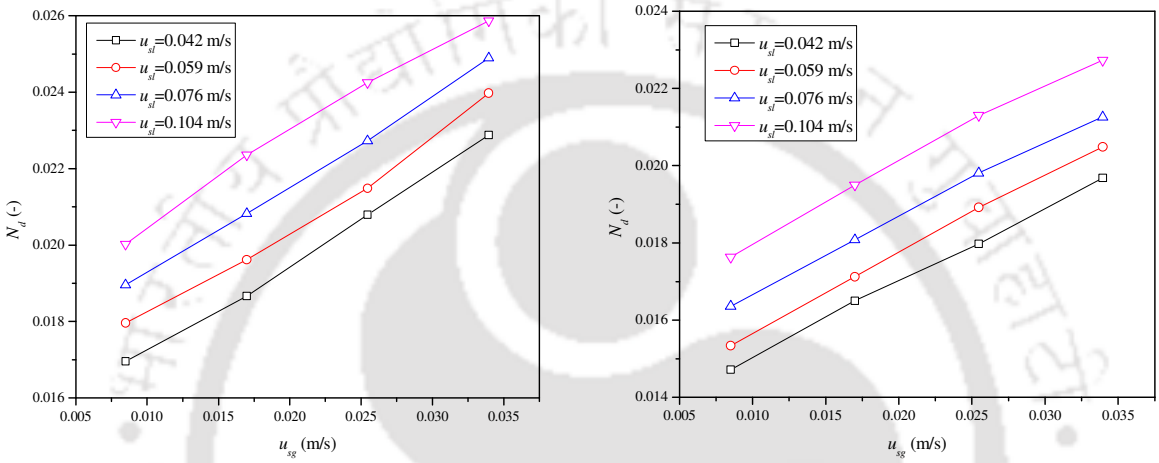

Figure 6. 5: Variations of dispersion number with gas and liquid velocities for (a) paraffin liquid and, (b) kerosene

From Figure 6.5, it can be seen that, with an increase in the superficial gas velocity, the dispersion number increases. As the gas velocity rises, more gas bubbles are formed in the column, which decreases the liquid-liquid mixture flow area in the column. The decrease in the flow area increases the actual velocity of the liquid, which is given as a function of the gas holdup ($v_{cl\text{-}dl} = u_{cl\text{-}dl} / 1\text{-}\varepsilon_g$). This can lead to an increase in the dispersion number. At a low superficial liquid velocity, the liquid jet entrains less gas into the liquid-liquid mixture, which causes the low dispersion number. With an increase in the superficial liquid velocity, more gas is entrained into the column (Goshika and Majumder, 2018). As a result, an intense mixing

between the phases occurs which increases the dispersion number. The variation of the dispersion number (N_d) with the gas holdup at a dispersed liquid volume of 5% v is shown in Figure 6.6. From Figure 6.6, it can be observed that the dispersion number is higher in paraffin liquid compared to the kerosene. This is due to the low viscosity of the kerosene which disperses quickly in the column at low gas holdup.

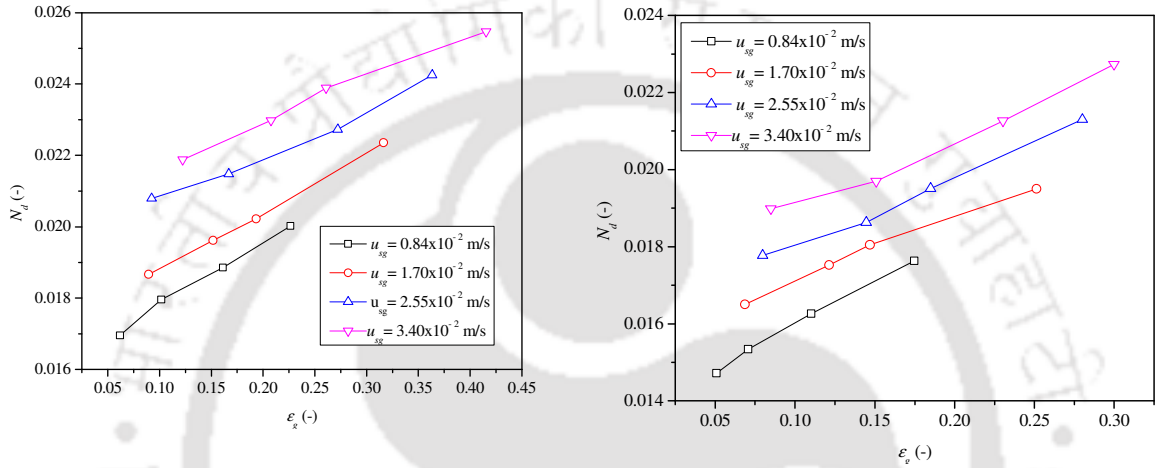

(a) (b)

Figure 6. 6: Variations of dispersion number with gas holdup for (a) air-paraffin liquid -water (b) air-kerosene –water

6.4.3.2 Effect of dispersed liquid volume on dispersion number

The variation of dispersion number with the volume of dispersed liquid at constant superficial gas velocity is shown in Figure 6.7. It is noted that the dispersion number increases with an increase in the volume of dispersed liquid. More droplets are formed with an increase in the volume of dispersed liquid, which increases the dispersion number. At lower concentrations, less liquid droplets formed, and more gas bubbles are there as compared to that at higher concentrations. As a result, the degree of mixing reduced results in less dispersion.

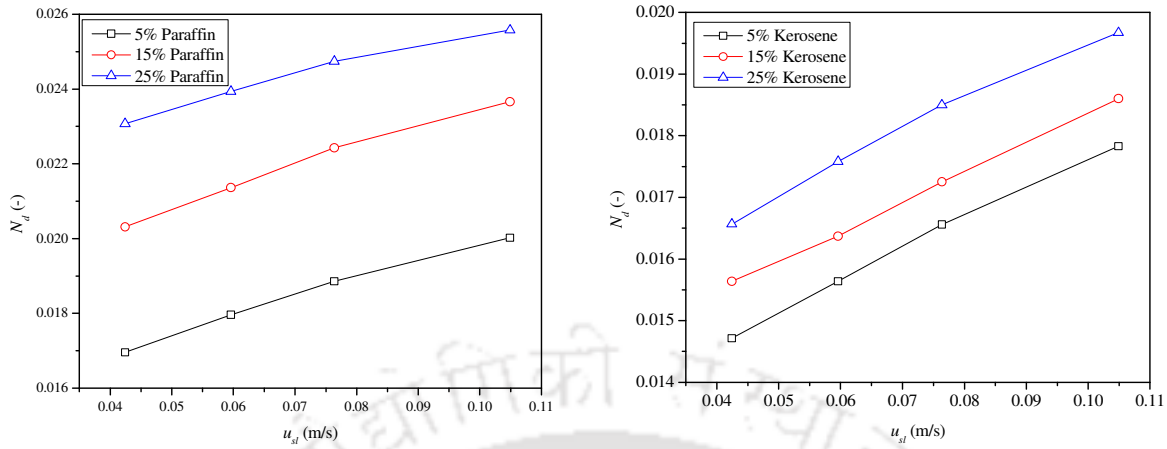

(a) (b)

Figure 6.7: Variations of dispersion number with dispersed liquid concentration for (a) paraffin liquid and, (b) kerosene

6.4 Analysis of the degree of mixing based on flow resistance

It is seen that the dispersion increases with the increase in jet velocity due to the jet kinetic energy supplied for dispersion, whereas it is decreased with the dispersed liquid holdup as the overall viscosity of the liquid mixture increases with the increase in the holdup of dispersed liquid. The kinetic energy distribution in the column depends on the overall resistance of the flow. The degree of mixing can be modeled in terms of the overall resistance of the flow as:

$$N_d = a \ln\left(\frac{1}{R_t}\right) - b \tag{6.7}$$

The coefficient *a,* and *b* can be obtained by fitting the model with experimental data. The overall resistance of the flow can be expressed as the summation of frictional resistance, hydrostatic resistance, and the acceleration or decelerative flow resistance which can be mathematically represented by

$$\frac{1}{R_t} = \frac{1}{R_f} + \frac{1}{R_h} + \frac{1}{R_d} \tag{6.8}$$

where R_t is the total resistance to flow, R_f is the frictional resistance to flow, R_h is the hydrostatic resistance to flow, and the resistance due to deceleration of liquid jet is R_d. The frictional resistance can be represented by

$$R_f = \frac{1}{A_c}\left[\Delta P_{TP} - \left(h_m \rho_{cl-dl}\left(1-\varepsilon_g\right)g\right) - \left(u_{cl}^2 \rho_{cl-dl}\left[\frac{d_c^2}{d_j^2} - \frac{1}{\left(1-\varepsilon_g\right)}\right]\right)\right]^{-1} \tag{6.9}$$

The hydrostatic resistance and the resistance due to deceleration (R_h) can be calculated respectively by

$$R_h = \frac{1}{A_c[h_m \rho_{cl-dl}\left(1-\varepsilon_g\right)g]} \tag{6.10}$$

and

$$R_d = \frac{1}{A_c}\left[u_{cl}^2 \rho_{cl-dl}\left\{\frac{d_c^2}{d_j^2} - \frac{1}{\left(1-\varepsilon_g\right)}\right\}\right]^{-1} \tag{6.11}$$

From the current study, it can be seen that the coefficients a and b depend on the volume fraction of dispersed liquid which can be expressed as follows

$$a = 0.693 - 0.750\varepsilon_{dl} \tag{6.12}$$

$$b = 1.9127 - 1.610\varepsilon_{dl} \tag{6.13}$$

6. 5 Analysis of degree of mixing based on penetration depth

The dispersion also increases with the increase in penetration depth. The degree of dispersion can be modeled in terms of the depth of the penetration of the liquid jet as

$$N_d = p\left(H_p\right)^q \tag{6.14}$$

The coefficients p and q in the Equation (6.14) can be obtained by fitting the model with

experimental data. From the present study, it is seen that those coefficients depend on the volume fraction of dispersed liquid which can be expressed as follows

$$p = 0.1544 - 0.265\varepsilon_{dl} \tag{6.15}$$

$$q = 0.592(\varepsilon_{dl})^{0.0826} \tag{6.16}$$

6.6 Mixing based on the velocity distribution model

Form the present experimental data, the dispersion number exhibits mixing performance depending on superficial liquid, superficial gas velocities, and dispersed liquid volume fraction. In this section, a model is developed to interpret the mixing behavior based on the velocity distribution model.

6.6.1 Velocity distribution model

In the bubble-droplet flow condition, liquid flows in the vertical direction, with a wide velocity distribution over the column cross-section. Liquid mixing takes place under the combined action of velocity variation and the motion of gas bubbles in the liquid. This is the basis for the model of velocity distribution, which is developed on the basis of Taylor's model [Taylor (1953)].

6.6.1.1 Model equations

According to Taylor (1953), when a non-uniform velocity stream transports a solute, the dispersion of the homogeneous system in the tube occurred. Aris (1956) generalized Taylor's work using the method of moments approach and obtained a general type of coefficient of dispersion as follows:

$$D_{ax} = \frac{d_c^2 u_o^2}{kD_m} + D_m \tag{6.17}$$

where u_o and D_m are the maximum velocities on the column axis, and the molecular diffusion coefficient, respectively, and the constant k determines the shape of the velocity distribution.

In the current gas-liquid-liquid downflow column, the Equation (6.17) was used to analyze the dispersion coefficient of the dispersed fluid motion, assuming that the flow is homogenous in the column, the uniform distribution of the dispersed liquid and the continuous mixing of the fluid. Based on these assumptions the molecular dispersion in Equation (6.17) is replaced with dispersion coefficient due to motion of droplet as

$$D_{ax} = \frac{d_c^2 u_o^2}{kD_d} + D_d \tag{6.18}$$

where D_d is the dispersion coefficient due to the motion of droplet. In the steady-state downflow system, the velocity in the center of the column is twice the average velocity (Majumder, 2016), which is expressed as

$$u_o = 2v_{cl-dl} \tag{6.19}$$

where u_o is the axial velocity of liquid-liquid mixture and $v_{cl\text{-}dl}$ is the average velocity which is defined as

$$v_{cl-dl} = \frac{u_{cl-dl}}{1-\varepsilon_g} \tag{6.20}$$

where $u_{cl\text{-}dl}$ is the superficial liquid velocity of the liquid-liquid mixture, and ε_g is the gas holdup. From the Equations (6.19) and (6.20) the overall dispersion coefficient can be written as

$$D_{ax} = \frac{4d_c^2 v_{cl-dl}^2}{kD_d} + D_d \tag{6.21}$$

6.6.2 Estimation of parameters D_d and k

The values of the droplet motion dispersion coefficient (D_d) and the velocity characteristic factor

(k) at different experimental conditions can be determined from the Equation (6.21) by plotting the overall dispersion coefficient (D_{ax}) versus the term ($4d_c^2 v_{cl-dl}^2$). These values are calculated at different experimental conditions from the slopes ($1/kD_d$) and the intercepts (D_d). The value of the characteristic factor of velocity distribution (k) is calculated from the reciprocal of the slope product and intercept.

$$\text{K= [slope} \times \text{intercept]}^{-1} = \left[\frac{1}{kD_d} \times D_d\right]^{-1} \tag{6.22}$$

From the experimental results, it is seen that at various experimental conditions the values of D_d and k vary. A model for D_d and k based on operational conditions are developed to predict the same. The correlations can be expressed as,

$$D_d = \gamma(u_{sg})^{\beta} \tag{6.23}$$

Where,

$$\gamma = 1.39\phi_{dl}^{\ 2} - 29.47\phi_{dl} + 237.24 \tag{6.24}$$

$$\beta = 0.002\phi_{dl}^{\ 2} - 0.03\phi_{dl} + 1.14 \tag{6.25}$$

$$k = A(u_{sg})^2 + B(u_{sg}) + C \tag{6.26}$$

where u_{sg} is the superficial gas velocity and, ϕ_{dl} is the volume concentration of the dispersed phase in the gas-liquid-liquid mixture.

$$A = -57.91\phi_{dl}^{\ 2} + 216.66\phi_{dl} - 935.04 \tag{6.27}$$

$$B = 4.17\phi_{dl}^{\ 2} - 141.88\phi_{dl} + 514.52 \tag{6.28}$$

$$C = -0.06\phi_{dl}^{\ 2} - 2.16\phi_{dl} - 6.32 \tag{6.29}$$

6.7 Development of general correlation for axial dispersion coefficient

A general empirical correlation for the gas-liquid-liquid system is developed for the prediction of the axial liquid dispersion coefficient based on the present experimental results. In the present study, the significant variables are considered to derive the correlation model. It is observed that the axial dispersion coefficient is a function of superficial liquid velocity, superficial gas velocity, the viscosity of the gas and liquid mixture, the density of gas and liquid mixture, the diameter of the column, interfacial tension, gravity, and height of the gas-liquid-liquid mixture. Based on the experimental data, the empirical correlation is expressed as a function of physical and dynamic variables of the system as,

$$D_{ax} = f\left(u_{sl}, u_g, \mu_{cl-dl}, \mu_g, \rho_{cl-dl}, \rho_g, \sigma_{cl-dl}, g, d_c, h_m, L\right) \tag{6.30}$$

From the Buckingham Pi theorem, the dimensional analysis of the above equation yields,

$$D_{ax} = f\left(\frac{u_{sl}}{u_{sg}}\right)\left(\frac{\rho_l}{\rho_g}\right)\left(\frac{\mu_{cl-dl}}{d_c u_{cl-dl}\rho_{cl-dl}}\right)\left(\frac{\mu_g}{d_c u_{cl-dl}\rho_{cl-dl}}\right)\left(\frac{\sigma}{d_c u_{cl-dl}^2 \rho_{cl-dl}}\right)\left(\frac{g d_c}{u_{cl-dl}^2}\right)\left(\frac{d_c}{h_m}\right)\left(\frac{d_c}{L}\right) \tag{6.31}$$

Incorporating the dimensional groups from the dimensional analysis, the following functional form was obtained for air-water-paraffin and air-water-kerosene systems,

$$\frac{D_{ax}}{u_{cl-dl} L} = f\left(\mathrm{Re}_{cl-dl}\right)^a \left(\mathrm{Re}_g\right)^b \left(We\right)^c \left(Fr\right)^d \left(H_r\right)^e \tag{6.32}$$

By multiple regression analysis with the experimental data, the functional relationship was deduced as follows:

$$Pe = 3.06\times10^{-2}\,\mathrm{Re}_j^{0.49}\,\mathrm{Re}_g^{-0.29}\,We^{0.19}\,Fr^{-0.73}\,Hr^{-0.54} \tag{6.33}$$

where Pe is the Peclet number ($V_l L/D_{ax}$). The proposed correlation is valid for predicting the dispersion coefficient within the ranges: 27.82 < Re_g < 83.46, 1005.8 < Re_j < 7186.7, 1.45 < We < 24.46, 0.004 < Fr < 0.065, 19 < Hr < 41. Equation (6.33) is found to predict the experimental values with a correlation coefficient of 0.97 and a standard error of 0.032. Figure 6.8 shows the parity plot of the experimental Peclet number values and that calculated by the Equation (6.33).

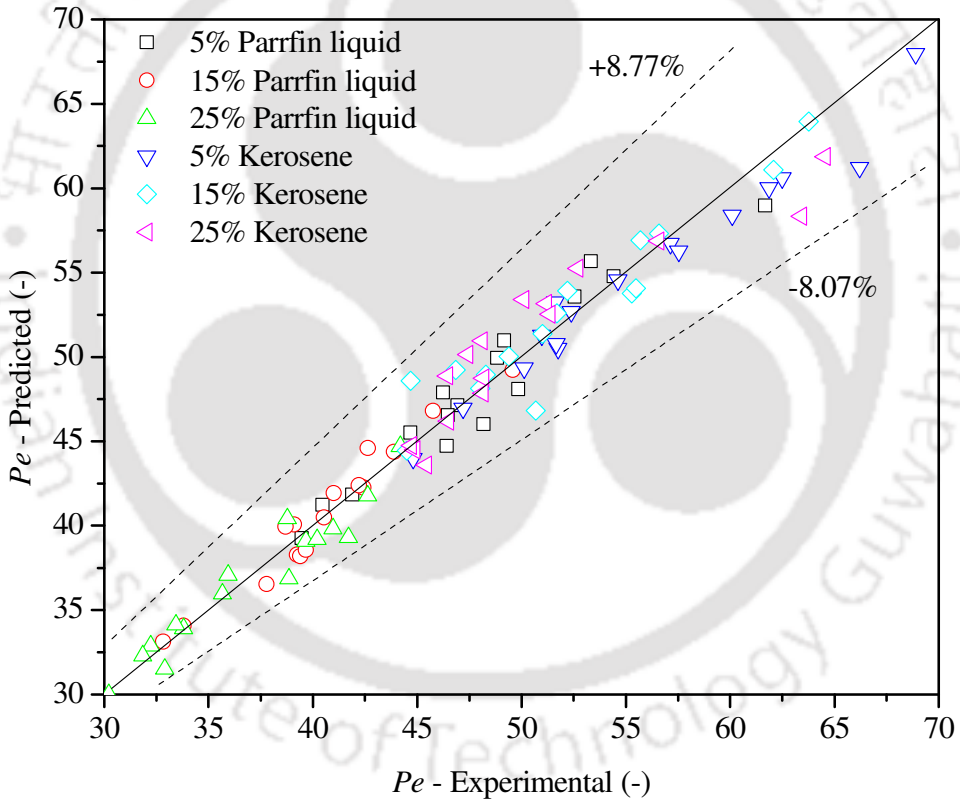

Figure 6. 8: Parity plot for Peclet number (Pe_l) for the gas-liquid-liquid system

6.8 Conclusions

In present work, an attempt has been made to study the mixing characteristics in the gas - liquid-liquid system. It has been found that the mixing phenomenon in this downflow column is

affected by variables such as gas flow rate, liquid flow rate, the concentration of the dispersed liquid. The tracer's mean residence time is greatly affected by the superficial liquid and gas velocities. The dispersion number increases with an increase in superficial liquid and gas velocity. The variation of the degree of dispersion is enunciated based on the velocity distribution model. The dispersion coefficient is predicted from the velocity distribution model, as a function of the dispersion coefficient due to the motion of droplet (D_d) and the characteristic velocity factor (k). The correlations developed by dimensional analysis for predicting the degree of dispersion as a function of different operating variables are satisfactory within the range of the experiments.

CHAPTER - 7

DROP SIZE CHARACTERISTICS AND DISTRIBUTION

In this chapter, the drop size and its distribution are enunciated as a function of superficial liquid, superficial gas velocities, and dispersed liquid concentration. The experimental drop size results are fitted with different distribution models. Correlations for estimating distribution function parameters are developed. An empirical correlation is developed for drop size and interfacial area by considering geometrical, operating variables, and the physical properties of the system.

7.1 Introduction

The Knowledge of drop size and its distribution is of paramount importance in the performance analysis and design of a liquid-liquid extraction column (Kumar and Hartland, 1996). Drop size affects the dispersed phase holdup, and the residence time of dispersed droplets (Kirou et al., 1988). Furthermore, drop size together with dispersed phase holdup is used to determine the interfacial area available for mass transfer. The interfacial area, in turn, indicates the mass transfer efficiency and affects both the dispersed and continuous phase mass transfer coefficients (Hemmati et al., 2015). Yoshida (1971) measured the average diameter of kerosene drops dispersed, which were operated batch-wise in vertical tubes. The mean drop diameter was correlated with the power input per unit mass of liquid and dispersed phase concentration. The average drop size was found to be a function of power input (power input$^{-0.5}$) and to the volume fraction of oil (volume fraction$^{0.25}$). They also found that, for an equal mean drop size, the power consumption in a vertical tube was much less than that in agitated vessels. Substantiating their claim that bubble columns are more efficient contactors for liquid-liquid systems than mechanically agitated vessels. They did not vary the physical properties of the dispersed phase to asses the drop size. An empirical correlation relating mean drop size to column diameter and

dispersed-phase viscosity was subsequently proposed by Hatate (1976). Kato et al. (1984) carried out experiments in a continuous, multistage column with the kerosene-water-air system and correlated mean drop diameter as a function of superficial gas velocity, total liquid velocity, and free area of a series of horizontal baffle plates. Bensalem et al. (1986) studied Sauter mean drop diameter and drop size distribution in a reciprocating plate extraction column with and without mass transfer, using the liquid system toluene-acetone-water. The measured drop size distribution showed that the first few plates achieved most of the break-up of the dispersed drops. The agitation rate was found to be the predominant factor in determining the mean drop diameter and the total interfacial mass transfer area. They reported that both the drop size distribution and the mean drop diameter affect the mass transfer. The mean drop diameter was smaller when the mass transfer occurred from the continuous to the dispersed phase. Takahashi and Nii (1999) have developed a high-performance multi-stage countercurrent extraction column (i.e. high extraction efficiency and high throughput). (i.e., high extraction efficiency and high throughput). The hydrodynamic behavior and the mass transfer characteristics of the column were studied experimentally. Each stage of the column consists of mixer part, settler part and a drop coalesce part between mixer and settler. The maximum throughput of column was independent of the drop size as the counter-current flow in the dispersion situation was avoided, by which the column is operated at a strong agitation where the extraction efficiency is high due to large interfacial area with small drops. The drop size in the mixer is shown as dependent on the residence time of the dispersed phase as well as the Weber number. The mass transfer characteristics were shown by a rigid sphere model of drop as the drop diameter was finer at a strong agitation in the mixer. Oliveira et al. (2008) studied the hydrodynamic behavior of a short Kuhni column using the binary system of water (continuous phase) and Exxsol D-80 (dispersed

phase). The counter-current flow pattern of the liquid phases was characterized as the Sauter mean drop diameter, drop size distribution and hold-up. Different operating variables such as rotor speed, the flow rate of both liquid phases and column stage were studied. The log-normal probability density function was shown to fit the experimental data along the column. They reported that smaller drops and more uniform drop size distributions were obtained with the increase of rotor speed and column stage number. Usman et al. (2009) studied the effect of drop size in a 5.0 cm pulsed sieve plate liquid-liquid extraction column with a total number of 80 sieve plates using the benzoic acid − kerosene − water system. They concluded that the mean drop diameter decreased more rapidly with increasing pulsation intensities and superficial velocities. The effect was not found to be significant at higher pulsation intensities and higher superficial velocities. They also reported that the drop size was observed to be a function of the operating regimes (mixer-settler, dispersion, and emulsion) of the pulsed sieve-plate extraction column. Lobry et al. (2013) studied liquid-liquid dispersion in co-current disc and doughnut pulsed column. Effects of various variables such as the dispersed phase holdup, the flow rate and pulsation conditions, packing material, and the physical properties on liquid dispersion were investigated. Breakage and coalescence rate models were applied in order to understand the various observed phenomena. They proposed a correlation to predict the mean droplet size depending on various dimensionless numbers characterizing the flow. Concerning the operating variables, an increase in pulsation velocity leads to a smaller mean droplet size. However, with more diluted liquid–liquid dispersion, the mean droplet size obtained was smaller. So, at higher dispersed phase holdup, the coalescence and breakage frequencies balances were modified. Samdavid et al. (2016) studied the drop size distribution for water-kerosene system. They reported that the kerosene droplets present inside the column resembled a shaped as honeycomb

structure where water molecules are encapsulated by a film of kerosene which was resulted before breaking into smaller drops of 5-7 cm. The drop size was within the range of 6 – 8 mm when the continuous kerosene phase changed into a dispersed phase. Beyond the transition velocity, a larger drop size was broken into smaller droplets and swept out of the column along with the water. They concluded that the holdup of kerosene was increased with increased kerosene flow rate leading to the formation of more droplets to break the encapsulated dispersed phase at high liquid throughput. Shirvani et al. (2016) measured drop size distributions using water-kerosene, Exxsol D-80, water-toluene and water-n-butyl acetate in Kühni columns. They reported that with an increase in rotors speed, the larger drop breaks into a smaller droplet and results in coalescence inside the column. They concluded that there was no significant change in drops size found for the flow rate of the dispersed phase. However, the flow rate of the continuous phase resulted in the significant effects of the size of the drop at a higher speed. Hendre et al. (2018) studied the effect of physical properties and operating parameters on drop size, dispersed phase holdup, and axial mixing. They proposed a correlation for the prediction of mean drop size in terms of power consumption per unit volume. A summary of the drop size range obtained by different investigators in various extraction columns is shown in Table 7.1. From the literature survey, it is observed that the intensification of extraction by different extraction columns depends on the size of the droplet. Different investigators proposed different approaches for intensification based on the interfacial area generated by the formation of droplets. Since jet-driven extraction is one of the ways of process intensification, which is gaining interest for its several advantages. One of the main advantages is the formation of fine droplets and possible applications on a large scale. Therefore, in this chapter, the drop size and its distribution are reported based on the present study in the jet-driven gas aided extraction

device.

Table 7.1: Drop size in different extraction columns

Author	Extraction Column	System	Column Geometry	Drop Size (d_{32})
Yu et al. (1989)	Pulsed sieve plate	Kerosene -water	i.d: 0.04 m	0.5 – 4 mm
Sohn and Doungdeethaveeratana (1998)	Horizontal vessel with bottom gas injection	$Cuso_4$- H_2SO_4-H_2O-LIX 860-kerosene	i.d: 0.1425 m	4 – 6 mm
Oliveira et al. (2008)	Short Kuhni column	Water -Exxsol D-80	i.d: 0.15 m,	0.5 – 8.5 mm
Usman et al. (2009)	Pulsed sieve plate	Benzoic acid - kerosene - water	i.d: 0.05 m,	5.32 –1.76 mm
Das et al. (2013)	SMX static mixer	Silicone oil -high fructose corn syrup	i.d: 0.04118 m	5 mm (max)

7.2 Experimental procedure

7.2.1 Mean drop size and interfacial area

The drop size was estimated by a photographic technique followed by the image analysis software. In this technique, the column was surrounded by a 150 mm × 150 mm clear perspex jacket. The jacket was filled with distilled water to avoid the optical distortions caused by the curved surface of the perspex column. The rear part of the column was illuminated by a 500 W halogen lamp, and the opposite wall is covered with a diffusion screen to avoid the undesired

reflections. Then images of different drop zones in the column were taken by the high-speed digital camera. Apart from all the images, good quality images were analyzed by the image processing software to obtain the drop size. The images taken were then processed and improved by image processing software (Digimizer, version: 4.2). The borders of drops were marked, avoiding the overlapped drops. Around 100 – 300 drops were manually be identified in each image. For the consistency of the experiments, three to five images were taken for each operating condition.

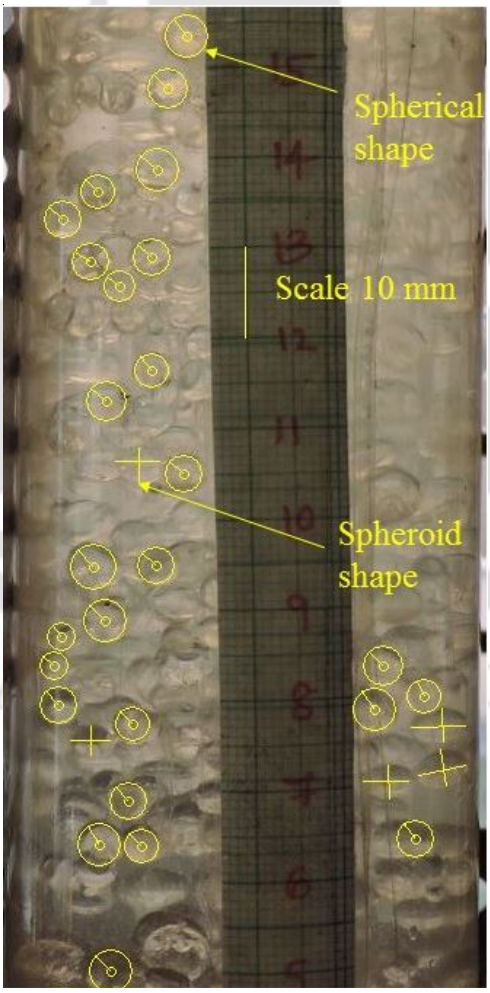

Figure 7.1: Typical image of paraffin droplets at 25% of volume fraction at u_{sg} = 2.5×10^{-2} m/s and u_{sl} = 7.64×10^{-2} m/s.

The mean drop diameter was considered as Sauter mean drop diameter (d_{32}) (also known as the volume-to-surface mean drop diameter) which was calculated by

$$d_{32} = \frac{\sum_{i=1}^{n} d_{di}^{3}}{\sum_{i=1}^{n} d_{di}^{2}} \tag{7.1}$$

where n is the number of classes used for distribution, and d_{di} is the droplet diameter. For the non-spherical droplet, the equivalent diameter (d_{eq}) was calculated by

$$d_{eq} = \left(l_{major}^{2} l_{\min or}\right)^{1/3} \tag{7.2}$$

where l_{major} and l_{minor} are the maximum and the minimum axial length of the droplet. A typical image of the drop size analysis is shown in Figure 7.1.

The specific interfacial area depends on drop size, and it is expressed by the equation:

$$a = \frac{6\varepsilon_{dl}}{d_{d,32}} \tag{7.3}$$

Once the drop size and the liquid hold up were estimated, the interfacial area was calculated by equation (7.3).

7.3 Theory on the drop size distribution

It was pointed out earlier that gas-liquid-liquid mixing occurs in the contactor within the present system. The liquid jet can be arrested in the contactor after coming out of the divergent diffuser, by adjusting the liquid height inside the column. It is observed that when a liquid jet from the nozzle discharges into the fluid with a uniform velocity, a tangential separation surface is formed between the liquid jet and the surrounding medium. The tangential surface instability forms eddies that move both in and across the direction of the flow. This creates a momentum

exchange with the surrounding media. As a result, a region of finite thickness with velocity is formed on the border of the jet and surrounding fluid. When this jet impinges on the liquid surface, it distributed the liquid as a droplet. The entrained liquid undergoes subsequent breakdown and disintegrates as fine droplet within a finite length, called mixing zone. In the intense mixing zone, jet energy is utilized to form the fine liquid droplet, which interacts with dispersed gas. The region below the intense mixing zone is referred to as a homogeneous bubble-drop distribution zone. The homogenous bubbly – drop flow zone consists of a relatively slow-moving packed bed of drops. The distributions are obtained by sorting the equivalent diameters of drops into different uniform classes. In the present experimental conditions, to measure the number density or drop size distribution at each run, the size of drops was divided into ten classes. In Tables, 7.2-7.3 typical range of drop size for each class is shown.

Table 7.2: Discretization in drop classes for 15% paraffin liquid at $u_{sg} = 0.84 \times 10^{-2}$ m/s and at different jet velocities

Bin	Frequency at u_j = 4.24 m/s	Frequency at u_j = 7.63 m/s	Frequency at u_j = 10.49 m/s	Cumulative Frequency at u_j = 4.24 m/s	Cumulative Frequency at u_j = 7.63 m/s	Cumulative Frequency at u_j = 10.49 m/s
0 – 0.748	0	0	0	0	0	0
0.74 – 1.04	4	0	0	16	0	0
1.04 – 1.34	12	0	0	48	0	0
1.34 – 1.63	4	0	0	16	0	0
1.63 – 1.93	0	0	0	0	0	0
1.93 – 2.23	0	0	0	0	0	0
2.23 – 2.52	0	22	0	0	88	0
2.53 – 2.82	0	3	0	0	12	0
2.82 – 3.12	0	0	0	0	0	0
3.12 – 3.42	0	0	13	0	0	52
3.42 – 3.71	0	0	11	0	0	44

Table 7.3: Discretization in drop classes for 15% kerosene at $u_{sg} = 0.84\times10^{-2}$ m/s and at different liquid jet velocities

Bin	Frequency at u_j = 4.24 m/s	Frequency at u_j = 7.63 m/s	Frequency at u_j = 10.49 m/s	Cumulative Frequency at u_j = 4.24 m/s	Cumulative Frequency at u_j = 7.63 m/s	Cumulative Frequency at u_j = 10.49 m/s
0 – 0.64	0	0	0	0	0	0
0.64 – 0.82	0	0	0	0	0	0
0.82 – 0.01	10	0	0	40	0	0
1.01 – 1.19	2	0	0	8	0	0
1.19 – 0.38	0	0	0	0	0	0
1.38 –1.56	0	13	0	0	52	0
1.56 – 1.75	0	10	0	0	40	0
1.75 – 0.94	0	2	0	0	8	0
1.94 – 0.12	0	0	5	0	0	20
2.12 – 0.31	0	0	16	0	0	64
2.31 – 2.50	0	0	3	0	0	12

7.4 Results and Discussion

7.4.1 Flow regime

The flow regime observed at various experimental studies is illustrated in Figure 7.2 a-c. In the present experimental conditions, an intense mixing zone is observed at the top section (Figure 2.1b) and a homogenous bubbly-droplet flow is observed in the middle and bottom column section, as shown in Figure 7.2. In the middle section of the homogenous bubbly-droplet flow regime, almost all the drops are spherical (at low liquid velocity $u_j < 7.63$ m/s) and spheroid in shapes (at high liquid velocity $u_j = 10.49$ m/s).

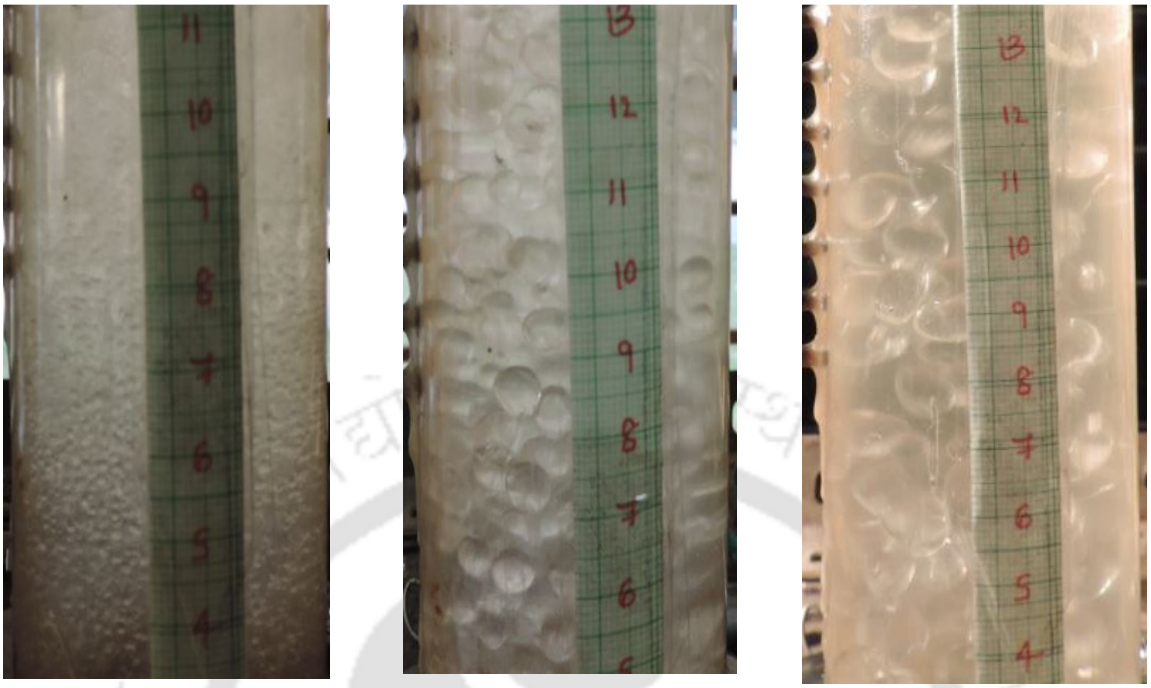

(a) u_j = 4.24 m/s (Middle section)

(b) u_j = 7.63 m/s (Middle section)

(c) u_j = 10.49 m/s (Middle section)

Figure 7.2: Images of paraffin droplets at 25% of volume fraction at constant gas velocity u_{sg} = 3.4×10^{-2} m/s with an increase in jet velocity

7.4.2 Effect of liquid and gas flow rate on mean drop size

The effect of the superficial liquid velocity and gas velocity on mean drop size for paraffin liquid-water and kerosene-water systems is shown in Figure 7.3. From the experimental results, it is observed that for a constant volume fraction of paraffin-liquid and kerosene, drop size increases with an increase in superficial liquid and gas velocity. With an increase in superficial liquid velocity, more gas is entrained in the column which increases gas holdup, increases more coalescence in the drops to increase the drop size in the column. From Figure 7.3a for a paraffin-liquid-water system, with an increase in the superficial gas velocity the mean drop size in the

column increases as the pressure in the column is decreased. From Figure 7.3a, it can be seen that at 5% of paraffin liquid, the range of mean drop size within 1.04 to 4.39 mm. When the volume fraction of paraffin-liquid is increased, it shows the same trend as discussed above, which is shown in Figure 7.4a, 7.5a, and 7.6a.

Similarly, the variation of drop size with the superficial liquid velocity of the kerosene-water system is shown in Figure 7.3b at different gas velocities. As in the case of paraffin liquid, in this case, also, the drop size is observed to increase with the superficial gas and liquid velocities. However, in the case of kerosene, the range of mean drop size is found to be lower than that of paraffin liquid. At a 5% volume fraction of kerosene, the mean drop size is within 0.69 to 3.17 mm. Also, it is observed that at a higher volume fraction (35% v) of kerosene, the drop size shows the same behavior as in lower volume fraction (5% v), but the drop size increases as the volume fraction increases, which is shown in Figure 7.4b, 7.5b and 7.6b.

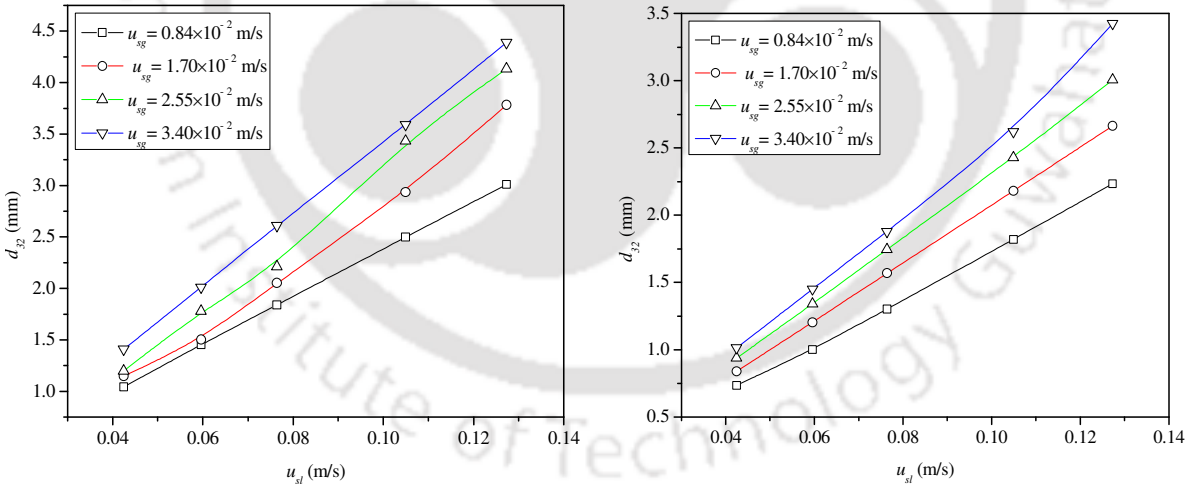

Figure 7.3: Variations of drop size with superficial liquid and gas velocities for 5% v of (a) paraffin liquid, (b) kerosene

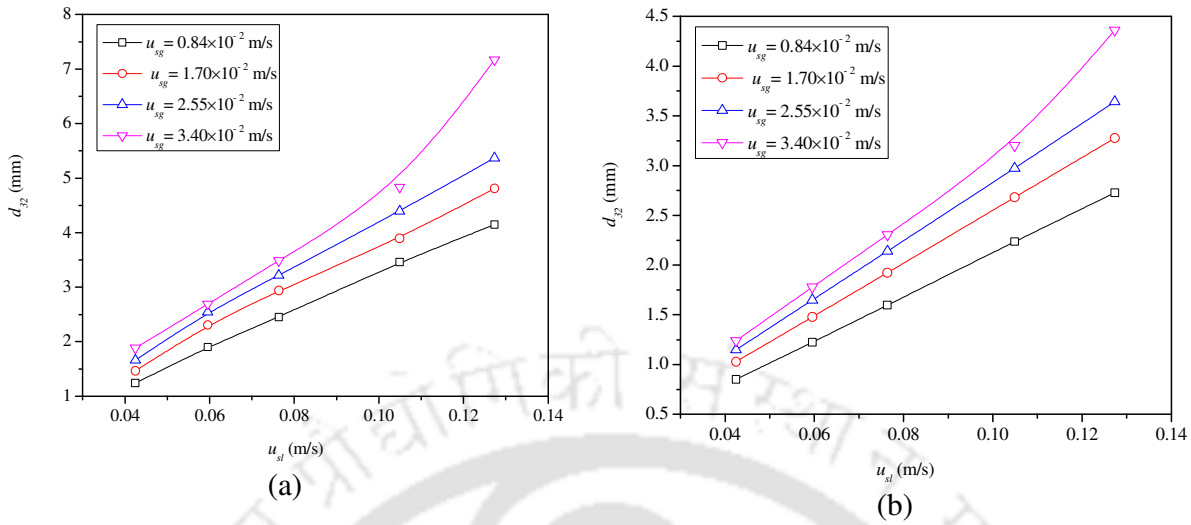

Figure 7.4: Variations of drop size with superficial liquid and gas velocities for 15% (v) of (a) paraffin liquid, (b) kerosene

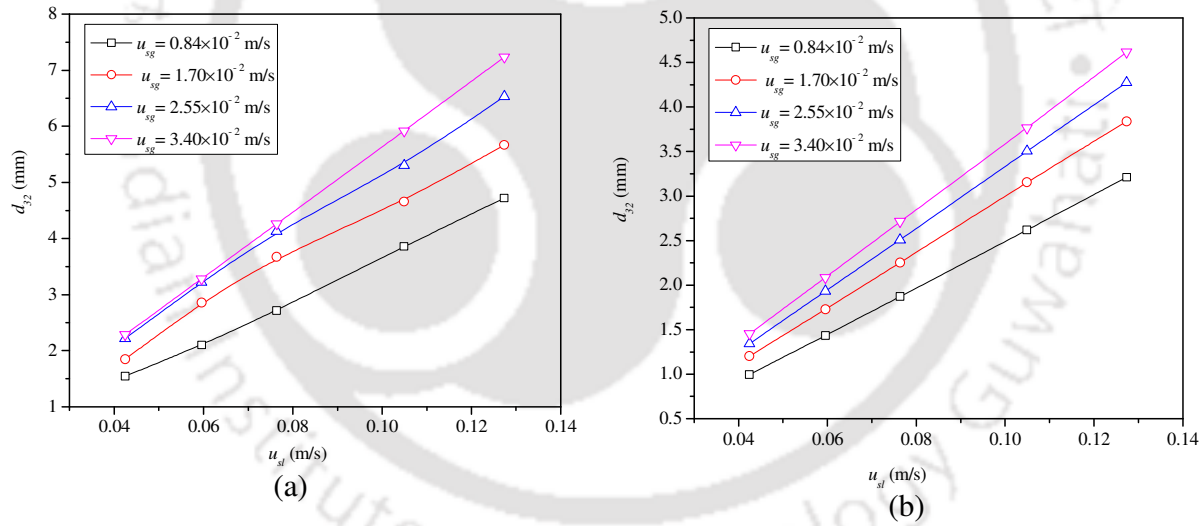

Figure 7.5: Variations of drop size with superficial liquid and gas velocities for 25% (v) of (a) paraffin liquid, (b) kerosene

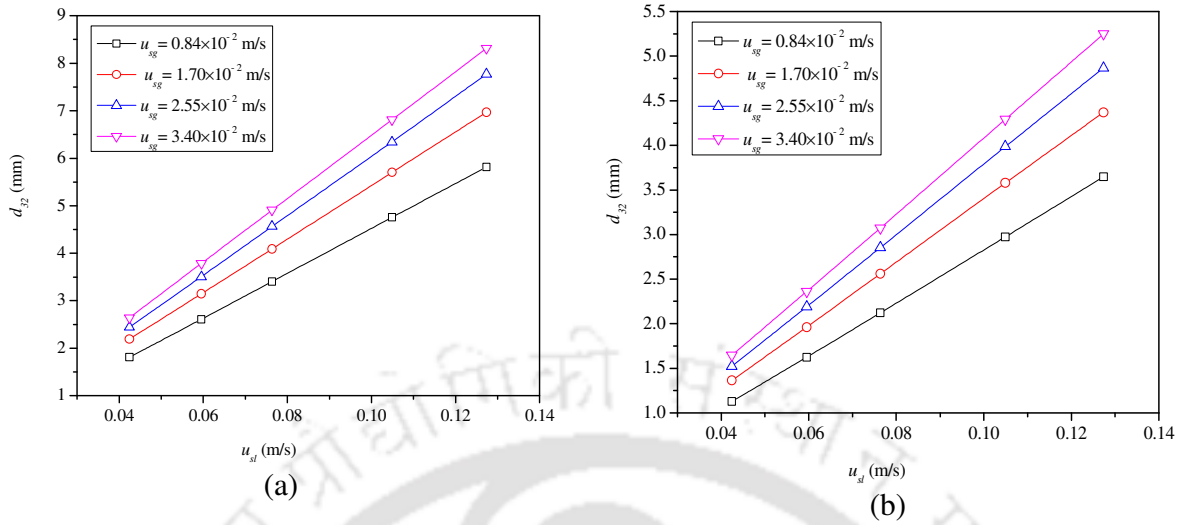

Figure 7.6: Variations of drop size with superficial liquid and gas velocities for 35% (v) of (a) paraffin liquid, (b) kerosene

7.4.3 Effect of dispersed liquid volume fraction on drop size

The effects of mean drop size with a superficial liquid velocity at different volume fractions of dispersed liquid at a constant gas flow rate are presented in Figure 7.7. It is observed that the drop size is larger at higher volume fractions of dispersed liquid than that of the lower volume fraction of dispersed liquid in the column. This happens because of the higher viscosity of the fluid mixture at a higher concentration of the dispersed liquid. From Figure 7.7a for the paraffin liquid-water system, it can be seen that the range of drop size is higher (d_{32} = 1.81–5.81 mm) at a higher volume fraction of dispersed liquid (35% v) than that at lower volume fraction (d_{32} = 1.04–3.01 mm at 5% v). With an increase in the volume concentration of the dispersed liquid the coalescence rate of the drops increases. A similar trend was reported by authors in the literature (Hatzikiriakos et al., 1990; Kato et al., 1984). From Figure 7.7b for the kerosene-water system, it is seen that the same pattern is observed as a paraffin liquid-water system. The deviation in drop size at different volume fractions of the paraffin liquid or kerosene at a higher gas flow rate is

shown in Figure 7.8.

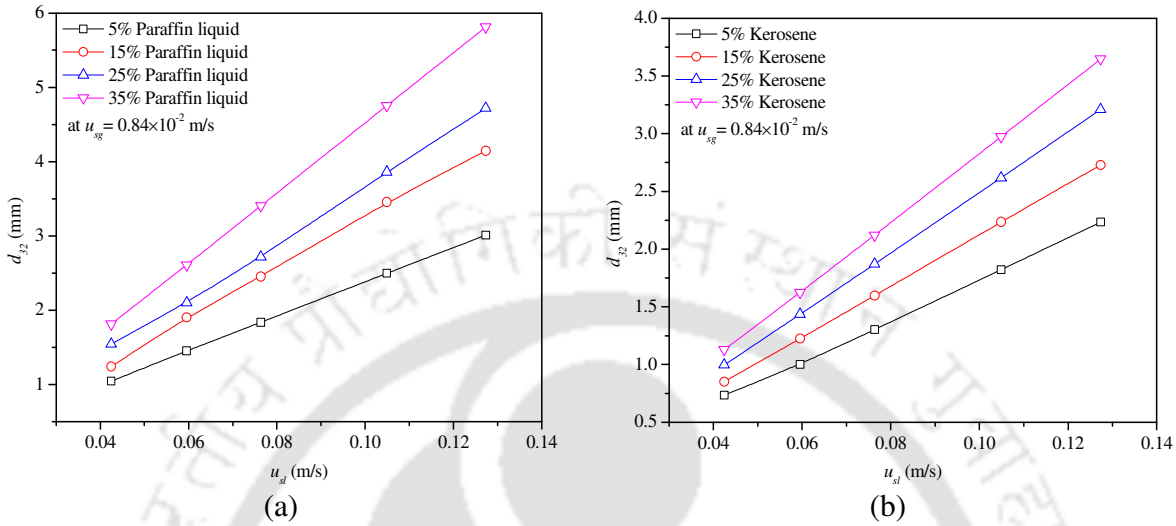

Figure 7.7: Variations of drop size with superficial liquid velocity at different concentrations of (a) paraffin liquid, (b) kerosene and at $u_{sg} = 0.84\times10^{-2}$ m/s

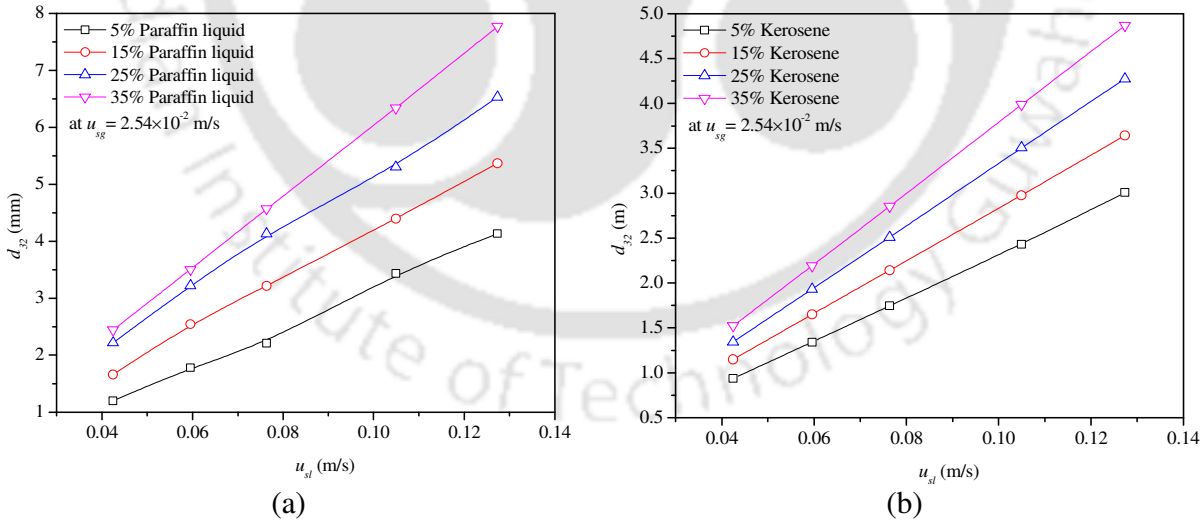

Figure 7.8: Variations of drop size with superficial liquid velocity at different concentrations of (a) paraffin liquid, (b) kerosene and at $u_{sg} = 2.54\times10^{-2}$ m/s

It is seen that the drop size increases with an increasing flow rate of gas. Also, it can be seen

from Figures 7.7 and 7.8 that the range of drop size is higher (d_{32} = 2.44 − 7.77 mm) at higher gas flowrate (u_{sg} = 2.54 ×10^{-2} m/s) than that at lower gas flowrate (d_{32} = 1.81–5.81 mm at u_{sg} = 0.84×10^{-2}m/s) of dispersed liquid (35% *v*). The liquid resistance decreases as the superficial gas velocity increases due to the increase in a gas holdup with an increase in superficial gas velocity.

7.5 Drop Size Distribution

7.5.1 Effect of gas and liquid flow rates on the drop size distribution

Influences of superficial liquid velocity with dispersed liquid of paraffin liquid-water at different gas velocities are shown in Figure 7.9. For the scale along the x-axis, the value "0.37" signifies the range of drop diameter ($d_d \leq$ 0.37 mm), and the second region denotes the drops of 0.37 mm ≤ $d_d \leq$ 0.74 mm. Figure 7.9a represents the number density curve of drop size in the presence of 5% paraffin liquid at different superficial liquid velocities and, at a constant gas velocity of 0.84×10^{-2} m/s. With an increase in the liquid velocity, it is observed that a broad drop size distribution results compared to that of lower liquid velocity (u_{sg} = 0.84×10^{-2} m/s − 2.54 ×10^{-2} m/s) in paraffin liquid system. This is due to the more momentum with an increase in superficial liquid velocity. The increase in the superficial liquid velocity from 4.24×10^{-2} m/s to 1.20×10^{-1} m/s, the drop size distribution region moved further to the larger drop diameter. The maximum number density of the drop size distribution curve shifted from 1.10 to 1.62 mm after an increase in the superficial liquid velocity of 7.64×10^{-2} m/s from 4.24×10^{-2} m/s. The drop size distribution curve shifted from 1.62 to 1.89 mm after an increase in the superficial liquid velocity of 1.05×10^{-1} m/s and a furthermore increase in the superficial liquid velocity of 1.20×10^{-1} m/s, it shifted to 2.42 mm drop diameter. When the volume fraction of paraffin-liquid is increased by 15% and

25%, it showed the same trend as discussed above, which is shown in Figure 7.10(a) and 7.11(a).

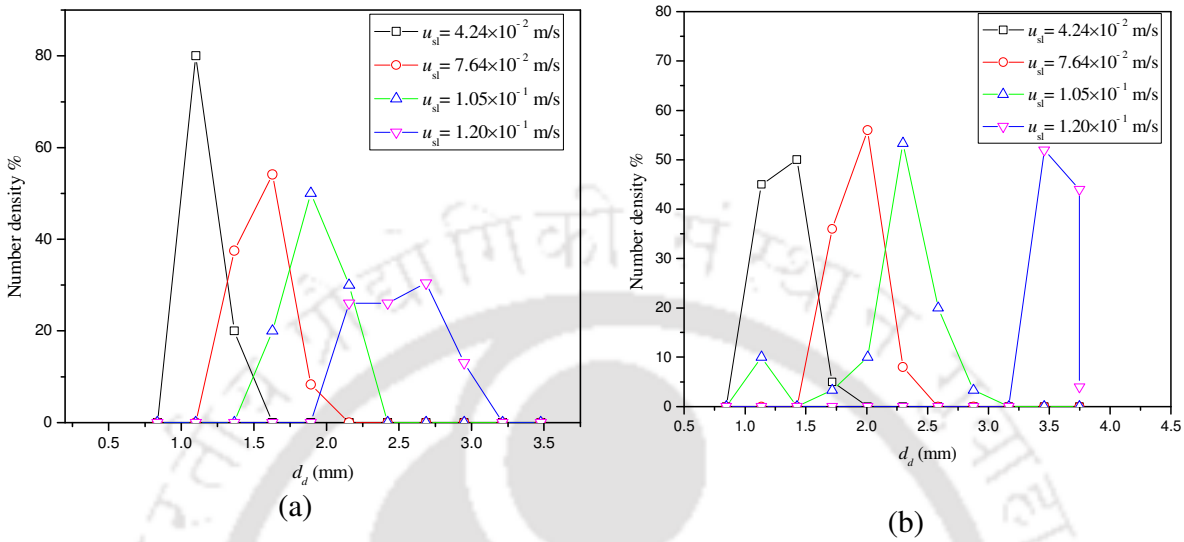

Figure 7.9: Variations of drop size distribution with superficial liquid for 5% (v) of paraffin liquid at (a) u_{sg} = 0.84×10^{-2} m/s, (b) u_{sg} = 2.544×10^{-2} m/s

Figure 7.9b shows the number density curve of drop size by increasing the gas velocity from 0.84×10^{-2} m/s to 2.54×10^{-2} m/s. It is seen that the size distributions of drops with paraffin liquid-water system at higher superficial gas velocity is higher than that at the lower superficial gas velocity. With an increase in the gas velocity, the drop coalescence increases in the column. It is observed that with an increase in superficial liquid velocity, the drop size distribution region moved further to the larger drop diameter. The maximum number density of the drop size distribution curve shifted from 1.42 to 2.00 mm after an increase in the superficial liquid velocity of 7.64×10^{-2} m/s from 4.24×10^{-2} m/s. The drop size distribution curve shifted from to 2.29 mm after an increase in the superficial liquid velocity of 1.05×10^{-1} m/s. Further increase in the superficial liquid velocity of 1.20×10^{-1} m/s, it shifted to 3.45 mm drop diameter. When the volume fraction of paraffin-liquid is increased by 15% and 25%, it shows the same trend as

discussed above, which is shown in Figure 7.10(b) and 7.11(b).

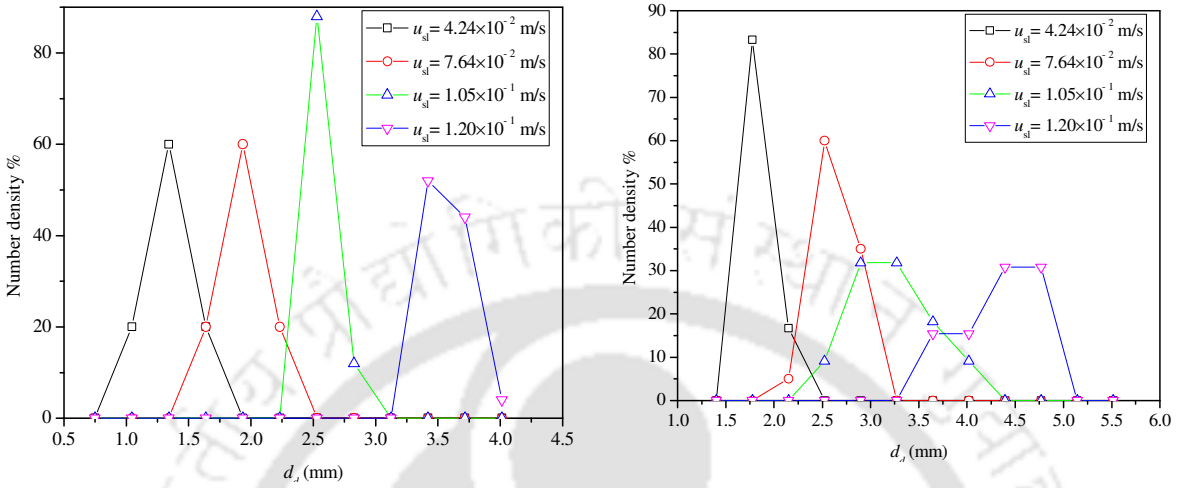

Figure 7.10: Variations of drop size distribution with superficial liquid velocity for 15% (v) paraffin liquid at (a) u_{sg} = 0.84×10^{-2} m/s, (b) u_{sg} = 2.544×10^{-2} m/s

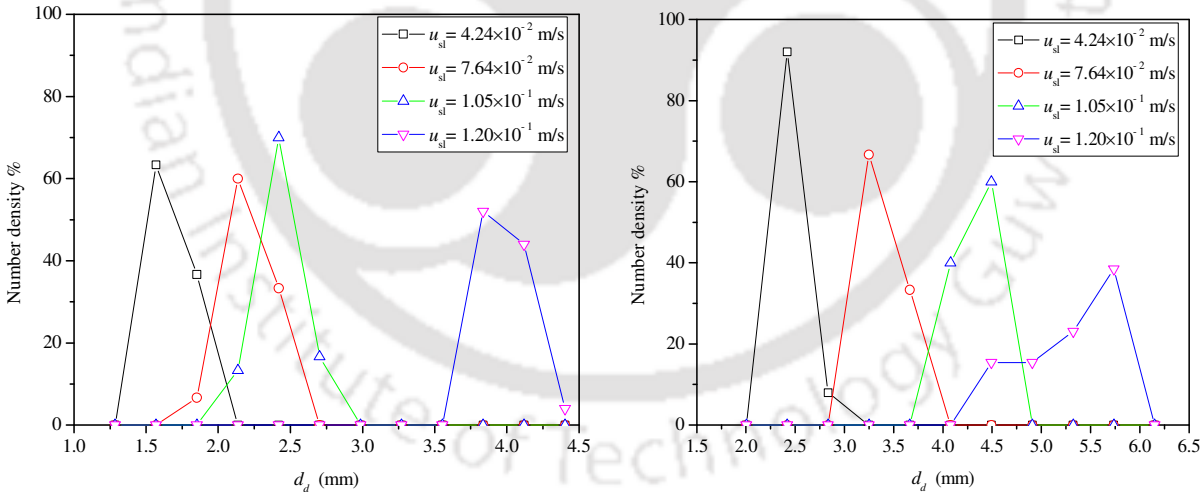

Figure 7.11: Variations of drop size distribution with superficial liquid velocity for 25% (v) of paraffin liquid at (a) u_{sg} = 0.84×10^{-2} m/s, (b) u_{sg} = 2.544×10^{-2} m/s

Figure 7.12 represents the number density curve of the drop size of the kerosene-water system at

different superficial gas and superficial liquid velocities. Figure 7.12a represents the number density curve of drop size in the presence of 5% kerosene at varying superficial liquid velocity and, at a constant gas flow rate of 0.84×10^{-2} m/s. As in the case of paraffin liquid, the drop size distribution is observed to increase with the superficial liquid velocities. However, in the case of kerosene, the range of drop size is found to be lower than that of paraffin liquid. As the kerosene viscosity is less than the paraffin liquid, it disperses in the continuous phase and forms smaller drops compared to that in paraffin liquid. From Figure 7.12a, it is observed that the maximum number density of the drop size distribution curve shifted from 0.76 to 0.92 mm after an increase in the superficial liquid velocity of 7.64×10^{-2} m/s from 4.24×10^{-2} m/s. The drop size distribution curve shifted from to 1.25 mm after an increase in the superficial liquid velocity of 0.105 m/s and a further increase in the superficial liquid velocity of 0.120 m/s, it shifted to 1.91 mm of drop diameter. When the volume fraction of kerosene is increased by 15% and 25%, it showed the same trend as shown in Figure 7.13a and 7.14a. Figure 7.12b shows the number density curve of drop size by increasing the gas velocity from 0.84×10^{-2} m/s to 2.54×10^{-2} m/s. It is seen that the size distributions of drops with the kerosene-water system at higher superficial gas velocity are higher than that at the lower superficial gas velocity with an increase in the gas velocity, the drop coalescence increases in the column. Figure 7.12b represents the number density curve of drop size in the presence of 5% kerosene-water at different superficial liquid velocity and, at a constant gas velocity of 0.0254 m/s. From Figure 7.12b, it is observed that the maximum number density of the drop size distribution curve shifted from 1.10 to 1.30 mm after an increase in the superficial liquid velocity of 7.64×10^{-2} m/s from 4.24×10^{-2} m/s. The drop size distribution curve shifted to 1.89 mm after an increase in the superficial liquid velocity of 0.105 m/s and a further increase in the superficial liquid velocity of 0.120 m/s, it shifted to 2.49 mm drop diameter.

When the volume fraction of kerosene is increased by 15% and 25%, it showed accordingly as is shown in Figure 7.13b and 7.14b.

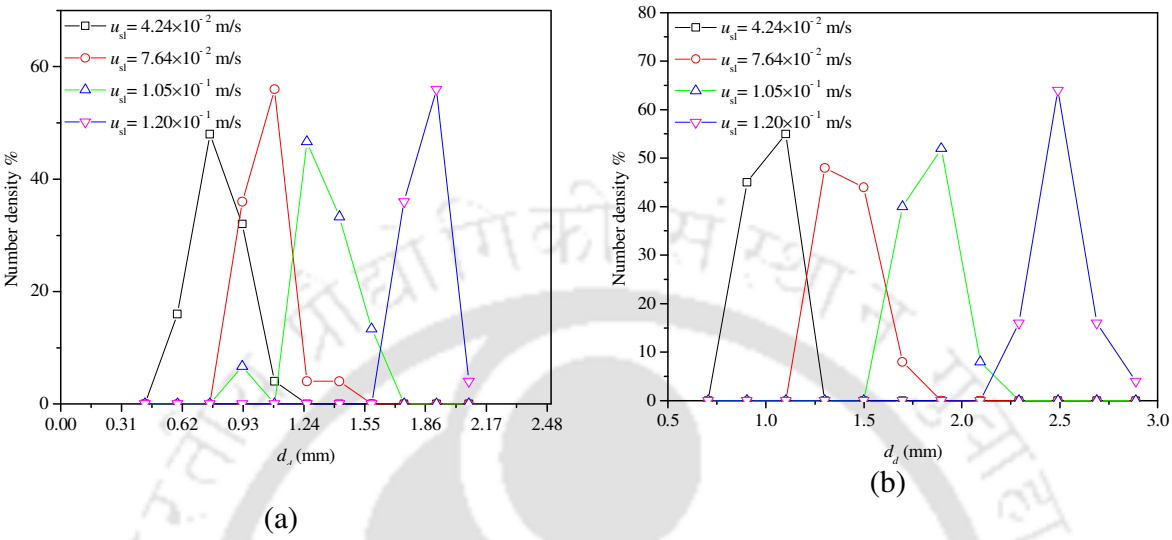

Figure 7.12: Variations of drop size distribution with superficial liquid velocity for 5% (v) kerosene at (a) u_{sg} = 0.84×10^{-2} m/s, (b) u_{sg} = 2.544×10^{-2} m/s

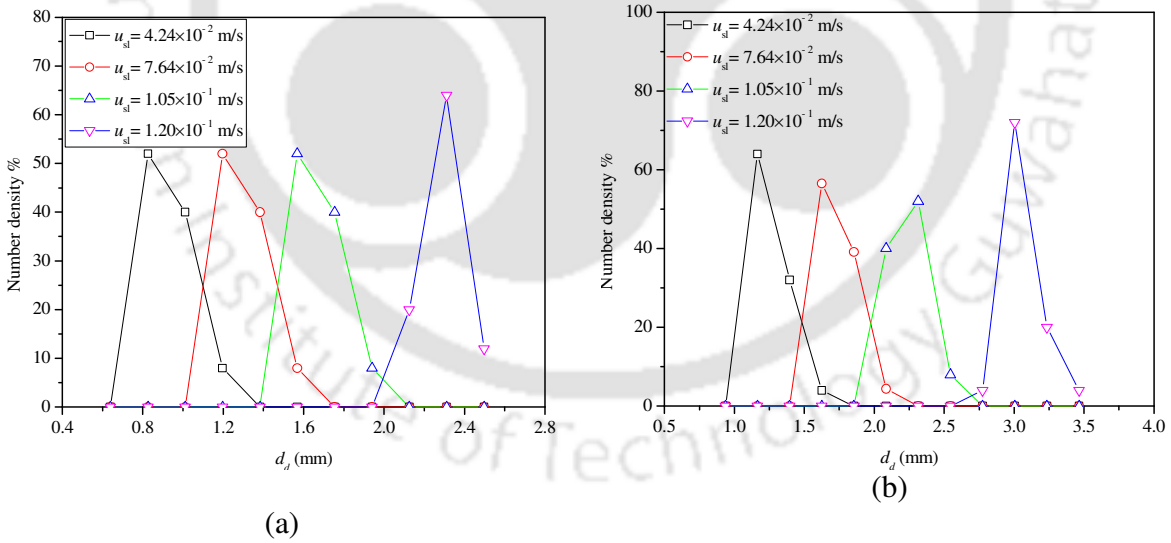

Figure 7.13: Variations of drop size distribution with superficial liquid velocity for 15% (v) kerosene at (a) u_{sg} = 0.84×10^{-2} m/s, (b) u_{sg} = 2.544×10^{-2} m/s

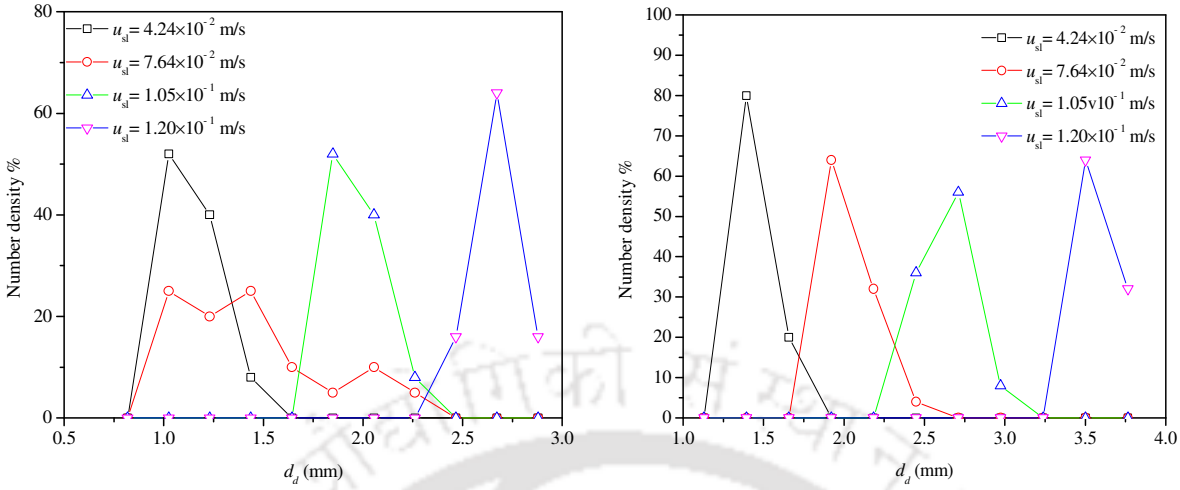

Figure 7.14: Variations of drop size distribution with superficial liquid velocity for 25% (v) kerosene at (a) $u_{sg} = 0.84\times10^{-2}$ m/s, (b) $u_{sg} = 2.544\times10^{-2}$ m/s

7.5.2 Effect of volume fraction of dispersed liquid on the drop size distribution

The effect of different volume fractions of dispersed liquid at a constant superficial liquid and gas flow rates on the drop size is presented in Fig.7.15. It is observed that the drop size distribution is wider at higher volume fractions of dispersed liquid than that of a lower volume fraction of dispersed liquid in the column. The distribution was found to merely shifted towards larger drop sizes as the dispersed phase volume fraction increases. This happens because of the higher viscosity of the fluid mixture at a higher concentration of the dispersed liquid. Figure 7.15a represents the number density curve of drop size in the presence of different paraffin liquid-water concentrations at constant superficial liquid velocity and, at a constant gas velocity. From Fig.7.15a, it can be observed that the trend of wider drop size distribution curves and shift towards larger drops are generally attributed to increasing in the collision rate of drops and the damping of turbulence, which collectively lead to an increase in the coalescence rate and a reduction in the breakage rates. The maximum number density of the drop size distribution curve

shifted from 1.24 to 1.40 mm after an increase in the paraffin liquid concentration of 15 % from 5 %. The drop size distribution curve shifted to 2.0 mm after an increase in the paraffin liquid concentration of 25 %.

Figure 7.15b represents the number density curve of drop size in the presence of different kerosene concentrations at constant superficial liquid velocity and, at a constant gas velocity. When the volume fraction of kerosene is increased by 15% and 25%, it showed the same trend as the paraffin liquid-water system. The maximum number density of the drop size distribution curve shifted from 0.78 to 0.95 mm after an increase in the kerosene concentration of 15 % from 5 %. The drop size distribution curve shifted to 1.04 mm after an increase in the kerosene concentration of 25 %.

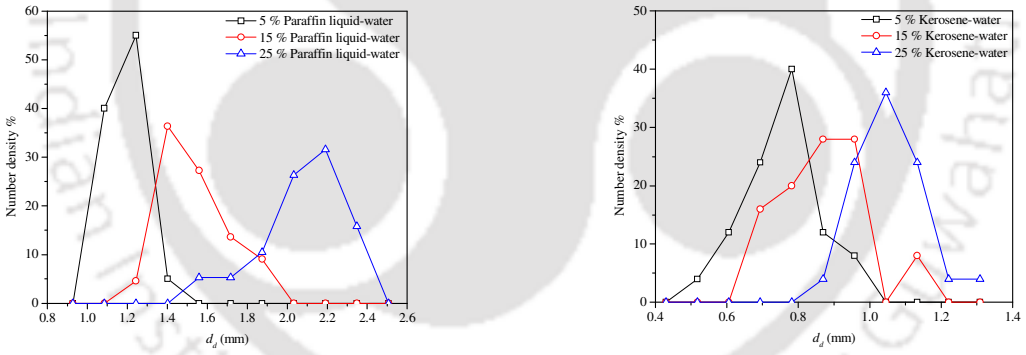

(a) (b)

Figure 7.15: Variations of drop size distribution with superficial liquid velocity within different systems (a) paraffin liquid- water, (b) kerosene-water volume fraction at $u_{sg} = 0.84\times10^{-2}$ m/s, $u_{sl} = 4.24\times10^{-2}$ m/s

7.5.3 Analysis of drop size distribution

In the present study, the drop size distributions were found to be non-symmetrical. The DSD can be denoted as density distribution function $F(d_d)$. For the present system, each experimentally

measured drop size data is fitted with a distribution model by using the least error method. It is observed that the log-logistic distribution fitted well to the experimental results with a minimum error at different operating variables. A typical well fitted distribution for each system compared with other distributions (e.g., Weibull, gamma, beta, log–logistic, etc.) is shown in Figure 7.16. The DSD follows the log logistic distribution, and it is expressed as

$$F(d_d) = \frac{\alpha}{\beta}\left(\frac{d_b}{\beta}\right)^{\alpha-1}\left(1+\left(\frac{d_b}{\beta}\right)^{\alpha}\right)^{-2} \tag{7.4}$$

where $F(d_d)$, α, and β are the density distribution function for a specific set of experimental conditions, shape parameter > 0, and the scale parameter > 0. Both the shape and scale parameters are calculated from the experimental values. Based on the present experimental results, the parameters are correlated with the operating variables.

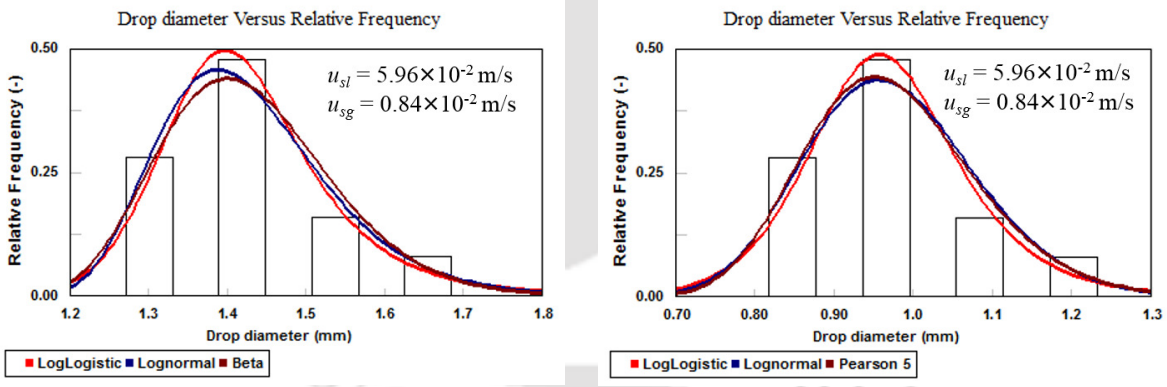

(a) (b)

Figure 7.16: Representation of various DSD for different dispersed liquid of 5% (v) (a) paraffin liquid, (b) kerosene

From the log-logistic, the constant parameters α, and β are correlated from the present

experimental results are given as,

$$\alpha = 1.41\times10^{-2}\times \mathrm{Re}_{sl}^{0.471}\,\mathrm{Re}_{g}^{-0.104}\,We^{0.067}\,Fr^{-0.373}\,Hr^{-0.428} \tag{7.5}$$

$$\beta = 4.77\times10^{-2}\times \mathrm{Re}_{sl}^{0.663}\,\mathrm{Re}_{g}^{-0.131}\,We^{-0.994}\,Fr^{0.613}\,Hr^{-0.685} \tag{7.6}$$

The two fitted parameters are expressed in terms of dimensionless numbers, which were obtained by dimensional analysis based on Buckingham's pi theorem. The accuracy of the predicted values with the experimental values is assessed by an average absolute percentage error. The average absolute relative percentage error (*AAPE*) is calculated by

$$AAPE = \left[\frac{1}{n}\sum_{i=1}^{n}\left[\left(\frac{\text{predicted} - \text{experimental}}{\text{experimental}}\right)^{2}\right]^{1/2}\right]\times 100 \tag{7.7}$$

Both functions of each distribution represented the data well within the investigated range of operating parameters. In Table 7.4, AAPE numbers were listed.

Table 7.4: Error analysis of Log-logistic distribution function

Function	Fitted parameter	AAPE (%)
Log-logistic	*A*	14
	β	11

The typical result of a comparison of experimental and predicted cumulative distribution functions (CDF) is shown in Figure 7.17. Figure 7.17a shows a comparison of data calculated by the log-logistic function with experimentally measured data. The AAPE of 2.43% (5% paraffin liquid) and 1% (at 25% paraffin liquid) were found. Figure 7.17b reports the comparison for the kerosene system with the AAPE of 7% (at 5% kerosene) and 14% (at 25% kerosene). It can be concluded that the developed empirical correlations for log-logistic distribution function are

suitable to predict the drop size distribution well within the acceptable range of error.

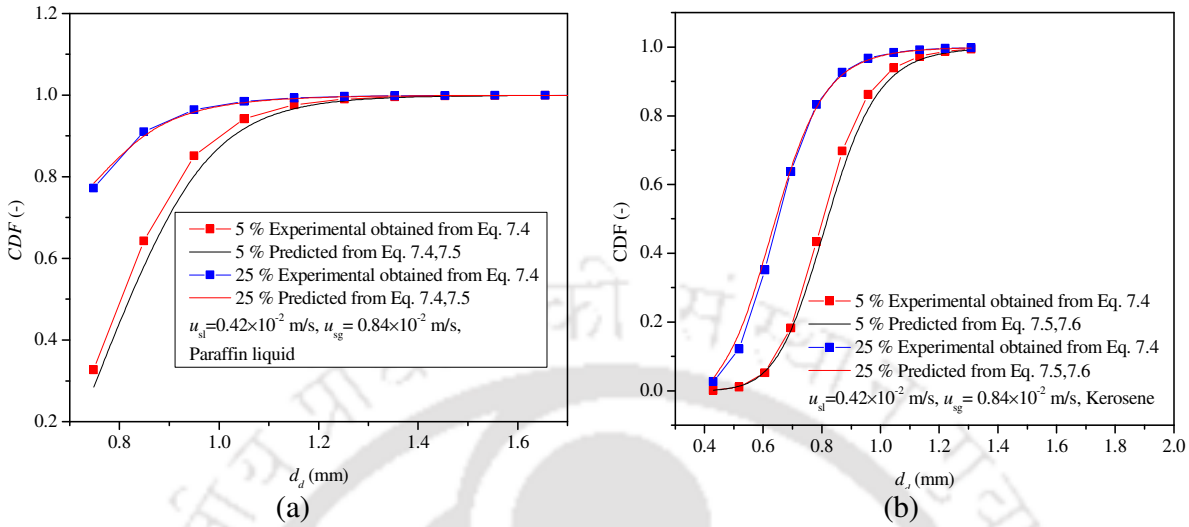

Figure 7.17: Comparison of drop size distribution (DSD) with experimental data at u_{sg} = 0.84×10^{-2} m/s, u_{sl}= 4.24x10^{-2} m/s for different concentration of (a) paraffin liquid, (b) kerosene

7.5.6 Development of general empirical correlation for drop size

The drop size is found to vary with (i) operating variables, namely liquid and gas flow rates, (ii) physical properties of the liquid and gas, namely density, viscosity, surface tension, (iii) geometric variables, namely, diameter of the column (*dc*). A function of drop size based on all these variables can be expressed as

$$d_{32} = f\left(u_{cl}, u_g, \rho_{cl-dl}, \rho_g, \mu_{cl-dl}, \mu_g, \sigma, g, d_c, h_m,\right) \tag{7.8}$$

By using the Buckingham pi theorem, the resulting equation for drop size,

$$\frac{d_{32}}{d_c} = \left(\frac{u_g}{u_{cl}}\right)\left(\frac{\rho_g}{\rho_{cl-dl}}\right)\left(\frac{\mu_l}{u_{cl}\rho_{cl-dl}d_c}\right)\left(\frac{\mu_{lg}}{u_{cl}\rho_{cl-dl}d_c}\right)\left(\frac{\sigma}{u_{cl}^2\rho_{cl-dl}d_c}\right)\left(\frac{d_c g}{u_{cl}^2}\right)\left(\frac{h_m}{d_c}\right)$$

(7.9)

By rearranging the final equation for drop size can be expressed as,

$$d_r = f\left(\mathrm{Re}_{sl}, \mathrm{Re}_g, We, Fr, Hr\right) = \lambda \mathrm{Re}_{cl}^a \mathrm{Re}_{sg}^b We_{cl}^c Fr_{cl}^d H_r^e \tag{7.10}$$

The multiple regression analysis of experimental data yields,

$$d_r = 9.01 \mathrm{Re}_{sl}^{0.6}\, \mathrm{Re}_g^{0.2}\, We^{-0.05} Fr^{0.77} H_r^{-0.69} \tag{7.11}$$

The above relationship was established on the basis of 160 experimental data. The values of drop size from the experimental results and calculated from the above correlation are compared, and a parity plot is presented in Figure 7.18.

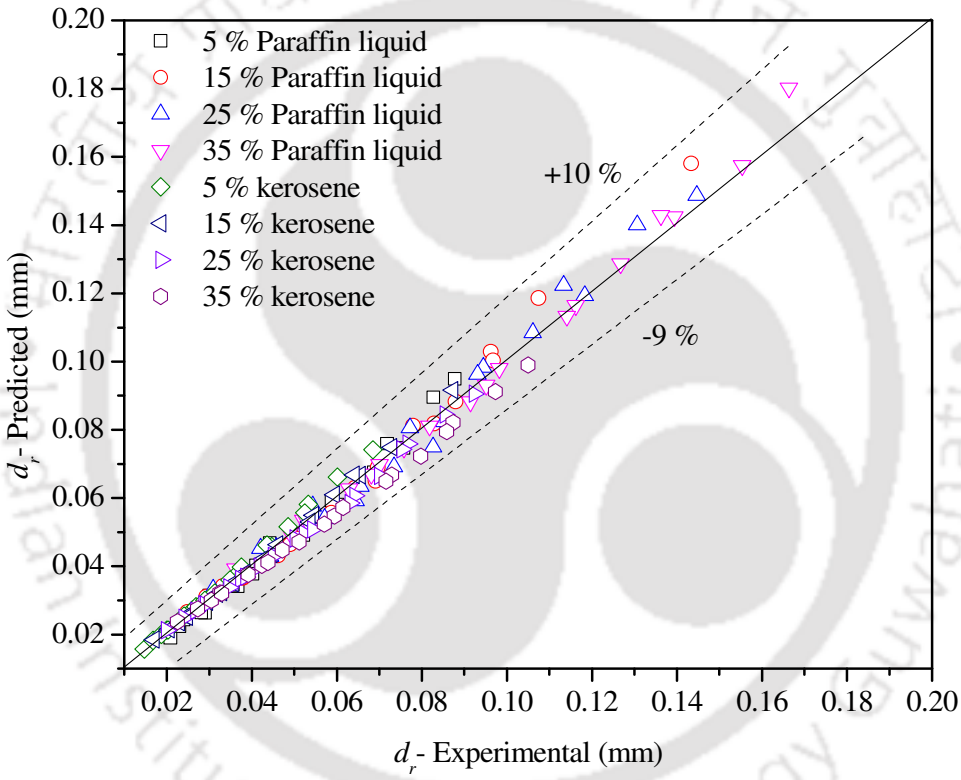

Figure 7.18: Parity plot of calculated values and experimental values of drop size at different concentrations (%) of Paraffin liquid and kerosene

The overall percentage error in drop size values from the experimental and correlation is found to be +10% and - 9%. The above correlation is valid for the following ranges of variables: 27.82 < Re_g < 111.28, 360.7 < Re_{sl} < 4021.9, 0.0028 < We < 0.029, 0.0036 < Fr < 0.033, 11 < H_r < 34.

7.6 Specific interfacial area

7.6.1 Effect of the specific interfacial area with gas and water flow rate

From the experimental result, it is seen that the specific interfacial area varies with the operating variables and dispersed liquid volume fraction. The variation of the interfacial area is shown in Figure 7.19 and 7.20. The specific interfacial area is related to the Sauter mean drop diameter and the dispersed phase holdup. As discussed earlier, the Sauter mean drop diameter increases with an increase in superficial gas and liquid velocities. The increase of Sauter mean drop diameter would result in a decrease in the specific interfacial area. From Figure 7.19a, it is observed that the specific interfacial area decreases with increasing superficial liquid and gas velocity. It can also be seen that at 5% paraffin, the range of specific interfacial area is 55 to 376 m^{-1}. As shown in Figure 7.20a, with an increase in dispersed phase volume fraction from 5 to 25% of paraffin liquid, the specific interfacial area increases within the range of 133 to 1012 m^{-1} respectively.

Similarly, the variation of the specific interfacial area with superficial liquid velocity is shown in Figure 7.19b for the constant volume fraction of kerosene (at 5%) at different gas velocities. As in the case of paraffin liquid, the interfacial area is observed to be decreasing with the superficial gas and liquid velocities. However, in the case of kerosene, the range of drop size is found to be lower than that of paraffin liquid. At a 5% volume fraction of kerosene, the interfacial area is 71 to 545 m^{-1}. From Figure 7.20b, it is observed that at a higher volume fraction of kerosene, the interfacial area shows the same trend as in lower volume fraction, but the specific interfacial area increases as the volume fraction increase from 245 to 1589 m^{-1}.

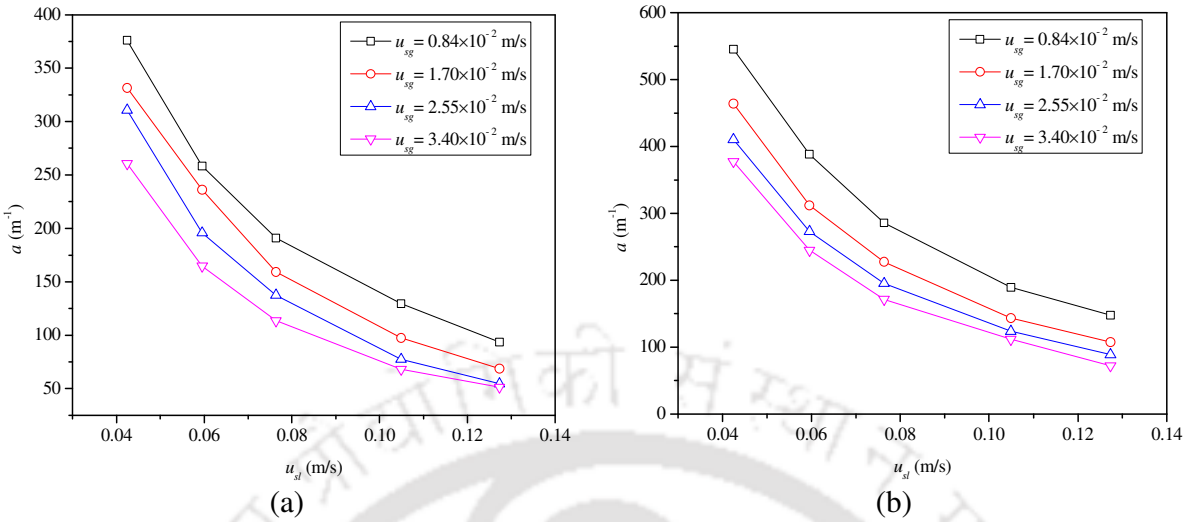

Figure 7.19: Variations of drop size with superficial liquid and gas velocities for 5% (v) (a) paraffin liquid, (b) kerosene

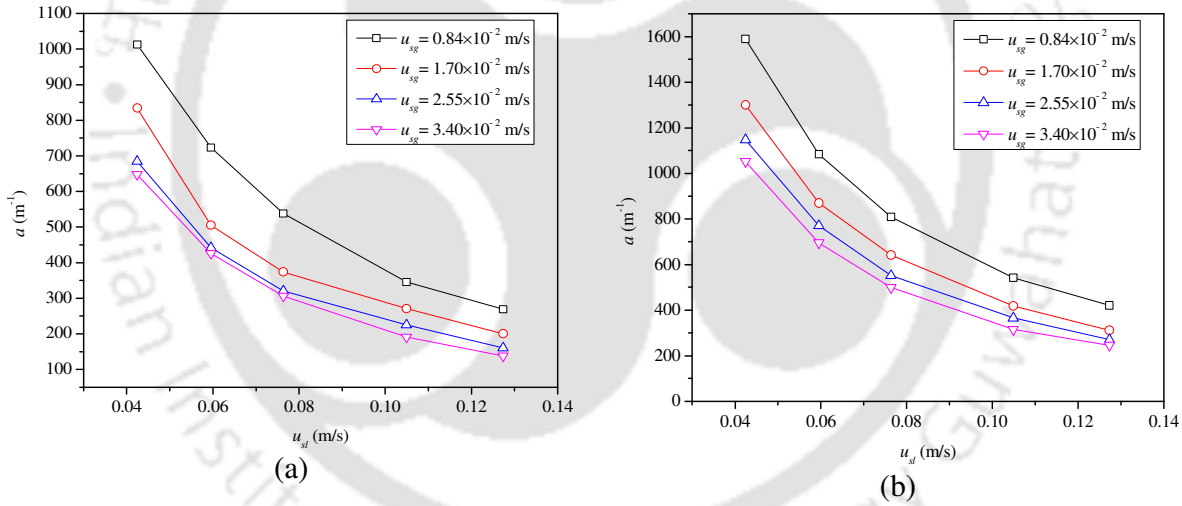

Figure 7.20: Variations of drop size with superficial liquid and gas velocities for 25% (v) (a) paraffin liquid, (b) kerosene

7.6.2 Interfacial area analysis by empirical correlation

A general correlation is established by using the Buckingham pi theorem to predict the interfacial area based on the operating variables.

The functionality of the specific interfacial area in term of various dimensionless groups by

dimensional analysis can be expressed as

$$ad_c = f\left(\mathrm{Re}_{sl}, \mathrm{Re}_g, We, Fr, H_r\right) \tag{7.14}$$

The multiple regression analysis of experimental data with this function yields,

$$ad_c = 1.94\times10^{-7}\,\mathrm{Re}_{sl}^{1.12}\,\mathrm{Re}_g^{0.55}\,We^{-3.57}\,Fr^{3.94}\,H_r^{1.86} \tag{7.15}$$

The above relationship was established on the basis of 160 experimental data. A parity plot is presented in Figure 7.21 to show the goodness of fit with experimental data.

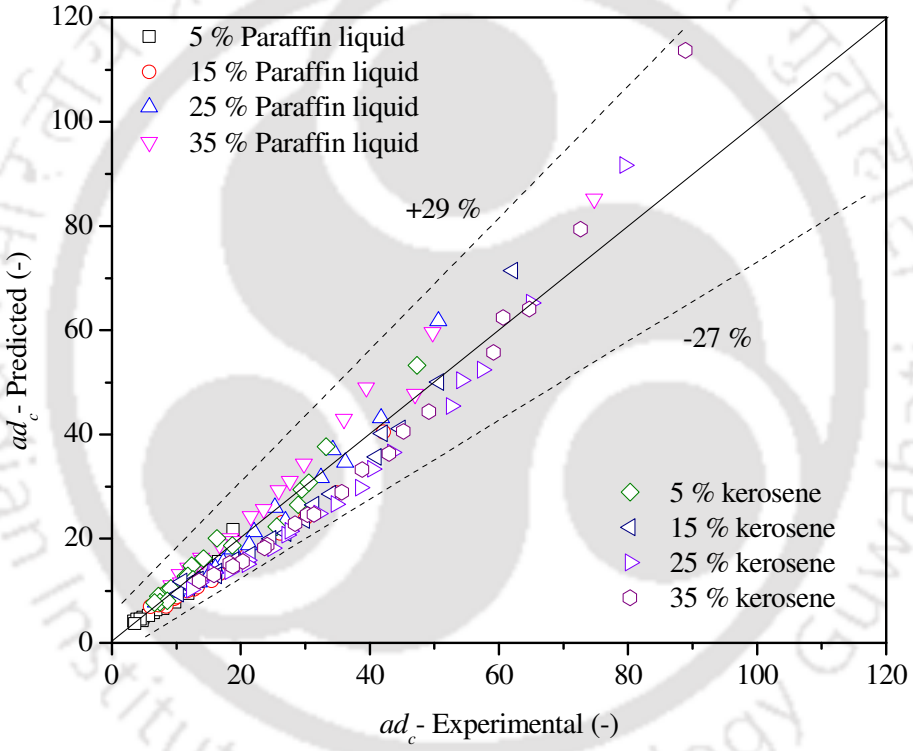

Figure 7. 21: Parity plot of calculated and experimental values of the specific interfacial area at different concentrations (%) of Paraffin liquid and kerosene

The overall percentage error is found to be in the range of +10% to - 9%. The above correlation is valid for the following ranges of variables: $27.82 < Re_g < 111.28$, $360.7 < Re_{sl} < 4021.9$, $0.0028 < We < 0.029$, $0.0036 < Fr < 0.033$, $11 < H_r < 34$.

7.7 Conclusions

In the present work, the effect of superficial liquid and gas velocities, and dispersed liquid volume concentration on drop size, drop size distribution were investigated. An increase in the drop size and its distribution was found with varying the gas and liquid superficial velocities and dispersed liquid volume. The drop size distribution results in the column with the paraffin liquid-water and kerosene-water system were not symmetrical. It has been observed that the distribution of droplet size follows the distribution function, namely log-logistic under various experimental conditions.

Correlations were developed for the estimation of the parameters of the distribution function. Empirical correlations are also proposed to interpret the sauter mean drop diameter and specific interfacial area in terms of operating variables such as superficial gas and liquid velocity and physical properties (i.e., mixture viscosity and density, surface tension) of the system.

CHAPTER - 8

MASS TRANSFER CHARACTERISTICS OF GAS-LIQUID-LIQUID EXTRACTION

In this chapter, the mass transfer characteristics of gas-liquid-liquid extraction are explained based on the present experiment. The effect of superficial liquid and gas velocities on extraction efficiency and mass transfer coefficient are enunciated. The effect of volume fraction of the dispersed liquid on extraction efficiency and mass transfer coefficient is explained. The generalized correlation model for the extraction efficiency and mass transfer coefficient based on the system properties are developed.

8.1 Introduction

Liquid-liquid extraction is the second most important separation process after distillation in chemical industries. There are various types of commonly used extraction columns, packed column, rotating disc contactor, Kuhni column, Oldshue-Rushton contactor, spray column, Scheibel extractor, reciprocating plate column, and pulsed sieve plate column. Although the non-agitated extraction columns, spray column, packed column, perforated plate column, sieve plate column, etc can handle high flow rates and are simple and cheap. There have been few applications of these columns because they suffer from serious back mixing of the continuous phase. It was shown that the back mixing is reduced when the spray column is operated with dense packing of drops. Another way of increasing the efficiency of a non-agitated extraction column is to introduce an inert gas (air, nitrogen, etc.) as a mixing agent in the two-phase liquid-liquid (L-L) system. This method of inert gas introduction increases the turbulence within the three-phase gas-liquid-liquid (G-L-L) system, which causes an improved dispersion of droplets, and, consequently, a higher dispersed phase holdup and therefore a great mass transfer area

(Dehkordi, 2002; Lü et al., 2005; Saien et al., 2006; Sohn and Doungdeethaveeratana, 1998; Tan et al., 2011). The efficiency of gas-liquid-liquid mass transfer is higher than the existing downcomer compared to liquid-liquid mass transfer without gas. Galkin et al. (1961) concluded that the extraction efficiency was nearly three times higher for conventional columns when the air was introduced into the extraction column, and claimed that the process is more efficient than that by the use of stirring or pulsation of the column. In the present study, a jet-driven downflow column is used for gas-liquid-liquid extraction studies. The column has many advantages over other conventional reactors. It has the capability of air dispersing into the column with a continuous phase without any external power requirement. As gas aided liquid-liquid extraction process has advantages over non-gas-aided extraction, it is gaining importance as a simple and inexpensive means of achieving such gas-liquid-liquid extraction in scientific and academic communities. For scale-up and the proper design of the downflow column with the gas-liquid-liquid system, several hydrodynamic characteristics and the transport processes are essential to study and its interpretation for the suitability of the industrial-scale operation. The previous chapters regarding entrainment and holdup characteristics (since it is important for interfacial area, mass transfer and design of the unit), pressure drop (since it is important for chemical reaction, mass transfer and design of the unit), droplet size distribution (since it is important for mass transfer through the interface) and mixing characterizes (it is important for mass and heat transfer), reveals the proof of concept of the feasibility of gas-liquid-liquid operation in the downflow column.

8.2 Literature review

Here some of the past research done on various types of extraction columns that are related to the present study are summarized as follows.

Morello and Poffenberger (1950) summarized all the available contemporary data on commercial extraction equipment**.** Their sources were the general literature, patent literature, and data from manufacturers and operators of extraction equipment. Vermijs and Kramers (1954) studied the extraction performance in a rotating disc contactor (R.D.C.) of small diameter at different rotor speeds, total throughput, and solvent to feed ratio using water-acetic acid-methyl isobutyl ketone system. By comparing the separating efficiency with the fractional volume of the dispersed phase under similar circumstances, it was found that under certain conditions, the efficiency decreases, although the hold-up of the dispersed phase increases. This effect is attributed to back-mixing in the continuous phase due to entrainment by the dispersed phase. The effectiveness of the R.D.C. was compared with that of similar extraction columns. Chantry et al. (1955) studied the application of pulsation to the liquid-liquid packed and sieve plate extraction columns. As extraction efficiencies in conventional counter-current columns are often poor, they observed that the application of pulsation to a packed column could be a practical interest for its efficiency improvement. The height of the packed section required is reduced as much as three times when the column liquids are pulsed. Optimum operating conditions was obtained by varying both frequency and amplitude of pulse. Greater efficiency is obtained with suitable low amplitude at high frequencies than that at low frequencies. The maximum throughput is reduced slightly when the column is pulsed. Changes in feed rates have less effect on the efficiency when pulsation is used than with the usually packed column operation. They also reported that in the Sieve-Plate column, average plate efficiencies as high as 70% is obtained by pulsating**.** Seibert and Fair (1988) studied mass-transfer efficiencies and hydraulic characteristics of a 10.2-cm packed extraction column. Different packings of ceramic Intalox saddles, metal Pall rings, ceramic Raschig rings, corrugated metal gauze and corrugated sheet metal were used. The performance

of the column was compared with these packings and that of an empty spray column. Two widely different chemical systems were used: toluene/acetone/water and 1-butanol/succinic acid/water. The influences of the direction of solute transfer, phase flow rates, and phase dispersion were studied and found to be significant. Fundamental models were developed to account for dispersed phase holdup, flooding, and mass-transfer efficiency. Yu et al. (1989) carried out mass transfer experiments in a 40 mm diameter pulsed sieve plate extraction column. Volumetric mass transfer coefficients and back mixing parameters in continuous and dispersed phases were simultaneously evaluated from steady-state concentration profiles of both phases based on the stage back mixing model. Drop sizes and dispersed phase hold up are measured at the same time. The mass transfer coefficient is predicted by a single turbulent circulating drop mechanism. Sohn and Doungdeethaveeratana (1998) studied a novel solvent extraction process in which the emulsion is generated by bottom gas injection rather than mechanical stirring. This process has a number of advantages over the mixer–settler unit or the spray column in terms of simple equipment configuration and the ease of cleaning and process control, while providing a sufficiently large interfacial area for mass transfer. The equipment consists of a horizontal cylindrical vessel in which the two immiscible liquids flow counter currently. High-strength gas jets are injected from the bottom at certain intervals along the length of the vessel. The gas jet creates a plume zone consisting of an emulsion of the two liquids which reults in a large interfacial area for rapid mass transfer. The two liquids then disengage and flow in the opposite directions before entering another plume zone. The process combines the simplicity of a cylindrical vessel, having no moving parts, with the contacting efficiency of a mixer–settler. The gas can be recycled in a closed-loop, thus eliminating mist and other emission problems. By using an inert gas, the oxidation degradation of the extractant solutes is prevented. The

advantages are useful for treating the large volume streams of hazardous materials. Venkatanarasaiah and Varma (1998) studied dispersed phase hold up and mass transfer in a liquid-liquid pulse column. The variation of volumetric mass transfer coefficient and the interfacial area with the experimental conditions are qualitatively similar. They reported that the mass transfer coefficient depends linearly on the drop diameter in the liquid pulsed column. Li et al. (2000) studied the mass transfer characteristics in a coalescence–dispersion sieve plate column. Experiments were carried with a system of 30% tri-butyl phosphate (in kerosene)–nitric acid–water in a 150 mm diameter of coalescence–dispersion pulsed sieve extraction (PSE) column. The direction of mass transfer was from continuous (aqueous) to the dispersed (organic) phase. The dynamic response method was used for the estimation of height of dispersion unit, the height of transfer unit and the apparent height of transfer unit. The efficiency of mass transfer at the low pulse intensity is little and at the high pulse intensity it is greater. The mass transfer performance is greatly effected in the column by the periodic coalescence and breakup of the drops. If the column is operated at high pulse intensity, the mass transfer efficiency can be increased by more than 30%. Dehkordi (2002) studied liquid-liquid extraction with chemical reaction in a novel impinging-jets reactor. Experiments were conducted on the physical extraction of n-butyl formate into distilled water and measured the overall volumetric mass-transfer coefficients. The results showed that due to both the impinging process and high shear forces acting on the phases, the overall volumetric mass transfer coefficients and volumetric extraction rates obtained by the physical and chemical methods, respectively, increased dramatically compared to those obtained by conventional reaction systems. An air-driven two-impinging-streams reactor was used in his experiment. Prabhakar et al. (2003) studied liquid-liquid mass transfer studies in the Karr extraction column of an internal diameter of 15.3 cm and

100 cm long with a stock of 17 plates. The counter-current liquid-liquid flow is employed with kerosene oil as a dispersed phase and water as a continuous phase with benzoic acid and n-butyric acids as solutes. The mass transfer coefficient in the column is influenced by the agitation rate of plate stock, free flow area, phase velocities and perforation diameter of the plate. The volumetric coefficients were found to be 15 to 20 times higher with agitation than that with no agitation of plate stack. Xu et al. (2005) designed a new membrane dispersion mini-extractor with a microfiltration membrane as the dispersion media for liquid-liquid extraction processes. The mass transfer and two-phase flow characteristics of the mini extractor along with the energy input were studied for six different systems. Their experiment results showed that the extraction efficiency as a function of the total volumetric flow rate. The extraction efficiency was close to 100% with residence times ranging from 0.15 to 0.45 s. The clarification time of the micromixing systems was less than 21 s, and the transmembrane pressure was below 200 kPa, potentially lower than the energy consumption of conventional extractors. This mini-extractor has advantages of high mass transfer performance, fast phase separation rate, and large capacity compared with other microchannel mixers. Lü et al. (2005) used a sieve-plate column to study the gas-liquid-liquid reactive extraction system for hydrogen peroxide production via the anthraquinone route. Experiments were conducted in a 50mm diameter of the sieve plate column for the oxidation of the hydrogenated anthraquinone solution by oxygen, and the extraction of hydrogen peroxide from the working solution with deionized water. The effects of superficial oxygen velocity were investigated for the 2-ethylanthrahydroquinone conversion and hydrogen peroxide extraction efficiency. The experimental results show that there is no hindrance between oxidation and extraction. Moreover, the presence of the gas encourages the transfer of hydrogen peroxide from the organic phase to the aqueous phase in the column. Also, a mathematical model

was developed to simulate the gas-liquid-liquid reactive extraction process. At different conditions the predicted values were compared with the experimental data, and the results were found to be satisfactory for the production of hydrogen peroxide in a sieve plate column. Saien et al. (2006) studied the liquid-liquid extraction process in a two impinging-jets contacting device (TIJCD) with the toluene-acetone-water system. The obtained overall volumetric mass transfer coefficient (capacity coefficient) results were more than three times higher than those reported in the conventional contactors and an air-driven two impinging-stream contactors. These experimental results demonstrated TIJCD's greater performance capability relative to conventional contactors. The influence of nozzles diameter, jets momentum, the inter nozzle distance and the enhancing effect of the impingement zone, parameters of the TIJCD have been studied using non-impinging-jets contacting device. An increase in the liquid flow rates increases the extraction efficiency and overall volumetric mass-transfer coefficient while increasing the distance between nozzles decreases the extraction efficiency. Furthermore, they showed the nozzle diameter effect on the extraction efficiency depends on the jet velocity. Torab-Mostaedi et al. (2008) studied the volumetric overall mass transfer coefficients using toluene-acetone-water system in a seven stage pilot plant Hanson mixer-settler extraction column. The effects of flow rates and agitation speed on volumetric overall mass transfer coefficients were studied. The results show that the volumetric overall mass transfer coefficient increases and reaches a maximum with increase in agitation speed. It falls with further increase in agitation speed after having reached its maximum. The overall volumetric mass transfer coefficient reduces significantly at high agitation speed, due to back mixing. With increase in the continuous phase flow rate the volumetric overall mass transfer coefficient decreases, while it increases with increase in dispersed phase flow rate. The overall mass transfer coefficients for continuous and

dispersed phases are determined through the use of the interfacial area from volumetric coefficients. An empirical correlation is proposed in terms of the Sherwood and Reynolds numbers to predict the overall mass transfer coefficient of the continuous phase. The experimental data of the investigated column are also compared with data for different columns of the extraction. Torab-Mostaedi and Safdari (2009) used a diffusion model for two different liquid-liquid systems to examine the volumetric overall mass transfer coefficients in a pulsed packed extraction column. The effects of operational variables such as continuous and dispersed phase flow rates and pulsation intensity on volumetric overall mass transfer coefficient have been investigated. The interfacial area, determined as a function of dispersed phase holdup and Sauter mean drop diameter, showed that the effects of phase flow rates are less significant than those of pulsation intensity and interfacial tension. An empirical correlation is proposed for the prediction of effective diffusivity as a function of viscosity ratio, Schmidt number and Reynolds number. The experimental and predicted values are found to be in good agreement for all operating conditions. The equation was used to calculate the overall mass transfer coefficients of the dispersed phase and, consequently, to finally size the height of the column. Torab-Mostaedi et al. (2009) studied the stage efficiency of a pilot plant Hanson mixer-settler extraction column with seven stages using the toluene-acetone-water system. The experiments were carried out for both directions of mass transfer. The parameters that are found to be significant on stage efficiency are flow ratio, agitation speed, solute concentration and total throughput. The stage efficiency of the investigated mixer-settler extraction column increased with agitation speed and reached a maximum, but it decreased with further increase in agitation speed after reaching its maximum, because axial mixing became significant for high agitation speed. It was observed that the stage efficiency varied little with total throughput for mass transfer direction continuous

to dispersed phase while it decreased with increase in total throughput for the opposite mass transfer direction. The results showed that, by increasing the flow ratio of dispersed phase to continuous phase, the stage efficiency has increased. Comparing the investigated column with some other type of extractors has shown that this column's stage efficiency is high, while its throughput is low. Finally, an empirical correlation was proposed for stage efficiency prediction and very good agreement was obtained between experimental data and calculated values. Ferial et al. (2010) investigated the mass transfer coefficient of liquid-liquid systems under jetting conditions. N-butanol-succinic acid-water chemical system is used in the experimental setup. The effects of different parameters on the mass transfer coefficient, such as nozzle diameter, jet velocity and the height of the continuous phase above the nozzle, were investigated. A correlation has also been derived in order to predict the mass transfer coefficient as a function of physical properties of both phases and aforementioned parameters. Based on the experimental results, mass transfer coefficient increases with an increase in the jet velocity and nozzle diameter, while increasing the height of the continuous phase above the nozzle decreases the mass transfer coefficient. These results revealed the importance of mass transfer during jet formation and breakage. Tan et al. (2011) studied a gas-liquid-liquid microdispersion system specially designed to realize a micro bubble-agitated extraction process for the intensification of extraction with a high phase ratio. The process with the phase ratio larger than 50 for H_2O_2 extraction was taken as a typical case. A microstructured system with microfiltration membranes as the dispersion medium was developed to generate the gas-liquid-liquid microdispersion system. The most efficient model suggested was with a lower addition of gas, by which the Murphree efficiency could reach higher than 90%, and the overall volumetric mass transfer coefficient could range in 0.2–21.9 s^{-1}, 10–30 times greater than the extraction process without

gas addition. Torab-Mostaedi et al. (2011) studied the mass transfer performance in a 76 mm diameter pulsed disc and doughnut extraction column for the toluene-acetone-water system. The mass transfer data are interpreted in terms of the axial diffusion model. The effect of operating parameters on the overall volumetric mass transfer coefficients has been investigated. With an increase in pulsation intensity the overall volumetric mass transfer coefficient increases. Due to increased entrainment and poor extraction efficiency, the mass transfer performance decreases at high pulsation intensity values, with the production of rigid dispersed droplets. The mass transfer performance is found to be higher for solute transfer in the direction of dispersed to continuous phase (d-c) due to the induced effect of interfacial turbulence. The experimental results indicated that the mass transfer performance of the column increases with an increase in continuous phase velocity and a decrease in dispersed phase velocity. An empirical correlation is predicted for the overall continuous phase Sherwood number as a function of Reynolds number and dispersed phase holdup for each mass transfer direction. These correlations can be used for the design and scale-up of the column. Tan et al. (2012) studied the recovery of butyl acetate (BA) from lovastatin wastewater by using a method of solvent extraction with liquid paraffin (LP) as the extractant. The results showed that the extraction efficiency of BA could reach 98% at room temperature, and the study on several operating factors demonstrated that the extraction efficiency is not significantly affected by the existence of lysozyme and the initial BA concentration. It takes about 15 min for the extraction process to reach equilibrium in their work. The loading capability of LP was found to be high by multi-stage extraction, in which the loaded LP was reused to extract the fresh wastewater. Finally, BA with high purity can be effectively recovered from the loaded LP by using vacuum evaporation. The unloaded LP can be easily regenerated using alkali treatment. The regenerated LP can be reused as many as 5 times without

noticeable decrease in extraction efficiency. Tan et al. (2013) investigated the process intensification mechanism for liquid-liquid extraction with a high phase ratio by forming a micro dispersion system of gas in water phase in organic phase. Extraction of H_2O_2 from an organic phase to an aqueous phase was selected as the model system. The influence of the gas phase addition as well as dispersion size on mass transfer performance is studied. The results showed that both the increase in the addition of gas phase and decrease in dispersion size lead to significant enhancement in mass transfer performance, especially for the overall mass transfer coefficient. As gas-to-water flow rate ratio increased from 25 to 600, the overall volumetric mass transfer coefficient increases by nearly two orders of magnitude. The result showed good coincidence with experimental values. Khawaja et al. (2017) studied the mass transfer performance in a tall, thin and low plate free area liquid pulsed sieve plate extraction column. The effects of pulsation intensity and dispersed phase velocity on the extraction efficiency of the column for the acetic acid-kerosene-water system were studied. A correlation for the measurement of overall mass transfer coefficient is developed that fits well the experimental data. In the present work, a mass transfer characteristics of extraction process in gas-liquid-liquid system in a jet driven downflow column. The aim of the study to understand the effect of jet energy to disperse the dispersed liquid as a droplet under the aid of inert gas for its possible enhancement of extraction efficiency based on contact area, retention time.

8.3 Methodologies

8.3.1 Theory to estimate the extraction efficiency

The extent of percentage extraction (E %) for continuous to dispersed phase was estimated by (Mondal and Majumder, 2018),

$$E(\%)=\frac{C_{cl,out}-C_{cl,in}}{C_{cl,in}}\times 100 \tag{8.1}$$

where $C_{cl,in}$ and $C_{cl,out}$ are concentrations of solute in the inlet and outlet of aqueous solutions respectively.

In the present study, the overall mass transfer coefficient was estimated based on the number of transfer units and height of the column as given by the following equation (Khawaja et al., 2017):

$$HTU=\frac{u_{sl}}{K_{cl}a}=\frac{H}{NTU_{cl}} \tag{8.2}$$

where u_{cl} is the continuous phase velocity, NTU_{cl} is the overall number of transfer units based on the continuous liquid, which is calculated using the experimental observations of inlet and exit molar concentrations of the phases. H is the height of the gas-liquid-liquid extraction column. The overall number of transfer units is given by the following equation:

$$NTU_{cl}=\frac{1}{\left(\frac{\left(C_{cl,out}-C_{cl,in}\right)}{m.\left(C_{dl,out}-C_{dl,in}\right)}\right)-1}\ln\left(\frac{C_{cl,in}-m\times C_{dl,out}}{C_{dl,out}-m\times C_{dl,in}}\right) \tag{8.3}$$

Where m is the distribution coefficient of solute between the continuous and dispersed phase.

The overall mass transfer coefficient based on the continuous phase was calculated using the following equation:

$$K_{cl}a=\frac{NTU_{cl}.u_{sl}}{H} \tag{8.4}$$

8.4 Experimental setup and procedure

The details of the experimental setup with its description described in chapter 2. In the present study, water is taken as a continuous phase. For the extraction efficiency and mass transfer

studies, the propionic acid is used as a solute in the water. The concentration of propionic acid in the water was varied as 0.01, 0.03, and 0.05 M. The physical properties of the fluids are shown in Table 2.1 in chapter 2. At the start of the experiment, for each run, a constant propionic acid concentration solution was prepared in water. Paraffin and kerosene as dispersed liquid are used as a solvent to extract the acid. The dispersed liquid is introduced as a batch mode by varying concentrations of 5, 15, 25, and 35% by volume into the column. The extraction in the present experiment is done for single-stage which means the dispersed liquid is taken new for every run. A sample was collected from the aqueous phase outlet after a regular interval and analyzed for the concentration of solute at a particular operating condition. The concentration of solute in outlet paraffin liquid and kerosene was estimated. When the system attained steady-state condition, 20 ml of sample is collected from liquid sampler port. The sample collected is then taken and titrate against sodium hydroxide solution of concentration 0.05 N. The efficiency of extraction is then calculated by the Equation (8.1).

8.5 Results and discussion

8.5.1 Effect of superficial gas and liquid velocity on extraction efficiency

The effect of liquid jet velocity on the extraction efficiency is shown in Fig.8.1. It is observed that with increasing the jet velocity and gas velocity, the extraction efficiency increases at a constant solvent liquid volume fraction (Paraffin liquid). The momentum of the jet increases with increasing liquid flow rate, which results in higher gas and dispersed liquid, thereby increases the drop formation, which enhances to increase the extraction efficiency. When the solvent paraffin liquid and kerosene volume fraction is increased by 15, 25, and 35% of the total volume of the column, it follows the same trend as discussed above, which is shown in Figures 8.2-8.4.

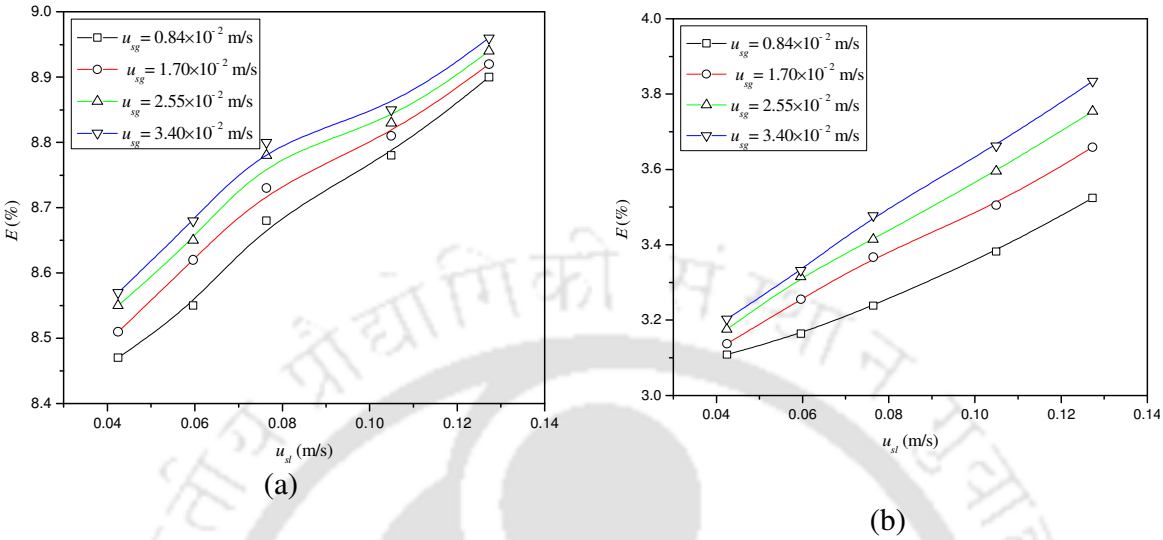

Figure 8.1: Variations of extraction efficiency with superficial liquid and gas velocities for 5% (v) of dispersed liquid (a) paraffin liquid-water + propionic acid and (b) kerosene-water + propionic acid

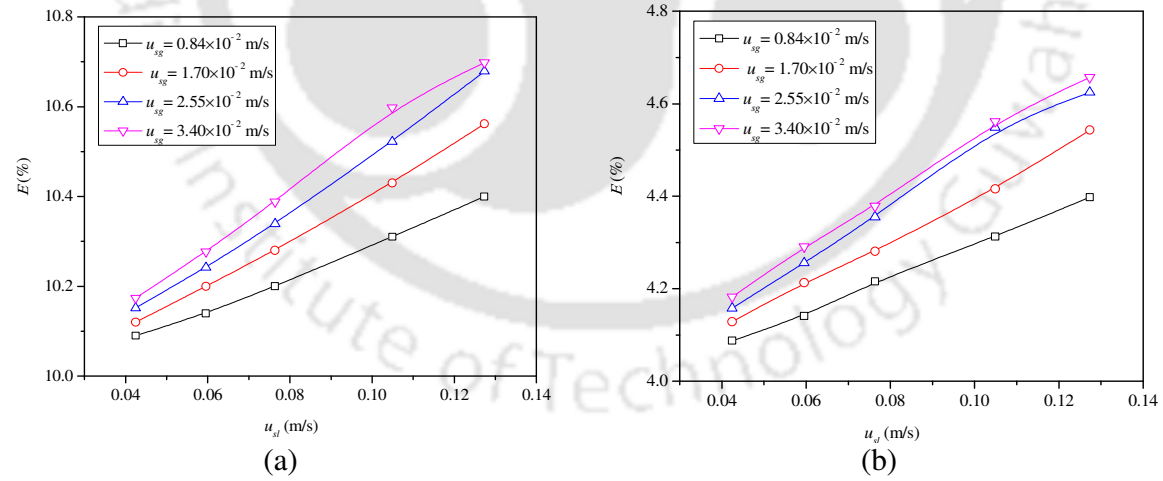

Figure 8.2: Variations of extraction efficiency with superficial liquid and gas velocities for 15% (v) of dispersed liquid (a) paraffin liquid-water + propionic acid and (b) kerosene-water + propionic acid

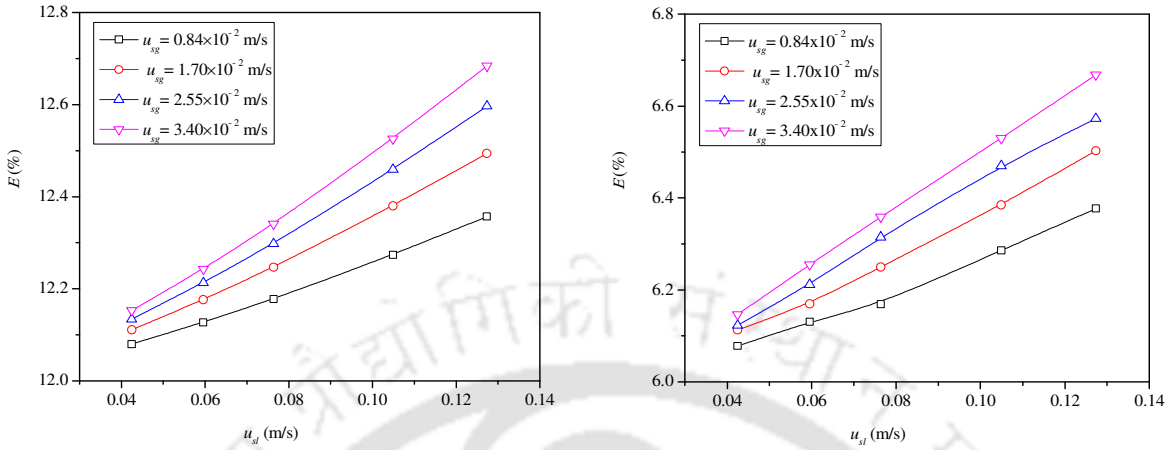

Figure 8.3: Variations of extraction efficiency with superficial liquid and gas velocity for 25% (v) of dispersed liquid (a) paraffin liquid-water + propionic acid and (b) kerosene-water + propionic acid

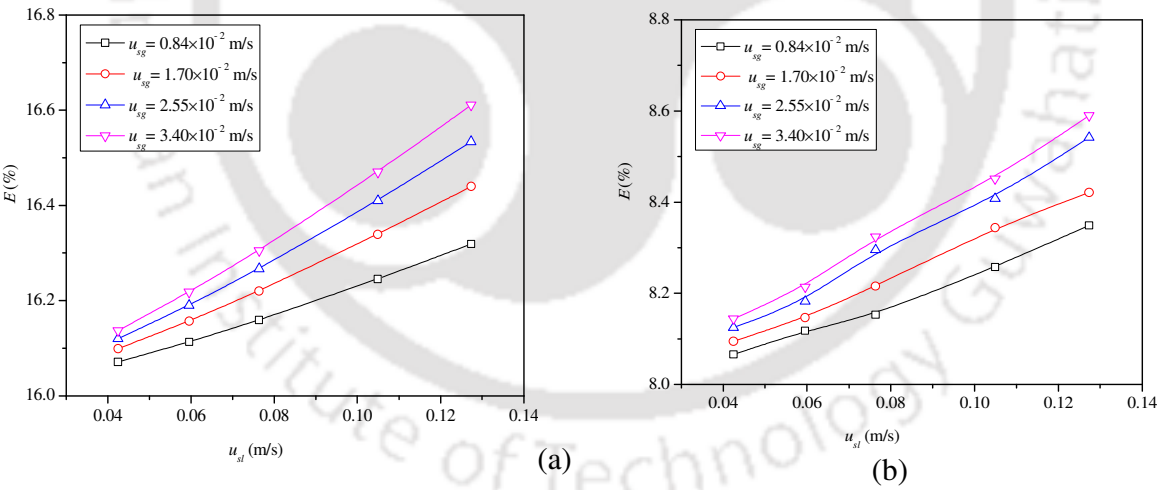

Figure 8.4: Variations of extraction efficiency with superficial liquid and gas velocity for 35% (v) of dispersed liquid (a) paraffin liquid-water + propionic acid and (b) kerosene-water + propionic acid

8.5.2 Effect of different solvent concentrations on extraction efficiency

The variations of extraction efficiency with different solvent concentrations at a constant gas flow rate is shown in Figure 8.5a, b for Paraffin liquid, and Kerosene respectively. It is observed that the extraction efficiency increases with an increase in the solvent volume in the column. From Figure 8.5a for paraffin liquid-water, it is observed that with an increase from 5 to 35% of the solvent, the extraction efficiency increases from 8.47 to 16.07 % for a single pass flow. From Figure 8.5b for kerosene-water, it is observed that with an increase from 5 to 35% of the solvent, the extraction efficiency increases from 3.10 to 8.06 %. With an increase in solvent volume the effective viscosity increases which increases the drop formation to enhance more mass transfer. The deviation in extraction efficiency with different concentrations of paraffin liquid and kerosene at a higher gas flow rate is shown in Figure 8.6a, b. It is observed that the extraction efficiency is increasing with respect to the gas flow rate.

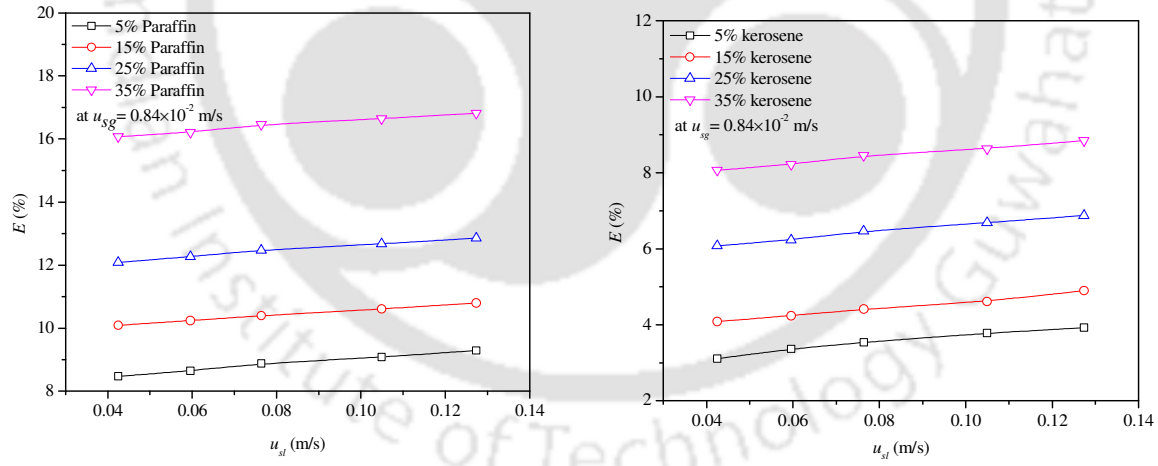

(a) (b)

Figure 8.5: Variations of extraction efficiency with superficial liquid velocity and at u_{sg} = 0.84×10^{-2} m/s for different dispersed liquid concentrations of (a) paraffin liquid and (b) kerosene

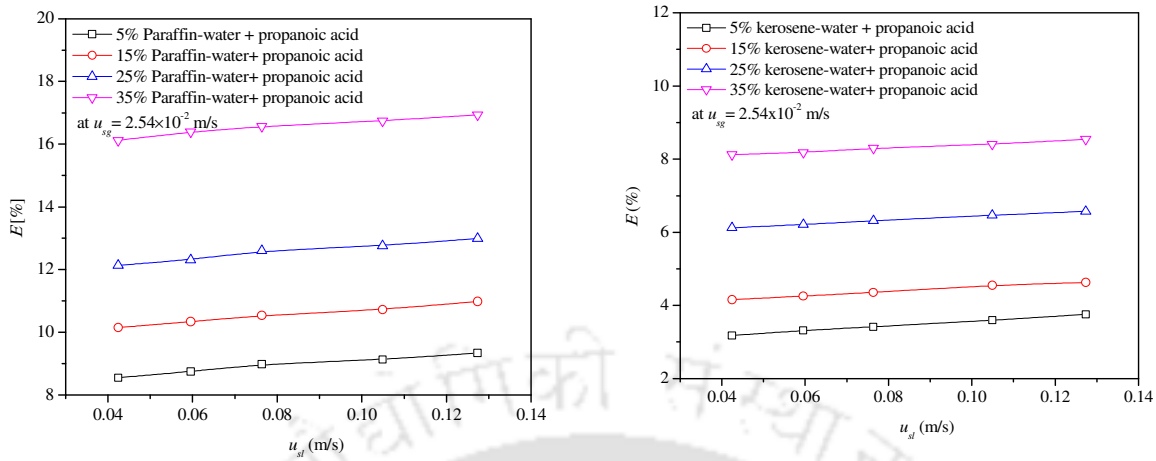

Figure 8.6: Variations of extraction efficiency with superficial liquid velocity and at u_{sg} = 2.54 $\times 10^{-2}$ m/s for different dispersed liquid concentrations of (a) paraffin liquid (b) kerosene

8.5.3 Comparison of extraction efficiency with different propionic acid concentrations

The extraction efficiency is compared with varying propionic acid concentrations (0.01, 0.03,005 M) for the present experimental system of water + propionic acid + paraffin liquid and water + propionic acid + kerosene system. The variations of extraction efficiency with different propionic acid concentrations at a constant solvent volume fraction and gas velocity are shown in Figure 8.7a, b. It is observed that the extraction efficiency is higher for the system with high solute concentration. The continuous liquid of high solute concentration has lesser surface tension, which enables the formation of the fine droplets in the column. The variations of extraction efficiency with different Propionic acid concentrations at a higher volume fraction of solvent and a constant gas flow rate is shown in Figure 8.8a, b. It is observed that the extraction efficiency is increasing with respect to the increase in the solvent fraction. With the increase in the solvent volume, the gas-liquid-liquid mixture forms more drops, which increases the interfacial area for mass transfer in the column and hence increased the extraction efficiency.

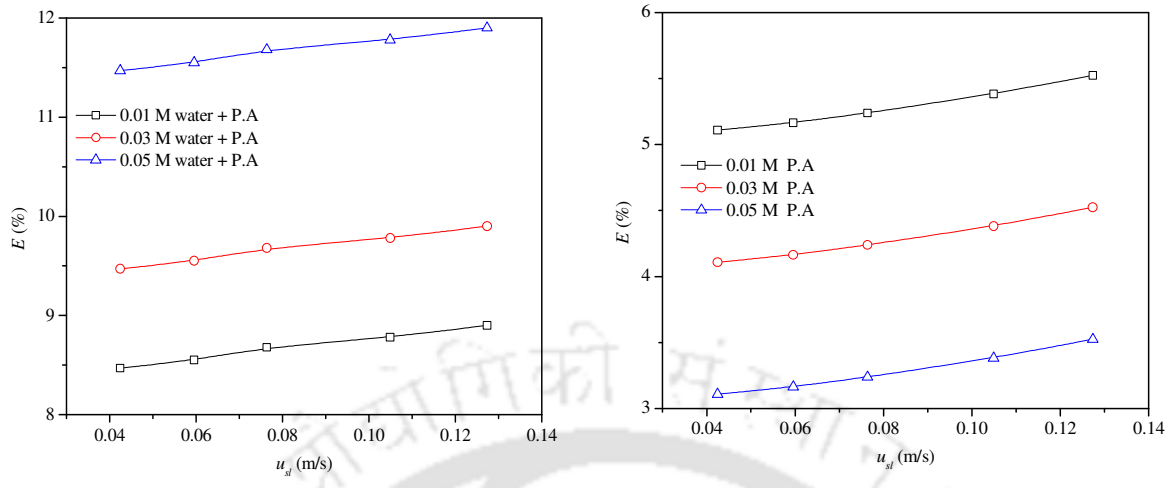

(a) (b)

Figure 8.7: Variations of extraction efficiency with different acid concentrations at u_{sg} = 0.84×10^{-2} m/s for 5% (v) of dispersed liquid (a) paraffin liquid - water + propionic acid and (b) kerosene - water + propionic acid

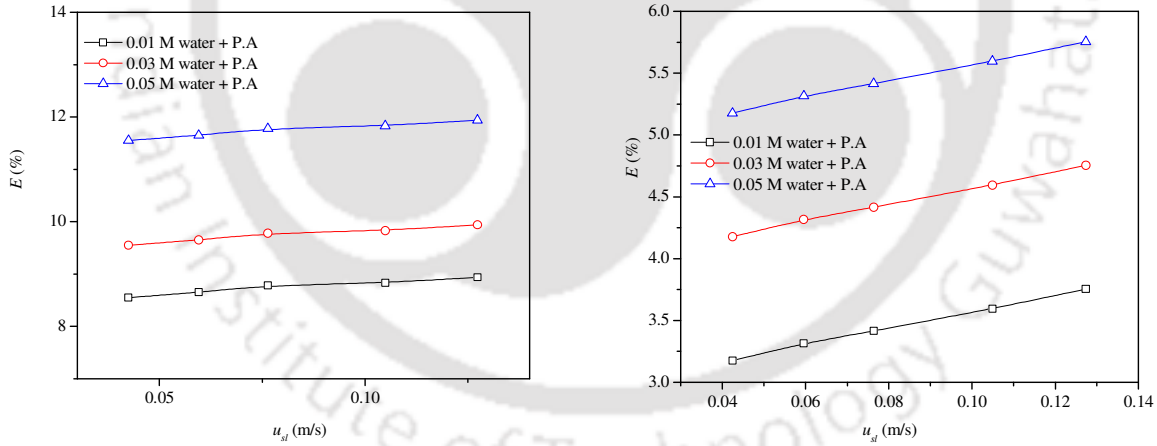

(a) (b)

Figure 8.8: Variations of extraction efficiency with different acid concentrations at u_{sg} = 0.84×10^{-2} m/s for 25% (v) of dispersed liquid (a) paraffin liquid - water + propionic acid and (b) kerosene - water + propionic acid

8.5.4 Effect of gas and liquid flow rate on height of transfer unit (HTU)

Figure 8.9a shows the effect of the height of transfer unit with superficial liquid velocity and gas velocity at 5% paraffin liquid volume fraction. It is observed that the height of transfer unit decreases gradually with an increase in the superficial liquid and gas velocities. At a constant volume fraction of dispersed phase with an increase in the superficial liquid velocity more gas is entrained into the column which decreases the dispersed phase holdup, which in effect decreases the height of transfer unit. A similar trend is reported in the literature (Khawaja et al., 2017; Lim et al., 1995; Usman et al., 2009). Figure 8.9b shows the effect of the height of transfer unit with superficial liquid velocity and gas velocities at 5% kerosene volume fraction. The height of transfer unit is smaller than the paraffin liquid because of the less viscosity of the kerosene which disperses quickly in the water. When the dispersed liquid paraffin and kerosene volume fraction is increased by 15, 25, and 35% of the total volume of the column, it follows the same trend, which is shown in Figure 8.10-8.12 respectively.

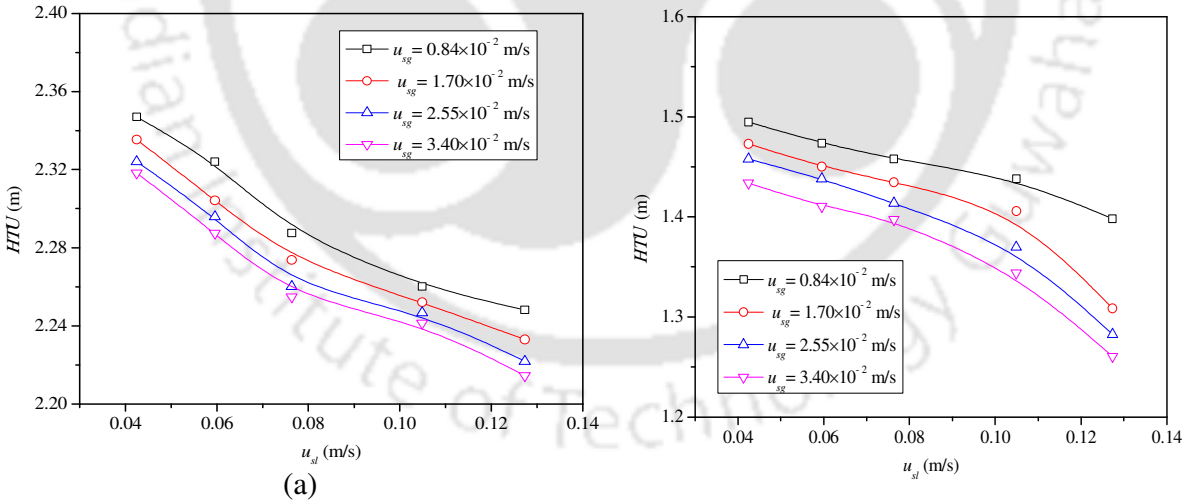

Figure 8.9: Effects of superficial liquid and gas velocities on height of transfer unit for 5% (v) of dispersed liquid (a) paraffin liquid-water + propionic acid and (b) kerosene-water + propionic acid

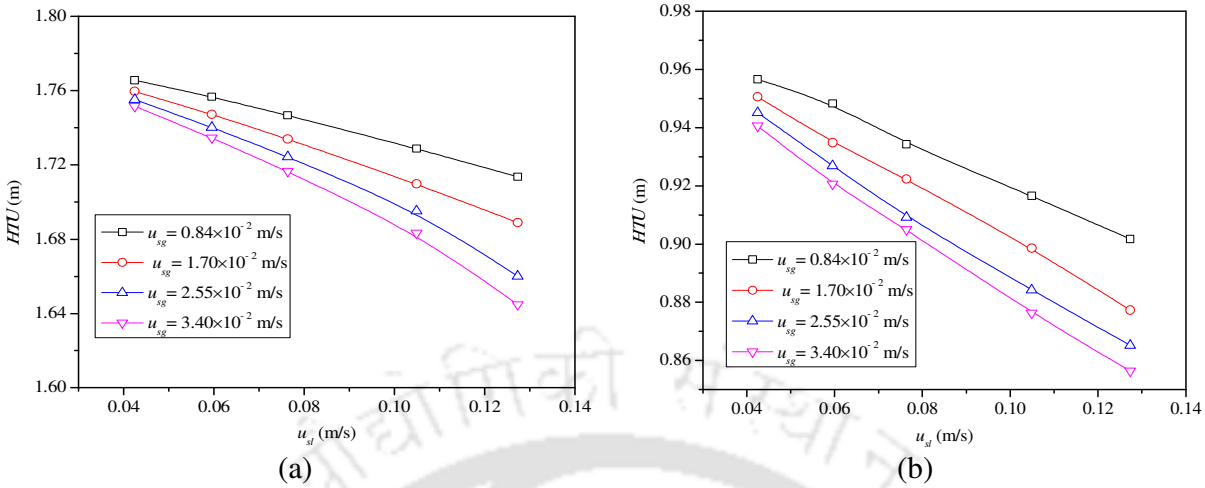

Figure 8.10: Effects of superficial liquid and gas velocities on height of transfer unit for 15% (v) of dispersed liquid (a) paraffin liquid-water + propionic acid and (b) kerosene-water + propionic acid

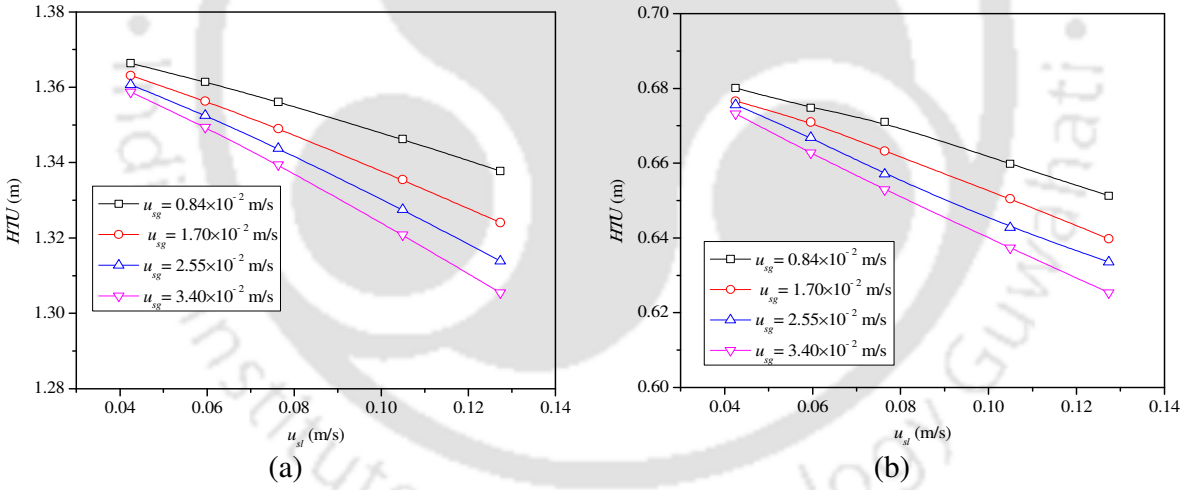

Figure 8.11: Effects of superficial liquid and gas velocities on height of transfer unit for 25% (v) of dispersed liquid (a) paraffin liquid-water + propionic acid and (b) kerosene-water + propionic acid

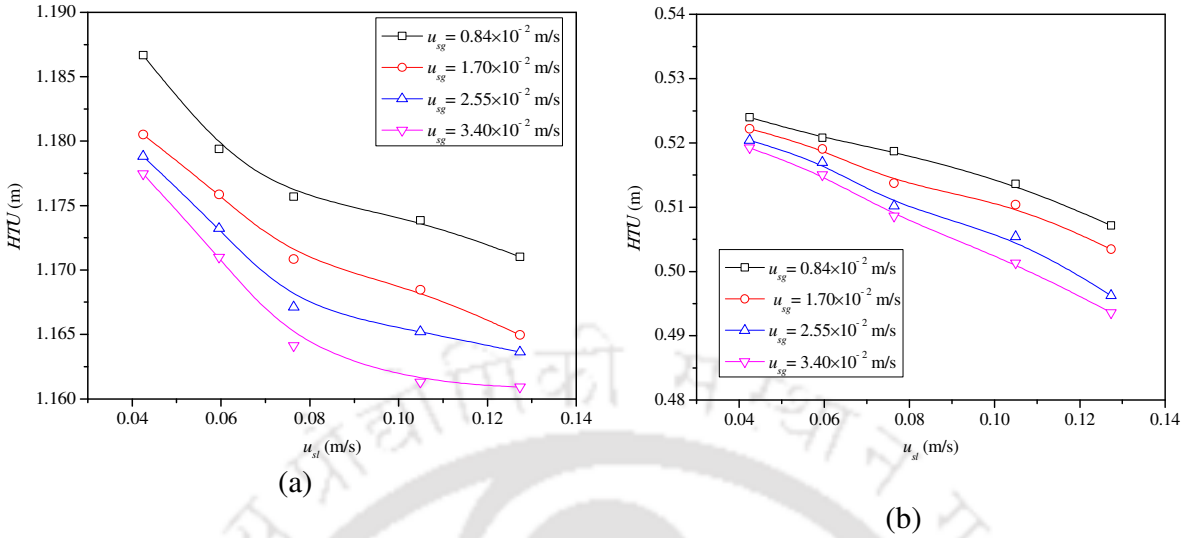

Figure 8.12: Effects of superficial liquid and gas velocities on height of transfer unit for 35% (v) of dispersed liquid (a) paraffin liquid-water + propionic acid and (b) kerosene-water + propionic acid

8.5.5 Effect of gas and liquid flow rate on mass transfer coefficient

Figure 8.13a shows the effect of superficial gas velocity on the mass transfer coefficient for different liquid velocities at a 5% paraffin liquid-water system. The overall volumetric mass transfer coefficient increases with an increase in superficial gas and liquid velocities. This increase in K_La with the increase in flow rate can be attributed to an increase in the specific interfacial area due to the generation of more droplets. The overall volumetric mass transfer coefficient, (which is a product of film mass transfer coefficient and specific interfacial area) increases with an increase in flow rate. A similar trend is reported in the literature (Khawaja et al., 2017; Lim et al., 1995; Usman et al., 2009). Figure 8.13b shows the effect of the mass transfer coefficient with superficial gas velocity for different liquid velocities of a 5% kerosene-water system. It is found that the overall volumetric mass transfer coefficient is higher in the kerosene-water system than that in the paraffin liquid-water system. At constant superficial

liquid and gas velocity, the kerosene drop size is lesser than the paraffin drops as discussed in chapter 7. With decreased drop size at constant superficial liquid and gas velocity, a higher specific interfacial area is observed which gives rise to an increased value of the mass transfer coefficient. When the dispersed liquid volume fraction is increased by 25 %, the mass transfer coefficient increases with superficial liquid and gas velocity, which is shown in Figure 8.14.

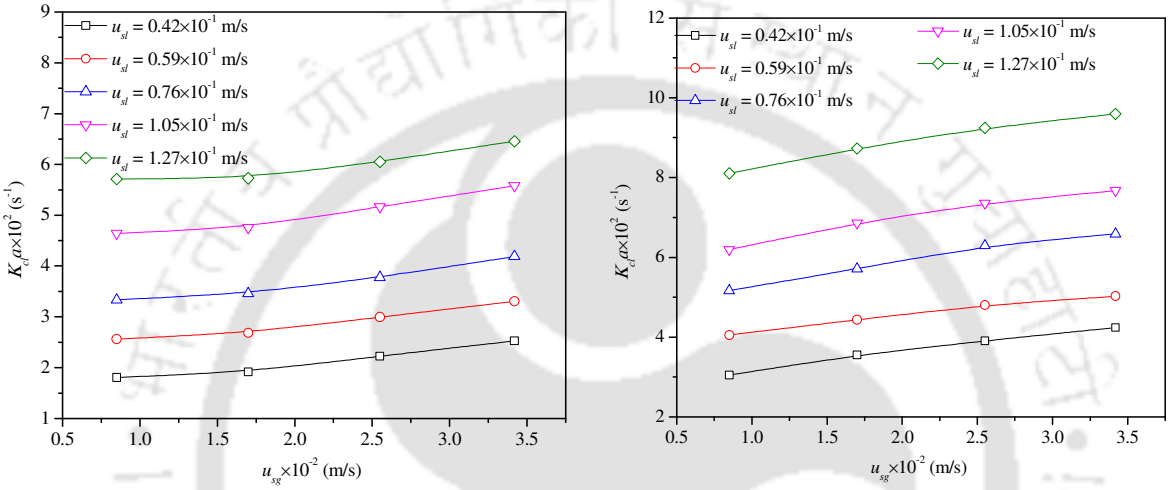

Figure 8.13: Effect of superficial gas and liquid velocity on MTC for 5% (v) of dispersed liquid (a) paraffin liquid-water + propionic acid and (b) kerosene-water + propionic acid

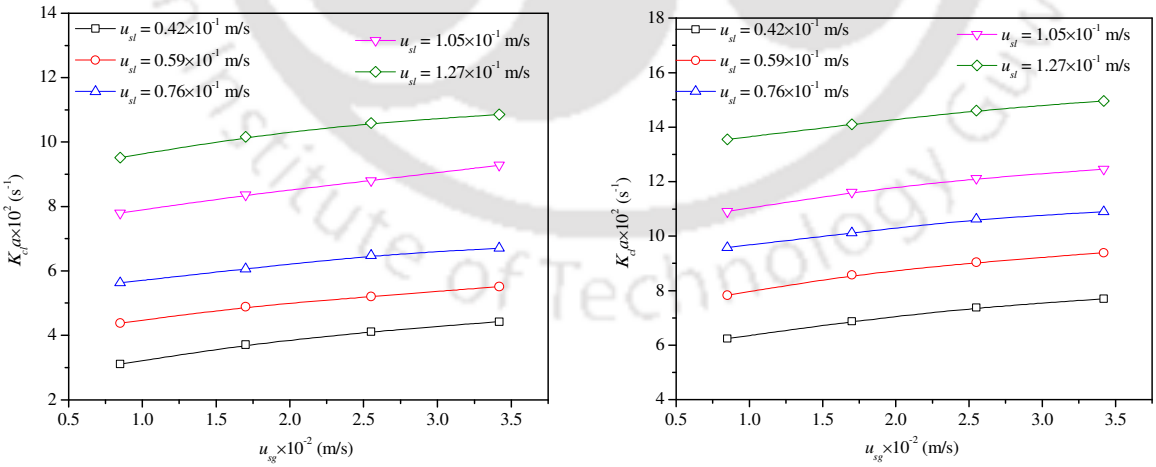

Figure 8.14: Effect of superficial gas and liquid velocity on mass transfer coefficient for 25% (v) of dispersed liquid (a) paraffin liquid-water + propionic acid and (b) kerosene-water + propionic acid

8.5.6 Effect of solvent volume fraction on mass transfer coefficient

Figure 8.15a shows the effect of superficial gas velocity on the mass transfer coefficient for different paraffin liquid concentrations at a constant liquid velocity. It is observed that the mass transfer coefficient increases with the increase in solvent concentration. With the increase in the solvent concentration the dispersed phase holdup increases which in effect increases the mass transfer coefficient. Figure 8.15b shows the effect of superficial gas velocity on the mass transfer coefficient for different kerosene concentrations at a constant liquid velocity. It is observed that the mass transfer coefficient increases with the increase in solvent concentration. The mass transfer coefficient is higher for kerosene than paraffin liquid in the column. This is occurred due to the higher interfacial area of kerosene than the paraffin liquid.

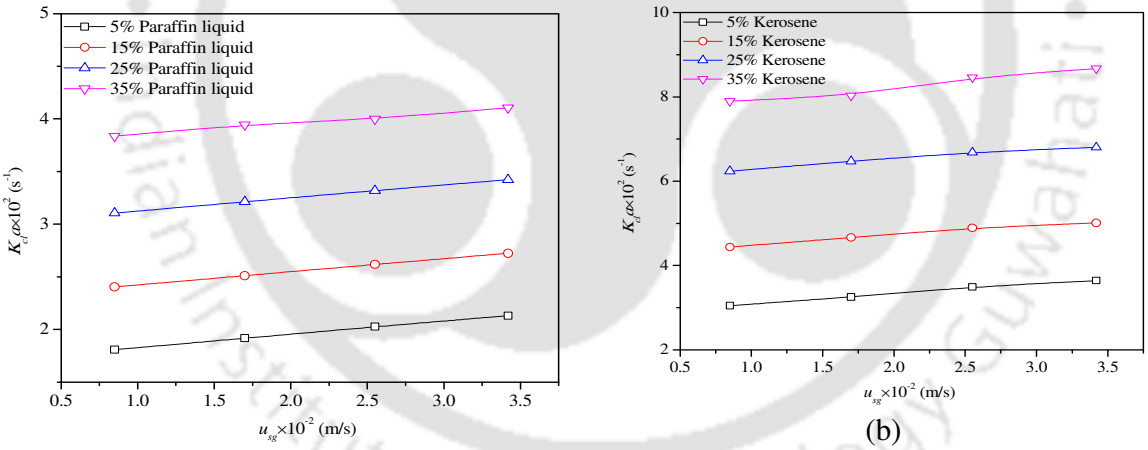

Figure 8.15: Variations of mass transfer coefficient with the superficial gas velocity in different systems (a) paraffin liquid-water + propionic acid and (b) kerosene-water + propionic acid concentrations at $u_{sl} = 0.42\times10^{-2}$ m/s

The variation in the mass transfer coefficient with different concentrations of paraffin liquid and

kerosene at a higher superficial liquid velocity is shown in Figure 8.16. It is observed that the mass transfer coefficient is increasing with the superficial liquid velocity as the intensity of the mixing increases in the column.

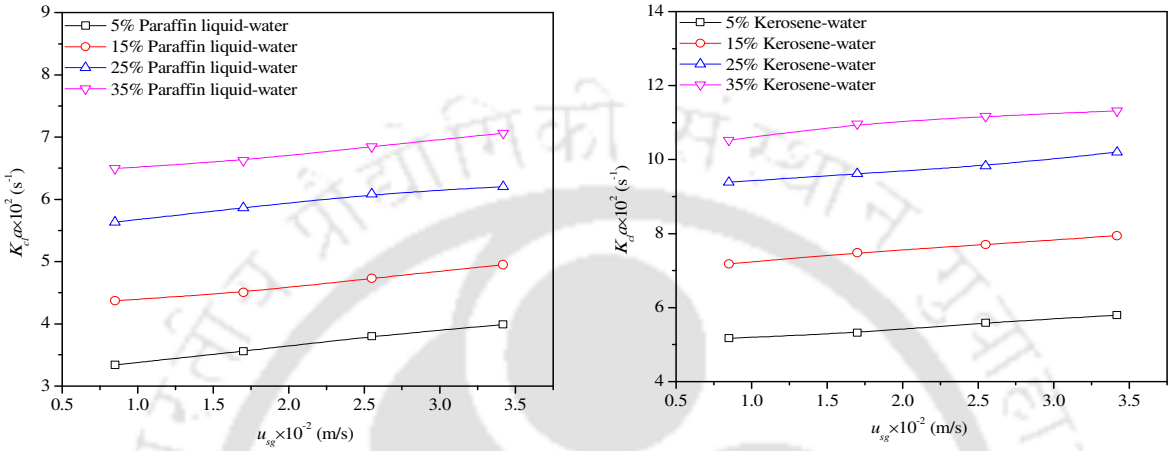

Figure 8.16: Variations of mass transfer coefficient with the superficial gas velocity in different systems (a) paraffin liquid-water + propionic acid and (b) kerosene-water + propionic acid concentrations at $u_{sl} = 7.64\times10^{-2}$ m/s

8.6 Empirical correlation model for mass transfer coefficient

A general correlation has been established by the Buckingham pi theorem of dimensional analysis to predict the mass transfer coefficient. The mass transfer coefficient is shown as a function of different operating and geometric variables. Therefore $K_{cl}a$ may be written as a function of all these variables as:

$$\frac{K_{cl}ad_c}{u_{sl}} = f\left(u_{sl}, u_g, \rho_{cl-dl}, \rho_g, \mu_{cl-dl}, \mu_g, \sigma, g, d_c, h_m\right) \tag{8.5}$$

After dimensional analysis

$$\frac{K_{cl}ad_c}{u_{sl}} = \left(\frac{u_g}{u_{sl}}\right)\left(\frac{\rho_g}{\rho_{cl-dl}}\right)\left(\frac{\mu_l}{u_{sl}\rho_{cl-dl}d_c}\right)\left(\frac{\mu_g}{u_{sl}\rho_g d_c}\right)\left(\frac{\sigma}{u_{sl}^2 d_c \rho_{cl-dl}}\right)\left(\frac{d_c g}{u_{sl}^2}\right)\left(\frac{h_m}{d_c}\right) \tag{8.6}$$

By rearranging the non-dimensional groups, the final equation for the mass transfer coefficient can be written as

$$\frac{K_{cl}ad_c}{u_{sl}} = f\left(\mathrm{Re}_{sl}, \mathrm{Re}_g, We, Fr, H_r\right) \tag{8.7}$$

The multiple regression analysis of experimental data with Equation (8.7) yields,

$$\frac{K_{cl}ad_c}{u_{sl}} = 4.55\times10^{-11}\,\mathrm{Re}_{sl}^{0.30}\,\mathrm{Re}_g^{0.23}\,We^{-2.89}\,Fr^{2.57}\,H_r^{2.55} \qquad R^2 = 0.945 \tag{8.8}$$

The above correlation is valid for the following ranges of variables: 2656.25 < Re_{sl} < 7975.59, 27.82 < Re_g < 111.28, 1.25 < We < 16.52, 0.0036 < Fr < 0.033, 0.023 < H_r < 0.051. The standard error of Equation (8.8) is 0.112. The correlation was established based on 480 experimental results at varying solvent volume fractions and operating conditions. The values $K_{cl}a$ calculated from the correlation and Equation (8.8) from the experimental values are compared, which are shown in Figure 8.17. The overall efficiency error in mass transfer coefficient values from the experimental and correlation is found to be +28 % and -24 %.

8.7 Extraction efficiency analysis by empirical correlation

The extraction efficiency is found to vary with (i) physical properties of the liquid and gas, namely density, viscosity, surface tension, (ii) operating variables namely, liquid and gas flow rates, (iii) geometric variables namely, the diameter of the column (d_c). A function of extraction efficiency E based on all these variables can be expressed as,

$$E = f\left(u_{sl}, u_g, \rho_{cl-dl}, \rho_g, \mu_{cl-dl}, \mu_g, \sigma, g, d_c, h_m\right) \tag{8.9}$$

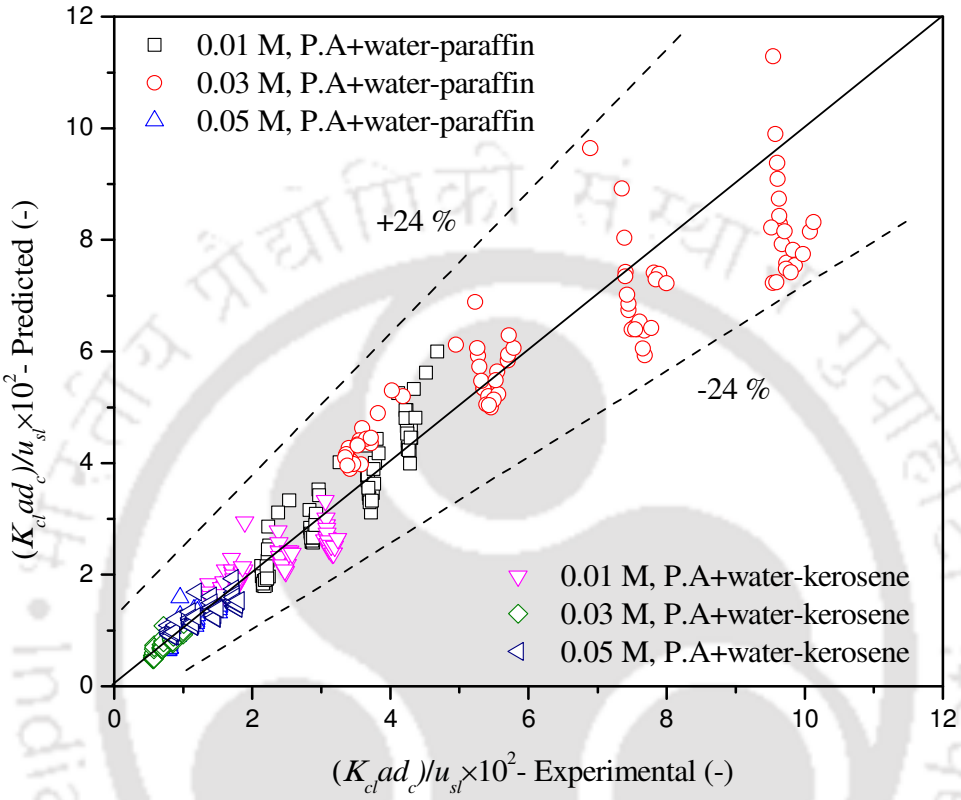

Figure 8.17: Parity plot of experimental values and calculated values of the mass transfer coefficient

Combining the non-dimensional groups from the dimensional analysis, the resulting equation for extraction efficiency of paraffin liquid- water + PA system can be expressed as,

$$E = \left(\frac{u_g}{u_{sl}}\right)\left(\frac{\rho_g}{\rho_{cl-dl}}\right)\left(\frac{\mu_l}{u_{sl}\rho_{cl-dl}d_c}\right)\left(\frac{\mu_g}{u_{sl}\rho_g d_c}\right)\left(\frac{\sigma}{u_{sl}^2 d_c \rho_{cl-dl}}\right)\left(\frac{d_c g}{u_{sl}^2}\right)\left(\frac{h_m}{d_c}\right) \tag{8.10}$$

By rearranging the non-dimensional groups into dimensional numbers, the final equation for extraction efficiency can be expressed as,

$$E = f\left(\mathrm{Re}_{sl}, \mathrm{Re}_{g}, We, Fr, H_r\right) \tag{8.11}$$

The multiple regression analysis of experimental data based on the Equation (8.11) yields,

$$E = 73.02\mathrm{Re}_{sl}^{0.55}\,\mathrm{Re}_{g}^{0.104}\,We^{0.864}\,Fr^{-0.99}\,H_r^{1.18} \qquad R^2 = 0.920 \tag{8.12}$$

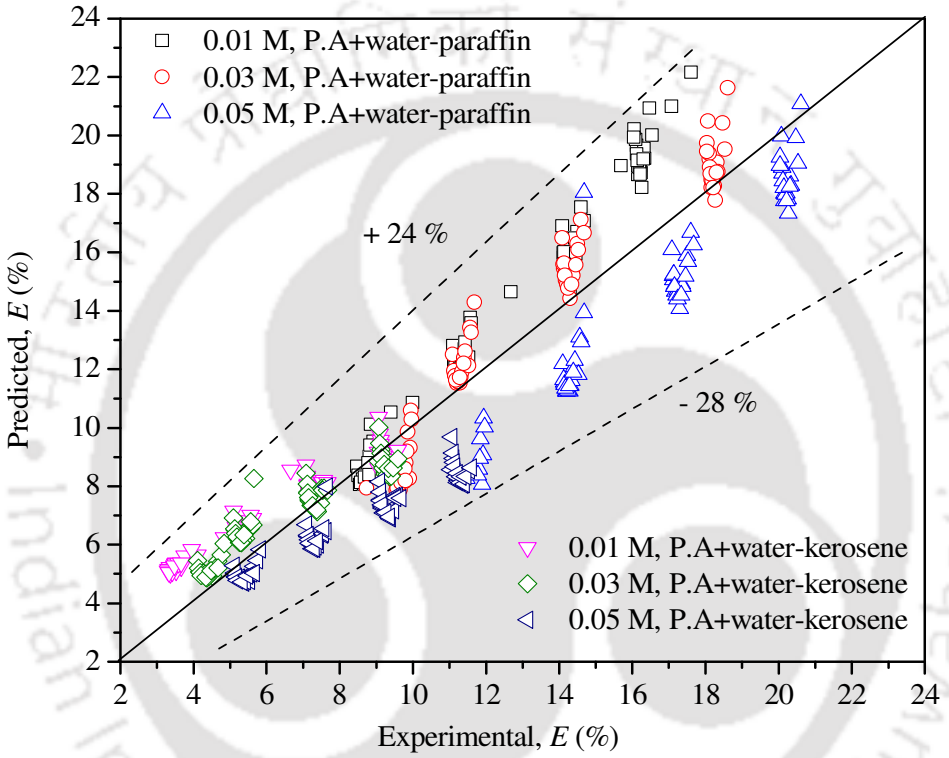

Figure 8.18: Parity plot of experimental values and calculated values of extraction efficiency at different solute concentrations

The above correlation is valid for the following ranges of variables: 2656.25 < Re_{sl} < 7975.59, 27.82 < Re_g < 111.28, 1.25 < We < 16.52, 0.0036 < Fr < 0.033, 0.023 < H_r < 0.051. The standard error of Equation (8.12) is 0.180. The correlation was established based on 480 experimental data at different solvent volume fractions and operating conditions. The overall percentage error between the experimental and correlation data is found to be within +24 % and -28 %. The

values of extraction efficiency calculated from the correlation and the experimental values are compared, which are shown in Figure 8.18.

8.8 Conclusions

The extraction efficiency of the gas-liquid-liquid system was experimentally investigated in a jet-driven gas-aided downflow column using air-water-paraffin liquid and air-water-kerosene system in the presence of mass transfer. The extraction efficiency is found to be strongly affected by the superficial liquid velocity and gas velocity. It is observed that the extraction efficiency increased with an increase in superficial gas and liquid velocities. The less extraction efficiency for kerosene compared to paraffin liquid is found as per the present investigation. This is occurred due to the low interfacial tension of kerosene solvent. The extraction efficiency is found to be higher with high solute concentration due to the lower surface tension of water and propionic acid mixture which enables to form more bubble-droplet mixture. The mass transfer coefficient appeared to be a strong function of both the superficial liquid and gas velocities. Mass transfer coefficient increases with an increase in the concentration of the dispersed liquid. The mass transfer coefficient of propionic acid in the kerosene phase was observed to be more than that when propionic acid is extracted with the paraffin liquid phase. The mass transfer coefficient is correlated with different operating system variables by developing a general correlation.

CHAPTER- 9

OVERALL CONCLUSIONS AND RECOMMENDATIONS FOR FUTURE WORKS

This chapter summarizes overall conclusions made from the present research findings of the thesis and also points out the possible scope for future research work

9.1 Overall conclusions

9.1.1 Entrainment characteristics:

- From this work, it was observed that gas entrainment varies with the liquid flow rate and system properties. It is increased with increasing gas and liquid flow rates.
- The liquid entrainment can be enhanced based on the liquid jet kinetic energy utilization. The penetration depth is correlated with the operating variables in terms of jet length to nozzle diameter ratio, Reynolds number, and the jet Froude number.
- A generalized correlation is proposed for entrainment of gas and liquid as a function of various operating variables within the range of experimental conditions.

9.1.2 Gas holdup characteristics:

- The gas holdup varies with the liquid flow rate and system properties. It is increased with increasing gas and liquid flowrates.
- Gas holdup data were analyzed by Lockhart-Martinelli correlation with modifications and by drift flux model.
- The slip velocity is also used to interpret the relative bubble velocity which indicates the interaction of the bubbles along with the liquid movement. This enables to bubble and droplet breakup to enhance the turbulence in the column which may be useful for intensification of the mass transfer process.

- A generalized correlation was proposed for entrainment of gas hold up as a function of various operating variables.

9.1.3 Frictional pressure drop characteristics:

- The frictional pressure drop rises with a rise in liquid and gas velocity. The variation of frictional pressure drop is found more significant at higher gas velocity (u_{sg} = 3.40×10^{-2} m/s) as compared to that at lower gas velocity (u_{sg} = 0.84×10^{-2} m/s).
- With the rise in the gas holdup of the system, the contact among the droplets and the liquid interface rises, and dispersed liquid droplets generate more friction and turbulence with the gas-liquid-liquid mixture.
- At a fixed superficial gas velocity, with a rise in liquid jet velocity, the intense mixing by higher momentum exchange inside the column leads to an increase in the friction in the column.
- The modified Lockhart-Martinelli model predicts the frictional pressure drop better compared to the Kato, Wallis, and Gharat and Joshi models for both low and high mixture Reynolds number. It is recommended for the prediction of frictional pressure drop in the proposed type of extraction column.
- A general empirical correlation is developed for frictional pressure drop and friction factor as a function of various operating variables and the system properties.

9.1.4 Mixing characteristics:

- It is found that the mixing phenomenon in this downflow column is affected by variables such as gas flow rate, liquid flow rate, the concentration of the dispersed liquid.

- The mean residence time of the tracer is greatly affected by superficial liquid and gas velocities. It decreases with an increase in superficial liquid velocity.
- At higher gas flow rates (u_{sg} = 3.40×10^{-2} m/s), variation is less compared to that at lower gas flow rates (u_{sg} = 0.84×10^{-2} m/s).
- The dispersion number of liquid increases with liquid flow rate. The dispersion number of liquid increases (34% for paraffin and kerosene) with increasing gas flow rate (u_{sg} = 0.84×10^{-2} m/s – 3.40×10^{-2} m/s). The amount of entrained gas in the column is increases with liquid velocity and dispersed liquid concentration.
- The variation of entrainment with time and the degree of dispersion are enunciated based on the axial dispersion model. The intensity of the dispersion is found to be a function of the flow resistance in the column.
- The correlations developed by dimensional analysis for Peclet number predict the intensity of mixing as a function of different operating variables.
- From the present experimental study of gas-liquid-liquid three-phase downflow, it is observed that the dispersion coefficient of bubble motion (D_b) is decreased, and the characteristic velocity factor (k) is increased with increase in dispersed liquid concentration.

9.1.5 Drop Size characteristics and its distribution:

- A detailed study was conducted to enunciate the effect of superficial liquid and gas velocities and dispersed liquid volume concentration on drop size, drop size distribution, and the type of the distribution function in a homogenous bubbly drop flow regime.

- A linear relationship was observed between superficial gas velocity and drop size. The obtained drop size distribution observed to follow log-logistic at different experimental conditions.
- Correlations were developed for the estimation of each distribution parameters of all of the distribution functions of the column.
- A generalized correlation model is also developed to predict the Sauter mean drop diameter and drop interfacial area. All of the developed correlations are suitable to predict the experimental data well within the error range of ± 29.90%.

9.1.6 Mass transfer characteristics of gas-liquid-liquid extraction:

- The extraction efficiency of the gas-liquid-liquid system was experimentally investigated in a jet-driven gas-aided downflow column using air-water-paraffin liquid and air-water-kerosene system.
- It was observed that the extraction efficiency increased with increasing superficial gas and water velocities. The interfacial tension of the solvent is one of the key factors for variation of extraction.
- The extraction efficiency is higher with high solute concentration due to the lower surface tension of water and propionic acid mixture which enables to form finer droplets.
- Mass transfer coefficient increases with an increase in superficial liquid and gas velocities and dispersed phase liquid concentration.
- An empirical correlation is developed for the mass transfer coefficient as a function of various operating variables and the system properties.

- The present work may be beneficial for the development of gas-liquid-liquid extraction processes for further understanding of gas – aided extraction process based on the bubble droplet interfacial area for its process intensifications.

9.2 Recommendations for future works

This work has reported the hydrodynamics and mass transfer phenomenon of details of gas-liquid-liquid flow in a jet-driven downflow contactor. The study includes gas holdup, gas entrainment, pressure drop, mixing characteristics, drop size distribution, and extraction efficiency. However, further works are required to have a complete idea in this field for proper designing and scaling of the gas-liquid-liquid contactor. Thus, possible recommendations for future research work in this system can be summarized as follows:

1. Prediction of gas holdup by different models and comparing with phase isolation method and development of different models especially for liquids with varying physical properties.

2. Study on different models for gas entrainment rate in the jet-driven downflow, especially for liquids with different physical properties.

3. Refinement of the theories predicting the pressure drop in the jet-driven downflow column with more experimental data with different liquids.

4. In the present study, mixing characteristics of the liquid has been studied only with paraffin liquid and kerosene system. In view of industrial applications, mixing characteristics should be done with different systems. So there is a scope to study the same with different system which has industrial importance.

5. Experiments for drop size distribution and interfacial area have been studied by photographic method with paraffin liquid and kerosene system. However, other methods can be used to study the drop size distribution. Thus, the authenticity of the results should be checked using other

methods.

6. Extraction studies in the present work are done at a low concentration of propionic acid. In view of industrial application, it is highly recommended for further study by varying different dispersed liquids.

7. Development of a Computational Fluid Dynamic (CFD) model and validation of the model by comparison with the experimental results.

APPENDIX-I

Calculation Procedure for Typical Multiple Regression [Equation (4.14)]

The regression equation is

$$\varepsilon_g = C_1 (\mathrm{Re}_{sl})^{b_1} (\mathrm{Re}_g)^{b_2} (We)^{b_3} (Fr)^{b_4} (Hr)^{b_5} \quad \text{(A1)}$$

Taking the logarithm of both side of the Equation (A1),

$$\log(\varepsilon_g) = \log(C_1) + b_1 \log(\mathrm{Re}_{sl}) + b_2 \log(\mathrm{Re}_g) + b_3 \log(We) + b_4 \log(Fr) + b_5 \log(Hr) \quad \text{(A2)}$$

The equation (A2) can be written as

$$Y = b_0 + b_1 X_1 + b_2 X_2 + b_3 X_3 + b_4 X_4 + b_5 X_5 + e \quad \text{(A3)}$$

Where Y = log (ε_g), X_1 = log (Re_{sl}), X_2 = log (Re_g), X_3 = log (We), X_4 = log (Fr), X_5 = log (H_r) and e is the error term which has to be minimized to estimate the regression model as

$$\hat{Y} = b_0 + b_1 X_1 + b_2 X_2 + b_3 X_3 + b_4 X_4 + b_5 X_5 \quad \text{(A4)}$$

Where $\hat{Y}$ is the predicted value of Y

The intercept b_o and the coefficients b_1, b_2, b_3, b_4, b_5 have been estimated by multiple regression analysis by 'Data Analysis Tool' of software 'Microsoft Excel'.

The software gives output on the basis of the following calculation

The equation (A4) can be written in matrix form for n (here n = 160) and k (here k = 5) variables as

$$\begin{bmatrix} Y_1 \\ Y_2 \\ . \\ . \\ Y_n \end{bmatrix} = \begin{bmatrix} 1 & X_{11} & ..... & X_{1k} \\ 1 & X_{21} & ..... & X_{1k} \\ . & & & \\ . & & & \\ 1 & X_{n1} & ..... & X_{1k} \end{bmatrix} \times \begin{bmatrix} b_1 \\ b_2 \\ . \\ . \\ b_{\backslash n} \end{bmatrix} + \begin{bmatrix} e_1 \\ e_2 \\ . \\ . \\ e_n \end{bmatrix} \quad \text{(A5)}$$

Y = X × B + e

Regression statistics

		Explanation
Multiple R	0.99	R = square root of R^2
R square	0.99	R^2 = coefficient of determination
Adjusted R square	0.99	Adjusted R^2 used if more than one X variable
Standard error	0.05	Estimate of the St. dev. Of the error e
Observations	160	Number of observations used in the regression

Analysis of variance

	Degrees of freedom	Sum of square	Mean of square	F-stat
Regression	5	60.12	12.02	4196.02
Residual	154	0.44	0.002	
Residual	159	60.56		

Regression sum of square = $B'X'Y - n\bar{Y}^2$

Total sum of square = $Y'Y - n\bar{Y}^2$

$$Y' = [Y_1 \quad Y_2 \quad Y_n]$$

$$B' = [B_1 \quad B_2 \quad B_n]$$

Residual sum of square = Total sum of square - Regression sum of square

$$R^2 = \frac{\text{Regression sum of square}}{\text{Residual sum of square}}$$

$$F - stat = \frac{R^2/(k-1)}{(1-R^2)/(n-k)}$$

Adjusted $R^2 = 1-(1-R^2)\left(\frac{n-1}{n-k}\right)$

Standard Error = $\sqrt{\frac{\text{Residual sum of square}}{\text{n - k}}}$

The F-stat gives the overall F-test of null hypothesis H_o: $b_1 = 0$. The F-stat gives the associated probability value. Since it is greater than 0.05 at 5% significance level we do not reject null hypothesis for the goodness of fit.

APPENDIX-II

Goodness of Fit for the Distributions Cited in Figure 7.16

Data points: 25

Estimates: Maximum likelihood estimates

Accuracy of Fit: 3×10^{-4}

Level of significance: 0.005

Details of the tests

Log Logistic: Min = 2, p = 6.74, β = 0.409

Chi Square		Kolmogorov-Smirnov		Anderson-Darling	
Total class	4	K-S Stat	7.75×10^{-2}	A-D Stat	0.19
Interval type	Equal probable	p-value	0.995	p-value	0.993
Degree of freedom	3	Result	Accept	Result	Accept
Chi square	0.44				
p-value	0.932				
result	Accept				

Beta: Min = 2, Max = 850.68

Chi Square		Kolmogorov-Smirnov		Anderson-Darling	
Total class	4	K-S Stat	7.89×10^{-2}	A-D Stat	0.227
Interval type	Equal probable	p-value	0.994	p-value	0.981
Degree of freedom	3	Result	Accept	Result	Accept
Chi square	7.81				
p-value	0.932				
result	Accept				

Chi Squared: Min = 2, $\upsilon = 1.17$

Chi Square		Kolmogorov-Smirnov		Anderson-Darling	
Total class	4	K-S Stat	0.462	A-D Stat	7.57
Interval type	Equal probable	p-value	2.08×10^{-5}	p-value	0.
Degree of freedom	3	Result	Reject	Result	Reject

Chi square	7.81				
p-value	5.12×10^{-13}				
result	Reject				

Erlang: Min = 2, m = 15, $\beta = 2.819\times10^{-2}$

Chi Square		Kolmogorov-Smirnov		Anderson-Darling	
Total class	4	K-S Stat	7.56×10^{-2}	A-D Stat	0.227
Interval type	Equal probable	p-value	0.997	p-value	0.981
Degree of freedom	3	Result	Accept	Result	Accept
Chi square	7.81				
p-value	0.932				
result	Accept				

Log normal: Min = 2, mu = -0.894, $\sigma = 0.260$

Chi Square		Kolmogorov-Smirnov		Anderson-Darling	
Total class	4	K-S Stat	7.79×10^{-2}	A-D Stat	2.49
Interval type	Equal probable	p-value	0.995	p-value	0.987
Degree of freedom	3	Result	Accept	Result	Accept
Chi square	7.81				
p-value	0.782				
result	Accept				

Weibull: Min = 2, $\alpha = 3.88$, $\beta = 0.465$

Chi Square		Kolmogorov-Smirnov		Anderson-Darling	
Total class	4	K-S Stat	0.123	A-D Stat	0.541
Interval type	Equal probable	p-value	0.799	p-value	0.705
Degree of freedom	3	Result	Accept	Result	Accept
Chi square	1.08				
p-value	0.782				
result	Accept				

Inverse Gaussian: Min = 2, $\alpha = 6.03$, $\beta = 0.42$

Chi Square		Kolmogorov-Smirnov		Anderson-Darling	
Total class	4	K-S Stat	7.83×10^{-2}	A-D Stat	0.213
Interval type	Equal	p-value	0.995	p-value	0.986

	probable				
Degree of freedom	3	Result	Accept	Result	Accept
Chi square	1.08				
p-value	0.782				
result	Accept				

Gamma: Min = 2, $\alpha = 14.88$, $\beta = 2.84\times10^{-2}$

Chi Square		Kolmogorov-Smirnov		Anderson-Darling	
Total class	4	K-S Stat	7.6×10^{-2}	A-D Stat	0.226
Interval type	Equal probable	p-value	0.996	p-value	0.981
Degree of freedom	3	Result	Accept	Result	Accept
Chi square	0.44				
p-value	0.932				
result	Accept				

Pearson 5: Min = 2, $\alpha = 14.98$, $\beta = 5.92$

Chi Square		Kolmogorov-Smirnov		Anderson-Darling	
Total class	4	K-S Stat	9.53×10^{-2}	A-D Stat	0.239
Interval type	Equal probable	p-value	0.961	p-value	0.976
Degree of freedom	3	Result	Accept	Result	Accept
Chi square	7.81				
p-value	0.782				
result	Accept				

The following distributions have been used to fit the experimental data in this study. Also goodness of fit has been tested by Chi Square test, Kolmogorov Smirnov test and Anderson Darling test by STAT::FIT Software. The methods of calculation for the different tests are also discussed in this section.

Beta Distribution

The Beta distribution is a continuous distribution that has both upper and lower finite bounds. The Beta distribution can approach zero or infinity at either of its bounds, with p controlling the lower bound and q controlling the upper bound (Johnson et al., 1995). It is defined as

$$F(x) = \frac{1}{B(p,q)} \frac{(x-\min)^{p-1}(\max-x)^{q-1}}{(\max-\min)^{p+q-1}}$$

where, min = minimum value of x,

Max=maximum value of x

P = lower shape parameter > 0

q = upper shape parameter > 0

B(p,q) Beta Function

Erlang Distribution

The Erlang distribution is a continuous distribution bounded on the lower side (Johnson et al., 1995). It is defined as

$$F(x) = \frac{(x - \min)^{m-1}}{\beta^m \Gamma(m)} \exp\left(-\frac{x - \min}{\beta}\right)$$

where, min = minimum x

m= shape factor = positive integer

β = scale factor > 0

Logistic Distribution

The logistic distribution is an unbounded continuous distribution which is symmetrical about its mean (Johnson et al., 1995). It is defined as

$$F(x) = \frac{\exp\left(-\frac{(x-\alpha)}{\beta}\right)}{\beta\left[1+\exp\left(-\frac{(x-\alpha)}{\beta}\right)\right]^2}$$

where, α = shift parameter

β = scale parameter > 0

Lognormal Distribution

The Lognormal distribution is a continuous distribution bounded on the lower side. The lognormal distribution is defined as

$$F(x) = \frac{1}{(x-\theta)\sqrt{2\pi\hat{\sigma}^2}} \exp\left(-\frac{[\log(x-\theta)-\hat{\mu}]^2}{2\hat{\sigma}^2}\right)$$

where, θ = minimum x

$$\hat{\mu} = \frac{\sum_{i=1}^{n} \ln(x_i)}{n}$$

$$\hat{\sigma} = \sqrt{\frac{\sum_{i=1}^{n} (\ln x_i - \hat{\mu})}{n}}$$

F(x) is always 0 at minimum *x*, rising to a peak that depends on both $\hat{\mu}$ and $\hat{\sigma}$, then decreasing monotonically for increasing *x*. By definition, the natural logarithm of a lognormal random variable is a Normal random variable. The lognormal distribution can also be used to approximate the normal distribution, for small sigma, while maintaining its strictly positive values of *x* (Johnson et al., 1995).

Weibull Distribution

The Weibull distribution is a continuous distribution bounded on the lower side. It provides one of the limiting distributions for extreme values (Johnson et al., 1995). It is defined as

$$F(x) = \frac{\alpha}{\beta}\left(\frac{x-\theta}{\beta}\right)^{\alpha-1} \exp\left(-\left(\frac{[x-\theta]}{\beta}\right)^{\alpha}\right)$$

where, θ = minimum x

α = shape parameter > 0

β = scale parameter > 0

F(x) has three distinct regions. For α =1, the Weibull distribution is reduced to the exponential distribution, starting at a finite value at minimum *x* and decreasing monotonically thereafter. For α < 1, the Weibull distribution tends to infinity at minimum *x* and decreases monotonically for increasing *x*. for α > 1, the Weibull distribution is 0 at minimum *x*, peaks at a value that depends on both α and β , decreasing monotonically thereafter.

Rayleigh Distribution

The Rayleigh Distribution is a continuous distribution bounded on the lower side (Shooman, 1990). It is defined as

$$F(x)=\frac{(x-\theta)}{\sigma^2}\exp\left(-\frac{(x-\theta)^2}{2\sigma^2}\right)$$

where, θ = minimum x

σ = scale parameter > 0

Inverse Weibull Distribution

The Inverse Weibull distribution is a continuous distribution with a bound on the lower side. It is uniquely zero at the minimum *x*, and always positively skewed. In general, the Inverse Weibull distributions distribution fits bounded, but very peaked, data with a long positive tail (Calabria and Pulcini, 1990). It can be expressed mathematically as

$$F(x)=\alpha\beta\left(\frac{1}{\beta(x-\theta)}\right)^{\alpha+1}\exp\left(-\left(\frac{1}{\beta(x-\theta)}\right)^{\alpha}\right)$$

where, θ = minimum x

α = shape parameter > 0

β = mixture of shape and scale > 0

Chi Squared Distribution

The Chi Squared is a bounded continuous distribution bounded on the lower side (Johnson et al., 1995). It is defined as

$$F(x)=\frac{1}{2^{\upsilon/2}\Gamma(\upsilon/2)}\exp\left(-\frac{(x-\theta)}{2}\right)(x-\theta)^{(\upsilon/2)-1}$$

where, θ = minimum *x*

υ = shape parameter

Inverse Gaussian distribution

The Inverse Gaussian distribution is a continuous distribution with a bound on the lower side. It is uniquely zero at the minimum *x*, distributions and always positively skewed. The Inverse Gaussian distribution is also known as the Wald distribution (Johnson et al., 1994). It is defined as

$$F(x)=\left(\frac{\alpha}{2\pi(x-\theta)^3}\right)^{1/2}\exp\left[-\frac{\alpha(x-\theta-\beta)^2}{2\beta^2(x-\theta)}\right]$$

where, θ= minimum x

α = shape parameter > 0

β = mixture of shape and scale > 0

The goodness of fit for distribution

To fit a distribution with the experimental data the parameters for each distribution are calculated by using either the moment equation or the maximum likelihood equation. Finally, the test for goodness of fit are calculated for each fitted distribution in order to ascertain the relative goodness of fit (Breinam, 1973: Law and Kelton, 1991; Banks and Carson, 1984; Stuart and Ord, 1991). The tests for goodness of fit are merely comparisons of the input data to the fitted distributions in a statistically significant manner. Each test makes the hypothesis that the fit is good and calculates a test statistic for comparison to a standard. There are different types of goodness of fit tests whereas the following three teat are more useful.

1. Chi Squared test
2. Kolmogorov Smirnov test
3. Anderson Darling test

If the choice of test is uncertain, even after consulting the descriptions, Kolmogorov Smirnov test is applicable over the widest range of data and fitted parameters.

While the test statistic for the Chi Squared test can be useful, the *p* value is more useful in determining the goodness of fit. The *p* value is defined as the probability that another sample will be as unusual as the current sample given that the fit is appropriate. A small p-value indicates that the current sample is highly unlikely, and therefore, the fit should be rejected. Conversely, a high *p*-value indicates that the sample is likely and would be repeated, and therefore, the fit should not be rejected. Thus, the higher the *p* value, the more likely that the fit is appropriate. When comparing two different fitted distributions, the distribution with the higher *p* value is likely to be the better fit regardless of the level of significance.

Chi Squared test

The Chi Squared test is attest of the goodness of fit of the fitted density ($F(x)$) to the

experimental data appropriately separated into different classes. Then the Chi-squared statistic for this data is calculated according to the equation:

$$\chi^2 = \sum_{i=1}^{k} \frac{(n_i - np_i)}{np_i^2}$$

where χ^2 is the Chi Squared statistic, n is the total number of data points, n_i is the number of data points in the ith continuous interval or ith discrete class, k is the number of intervals or classes used, and p_i is the expected probability of occurrence in the interval or class for the fitted distribution. The resulting test statistic is then compared to a standard value of Chi Squared with the appropriate number of degrees of freedom and level of significance. The number of degrees of freedom is always taken to be the net number of data bins (intervals, classes used in the calculation minus 1; because this is the most conservative test, that is, the least likely to reject the fit in error (Law and Kelton, 1991; Brunk, 1960; Stuart and Ord, 1991)

Kolmogorov Smirnov test

The Kolmogorov Smirnov test is a statistical test of the goodness of fit of the fitted cumulative distribution to the experimental data. The Kolmogorov Smirnov test (KS) calculates the largest absolute difference between the cumulative distributions for the experimental data and for the fitted distribution according to the equations:

$$D = Max\left(D^+, D^-\right)$$

$$D^+ = Max\left(\frac{i}{n} - F(x)\right), i = 1,....., n$$

$$D^- = Max\left(F(x) - \frac{i-1}{n}\right), i = 1,....., n$$

where D is the KS statistic, x is the value of the ith point out of n total data points, and $F(x)$ is the fitted cumulative distribution. The difference is determined separately for positive and negative discrepancies on a point by point basis. The resulting test statistic is then compared to a standard value of KS statistic with the appropriate number of data points and level of significance [Law and Kelton (1991), Brunk (1960), Stuart and Ord (1991)]. The goodness of fit view also reports a REJECT or ACCEPT decision for each KS test based on the comparison between the calculated test statistic and the standard statistic for the given level of significance.

Anderson Darling test

The Anderson Darling test is also a test of the goodness of fit of the fitted cumulative distribution to the experimental data, weighted heavily in the tails of the distributions. The Anderson Darling (AD) test calculates the integral of the squared difference between the experimental data and the fitted distribution, with increased weighting for the tails of the distribution, by the equation:

$$W_n^2 = n\int_{-\infty}^{\infty} \frac{[F_n(x) - F(x)]^2}{F(x)[1 - F(x)]} dF(x)$$

where W_n^2 is the AD statistic, n is the number of data points, $F(x)$ is the fitted cumulative distribution, and $F_n(x)$ is the cumulative distribution of the experimental data. This can be reduced to the more useful computational equation:

$$W_n^2 = -n - \frac{1}{n}\sum_{i=1}^{n}(2i-1)[\log\mu_i + \log(1-\mu_{n-i+1})]$$

where μ_i is the value of the fitted cumulative distribution, $F(x_i)$, for the ith data point [Law and Kelton (1991) and Anderson and Darling (1994)]. The resulting test statistic is then compared to a standard value of AD statistic with the appropriate number of data points and level of significance. The goodness of fit view also reports a REJECT or ACCEPT decision for each AD test base on the comparison between the calculated test statistic and the standard statistic for the given level of significance.

NOMENCLATURE

Chapter-2

C	Concentration of solute in the continuous liquid (mol/l)
$C_{cl,\ in}$	Inlet concentration of solute in the continuous liquid (mol/l)
$C_{cl,\ out}$	Outlet concentration of solute in the continuous liquid (mol/l)
$C_{dl,\ in}$	Inlet concentration of solute in the dispersed liquid (mol/l)
$C_{dl,\ out}$	Outlet concentration of solute in the dispersed liquid (mol/l)
d_c	Column diameter (m)
d_s	Suction diameter (m)
d_i	Air inlet diameter (m)
d_t	Throat diameter (m)
E	Extraction percentage (%)
h_s	Suction chamber height (m)
H	Height of the extraction column (m)
H_{cl}	Height of continuous liquid (m)
H_{dl}	Height of dispersed liquid (m)
$H_{dl\text{-}cl}$	Height of liquid-liquid mixture in the column (m)
$H_{g\text{-}dl\text{-}cl}$	Height of gas-liquid-liquid mixture interface (m)
HTU_{cl}	Height of transfer unit based on continuous phase (m)
K	Conductivity of the solution (micro-Siemens)
$K_{cl}a$	Volumetric mass transfer coefficient based on continuous phase (1/s)
L_d	Length of diffuser (m)
L_t	Length of Throat (m)
m	Equilibrium constant
M	Molar Concentration (mol/l)
M_{cl}	Molecular weight of continuous liquid (kg/kmol)
M_{dl}	Molecular weight of dispersed liquid (kg/kmol)
NTU_{cl}	Number of transfer unit based on continuous phase (m)
ΔP_a	Acceleration component of pressure drop (Pa)
ΔP_{ftp}	Frictional pressure drop for three phase flow (Pa)

ΔP_h	Hydrostatic pressure drop, (Pa)
ΔP_{TP}	Total pressure drop for three phase flow (Pa)
Q_g	Gas entrainment rate (m^3/s)
$Q_{cl\text{-}dl}$	Continuous and dispersed liquid mixture flowrate (m^3/s)
Q_{dl}	Entrainment of dispersed liquid (m^3/s)
u_{cl}	Continuous liquid velocity (m/s)
V_{cl}	Volume of continuous liquid (m^3)
V_{dl}	Volume of dispersed liquid (m^3)
V_{tot}	Total volume of liquid-liquid mixture (m^3)

Greek Letters

α_{cl}	Volume fraction of continuous liquid (-)
α_{dl}	Volume fraction of dispersed liquid (-)
ε_{dl}	Dispersed liquid hold up (-)
ε_g	Gas phase hold up (-)
ρ_{cl}	Continuous phase density (kg/m^3)
ρ_{dl}	Dispersed phase density (kg/m^3)
ρ_{cl-dl}	Density of dispersed and continuous liquid mixture (kg/m^3)
ρ_g	Gas phase density (kg/m^3)
μ_{cl}	Continuous liquid viscosity (kg/m.s)
μ_{dl}	Dispersed liquid viscosity (kg/m.s)
μ_{cl-dl}	Continuous liquid and dispersed liquid mixture viscosity (kg/m.s)
σ_{cl}	Surface tension of continuous liquid (N/m)
σ_{dl}	Surface tension of dispersed liquid (N/m)
σ_{cl-dl}	Surface tension of continuous and dispersed liquid mixture (N/m)

Chapter -3

d_c	Column diameter (m)
d_n	Nozzle diameter (m)
E_s	Supplied kinetic energy (W)
E_{min}	Minimum energy (W)
$E_{u,min}$	Minimum energy utilized (W)
$f_{v,cum}$	Cumulative entrainment rate (-)
Fr	Froude number ($=u_{sl}^2 / gd_c$) (-)
g	Gravitational acceleration (m/s^2)
$h_{g\text{-}cl\text{-}dl}$	Height of gas-liquid-liquid mixing height (m)
H_{cl}	Height of continuous liquid (m)
H_{dl}	Height of dispersed liquid (m)
$H_{cl\text{-}dl}$	Height of continuous liquid-dispersed liquid (m)
$H_{g\text{-}dl\text{-}cl}$	Height of gas-liquid-liquid mixture interface (m)
H_p	Height of penetration depth (m)
H_{pR}	Ratio of height of penetration depth and nozzle diameter (H_p/d_n) (-)
H_r	Height ratio of three phase mixture to diameter of the mixing column (h_m/d_c) (-)
$i.d$	Inner diameter (m)
L_j	Jet length (m)
L_c	Length of the column (m)
L_{jR}	Ratio of length of jet and nozzle diameter (L_j/d_n) (-)
M	Parameter defined in Equation (3.8) (-)
M_{cl}	Molecular weight of continuous liquid (kg/kmol)
M_{dl}	Molecular weight of dispersed liquid (kg/kmol)
p	Parameter defined in Equation (3.6)
q	Parameter defined in Equation (3.6)
Q_g	Gas entrainment rate (m^3/s)
$Q_{cl\text{-}dl}$	Continuous and dispersed liquid mixture flowrate (m^3/s)
Q_{dl}	entrainment of dispersed liquid (m^3/s)
R^2	Correlation coefficient (-)

Re_j	Jet Reynolds number ($=\rho_l d_c u_j / \mu_l$), (-)
Re_g	Gas Reynolds number ($=\rho_g d_c u_{sg} / \mu_g$), (-)
u_j	Jet velocity (m/s)
u_{sg}	Superficial gas velocity (m/s)
u_{sl}	Superficial liquid velocity (m/s)
$u_{e,min}$	Minimum entrainment velocity (m/s)
V_{cl}	Volume of continuous liquid (m^3)
V_{dl}	Volume of dispersed liquid (m^3)
V_{tot}	Total volume of liquid-liquid mixture (m^3)
We	Weber number ($=\rho_{sl} u_j^2 d_n / \sigma$) (-)

Greek letters:

α	Parameter defined in Equation (3.16)
β	Parameter defined in Equation (3.16)
γ	Parameter defined in Equation (3.16)
Γ	Parameter defined in Equation (3.7)
α_{cl}	Volume fraction of continuous liquid (-)
α_{cl}	Volume fraction of dispersed liquid (-)
η_m	Efficiency of mixture (-)
ϕ_{dl}	Volume concentration of the dispersed phase (-)
ε_{cl}	Continuous liquid hold up (-)
ε_{dl}	Dispersed liquid hold up (-)
ε_g	Gas phase hold up (-)
ρ_{cl}	Continuous phase density (kg/m^3)
ρ_{cl-dl}	Continuous liquid and dispersed liquid mixture density (kg/m^3)
ρ_g	Gas phase density (kg/m^3)
μ_g	Gas phase viscosity (kg/m.s)

μ_{cl}	Continuous liquid viscosity (kg/m.s)
μ_{dl}	Dispersed liquid viscosity (kg/m.s)
μ_{cl-dl}	Continuous liquid and dispersed liquid mixture viscosity (kg/m.s)
σ_{cl}	Surface tension of continuous liquid (N/m)
σ_{dl}	Surface tension of dispersed liquid (N/m)
σ_{cl-dl}	Surface tension of continuous liquid and dispersed liquid (N/m)

Subscripts

cl	Continuous liquid
dl	dispersed liquid
g	Gas
g-cl-dl	Gas- continuous-dispersed liquid mixture
j	Jet velocity
m	Mixture
cl-dl	Continuous liquid and dispersed liquid mixture

Chapter-4

a_1-a_4	Parameters used in Equation (4.1)
A_r	Area ratio (-)
C_o	Distribution parameter (-)
d_c	Column diameter (m)
d_d	Drop diameter (m)
Fr	Froude number ($=u_M^2 / gd_c$) (-)
g	Gravitational acceleration (m/s^2)
h_c	Height of column (m)
h_m	Mixing height (m)
H_r	Height ratio of three phase mixture to diameter of the mixing column (h_m/d_c) (-)
i.d	Inner diameter (m)

k_m	Mixing loss coefficient (-)
m_g	Mass flow rate of gas (kg/s)
m_m	Mass flow rate of mixture (kg/s)
Mo	Morton number ($g\mu_{dl-cl}^4 / \rho_{dl-cl}\sigma_{dl-cl}^3$) (-)
N	Number of repeated experiments (-)
Q_g	Gas entrainment rate (m^3/s)
$Q_{cl\text{-}dl}$	Continuous and dispersed liquid flowrate (m^3/s)
R^2	Correlation coefficient (-)
Re_j	Jet Reynolds number (= $\rho_l d_c u_j / \mu_l$), (-)
Re_g	Gas Reynolds number (= $\rho_g d_c u_{sg} / \mu_g$), (-)
SE	Standard error (-)
$STDEV$	Standard deviation (-)
u_b	Rise velocity of bubble (m/s)
u_c	Velocity of continuous phase (m/s)
u_d	Drift velocity (m/s)
u_j	Jet velocity (m/s)
u_l	Interstitial liquid velocity (m/s)
u_s	Slip velocity (m/s)
u_{sg}	Superficial gas velocity (m/s)
u_{sl}	Superficial liquid velocity (m/s)
U	Standard uncertainty (-)
We	Weber number (= $\rho_{sl} u_j^2 d_n / \sigma$) (-)
x	Mass quality (-)
x_i	Experimental value at i (-)
$\bar{x}$	Mean of repeated experiments (-)
X	Lockhart-Martinelli parameter (-)
Δz	Vertical length (m)

Greek letters:

α	Parameter defined in Equation (4.23)
β	Parameter defined in Equation (4.23)
$\bar{\epsilon}$	Average energy dissipation rate per unit volume (kg/ms^3)
ε_{cl}	Continuous liquid hold up (-)
ε_{dl}	Dispersed liquid hold up (-)
ε_g	Gas phase hold up (-)
ρ_{cl}	Continuous liquid density (kg/m^3)
$\rho_{cl\text{-}dl}$	Continuous and dispersed liquid mixture density (kg/m^3)
ρ_g	Gas phase density (kg/m^3)
μ_{cl}	Continuous liquid viscosity (kg/m.s)
μ_{dl}	Dispersed liquid viscosity (kg/m.s)
$\mu_{cl\text{-}dl}$	Dispersed liquid and continuous liquid mixture viscosity (kg/m.s)
σ_{cl}	Surface tension of continuous liquid (N/m)
σ_{dl}	Surface tension of dispersed liquid (N/m)
$\sigma_{cl–dl}$	Surface tension of continuous liquid and dispersed liquid (N/m)

Subscripts

cl	Continuous liquid
dl	Dispersed liquid
g	Gas
g- cl-dl	Gas-dispersed liquid-continuous liquid mixture
j	Jet velocity
m	Mixture
cl-dl	Continuous liquid-dispersed liquid mixture
sg	Superficial gas
sl	Superficial liquid

Chapter-5

a_j	Acceleration due to jet velocity (m/s^2)

A	Cross-sectional area (m^2)
$AAPE$	Average absolute relative percentage error (%)
C	Chisholm constant (-)
d_c	Diameter of the column (m)
d_j	Diameter of jet in the column (m)
d_{vs}	Bubble diameter (m)
Eu	Euler number ($=\Delta P_{TP}/\rho_{dl-cl}u_{dl-cl}^2$)), (-)
f	Friction factor (-)
f_{TP}	Three-phase friction factor (-)
F	Force (N)
Fr	Froude number ($=u_M^2/gd_c$) (-)
g	Acceleration due to gravity (m/s^2)
h_c	Height of column (m)
h_m	Height of the gas-liquid-liquid mixture in column (m)
H_r	Ratio of height of three phase mixture to diameter of column (h_m/d_c) (-)
H_{cl}	Height of continuous liquid (m)
H_{dl}	Height of dispersed liquid (m)
$H_{dl\text{-}cl}$	Height of liquid-liquid mixture in column (m)
$H_{g\text{-}dl\text{-}cl}$	Height of total mixture in column (m)
L_j	Jet length (m)
L_c	Length of the column (m)
ΔP_a	Acceleration component of pressure drop (Pa)
ΔP_{fO}	Frictional pressure drop for single phase flow (Pa)
ΔP_{fT}	Frictional pressure drop for three phase flow (Pa)
ΔP_h	Hydrostatic head (Pa)
ΔP_{TP}	Total pressure drop for three phase flow (Pa)
$\Delta P_{f0,\ dl\text{-}cl}$	Frictional pressure drop of continuous liquid phase flow (Pa)
ΔP_{f0g}	Frictional pressure drop of gas phase flow (Pa)
m	Mass flow rate (kg/s)
Mo	Morton number ($g\mu_{dl-cl}^4/\rho_{dl-cl}\sigma_{dl-cl}^3$) (-)

R^2	Correlation coefficient (-)
Re_j	Reynolds number based on jet velocity ($\rho_l d_c u_j / \mu_l$), (-)
Re_G	Reynolds number based on superficial gas velocity ($\rho_G d_c u_{sg} / \mu_g$), (-)
SE	Standard error (-)
u	Velocity (m/s)
u_j	Jet velocity (m/s)
u_s	Slip velocity (m/s)
u_{sg}	Superficial gas velocity (m/s)
u_{sl}	Superficial liquid velocity (m/s)
$u_{dl\text{-}cl}$	Superficial continuous phase liquid velocity (m/s)
U_r	Ratio of superficial liquid velocity to gas velocity (-)
V_O	Velocity of single phase (m/s)
V_c	Volume of continuous phase (ml)
V_s	Volume of solvent (ml)
x	Mass quality (-)
X	Lockhart-Martinelli parameter (-)
X_{mod}	Modified Lockhart – Martinelli parameter (-)
ϕ_g, $\phi_{dl\text{-}cl}$	Lockhart–Martinelli parameters (-)

Greek letters

ε_{cl}	Continuous liquid holdup (-)
ε_{dl}	Dispersed liquid holdup (-)
ε_g	Gas phase hold up (-)
ρ_0	Single phase liquid density (kg/m^3)
ρ_{cl}	Continuous liquid density (kg/m^3)
$\rho_{dl\text{-}cl}$	Dispersed and continuous liquid mixture density (kg/m^3)
ρ_g	Gas phase density (kg/m^3)
μ_{cl}	Continuous liquid viscosity (kg/m.s)
μ_{dl}	Dispersed liquid viscosity (kg/m.s)
$\mu_{dl\text{-}cl}$	Dispersed liquid and continuous liquid mixture viscosity (kg/m.s)

σ_l	Surface tension of liquid (N/m)

Subscripts

AT	Additional turbulence
c	Column
cl	Continuous liquid
dl	Dispersed liquid
dl-cl	Dispersed liquid-continuous liquid mixture
g	Gas
g-dl-cl	Gas-dispersed liquid-continuous liquid mixture
j	Jet velocity
k	Kato
l	Liquid
m	Mixture
o	Single phase
s	Superficial / slip
sg	Superficial gas
sl	Superficial liquid
tp	Three phase
w	Wallis
y	Transverse

Chapter-6

A_c	Column cross section area (m^2)
C_t	Concentration of Tracer at time t (kg/m^3)
C_o	Initial tracer concentration (kg/m^3)
d_c	Diameter of column (m)
D_d	Dispersion coefficient of the droplet motion
D_{ax}	Longitudinal or axial dispersion coefficient (m^2/s)
E_z	Axial dispersion coefficient (m^2/s)
f_v	Volume fraction of dispersed liquid (-)

Fr	Froude number ($=u_{sl}^2/d_c g$) (-)
h_m	Gas-liquid-liquid mixing height (m)
h_m	Clear liquid-liquid height (m)
H_p	Height of penetration depth (m)
H_r	Ratio of height of three phase mixture to diameter of the column (h_m/d_c) (-)
g	Acceleration due to gravity (m/s^2)
N_d	Dispersion number (-)
ΔP_{TP}	Total pressure drop for three phase flow, (Pa)
Pe	Peclet Number (-)
Q_G	Gas flow rate (m^3/s)
Q_L	Liquid flow rate (m^3/s)
RTD	Residence time distribution
R^2	Correlation coefficient, (-)
Re_j	Reynolds number based on jet velocity (-)
Re_l	Reynolds number based on liquid velocity (-)
Re_g	Reynolds number based on superficial gas velocity (-)
R_T	Overall resistance of flow
R_f	Frictional resistance of flow
R_h	Hydrostatic resistance of flow
R_d	Accelerate resistance of flow
t	Time (s)
t_m	Mean residence time (s)
Vg	Interstitial gas velocity ($u_{sg}/(\varepsilon_g)$) (m/s)
V_l	Interstitial liquid velocity ($u_{sl}/(1-\varepsilon_g)$) (m/s)
u_{sg}	Superficial gas velocity (Q_g/A_c) (m/s)
u_{sl}	Superficial liquid velocity (Q_l/A_c) (m/s)
u_j	Jet velocity (m/s)
V	Volume of dispersed liquid (ml)
We	Weber number $\left(u_{sl}^2 \rho_{cl-dl} d_c/\sigma\right)$ (-)

Greek letters

ϕ_{dl}	Volume concentration of the dispersed phase
ε_{cl}	Continuous liquid hold up (-)
ε_{dl}	Dispersed liquid hold up (-)
ε_g	Gas phase hold up (-)
ρ_{cl}	Continuous liquid density (kg/m^3)
$\rho_{cl\text{-}dl}$	Continuous and dispersed liquid mixture density (kg/m^3)
ρ_g	Gas phase density (kg/m^3)
μ_{cl}	Continuous liquid viscosity (kg/m.s)
μ_{dl}	Dispersed liquid viscosity (kg/m.s)
$\mu_{cl\text{-}dl}$	Dispersed liquid and continuous liquid mixture viscosity (kg/m.s)
σ_{cl}	Surface tension of continuous liquid (N/m)
σ_{dl}	Surface tension of dispersed liquid (N/m)
σ_{cl-dl}	Surface tension of continuous liquid and dispersed liquid (N/m)
σ_θ^2	Variance (-)
σ^2	Mean (-)

Chapter -7

a	Interfacial area (m^{-1})
AAPE	Absolute average percentage error (%)
CDF	Cumulative distribution function (-)
DSD	Drop size distribution (-)
d_c	Diameter of the column (m)
d_{32}	Sauter mean drop diameter (m)
d_d	Droplet diameter (m)
d_{eq}	Equivalent drop diameter (m)
$F(d_b)$	Drop distribution function (-)
Fr	Froude number (u_M^2 / gd_c) (-)
g	Acceleration due to gravity (m/s^2)
h_c	Height of column (m)

H_{cl}	Height of continuous liquid (m)
H_r	Ratio of height of three phase mixture to diameter of the mixing column (h_m/d_c) (-)
H_{dl}	Height of dispersed liquid (m)
$H_{cl\text{-}dl}$	Height of continuous liquid-dispersed liquid (m)
$H_{g\text{-}dl\text{-}cl}$	Height of interface of the mixture (m)
i.d	Inner diameter (m)
L	Distance between input and output of the tracer (m)
L_j	Jet length (m)
L_c	Length of the column (m)
l_{major}	Maximum axial length of the bubble (m)
l_{minor}	Minimum axial length of the bubble (m)
n_i	Number of bubbles (-)
R^2	Correlation coefficient (-)
Re_j	Reynolds number based on jet velocity ($\rho_l d_c u_j / \mu_l$) (-)
Re_{cl}	Reynolds number based on liquid velocity ($\rho_l d_c u_l / \mu_l$) (-)
Re_g	Reynolds number based on superficial gas velocity ($\rho_g d_c u_{sg} / \mu_g$) (-)
SE	Standard error (-)
u_{cl}	Continuous phase velocity (m/s)
u_j	Jet velocity (m/s)
u_{sg}	Superficial gas velocity (m/s)
u_{sl}	Superficial liquid velocity (m/s)
U_r	Ratio of superficial liquid velocity to gas velocity (-)
V_c	Volume of continuous phase (ml)
V	Volume of solvent (ml)
We	Weber number (= $\rho_{sl} u_j^2 d_n / \sigma$) (-)

Greek letters

α	Shape parameter of drop in Equation (7.4)
β	Scale parameter of drop in Equation (7.4)

ε_{cl}	Continuous liquid hold up (-)
ε_{dl}	Dispersed liquid hold up (-)
ε_{g}	Gas phase hold up (-)
ε_{s}	Volumetric flow fraction (-)
ρ_{cl}	Continuous phase density (kg/m^3)
ρ_{cl-dl}	Continuous liquid and dispersed liquid mixture density (kg/m^3)
ρ_{g}	Gas phase density (kg/m^3)
μ_{cl}	Continuous liquid viscosity (kg/m.s)
μ_{dl}	Dispersed liquid viscosity (kg/m.s)
μ_{cl-dl}	Continuous liquid and dispersed liquid mixture viscosity (kg/m.s)
σ_{cl-dl}	Surface tension of continuous liquid and dispersed liquid (N/m)

Subscripts

cl	Continuous liquid
dl	Dispersed liquid
d	Drop
g	Gas
g-cl-dl	Gas- continuous-dispersed liquid mixture
j	Jet velocity
m	Mixture
cl-dl	Continuous liquid and dispersed liquid mixture
sg	Superficial gas
sl	Superficial liquid

Chapter-8

a	Specific Interfacial area (m^{-1})
$C_{cl,\ in}$	Inlet concentration of solute in the continuous liquid (mol/l)

$C_{cl,\ out}$	Outlet concentration of solute in the continuous liquid (mol/l)
$C_{dl,\ in}$	Inlet concentration of solute in the dispersed liquid (mol/l)
$C_{dl,\ out}$	Outlet concentration of solute in the dispersed liquid (mol/l)
d_c	Column diameter (m)
E	Extraction efficiency (%)
Fr	Froude number (u_M^2 / gd_c) (-)
g	Gravitational acceleration (m/s^2)
H_r	Ratio of height of three phase mixture to diameter of column (-)
H	Height of the extraction column (m)
H_{cl}	Height of continuous liquid (m)
$H_{dl\text{-}cl}$	Height of mixture in column (m)
$H_{g\text{-}dl\text{-}cl}$	Height of gas-liquid-liquid interface of the mixture (m)
HTU	Height of transfer unit based on continuous phase (m)
$K_{cl}a$	Mass transfer coefficient based on continuous phase (1/s)
m	Equilibrium constant
M	Molar Concentration (mol/l)
NTU_{cl}	Number of transfer unit based on continuous phase (m)
P.A	Propionic acid
Re_{cl}	Reynolds number based on liquid velocity ($\rho_l d_c u_l / \mu_l$), (-)
Re_g	Reynolds number based on superficial gas velocity ($\rho_g d_c u_{sg} / \mu_g$), (-)
u_j	Jet velocity (m/s)
u_{sl}	Superficial liquid velocity (m/s)
u_g	Superficial gas velocity (m/s)
We	Weber number (= $\rho_{sl} u_j^2 d_n / \sigma$) (-)

Greek Letters

ρ_{cl}	Density of continuous liquid (kg/m^3)
$\rho_{cl\text{-}dl}$	Density of dispersed and continuous liquid mixture (kg/m^3)
ρ_g	Density of gas phase (kg/m^3)
μ_{cl}	Viscosity of continuous liquid (kg/m.s)

μ_{dl}	Dispersed liquid viscosity (kg/m.s)
$\mu_{cl\text{-}dl}$	Viscosity of dispersed and continuous liquid mixture (kg/m.s)
σ	Surface tension of liquid (N/m)

Abbreviation

cl	Continuous liquid
dl	Dispersed liquid
dl-cl	Dispersed liquid-continuous liquid
g	Gas
g-dl-cl	Gas-dispersed liquid-continuous liquid
sg	Superficial gas
sl	Superficial liquid

REFERENCES

- Aris, R., 1956. On the dispersion of a solute in a fluid flowing through a tube. Proceedings of the Royal Society of London. Series A. Mathematical and Physical Sciences 235, 67-77.
- Asai, S., Yoshizawa, H., 1991. Longitudinal holdup distribution of gas and dispersed liquid in bubble columns with two immiscible liquids. Industrial & Engineering Chemistry Research 30, 745-751.
- Assmann, N., von Rohr, P.R., 2011. Extraction in microreactors: intensification by adding an inert gas phase. Chemical Engineering and Processing: Process Intensification 50, 822-827.
- Babu, P., Kundu, G., Mukherjee, D., 1999. Studies on liquid-liquid dispersion in a downflow bubble column. Indian Journal of Chemical Technology 6, 243-246.
- Bagul, R., Pilkhwal, D., Vijayan, P., Joshi, J., 2013. Entrainment phenomenon in gas–liquid two-phase flow: A review. Sadhana 38, 1173-1217.
- Baidossi, W., Goren, N., Blum, J., Schumann, H., Hemling, H., 1993. Homogeneous and biphasic oligomerization of terminal alkynes by some water soluble rhodium catalysts. Journal of Molecular Catalysis 85, 153-162.
- Bandyopadhyay, N., Ray, P., Dutta, B., 1988. Gas holdup in a bubble column with immikible liquid mixtures. The Canadian Journal of Chemical Engineering 66, 995-999.
- Bart, H.-J., Stevens, G., 2004. Reactive solvent extraction. Ion Exchange and Solvent Extraction 17, 37-83.
- Behringer, H., 1952. The flow of liquid-gas mixtures in vertical tubes. VDI-Union of German Engineers, Amsterdam (Netherlands).
- Bensalem, A., Steiner, L., Hartland, S., 1986. Effect of mass transfer on drop size in a Karr column. Chemical Engineering and Processing: Process Intensification 20, 129-135.

- Biń, A., 1988. Minimum air entrainment velocity of vertical plunging liquid jets. Chemical Engineering Science 43, 379-389.
- Bin, A., Smith, J.M., 1982. Mass transfer in a plunging liquid jet absorber. Chemical Engineering Communications 15, 367-383.
- Bonsignore, D., Volpicelli, G., Campanile, A., Santoro, L., Valentino, R., 1985. Mass transfer in plunging jet absorbers. Chemical Engineering and Processing: Process Intensification 19, 85-94.
- Botton, R., Cosserat, D., Charpentier, J., 1978. Influence of column diameter and high gas throughputs on the operation of a bubble column. The Chemical Engineering Journal 16, 107-115.
- Butterworth, D., 1975. A comparison of some void-fraction relationships for co-current gas-liquid flow. International Journal of Multiphase flow 1, 845-850.
- Chantry, W.A., Berg, R.V., Wiegandt, H., 1955. Application of pulsation to liquid-liquid extraction. Industrial & Engineering Chemistry 47, 1153-1159.
- Chaudhari, R., Bhattacharya, A., Bhanage, B., 1995. Catalysis with soluble complexes in gas-liquid-liquid systems. Catalysis today 24, 123-133.
- Cheng, D., Cheng, J., Li, X., Wang, X., Yang, C., Mao, Z.S., 2012. Experimental study on gas–liquid–liquid macro-mixing in a stirred tank. Chemical Engineering Science 75, 256-266.
- Chisholm, D., 1967. A theoretical basis for the Lockhart-Martinelli correlation for two-phase flow. International Journal of Heat and Mass Tansfer 10, 1767-1778.
- Cramers, P., Beenackers, A., 2001. Influence of the ejector configuration, scale and the gas density on the mass transfer characteristics of gas–liquid ejectors. Chemical Engineering

Journal 82, 131-141.

- Cumming, I.W., 1975. The impact of failing liquids with liquid surfaces. PhD Thesis, Loughborough University of Technology, London.
- Das, M.D., Hrymak, A.N., Baird, M.H., 2013. Laminar liquid–liquid dispersion in the SMX static mixer. Chemical Engineering Science 101, 329-344.
- Datta, A., 1976. Effect of mixing throat length on the performance of a liquid jet ejector. M. Sc. thesis, Chemical Engineering Department, IIT, Kharagpur, India.
- Davies, G., Mitra, A., Roy, A., 1967a. Momentum Transfer Studies in Ejectors. Correlalations for Single-Phase and Two-Phase Systems. Industrial & Engineering Chemistry Process Design and Development 6, 293-299.
- Davies, G., Mitra, A., Roy, A., 1967b. Momentum Transfer Studies in Ejectors. Correlation for Three-Phase (Air-Liquid-Solid) System. Industrial & Engineering Chemistry Process Design and Development 6, 299-302.
- Davis, W., 1963. The effect of the Froude number in estimating vertical two-phase gas-liquid friction losses. British Chemical Engineering 8, 462-465.
- Deckwer, W.-D., Field, R.W., 1992. Bubble column reactors. Wiley, New York.
- Dehkordi, A.M., 2002. Liquid–liquid extraction with chemical reaction in a novel impinging-jets reactor. AIChE Journal 48, 2230-2239.
- Descamps, M., Oliemans, R., Ooms, G., Mudde, R., Kusters, R., 2006. Influence of gas injection on phase inversion in an oil–water flow through a vertical tube. International Journal of Multiphase Flow 32, 311-322.
- Desouky, S.E.-D.M., 1991. A new laminar-turbulent-transition criterion for pseudoplastic fluids. Journal of Petroleum Science and Engineering 5, 285-291.

- Din, G.U., Chughtai, I.R., Inayat, M.H., Khan, I.H., 2009. Study of axial mixing, holdup and slip velocity of dispersed phase in a pulsed sieve plate extraction column using radiotracer technique. Applied Radiation and Isotopes 67, 1248-1253.
- Drumm, C., Attarakih, M., Hlawitschka, M.W., Bart, H.-J.r., 2010. One-group reduced population balance model for CFD simulation of a pilot-plant extraction column. Industrial & Engineering Chemistry Research 49, 3442-3451.
- Eberhart, J., 1966. The Surface Tension of Binary Liquid Mixtures1. The Journal of Physical Chemistry 70, 1183-1186.
- Evans, G., Jameson, G., Atkinson, B., 1992. Prediction of the bubble size generated by a plunging liquid jet bubble column. Chemical Engineering Science 47, 3265-3272.
- Evans, G., Jameson, G., Rielly, C., 1996. Free jet expansion and gas entrainment characteristics of a plunging liquid jet. Experimental Thermal and Fluid Science 12, 142-149.
- Evans, G.M., 1990. A study of a plunging jet bubble column. Ph.D. Thesis, University of Newcastle, Australia.
- Fukuda, H., Sumino, Y., Kanzaki, T., 1968. Scale-up of fermentors. 2. Modified equations for power requirment. Journal of Fermentation Technology 46, 838.
- Galkin, N., Tikhomirov, V., Goriainov, N., Fedorov, V., 1961. The mechanism of distribution of liquids in a plate extractor. Journal of Nuclear Energy. Parts A/B. Reactor Science and Technology 14, 132-133.
- Gharat, S., Joshi, J., 1992. Transport phenomena in bubble colunm reactor II: Pressure drop. The Chemical Engineering Journal 48, 153-166.
- Ghosh, S., Das, G., Das, P., 2011. Pressure drop analysis for liquid-liquid downflow through vertical pipe. Journal of Fluids Engineering 133, 011202.

- Goshika, B.K., Majumder, S.K., 2018. Entrainment and holdup of gas-liquid-liquid dispersion in a downflow gas-liquid-liquid contactor. Chemical Engineering and Processing-Process Intensification 125, 112-123.
- Goshika, B.K., Majumder, S.K., 2019a. Dispersion of liquid–liquid phase by a jet-induced gas–liquid–liquid mixing column developed for separation of organic pollutants. Separation Science and Technology 54, 535-548.
- Goshika, B.K., Majumder, S.K., 2019b. Frictional pressure drop of gas–liquid–liquid dispersion in an ejector-induced downflow column. Multiphase Science and Technology 31, 151-174.
- Hatate, Y., 1976. Drop Size in Gas-Liquid-Liquid System Bubble Column. Kagaku Kogaku Ronbunshu 2, 133-137.
- Hatzikiriakos, S.G., Gaikwad, R.P., Nelson, P.R., Shaw, J.M., 1990. Hydrodynamics of gas-agitated liquid-liquid dispersions. AIChE Journal 36, 677-684.
- Hemmati, A., Torab-Mostaedi, M., Shirvani, M., Ghaemi, A., 2015. A study of drop size distribution and mean drop size in a perforated rotating disc contactor (PRDC). Chemical Engineering Research and Design 96, 54-62.
- Hendre, N.V., Venkatasubramani, V., Farakte, R.A., Patwardhan, A.W., 2018. Hydrodynamics and Mass Transfer Characteristics of Asymmetric Rotary Agitated Columns. Industrial & Engineering Chemistry Research 57, 1630-1644.
- Hu, B., Angeli, P., 2006. Phase Inversion and Associated Phenomena in Oil-Water Vertical Pipeline Flow. The Canadian Journal of Chemical Engineering 84, 94-107.
- Jawad, A.H., 2009. Studies Pressure Drop of gas-Non-Newtonian Liquid Two Phase Flow in Bubble Column. Engineering and Technology Journal 27, 1336-1350.

- Kantarci, N., Borak, F., Ulgen, K.O., 2005. Bubble column reactors. Process Biochemistry 40, 2263-2283.
- Kastner, L., Spooner, J., 1950. An investigation of the performance and design of the air ejector employing low-pressure air as the driving fluid. Proceedings of the Institution of Mechanical Engineers 162, 149-166.
- Kato, Y., Kago, T., Morooka, S., 1984. Longitudinal concentration distribution of droplets in multi-stage bubble columns for gas-liquid-liquid systems. Journal of Chemical Engineering of Japan 17, 429-435.
- Kawase, Y., Moo-Young, M., 1989. Hydrodynamics in bubble column bioreactors with fermentation broths having a yield stress. Applied Microbiology and Biotechnology 30, 596-603.
- Khawaja, S.Y., Usman, M.R., Nasif, M., Akram, M.S., Afzal, W., Akhtar, N.A., 2017. Mass transfer efficiency of a tall and low plate free area liquid pulsed sieve-plate extraction column. International Journal of Industrial Chemistry 8, 397-410.
- Khooshechin, S., Safdari, J., Moosavian, M.A., Mallah, M.H., 2013. Prediction of pressure drop in liquid–liquid pulsed packed extraction countercurrent columns. International Journal of Heat and Fluid Flow 44, 684-691.
- Kirchner, W., 1974. Gas entrainment by plunging liquid jets, Proceedings of 5th Australasian Conference on Hydraulics and Fluid Mechanics, Christchurch, New Zealand.
- Kirou, V., Tavlarides, L.L., Bonnet, J., Tsouris, C., 1988. Flooding, holdup, and drop size measurements in a multistage column extractor. AIChE Journal 34, 283-292.
- Kumagai, M., Endoh, K., 1982. Effects of kinematic viscosity and surface tension on gas entrapment rate of an impinging liquid jet. Journal of Chemical Engineering of Japan 15,

427-433.

- Kumar, A., Hartland, S., 1996. Unified correlations for the prediction of drop size in liquid–liquid extraction columns. Industrial & Engineering Chemistry Research 35, 2682-2695.
- Kundu, G., Mukherjee, D., Mitra, A., 1995. Experimental studies on a co-current gas-liquid downflow bubble column. International Journal of Multiphase Flow 21, 893-906.
- Kusabiraki, D., Niki, H., Yamagiwa, K., Ohkawa, A., 1990. Gas entrainment rate and flow pattern of vertical plunging liquid jets. The Canadian Journal of Chemical Engineering 68, 893-903.
- Lapidus, L., Elgin, J., 1957. Mechanics of vertical-moving fluidized systems. AIChE Journal 3, 63-68.
- Lapple, C., 1951. Fluid and Particle Mechanics. Newark: University of Delaware.
- Law, J.D., Todd, T.A., 2008. Liquid-liquid extraction equipment, Hydrometallurgy 42, 1-14.
- Levenspiel, O., 1972. Chemical Reaction Engineering John Wiley & Sons. Inc., New York.
- Levenspiel, O., Smith, W., 1957. Notes on the diffusion-type model for the longitudinal mixing of fluids in flow. Chemical Engineering Science 6, 227-235.
- Li, H., Luo, G., Fei, W., Wang, J., 2000. Mass transfer performance in a coalescence–dispersion pulsed sieve plate extraction column. Chemical Engineering Journal 78, 225-229.
- Lim, J.S., Lee, Y.-W., Kim, J.-D., Lee, Y.Y., Chun, H.-S., 1995. Mass-transfer and hydraulic characteristics in spray and packed extraction columns for supercritical carbon dioxide-ethanol-water system. The Journal of Supercritical Fluids 8, 127-137.
- Lin, T.J., Donnelly, H.G., 1966. Gas bubble entrainment by plunging laminar liquid jets. AIChE Journal 12, 563-571.
- Lobry, E., Gourdon, C., Xuereb, C., Lasuye, T., 2013. Liquid–liquid dispersion in co-current

disc and doughnut pulsed column effect of the operating conditions, physical properties and materials parameters. Chemical Engineering Journal 233, 24-38.

- Lockhart, R., Martinelli, R., 1949. Proposed correlation of data for isothermal two-phase, two-component flow in pipes. Chemical Engineering Progress 45, 39-48.
- Lü, S., Mi, Z., Wang, L., Wang, Y., Zhu, Z., Fu, S., 2005. Experimental investigation and simulation of gas–liquid–liquid reactive extraction process for the production of hydrogen peroxide. Chemical Engineering Science 60, 6298-6306.
- Majumder, S.K., 2008. Analysis of dispersion coefficient of bubble motion and velocity characteristic factor in down and upflow bubble column reactor. Chemical Engineering Science 63, 3160-3170.
- Majumder, S.K., 2016. Hydrodynamics and transport processes of inverse bubbly flow. Elsevier, Amsterdam.
- Mandal, A., 2010. Characterization of gas-liquid parameters in a down-flow jet loop bubble column. Brazilian Journal of Chemical Engineering 27, 253-264.
- Mandal, A., Kundu, G., Mukherjee, D., 2004. Gas-holdup distribution and energy dissipation in an ejector-induced downflow bubble column: the case of non-Newtonian liquid. Chemical Engineering Science 59, 2705-2713.
- Matsumura, M., Sakuma, H., Yamagata, T., Kobayashi, J., 1982. Gas entrainment in a new gas entraining fermentor. Journal of Fermentation Technology 60, 457-467.
- McKeogh, E., Ervine, D., 1981. Air entrainment rate and diffusion pattern of plunging liquid jets. Chemical Engineering Science 36, 1161-1172.
- Mitra, A., Roy, A., 1963. Performance of slurry reactor for Fischer-Tropsch and related syntheses. Indian Chemical Engineer. 5, 127-132.

- Mondal, S., Majumder, S.K., 2018. Studies on the copper extraction in a channel-based packed extraction device. Minerals Engineering 126, 194-206.
- Morello, V., Poffenberger, N., 1950. Commercial extraction equipment. Industrial & Engineering Chemistry 42, 1021-1035.
- Mukherjee, D., Biswas, M.N., Mitra, A.K., 1988. Hydrodynamics of liquid-liquid dispersion in ejectors and vertical two phase flow. The Canadian Journal of Chemical Engineering 66, 896-907.
- Napeida, M., Asl, A.H., Safdari, J., Torab-Mostaedi, M., 2010. Holdup and characteristic velocity in a Hanson mixer–settler extraction column. Chemical Engineering Research and Design 88, 703-711.
- Ohkawa, A., Kusabiraki, D., Kawai, Y., N. Sakai, N., 1986. Some Flow Characteristics of a Vertical Liquid Jet System having Downcomers. Chemical Engineering Science 41, 2347-2361.
- Ohkawa, A., Kusabiraki, D., Kawai, Y., Sakai, N., 1987. Flow characteristics of an air-entrainment type aerator having a long downcomer. Chemical Engineering Science 42, 2788-2790.
- Ohkawa, A., Kusabiraki, D., Kawai, Y., Sakai, N., Endoh, K., 1986. Some flow characteristics of a vertical liquid jet system having downcomers. Chemical Engineering Science 41, 2347-2361.
- Ohkawa, A., Shiokawa, Y., Sakai, N., Imai, H., 1985. Flow characteristics of downflow bubble columns with gas entrainment by a liquid jet. Journal of Chemical Engineering of Japan 18, 466-469.
- Oliveira, N., Silva, D.M., Gondim, M., Mansur, M.B., 2008. A study of the drop size

distributions and hold-up in short Kühni columns. Brazilian Journal of Chemical Engineering 25, 729-741.

- Pietrzak, M., Płaczek, M., Witczak, S., 2017. Upward flow of air-oil-water mixture in vertical pipe. Experimental Thermal and Fluid Science 81, 175-186.
- Poettman, F.H., Carpenter, P.G., 1952. The multiphase flow of gas, oil, and water through vertical flow strings with application to the design of gas-lift installations, Drilling and Production Practice. American Petroleum Institute.
- Rathilal, S., Carsky, M., Heyberger, A., Rouskova, M., 2013. Difference of hydrodynamics for a VPE with and without mass transfer and effect of agitation level on extent of mass transfer. South African Journal of Chemical Engineering 18, 29-39.
- Reith, T., Renken, S., Israel, B., 1968. Gas hold-up and axial mixing in the fluid phase of bubble columns. Chemical Engineering Science 23, 619-629.
- Sa, R., Gois, L., Cavalcanti, C., 2010. Dispersed phase holdup in a liquid-liquid extraction column. Latin American applied research 40, 373.
- Saien, J., Zonouzian, S.A.E., Dehkordi, A.M., 2006. Investigation of a two impinging-jets contacting device for liquid–liquid extraction processes. Chemical Engineering Science 61, 3942-3950.
- Samdavid, S., Renganathan, T., Krishnaiah, K., 2016. Hydrodynamics of a cocurrent downward liquid–liquid extraction column. RSC Advances 6, 12439-12445.
- Seibert, A.F., Fair, J.R., 1988. Hydrodynamics and mass transfer in spray and packed liquid-liquid extraction columns. Industrial & Engineering Chemistry Research 27, 470-481.
- Shirvani, A., Ghaemi, A., Torab, M.M., 2016. Experimental Investigation of Flooding and Drop Size in a Kuhni Extraction Column. International Journal of Engineering 29, 288-296.

- Sivaiah, M., Majumder, S.K., 2013a. Dispersion characteristics of liquid in a modified gas-liquid-solid three-phase downflow bubble column. Particulate Science and Technology 31, 210-220.
- Sivaiah, M., Majumder, S.K., 2013b. Hydrodynamics and mixing characteristics in an ejector-induced downflow slurry bubble column (EIDSBC). Chemical engineering journal 225, 720-733.
- Sivaiah, M., Parmar, R., Majumder, S.K., 2012. Gas entrainment and holdup characteristics in a modified gas–liquid–solid down flow three-phase contactor. Powder technology 217, 451-461.
- Smith, J.S., Valsaraj, K.T., Thibodeaux, L.J., 1996. Bubble Column Reactors for Wastewater Treatment. 1. Theory and Modeling of Continuous Countercurrent Solvent Sublation. Industrial & Engineering Chemistry Research 35, 1688-1699.
- Smith, R., 1951. Some Aspects of Fluid Flow. Edward Arnold, London, 229.
- Sohn, H., Doungdeethaveeratana, D., 1998. A novel solvent extraction process with bottom gas injection without moving parts. Separation and Purification Technology 13, 227-235.
- Sovilj, M., Kneževic, G., 1994. Gas-agitated liquid-liquid extraction in a spray column. Collection of Czechoslovak Chemical Communications 59, 2235-2243.
- Spedding, P., Woods, G., Raghunathan, R., Watterson, J., 2000. Flow pattern, holdup and pressure drop in vertical and near vertical two-and three-phase upflow. Chemical Engineering Research and Design 78, 404-418.
- Stapelberg, H.H., Mewes, D., 1994. The pressure loss and slug frequency of liquid-liquid-gas slug flow in horizontal pipes. International Journal of Multiphase Flow 20, 285-303.
- Stokes, G.G., 1880. Supplement to a paper on the theory of oscillatory waves. Mathematical

and Physical papers 1, 14.

- Suciu, G.D., Smigelschi, O., 1976. Size of the submerged biphasic region in plunging jet systems. Chemical Engineering Science 31, 1217-1220.
- Takahashi, K., Nii, S., 1999. Behavior of Multistage Mixer-Settler extraction Column. Memoris-school of engineering, Nagoya University 51, 1-51.
- Tan, J., Liu, Z., Lu, Y., Xu, J., Luo, G., 2011. Process intensification of H_2O_2 extraction using gas–liquid–liquid microdispersion system. Separation and Purification Technology 80, 225-234.
- Tan, J., Lu, Y., Xu, J., Luo, G., 2013. Modeling investigation of mass transfer of gas–liquid–liquid dispersion systems. Separation and Purification Technology 108, 111-118.
- Tan, S., Xu, D., Dong, L., Wei, S., Luo, Z., Zhang, H., 2012. Solvent extraction of butyl acetate from lovastatin wastewater using liquid paraffin. Desalination 286, 94-98.
- Taylor, G.I., 1953. Dispersion of soluble matter in solvent flowing slowly through a tube. Proceedings of the Royal Society of London. Series A. Mathematical and Physical Sciences 219, 186-203.
- Thornton, J.D., 1992. Science and Practice of Liquid-liquid Extraction: Process chemistry and extraction operations in the hydrometallurgical, nuclear, pharmaceutical, and food industries. Oxford University Press, USA.
- Topiwala, H., Hamer, G., 1974. Mass transfer and dispersion properties in a fermenter with a gas-inducing impeller. Transactions of the Institution of Chemical Engineers 52, 113-120.
- Torab-Mostaedi, M., Ghaemi, A., Asadollahzadeh, M., Pejmanzad, P., 2011. Mass transfer performance in pulsed disc and doughnut extraction columns. Brazilian Journal of Chemical Engineering 28, 447-456.

- Torab-Mostaedi, M., Safdari, J., 2009. Prediction of mass transfer coefficients in a pulsed packed extraction column using effective diffusivity. Brazilian Journal of Chemical Engineering 26, 685-694.
- Torab-Mostaedi, M., Safdari, J., Moosavian, M.A., Maragheh, M.G., 2009. Stage efficiency of Hanson mixer-settler extraction column. Chemical Engineering and Processing: Process Intensification 48, 224-228.
- Torab-Mostaedi, M., Safdari, S., Moosavian, M., Maragheh, M.G., 2008. Mass transfer coefficients in a Hanson mixer-settler extraction column. Brazilian Journal of Chemical Engineering 25, 473-481.
- Upadhyay, R.K., Kaim, J., Roy, S., 2009. Investigation of downflow bubble columns: experiments and modeling. Journal of Chemical Engineering of Japan 42, 156-161.
- Usman, M., Sattar, H., Hussain, S., Muhammad, H., Asghar, A., Afzal, W., 2009. Drop size in a liquid pulsed sieve-plate extraction column. Brazilian Journal of Chemical Engineering 26, 677-683.
- Van de Donk, J.A.C., 1981. Water aeration with plunging jets. PhD Thesis. Technische Hogeschool Delft.
- Van de Sande, E., Smith, J.M., 1975. Mass transfer from plunging water jets. The Chemical Engineering Journal 10, 225-233.
- Veera, U.P., 2001. Gamma ray tomography design for the measurement of hold-up profiles in two-phase bubble columns. Chemical Engineering Journal 81, 251-260.
- Venkatanarasaiah, D., Varma, Y., 1998. Dispersed phase holdup and mass transfer in liquid pulsed column. Bioprocess Engineering 18, 119-126.
- Vermijs, H., Kramers, H., 1954. Liquid-liquid extraction in a rotating disc contactor.

Chemical Engineering Science 3, 55-64.

- Wallis, G., 1969. One-Dimensional Two-Phase Flow McGraw-Hill Book Company. New York.
- Wang Li, Cheng Yong-xi, Lu Shu-xiang, Zhen-tao, M., 2007. Calculation of Organic Dispersed Holdup in Gas-Agitated Extraction Columns. Journal of Tianjin University 40, 260-264.
- Wang, Y., Fei, W., Sun, J., Wan, Y., 2002. Hydrodynamics and mass transfer performance of a modified rotating disc contactor (MRDC). Chemical Engineering Research and Design 80, 392-400.
- Xu, J., Luo, G., Chen, G., Tan, B., 2005. Mass transfer performance and two-phase flow characteristic in membrane dispersion mini-extractor. Journal of Membrane Science 249, 75-81.
- Xu, J.Y., Zhang, J., Liu, H.F., Wu, Y.X., 2012. Oil–gas–water three-phase upward flow through a vertical pipe: Influence of gas injection on the pressure gradient. International Journal of Multiphase Flow 46, 1-8.
- Yamagiwa, K., Kusabiraki, D., Ohkawa, A., 1990. Gas holdup and gas entrainment rate in downflow bubble column with gas entrainment by a liquid jet operating at high liquid throughput. Journal of Chemical Engineering of Japan 23, 343-348.
- Yoshida, F., and Yamada,T, 1971. Average size of oil drops in hydrocarbon fermentation. Journal of fermentation technology 49, 235-244.
- Yu, Q., weiyang, F., jiading, W., 1989. A study on mass transfer in pulsed sieve-plate extraction column. Journal of Chemical Industry and Engineering, 218-228.
- Zahradnik, J., Fialova, M., Linek, V., Sinkule, J., Řezníčková, J., Kaštánek, F., 1997.

Dispersion efficiency of ejector-type gas distributors in different operating modes. Chemical Engineering Science 52, 4499-4510.

- Zuber, N., Findlay, J., 1965. Average volumetric concentration in two-phase flow systems. Journal of Heat Transfer 87, 453-468.
- Zundelevich, Y., 1979. Power consumption and gas capacity of self-inducting turbo aerators. AIChE Journal 25, 763-773.